Energy recovery maximisation modelling subject to constrained cooling

JP Bester

orcid.org/ 0000-0002-1758-2743

Thesis accepted in fulfilment of the requirements for the degree Doctor of Philosophy in Mechanical Engineering at the North-West University

Promoter:	Dr PvZ Venter
Co-promoter:	Prof M van Eldik

Graduation: June 2025

ACKNOWLEDGEMENTS

The author of this thesis has been blessed with both a professional and personal support structure, and would like to thank:

- My supervisor Dr. Philip Venter, for his insight, enthusiasm, time, endless patience, and invaluable guidance throughout the course of this study.
- My co-supervisor Dr. Martin van Eldik, for his expert advice, constructive feedback, and support in refining this research to its completion.
- My colleague and friend, Dr. Cronier van Niekerk, for his unwavering encouragement, critical insights, and for always being a sounding board for new ideas.
- My parents, Johan and Elizma, for their unconditional love, sacrifices, life lessons, strong work ethic, and belief in my ability to persevere.
- My lovely wife, Ansuné, and son Hanro, for their boundless love, understanding, for the patience during the demanding periods of this journey, and for being my constant source of strength, inspiration and joy.
- I also thank the Lord for granting me the capacity to start, to persevere and for the support to complete this thesis.

ABSTRACT

The heat rejection cycle in a metal production plant involves the transfer of thermal energy from warm (1200°C –1500°C) flue gas to a closed cooling water cycle. This closed cycle is operated to, furthermore, remove the absorbed thermal energy from the circulating cooling water. Monitoring and controlling this heat-absorption-and-rejection cycle is critical. Process stability requires maintaining the temperatures of both the flue gas and cooling water in respective design operational envelopes and is also critical for preventing corrosion in the gas cooler, and overall equipment integrity. To maintain both temperature envelopes, the absorbed waste heat in the cooling water is transferred to the environment via an air-cooled heat exchanger (ACHX) and/or used to generate power through a Rankine cycle (PGEN).

Several studies have focused on evaluating the performance of waste heat recovery Rankine cycles and air-cooled heat exchangers, mostly considering these systems in isolation. These studies typically aim to maximise parameters such as heat recovery efficiency. Relevant studies on combined systems have also demonstrated the use of design conditions and non-fluctuating heat sources. The combined control of power generation and air-cooled heat exchangers; however, specifically the dynamic distribution of flow to increase energy recovery while sustaining the operational envelope with a fluctuating heat source, remains underexplored. Addressing this gap can improve the operational efficiencies of combined heat and power systems that are commonly deployed in industry. Furthermore, filling this gap also provides insights into practical solutions for enhancing power generation performance and reducing operational costs.

To achieve this objective, representative models for the PGEN, ACHX, gas cooler, and heat loss components were formulated. Internal control philosophies have also been formulated for controllable components. This ensures that phenomena such as trips during periods of low heat availability and constrained restart procedures are accounted for over the time horizon of the plant-specific waste-heat profile. These models are then used in the novel control philosophies of this thesis to maximise net power generation without breaching the operational temperature envelope.

The first novel philosophy improves on the current philosophy by providing a framework for the dynamic flow adjustment between the PGEN and ACHX with the aim of maximising net power generation. This philosophy maximises the power generation for the available heat in the cooling water. The second novel philosophy improves on the first by solving for increased available heat in the cooling water through adjustment of the cooling water flow rate. This is followed by dynamically adjusting the flow distribution between the PGEN and ACHX. This philosophy provides the framework that ensures maximum power generation for the available heat in the flue gas. The third novel formulation improves on the second by adjusting the approach to allow for a

thermal energy storage system to dampen the heat source fluctuations and reduce the number of low heat availability trips the PGEN experiences. The approach from this philosophy maximises power generation over the time horizon by managing the charging and discharging of the thermal energy storage with the cooling water exiting the gas cooler.

The frameworks provided by the novel control philosophies is solved for on a historical dataset and increased the energy transferred from flue gas to cooling water from 92.24% to 99.57%. The average power generation over the time horizon also increased from 1.134 MW to 1.485 MW when applying the first philosophy. The second and third philosophy resulted in average power generation of 1.615 and 1.631 MW. The energy recovery ratio, defined as the ratio of electrical energy generated to the available energy in the flue gas, increased from 8.66% for the Work's philosophy to 11.34%, 12.38%, and 12.96% for the first, second, and third novel philosophies, respectively. These results were obtained through simulation-based evaluations of the proposed approaches.

Keywords: dynamic control, temperature control, waste heat recovery, flow distribution, industrial cooling system, gas cooler, power generation, historical heat profile, fluctuating heat source

TABLE OF CONTENTS

ACKNOWLEDGEMENTS ..... **I**

ABSTRACT ..... **II**

TABLE OF CONTENTS ..... **IV**

LIST OF TABLES ..... **XI**

LIST OF FIGURES ..... **XII**

1 BACKGROUND AND PROBLEM STATEMENT **1**

1.1 Introduction **1**

1.2 Research Need **4**

1.3 Objective of This Study **5**

1.4 Methodology of Investigation **5**

1.5 Contributions of This Study **6**

1.6 Layout of The Thesis **7**

CHAPTER 2 LITERATURE REVIEW **9**

2.1 Basic Definitions and Theory **9**

2.1.1 Fluid 9

2.1.2 Steady State and Transient Processes 9

2.1.3 Specific Enthalpy 9

2.1.4 Specific Heat Capacity 9

2.1.5 Conservation laws 10

2.1.6 Measurable Energy Transfer 11

2.1.7 Heat Transfer Mechanisms 12

2.1.8 Thermal Resistance 17

2.1.9 Overall heat transfer coefficient 18

2.2 Systems and Devices Theory **18**

2.2.1 Heat Rejection Process of the Metal Production Plant 18

2.2.2 Gas Cooler 19
2.2.3 Heat Exchangers 20
2.2.4 Pumps and Fans 23
2.2.5 Energy Recovery Process – Power Generation 25
2.2.5.1 Turbines 26
2.2.5.2 Turbine Trips and Controlled Startup 27
2.3 Control Philosophy and Methods 28
2.3.1 Heat Exchanger Efficiency Maximisation 28
2.3.2 Parallel Heat Recovery Operations with a Fluctuating Heat Source 29
2.3.3 Energy Recovery with a Fluctuating Waste Heat Profile 30
2.4 Identified Gap in Literature 33
2.5 Summary 34

CHAPTER 3 PROCESS AND COMPONENT CONSIDERATIONS 36
3.1 Heat Rejection System 36
3.1.1 Layout 36
3.1.2 Control Requirements 37
3.2 Gas-Cooler Operational Considerations 38
3.2.1 Flue Gas Temperature Envelope 38
3.2.2 Cooling Water Operational Envelope 39
3.2.3 Fluctuating Waste Heat Profile 40
3.3 Air Cooled Heat Exchanger Operational Considerations 44
3.3.1 ACHX Original Design 44
3.3.2 ACHX Operational Model 45
3.3.2.1 Heat Transfer without Forced Convection 45
3.3.2.2 Heat Transfer with Forced Convection 46
3.3.2.3 Combined Operational Regime 48
3.4 Power Generation System Operational Considerations 49

3.4.1 PGEN Layout and Design Limitations 49
3.4.1.1 PGEN Cycle Layout 49
3.4.1.2 Design and Operational Limitations 50
3.4.2 PGEN Operational Performance Model 52
3.4.2.1 PGEN Component Models 52
3.4.2.2 PGEN Off-Design Operational Model Results 55
3.5 Heat Losses from Uninsulated Components 56
3.5.1 Details on Uninsulated Components 57
3.5.2 Quantifying Heat Loss to the Environment 58
3.6 Unplanned trip events 61
3.7 Conclusion 62

CHAPTER 4 RECURRING COMPONENT CONTROL PHILOSOPHIES 64
4.1 Flue Gas Temperature Control Philosophy 64
4.1.1 Cooling Water Flow Control (CWFC) 64
4.1.2 CWFC Results on Demonstrative Dataset 66
4.2 PGEN Control Philosophy 68
4.2.1 Changing the Outlet Pressure of the Cycle Pump 68
4.2.2 Changing the Degree of Superheat on the Evaporator Exit 69
4.2.3 Control Philosophy for Maximum Power Generation (PGCP) 70
4.2.4 PGCP Results on Demonstrative Dataset 72
4.3 ACHX Control Philosophy 74
4.3.1 Control Philosophy for Efficient Heat Transfer (ACCP) 74
4.3.2 ACCP Results on Demonstrative Dataset 77
4.4 Setpoint Temperature Control Model 79
4.4.1 Control Philosophy for Temperature Setpoint Determination (TSD) 80
4.4.2 TSD Results on Demonstrative Dataset 81
4.5 Summary and Conclusion 82

CHAPTER 5 THE WORKS PHILOSOPHY 84

5.1 Sub-algorithms for Sustained Operations 84

5.1.1 Heat Flow From ACHX with No Operational Fans 84

5.1.2 Bypass Flow and Restart of flow through ACHX 86

5.1.2.1 Bypassing Flow to Maintain Operational Envelope 86

5.1.2.2 Restarting the ACHX 87

5.1.3 Tripped PGEN Scenario 89

5.1.3.1 Cold and Warm Start Procedures 89

5.1.3.2 Time Delay and Start Procedures for PGEN 90

5.2 Formulation of the Works Philosophy (WP) 92

5.3 Performance Evaluation of WP 96

5.3.1 Demonstrative Dataset 96

5.3.1.1 Results for Distribution of Flow and Heat 96

5.3.1.2 Results for ACHX and PGEN Operation 97

5.3.2 Historical Dataset 100

5.3.2.1 Demonstration of SAAR 100

5.3.2.2 Unplanned Trip of PGEN 101

5.3.2.3 Summary of Performance Results 101

5.3.3 Adjustment to Ratio 104

5.4 Conclusion 105

CHAPTER 6 DISCRETE ADJUSTMENT TO DISTRIBUTION 107

6.1 Approach Changes from WP 107

6.2 Additional Sub-Algorithms for Sustained Operation 107

6.2.1 Minimum and Maximum Cooling Water Flow through ACHX 108

6.2.1.1 Change in Minimum Flow Approach for DADP 108

6.2.1.2 Minimum flow through ACHX for Demonstrative Dataset 109

6.3 Nett Power Generation vs Flow Distributed to PGEN 110

6.3.1 Case study for PGEN Flow Distribution Calculation 110
6.3.2 Bisection Method 112
6.4 Formulation of the Discrete Adjustment to Distribution (DADP) 113
6.5 Performance Evaluation of the DADP 117
6.5.1 Demonstrative Dataset 117
6.5.1.1 Results for Distribution of Flow and Heat 118
6.5.1.2 Results for ACHX and PGEN Operation 119
6.5.2 Historical Dataset 121
6.5.2.1 Performance and Operational Parameters on the Historical Dataset 122
6.5.2.2 Comparison between DADP and WP 123
6.5.2.3 Comparison to Maximum flow to PGEN Philosophy 124
6.6 Conclusion 125

CHAPTER 7 DISCRETE ADJUSTMENT TO FLOW 128
7.1 Approach Changes from DADP 128
7.1.1 Maximising Energy Recovered from Flue Gas 128
7.1.2 Minimise Power Consumption from Cooling Water Pumps 129
7.2 Flow influences on Gas Cooler Heat Transfer 130
7.2.1 Simplified Gas Cooler Model 130
7.2.2 Case Study for Cooling Water Flow Control 132
7.3 Formulation of the Cooling Water Flow Range (CWFR) Algorithm 134
7.4 Formulation of the Discrete Adjustment to Flow Philosophy (DAFP) 136
7.5 Performance Evaluation of the DAFP 138
7.5.1 Demonstrative Dataset 138
7.5.1.1 Operational Status of Components 139
7.5.1.2 Flow and Temperature Adjustments 139
7.5.1.3 Nett Power Generation 142
7.5.1.4 Summary of Demonstrative Dataset Results 142

7.5.2 Historical Dataset 143
7.5.2.1 Performance and Operational Parameters on Historical Dataset 143
7.5.2.2 Comparison to DADP 145
7.6 Conclusion 146

CHAPTER 8 POTENTIAL SYSTEM IMPROVEMENTS 149
8.1 Addition of a TESS 149
8.1.1 Updated System Layout with TESS 149
8.1.2 TESS Parameters 150
8.2 Adjustments to DAFP 152
8.2.1 TESS Control Algorithm (TCA) 152
8.2.2 Evaluation on Demonstrative Dataset 154
8.2.3 Changes Required to CWFR (CWFR-T) 156
8.3 Formulation of DAFP with integrated TESS control (DAFP-T) 158
8.4 Performance Evaluation of DAFP-T 161
8.4.1 Demonstrative Dataset 161
8.4.1.1 Changes in Heat Availability, Flow and Temperatures 161
8.4.1.2 Nett Power Generation 163
8.4.1.3 Summary of Demonstrative Dataset Results 164
8.4.2 Historical Dataset 164
8.4.2.1 Performance and Operational Parameters on Historical Dataset 164
8.4.2.2 Comparison to DAFP 167
8.5 Conclusion 168

CHAPTER 9 SUMMARY AND CONCLUSION 172
9.1 Chapter Summaries 173
9.2 Future research 176
BIBLIOGRAPHY 178
APPENDIX A – ACHX PERFORMANCE PREDICTION MODEL 184

APPENDIX B – HEAT LOSS PREDICTION MODEL 188

APPENDIX C – POWER GENERATION CONTROL (PGCP) 194

APPENDIX D – AIR-COOLED HEAT EXCHANGER CONTROL (ACCP) 198

APPENDIX E – TEMPERATURE SETPOINT DETERMINATION (TSD) 202

APPENDIX F – SAMPLE SCRIPT FOR WP 207

APPENDIX G – SAMPLE SCRIPT FOR DADP 214

APPENDIX H – SCRIPT FOR DAFP 219

APPENDIX I – SCRIPT FOR DAFP-T 222

APPENDIX J – PUBLISHED ARTICLE 224

LIST OF TABLES

Table 3-1: Gas Cooler Design Parameters and Operational Envelope for Cooling Water 39

Table 3-2: Design Parameters of an ACHX 44

Table 3-3: PGEN Operational Limits and Design Parameters 51

Table 3-4: Uninsulated Components Between PGEN and ACHX and the Gas Cooler 57

Table 4-1: Results for PGCP on Demonstrative Dataset 72

Table 4-2: Section of Results for ACCP on Demonstrative Dataset 78

Table 5-1: Summary of Performance Evaluation for WP 102

Table 5-2: Comparison of performance for different α parameters under WP 104

Table 6-1: The Bisection Method Algorithm 112

Table 6-2: Modified Bisection Method Algorithm for use in DADP (BM-PGEN) 113

Table 6-3: Comparison of Performance between WP and DADP 124

Table 6-4: Comparison of Performance Evaluation between Maximum Flow Philosophy and DADP 125

Table 7-1: Selection of Results for Flow Control Case Study 133

Table 7-2: Comparison of DAFP, DADP and WP on Demonstrative Dataset 143

Table 7-3: Comparison of Performance between DAFP, DADP and WP 145

Table 8-1: TESS Design Parameters 151

Table 8-2: Comparison of DAFP-T, DAFP, DADP and WP on Demonstrative Dataset 164

Table 8-3: TESS Depletion and Recharging in Historical Dataset 166

Table 8-4: Comparison of Performance between DAFP-T, DAFP, DADP and WP 168

LIST OF FIGURES

Figure 1-1: Closed Loop Cooling Cycle Layout 2

Figure 2-1: Boundary Layer Development in Convective Heat Transfer, as in [8] 13

Figure 2-2: Heat Transfer Across Composite Wall as in [3] 17

Figure 2-3: Concentric Tube Heat Exchanger, as in [2] 20

Figure 2-4: Thermal Resistance Circuit for Concentric Tube Heat Exchanger with Fouling 21

Figure 2-5: Rankine Cycle for Power Generation from Waste Heat Recovered 26

Figure 3-1: Detailed Layout of Heat Rejection Process 37

Figure 3-2: Representative Dataset of Waste Heat Over Time 42

Figure 3-3: Demonstrative Waste Heat Dataset 43

Figure 3-4: Maximum and Minimum Heat Transferred every Time Interval for the Demonstrative Dataset 43

Figure 3-5: Heat Transfer Rate vs Cooling Water Temperature during Natural Convection per ACHX 46

Figure 3-6: Fluid Mass Flows vs Predicted Heat Transfer Performance in the ACHX (Per Fan) for a Heat Source Temperature of 180 ℃ 47

Figure 3-7: Combination of Forced and Natural Convection Heat Transfer in the ACHX 48

Figure 3-8: Heat Transfer Rate Range for the Four Fans in the ACHX 49

Figure 3-9: PGEN Component Layout 50

Figure 3-10: Thermal Efficiency vs Heat Source Parameters for $\mathbf{P3} = 22.8$ bar and $\mathbf{Tevap} *=$ 20 ℃ 56

Figure 3-11: Heat Loss to the Environment Between PGEN, ACHX and the Gas Cooler 57

Figure 3-12: Thermal Resistance System for Heat Loss through Pipe and Tank 58

Figure 3-13: Heat Loss versus Temperature and Mass Flow Rate of Cooling Water 60

Figure 3-14: Progress to Control Algorithms after Chapter 3 63

Figure 4-1: Cooling Water Flow Control Based on Flue Gas Temperature Exiting the Gas Cooler 65

Figure 4-2: Cooling Water Flow Rate Adjustments through CWFC 66

Figure 4-3: Heat Transferred in Gas Cooler at Time t for CWFC 67

Figure 4-4: Thermal Efficiency of PGEN with a Varying **P3** at $\mathbf{Tevap} *= \mathbf{10}$℃, $\mathbf{mhs} = \mathbf{60\ kgs}$ and $\mathbf{Ths} = 200$ ℃ 68

Figure 4-5: Efficiency of PGEN with varying $\mathbf{Tevap} *$ at $\mathbf{Pevap} = \mathbf{20\ bar}$, $\mathbf{mhs} = \mathbf{60\ kgs}$, $\mathbf{Ths} = 200$ ℃ 69

Figure 4-6: PGEN Control Philosophy (PGCP) 71

Figure 4-7: Power Generation Comparison of PGCP to Fixed Philosophy on Demonstrative Dataset 73

Figure 4-8: Evaporating Pressure and Degree of Superheat Variation for PGCP on Demonstrative Dataset 74

Figure 4-9: ACHX Control Philosophy (ACCP) 75

Figure 4-10: Heat Transfer Achieved in ACHX under ACCP on Demonstrative Dataset 78

Figure 4-11: Fan Operational Speed Assigned by ACCP on Demonstrative Dataset 79

Figure 4-12: Temperature Setpoint Control Philosophy (TSD) 80

Figure 4-13: Rate of Heat Loss from Uninsulated Components over Time for Demonstrative Dataset 81

Figure 4-14: Total Heat Loss Rate and Setpoint Temperature over Time for Demonstrative Dataset 82

Figure 4-15: Summary of Control Philosophies Demonstrated in Chapter 4 83

Figure 5-1: Temperature of Stagnant Cooling Water in ACHX over time for $\mathbf{T0} = 210$ ℃ 85

Figure 5-2: Restarting Flow through the ACHX 88

Figure 5-3: Time Delay in Start Procedure of PGEN 91

Figure 5-4: Flow Diagram of WP 95

Figure 5-5: Heat Transferred by ACHX and PGEN for WP on a Demonstrative Dataset 96

Figure 5-6: Flow Distribution between ACHX and PGEN 97

Figure 5-7: ACHX Operational Settings for WP on Demonstrative Dataset 98

Figure 5-8: Power Generation by PGEN for WP on Demonstrative Dataset 98
Figure 5-9: Efficiency over Time for PGEN with WP on Demonstrative Dataset 99
Figure 5-10: PGEN Settings for WP on Demonstrative Dataset 99
Figure 5-11: Demonstration of SAAR in Historical Dataset 100
Figure 5-12: Unplanned Trip Response of WP 101
Figure 5-13: Operational Speed of Fans over Time Horizon of Historical Dataset 102
Figure 5-14: Thermal Efficiency of PGEN over time horizon of Historical Dataset 103
Figure 5-15: Temperature at Point 5 with WP 103
Figure 5-16: Summary of Control Philosophies of WP after Conclusion of Chapter 5. 106
Figure 6-1: Minimum Flow Assignment to ACHX through WCP (SAMF) 108
Figure 6-2: Minimum Flow through ACHX for Demonstrative Dataset 109
Figure 6-3: Nett Power Generation vs Cooling Water Flow Rate to PGEN 111
Figure 6-4: Flow Diagram of DADP 115
Figure 6-5: Flow Distribution between ACHX and PGEN under DADP 118
Figure 6-6: Comparison of PGEN Cooling Water Flow under DADP and WP 118
Figure 6-7: Setpoint Temperature and Average Heat Transfer Comparison between DADP and WP 119
Figure 6-8: ACHX Operational Settings for WP on Demonstrative Dataset 120
Figure 6-9: Power Generation by PGEN for WP on Demonstrative Dataset 120
Figure 6-10: PGEN Efficiency Comparison between DADP and WP on Demonstrative Dataset 121
Figure 6-11: Operational Speed of Fans over Time Horizon of Historical Dataset 122
Figure 6-12: Thermal Efficiency of PGEN over Time Horizon of Historical Dataset 122
Figure 6-13: Temperature at point 5 with DADP 123
Figure 6-14: Summary of DADP after Conclusion of Chapter 6. 127
Figure 7-1: Exit Temperature of Flue Gas at the Gas Cooler for CFWC 128

Figure 7-2: Residual Heat in Flue Gas with CWFC..... 129
Figure 7-3: Cooling Water Flow Range (CWFR) for Operational Envelope in Gas Cooler135
Figure 7-4: Flow Diagram of DAFP 137
Figure 7-5: Operational Status of Components with DAFP in Demonstrative Dataset .. 139
Figure 7-6: $\mathbf{Ths,t}$ Comparison between DADP and DAFP and $\mathbf{Tfg}$ for DAFP 140
Figure 7-7: Allowable Cooling Water Flow Rate in DAFP 140
Figure 7-8: Available Heat Comparison between DAFP and DADP 141
Figure 7-9: Flow Distribution between ACHX and PGEN for DAFP 142
Figure 7-10: Comparison of Nett Power Generation for DADP and DAFP..... 142
Figure 7-11: Relative Changes in Thermal Efficiency from DADP to DAFP 144
Figure 7-12: Increase in Power Generation from DADP to DAFP..... 144
Figure 7-13: Summary of DAFP after Conclusion of Chapter 7. 147
Figure 8-1: Layout of Heat Rejection System with Addition of a TESS 150
Figure 8-2: Temperature at which PGEN tripped for DAFP 151
Figure 8-3: Temperature of Cooling Water exiting Gas Cooler for DAFP..... 152
Figure 8-4: TESS Control Algorithm (TCA) to Adjust Cooling Water Temperature entering DAFP 153
Figure 8-5: Heat Availability in Cooling Water Before and After TESS..... 155
Figure 8-6: Additional Flow Required to Meet Heat Requirement with TESS Compared to DAFP Flow Rate 156
Figure 8-7: CWFR-T for Use in DAFP with an Integrated TESS 157
Figure 8-8: Flow Diagram of DAFP-T 160
Figure 8-9: TESS Influence on Available Heat in Cooling Water for Demonstrative Dataset161
Figure 8-10: Changes in Cooling Water Flow Rate from DAFP to DAFP-T 162
Figure 8-11: Differences in Cooling Water Temperatures $\mathbf{T2}*$ between DAFP and DAFP-T163
Figure 8-12: Impact of TESS on Nett Power Generation for Demonstrative Dataset 163

Figure 8-13: Difference in Heat Available in Cooling Water from DAFP to DAFP-T 165

Figure 8-14: TESS Level over Time Horizon of Historical Dataset for DAFP-T 165

Figure 8-15: Increase in Power Generation from DADP to DAFP 166

Figure 8-16: Summary of DAFP-T after Conclusion of Chapter 8. 170

1 BACKGROUND AND PROBLEM STATEMENT

1.1 Introduction

All metal production plants utilise a material conversion process to produce a desired product. Within the metal industry, steel production processes consume approximately 4.78% of global energy usage [1]. In addition, Gupta [1] also stated that 48% of the energy inputs are wasted in a steel plant. It is further stated by Zeelie et al. [2] that, due to increasing energy costs, the South African steel industry requires energy-saving measures to continue ensuring global market competitiveness.

Production processes, such as blast furnaces (BFs), basic oxygen furnaces (BOFs), and electric arc furnaces (EAFs), require heat to convert raw materials into workable products for downstream use. These processes also produce by-products in the form of high-temperature flue gases [3]. For example, the carbon-oxygen reaction within a BOF converter produces flue gas at temperatures ranging between 1200 ℃ and 1500 ℃ [4].

The high-temperature flue gas is typically cooled and cleaned before it is either released into the atmosphere through a flare or used in interdependent processes and plants in the vicinity, referred to as the Works. The flue gas temperature is reduced in a gas cooler, which is a component that forms part of a closed-loop cooling cycle.

To effectively control the flue gas temperature at the exit of the gas cooler, an acceptable range must first be established. The maximum temperature for the flue gas exiting the gas cooler can be based on downstream equipment requirements, such as a maximum temperature of 400 ℃ to protect the filters in the baghouse [5]. A lower temperature limit is also used to prevent acid dew point corrosion, with a specific value depending on the flue gas composition [6]. A sensible value for flue gas from fossil fuels with higher sulphur content ranges from 150 ℃ to 175 ℃ [7].

The exit temperature of the flue gas from the gas cooler depends on the heat transferred from the flue gas to the cooling water. The flue gas flow rate and temperature entering the gas cooler are process-related and can fluctuate significantly. A study by Lecompte et al. [8] used an EAF as a case study in which the available waste heat, calculated from the temperature and mass flow rate for the flue gas, ranged from 0 to 28 MW with an average of 8.8 MW.

The heat transfer from flue gas to cooling water is influenced by the temperature and mass flow of both fluids [9]. Therefore, continuously controlling the flow rate and temperature of the cooling water entering the gas cooler is critical for ensuring that the gas cooler exit temperature is acceptable.

To control the cooling-water temperature and flow rate, an allowable range is typically established, which is referred to as the temperature envelope. The temperature envelope is typically indicated

by the manufacturer and is based on the design of the gas cooler, pump flow ranges, and expected process parameters. Failure to adhere to the temperature envelope for the cooling water results in noncompliance with the gas cooler operational limits.

This thesis focuses on the closed-loop cooling water cycle and its control philosophy. The layout in Figure 1-1 shows that the cooling water is pumped to point 1, which is referred to as the gas cooler inlet. In the gas cooler, the cooling water absorbs heat from the flue gas and exits at point 2. As noted earlier, the flue gas temperature and flow rates can fluctuate significantly, and such fluctuations are observed in the cooling water temperature at point 2. The average temperature at point 2 over a discrete time interval t, $\overline{T}_2$, stays within the higher and lower temperature limits, denoted as $\overline{T}_2^H$ and $\overline{T}_2^L$, respectively.

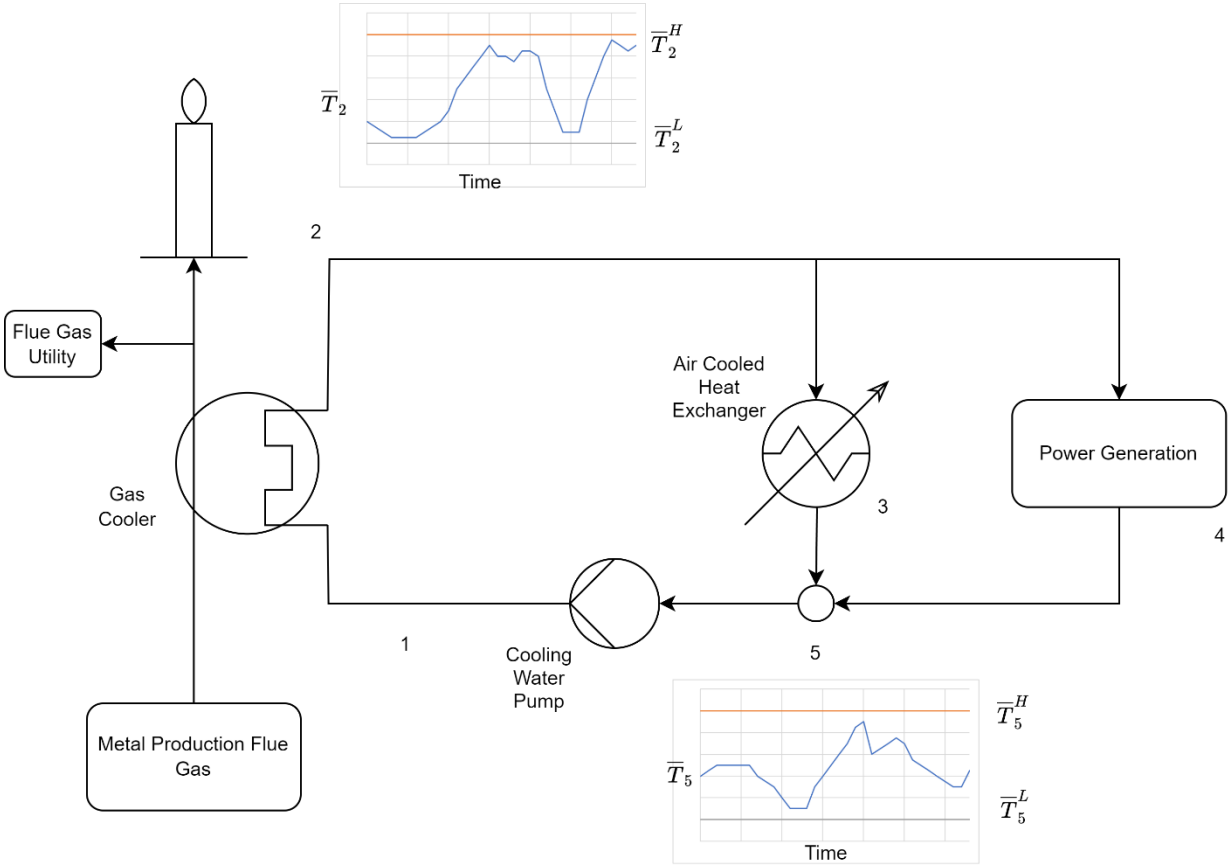


Figure 1-1: Closed Loop Cooling Cycle Layout

The cooling water moves through an air-cooled heat exchanger (ACHX) at point 3, where the ambient air moves through the tube bundles and transfers heat from the cooling water. This is the conventional method for transferring heat from the cooling water [10].

However, with the increasing need for metal producers to remain competitive, the adoption of waste heat utilisation methods is becoming increasingly prevalent within production plants. In response to this transition, production facilities are continually exploring integrated heat-rejection processes that combine conventional heat removal and waste heat utilisation techniques [11].

In this system, a power generation (PGEN) cycle is introduced parallel to the ACHX. Therefore, cooling water can also be distributed to the power generation system at point 4. The cooling water exiting both the power generation and the air-cooled heat exchanger combines at point 5 before being pumped into the gas cooler.

Using the cooling water flow rate and $\overline{T}_2$ as inputs, the control philosophy must distribute the flow rate between the air-cooled heat exchanger and power generation processes. In addition, the control philosophy must assign target temperatures, referred to as setpoints, to each process. The flow distributed to each process joins again at point 5. Therefore, the control philosophy must ensure that the flow distribution and temperature setpoint result in an average temperature $\overline{T}_5$ within the required maximum and minimum temperatures of $\overline{T}_5^H$ and $\overline{T}_5^L$, respectively.

The section of the system between points 5 and 1 contains uninsulated piping. This allows for heat transfer to the environment that will result in further reduction of the cooling water temperature and, therefore, needs to be considered when determining the values of $\overline{T}_5^H$ and $\overline{T}_5^L$. The heat transfer to the environment can be calculated based on the cooling water flow rate and temperature [9]. Accurately determining the heat transfer and maintaining the value $\overline{T}_5$ within the allowable range ensures that the gas-cooler temperature envelope is maintained.

As per the design intent, the ACHX has a significant heat transfer area exposed to the environment. Heat transfer can thus be expected at the ACHX, even with no forced draft. If the control philosophy prevents the flow from moving through the ACHX, the stagnant water inside the tube bundles will cool down due to the difference to atmospheric temperature. This will continue until sufficient time has passed, such that there is no temperature difference to the ambient air [12]. If the PGEN becomes unavailable, the ACHX will once again receive all of the flow. This results in cooling water outside the temperature envelope entering the gas cooler. The control philosophy must, therefore, ensure that ACHX is distributed a portion of the cooling water flow.

The PGEN is a Rankine-type cycle in which the heat transferred from the cooling water is used to generate electrical power [13]. The flow rate and temperature of the cooling water distributed to the Rankine cycle influence the efficiency of the power generation system. The power generated for two different flow rates can differ, even though the same amount of heat is transferred over time t [13]. The PGEN has an internal control philosophy that maximises power generation for the flow that is distributed to it by controlling the pressure and degree of superheat achieved in the evaporator [14].

Note that the PGEN can enter a tripped state, where no heat transfer or power generation can occur, due to low heat availability or external factors [15]. The PGEN would have to undergo a controlled restart procedure before it could generate power again [15]. During this phase, the

ACHX will need to transfer all the required heat to ensure that the operational temperature envelope is maintained.

The current Works philosophy is to operate PGEN and ACHX as independent processes. The flow is distributed with a fixed ratio, whereas the setpoint temperature for each process is also determined independently. This approach ensures that the temperature envelope is maintained. However, due to the fluctuating nature of the waste heat in terms of both temperature and flow rate, improvements in terms of energy recovery are possible.

1.2 Research Need

Numerous studies have investigated the control and performance maximisation of waste heat recovery Rankine cycles and air-cooled heat exchangers separately. The studies by Miao et al. [13] and Hu et al. [16] investigated the Rankine cycle performance under variable heat source conditions with a focus on maximising the power output and efficiency through control strategies that adjust internal process parameters. Similarly, van Rooyen [17] and Gao et al. [18] conducted comprehensive studies on the operational dynamics of air-cooled heat exchangers, examining their adjustability and performance under different operational conditions.

Existing literature primarily addresses these systems in isolation on an industrial plant. The closest literature to the system in this study is the use of flue gas from a boiler to generate power and provide heating to an entity [19], referred to as a combined heat and power (CHP) cycle. Thermo-economical optimisations of CHPs are well represented in the literature, such as in [20] and [21]. It is noted that comprehensive performance analysis of CHP systems under different control strategies is not well represented [19]. The study then formulates control strategies for different objectives using design conditions instead of a fluctuating heat source.

The study by Bester et al. [22] used a fluctuating heat source and several control philosophies to evaluate the influence different frameworks has on the off-design operation of PGEN and ACHX. The study stated that significant savings can be observed by only changing operational approaches when a fluctuating heat source is present. It is noted by this study that higher fidelity models are required for ACHX and PGEN to accurately simulate the system over the time horizon.

The combined control of power generation and air-cooled heat exchangers, specifically the dynamic distribution of flow between them to increase energy recovery while maintaining the operational envelope with a fluctuating heat source, remains underexplored. Filling this gap is critical, because improving the interaction between the power generation system and air-cooled heat exchanger can lead to significant improvements in the operational efficiency of CHP systems. Addressing this gap would provide valuable insights into practical solutions for enhancing energy recovery and reducing operational costs in such integrated systems.

1.3 Objective of This Study

The aim of this study is to formulate a control philosophy that dynamically adjusts the cooling water flow rate and distribution between an air-cooled heat exchanger and a power generation system to maximise energy recovery, while still adhering to all process constraints. In doing so, this study will contribute knowledge regarding practical implications for both operating philosophies and the design of more efficient energy recovery systems.

Specifically, the study focuses on three key objectives:

1. Provide a framework for dynamically distributing the flow between the PGEN and ACHX with the aim of maximising net power generation for the available heat in the cooling water.
2. Provide a framework for increasing the available heat in the cooling water by adjusting the flowrate thereof and then adjusting the flow between the PGEN and ACHX for maximum net power generation from the available heat in the flue gas.
3. Provide a framework that would make (2) applicable to a system with an integrated thermal energy storage, which is introduced with the intent of dampening the fluctuations observed in the cooling water distributed between PGEN and ACHX.

1.4 Methodology of Investigation

The method of investigating followed to reach the objectives of this study is to:

- Review the relevant literature on control methodologies and compile all relevant information on the operational limitations of ACHX and PGEN.
- Formulate a model that predicts the heat transfer rates in the ACHX based on the flow rate and temperature of the cooling water. This model must also consist of an internal control philosophy that determines the required parameters, such as the number of fans in operation as well as the required rotational speed, to achieve the desired target temperature for the cooling water.
- Formulate a model that predicts the power generation in the PGEN based on the flow rate and temperature of the cooling water. This model must also consist of an internal control philosophy where PGEN process parameters are adjusted to maximise power generation, as can be found in the literature.
- Formulate a heat loss prediction model that will provide a suitable setpoint temperature for point 5 in Figure 1-1.
- Use the current Works philosophy and a comprehensive historical dataset to evaluate current operational efficiencies and performance. The current Works philosophy must include the restart procedures of both the PGEN and ACHX after a trip occurrence, as

dictated by the manufacturer. This will ensure that the evaluated performance of the current and future philosophies is realistic and practical.

- Formulate novel control philosophies from this evaluation to improve the energy recovered until it is shown that maximum power generation has been achieved for the currently installed system.
- Algorithm formulations and processing are performed using Python 3 code and Microsoft Excel. Additional modules, such as NumPy, Pandas and CoolProp are imported to handle and process the relevant data.

1.5 Contributions of This Study

This thesis proposes three novel control philosophies. These control formulations determine suitable flow distributions and setpoint temperatures for each period to ensure that the temperature envelope of the gas cooler is maintained. The three novel control formulations are as follows:

1. A control formulation that changes the minimum setpoint flow for the ACHX to a variable flow distribution. The setpoint temperatures for each process are treated as variable parameters. While the PGEN is in normal operation mode, the control formulation determines the minimum flow to the ACHX that will sustain the operation of the PGEN and operational envelope. The flow distribution is iteratively adjusted until no improvement in power generation is observed. This control formulation thus maximises the power generation from available thermal energy available in the cooling water for each period. This control formulation can be used by any combined heat and power plant to determine the maximum power generation achievable from a fluctuating heat source while ensuring the operational envelope is maintained.
2. The second control formulation uses the variable cooling water flow distribution and setpoint temperatures from the previous formulation. It introduces a more advanced use of the gas cooler model to adjust the rate of cooling water flow throughout the system with the aim of maximising the power generation. The iterative adjustments to the flow distribution are still made until no increase in power generation is noted. This model can be used by any energy recovery plant that has or is investigating increased control on the heat supplying heat exchanger with the aim of maximising power generation.
3. The third control formulation is based on the second control formulation, with an additional component in the form of a thermal energy storage system (TESS). This model can be used by any combined heat and power generation system to model the effect on power generation performance, should investments into a TESS be made. Several options, along

with the expected investment, can be modelled with the same signature fluctuations in heat source to determine the desired option in terms of return on investment.

This study also led to the publication of one article in a peer-reviewed journal.

1. **Title of Article:** “Energy Recovery Maximisation Modelling Subject to Constrained Cooling”
   Journal: energies
   Date Published: 25 December 2023
   DOI: https://doi.org/10.3390/en17010131
   Summary: This article provides control philosophy comparisons with the Works philosophy based simplified ACHX and PGEN models to evaluate potential room for improvement. The findings in this study demonstrate the effectiveness of control philosophies that remove the independent operation of the ACHX and PGEN and rather make holistic flow distribution and setpoint temperature assignments.

A reprint of this article is provided in Appendix J.

1.6 Layout of The Thesis

Engineering principles are given in Chapter 2 along with a sufficient background to fully understand the detailed engineering process and applied control algorithms from Chapter 3 onwards. Chapter 2 also includes a literature survey relevant to control formulations for heat exchangers and energy recovery processes.

The engineering plant used to demonstrate and compare the application of the control algorithms and strategies is described in Chapter 3. The detailed description includes design parameters for the ACHX and PGEN along with relevant information on the piping and equipment where environmental heat loss will occur. Chapter 3 also provides the relevant ACHX and PGEN process models to be used in future chapters.

Chapter 4 delivers insight into the determination of the cooling water flow rate based on the flue gas exit temperature at the gas cooler. It further contains the formulation of the specific control philosophies of ACHX and PGEN, based on studied literature. The chapter also contains the model that is used to determine a suitable temperature at point 5.

The current Works’ Philosophy is given in Chapter 5. The formulation and performance of the Works’ Philosophy is preceded by reoccurring models for the ACHX and PGEN restart procedures to be followed for all control philosophies as dictated by the plant. The performance of the Works’ Philosophy is evaluated on both a demonstrative and historical dataset.

In Chapter 6, a novel control formulation is provided that improves on the Work’s philosophy by removing the independent approach of operating the two systems. A model is introduced that

determines the allowable flow rate range to the PGEN as well as a method that is used to iteratively determine the flow rate that maximises the power generation of the system. The cooling water flow rate is controlled with the same approach as with the Works' Philosophy.

Chapter 7 introduces another novel control philosophy that improves on the previous formulation by adjusting the cooling water flow rate through the gas cooler. The adjustments are made based on the expected nett power generation of the system for the allowable cooling water flow rate range. The approach also ensures that the minimum power is consumed when the PGEN is not available. The cooling water flow rate limits are determined by the operational envelopes of both the fluids in the gas cooler and can thus change from between time steps.

Chapter 8 contains the third novel control philosophy that improves on the first two with the addition of a thermal energy storage. Adjustments are made to the cooling water flow rate algorithms to manage the heat transfer to and from the thermal energy storage in order to reduce the frequency of tripped states as well as the constrained restart procedures. The previous approaches of determining the desired cooling water flow rate and distribution between the ACHX and PGEN are still used.

Finally, Chapter 9 summarises the unique contributions of this thesis along with recommendations for future studies.

CHAPTER 2 LITERATURE REVIEW

This chapter provides the background required to follow all algorithms and decision-making processes.

This includes the fundamental laws governing the working principles of all engineering equipment that form a part of the heat transfer processes under investigation.

2.1 Basic Definitions and Theory

The following section will delve into the engineering theory on the principles of heat transfer. To comprehend the working principles of equipment operation and its control philosophies in subsequent chapters, it is imperative to understand the following thermal fluid definitions.

2.1.1 Fluid

By definition, a fluid is a substance that is not bound to a fixed shape. For this study, a fluid is in one of three states: liquid, gas, or a combination of liquid and gas. The combination of liquid and gas phases in a fluid is typically referred to as a two-phase mixture [12].

2.1.2 Steady State and Transient Processes

A steady state process is in a condition where the mass and energy flow across the control volume remains constant. Therefore, the thermodynamic properties of a fluid within all discrete points of the control volume are independent of the time [23]. In a steady-state process, no accumulation of mass or energy is observed within the control volume [24].

When variations in mass or energy across the control surface are observed over time, it is commonly referred to as transient processes [23]. A transient process typically corresponds to the accumulation or reduction of mass and energy over a time period within the process [24].

2.1.3 Specific Enthalpy

Enthalpy is an important thermodynamic measure equivalent to the energy contained in a fluid, referred to as internal energy u, in combination with the potential flow energy of a fluid [25]. The potential flow energy is the product of the pressure and volume [23]. Considering these definitions per unit mass, the following formula defines specific enthalpy (energy per unit mass):

$$h = u + \frac{p}{\rho} \tag{2.1}$$

2.1.4 Specific Heat Capacity

The fundamental definition of c_p is as follows:

$$c_p = \left(\frac{\partial h}{\partial T}\right)_p \tag{2.2}$$

Thus, the value of c_p is a measure of the capacity of the fluid to absorb energy during a constant-pressure process. This energy absorption typically occurs in the form of heat. It is also implied that if a fluid has a higher heat capacity than another fluid, it is able to absorb a larger quantity of energy while only undergoing the same change in temperature [24].

2.1.5 Conservation laws

Three conservation laws are critical to any thermo-fluid modelling process. These laws are based on the conservation of mass, momentum, and energy.

2.1.5.1 Conservation of Mass

The following equation holds for mass conservation [24].

$$V\frac{\partial \rho}{\partial t} + \dot{m}_e - \dot{m}_i = 0 \tag{2.3}$$

where $\dot{m}$ is the mass flow rate of the fluid in the control volume with subscripts "e" and "i" referring to the outlet and inlet, respectively. With steady state flows, it follows that $\frac{\partial \rho}{\partial t} = 0$, thus, the equation in reduces to:

$$\dot{m}_e - \dot{m}_i = 0 \tag{2.4}$$

From the equation above, it is implied that the mass flow entering and exiting the control volume is equal under steady state conditions and thus $\dot{m} = \dot{m}_i = \dot{m}_e$. The mass flow rate can be calculated by:

$$\dot{m} = \rho V A \tag{2.5}$$

where A is the flow area normal to the direction of fluid motion and V is the flow velocity. Thus, the formula for A is dependent on the cross-sectional geometry of the profile of the carrying components.

2.1.5.2 Conservation of Momentum

The following equation is valid for incompressible flows [24].

$$\rho L\frac{\partial V}{\partial t} + (p_{0e} - p_{oi}) + \rho g(z_e - z_i) + \Delta p_{0L} = 0 \tag{2.6}$$

The following equation is valid for compressible flow [24]:

$$\rho L\frac{\partial V}{\partial t}+\frac{p}{p_0}(p_{0e}-p_{oi})+\frac{\rho V^2}{2}\frac{1}{T_0}(T_{0e}-T_{0i})+\ \rho g(z_e-z_i)+\ \Delta p_{0L}=0 \tag{2.7}$$

where L (displacement) and z (displacement) are the length and elevation height of the control, respectively, and g (displacement per time squared) is the gravitational acceleration. The pressure drop across the control volume is given by Δp_{0L} (force per area). If steady state is valid, $\frac{\partial V}{\partial t}=0$ and the following two equations are valid for incompressible and compressible flow respectively:

$$p_{0e}-p_{0i}+\rho g(z_e-z_i)+\ \Delta p_{0L}=0 \tag{2.8}$$

$$\frac{p}{p_0}(p_{0e}-p_{oi})+\frac{\rho V^2}{2}\frac{1}{T_0}(T_{0e}-T_{0i})+\ \rho g(z_e-z_i)+\ \Delta p_{0L}=0 \tag{2.9}$$

2.1.5.3 Conservation of Energy

The following equation holds for energy conservation [24].

$$\dot{Q}+\dot{W}=V\frac{\partial(\rho h_0-p)}{\partial t}+\ \dot{m}_e h_{0e}-\ \dot{m}_i h_{0i}+\ \dot{m}_e g z_e-\ \dot{m}_i g z_i \tag{2.10}$$

where $\dot{Q}$ and $\dot{W}$ (energy per time) are the total rates of heat transfer and work done on the fluid, respectively. Under steady state conditions, $\frac{\partial(\rho h_0-p)}{\partial t}=0$, the equation above is reduced to:

$$\dot{Q}+\dot{W}=\dot{m}_e h_{0e}-\ \dot{m}_i h_{0i}+\ \dot{m}_e g z_e-\ \dot{m}_i g z_i \tag{2.11}$$

Under steady state conditions where $\dot{m}=\dot{m}_i=\dot{m}_e$ holds and the change in elevation is negligible, the conservation of energy reduces further:

$$\dot{Q}+\dot{W}=\dot{m}(h_{0e}-\ h_{0i}) \tag{2.12}$$

The above equation states that the change in specific enthalpy within the fluid can be calculated by the combination of the rate of work done on the fluid with the rate of heat added.

These are the fundamental thermal-fluid properties; basic definitions relating to engineering equipment are presented in the next section.

2.1.6 Measurable Energy Transfer

The conservation of energy law, under the assumption of steady-state conditions and no significant elevation change, is reduced to (2.12). Using the definition of specific enthalpy (2.1), $h=u+p\upsilon$, (2.12) can be expressed as:

$$\dot{Q}+\dot{W}=\dot{m}((u_e+p_e v_e)-(u_i+p_i v_i)) \tag{2.13}$$

where u and v are the specific internal energy and the specific volume of the fluid, respectively. The pressure is denoted as p. The subscripts "e" and "i" refer to the fluid conditions when exiting and entering the control volume, respectively.

Assuming a constant specific heat at constant volume across the control volume, the change in specific internal energy can be expressed as [9]:

$$u_e - u_i = c_v(T_e - T_i) \tag{2.14}$$

If the work done on the fluid is negligible, equation (2.13) is reduced to:

$$\dot{Q} = \dot{m}c_p(T_e - T_i) \tag{2.15}$$

As stated by Incropera et al. [9], there are four cases in which equation (2.15) holds. Two are relevant to this study, with the first being an ideal gas with negligible kinetic and potential energy changes, and no work other than flow work is applicable. The second case is an incompressible liquid with negligible kinetic and potential energy changes and negligible work, including flow work.

2.1.7 Heat Transfer Mechanisms

There are three processes in which heat is transferred. These processes are conduction, convection and radiation. These processes also have specific rate equations that can be used to determine the heat transferred per unit of time.

2.1.7.1 Conduction

The transfer of energy from high energy particles to low energy particles due to the interaction of particles within a substance, is known as conduction [9]. The rate equation for conduction is known as Fourier's law. For a 1D plane wall with a temperature distribution of $T(x)$, the rate equation can be expressed as:

$$q_x'' = -k\frac{dT}{dx} \tag{2.16}$$

where q_x'' is the heat flux (energy rate per unit area) and k is the wall material property known as thermal conductivity (energy rate per unit length and temperature). The negative sign is indicative of the heat being transferred in the direction of decreasing temperature. Assuming steady-state conditions, the temperature distribution is expected to be linear. Thus, the temperature gradient, $\frac{dT}{dx}$, can be expressed as $\frac{dT}{dx} = \frac{\Delta T}{L}$. The rate equation in (2.16) then changes to:

$$q_x'' = -k\frac{\Delta T}{L} \tag{2.17}$$

The heat rate by conduction, $\dot{Q}_x$, is the product of the heat flux in equation (2.17) and the area of heat transfer [9]:

$$\dot{Q}_x = -kA\frac{\Delta T}{L} \tag{2.18}$$

2.1.7.2 Convection

Convective heat transfer comprises of two mechanisms: the diffusion and bulk motion of the fluid [9]. A fluid-surface interaction typically leads to the development of a velocity boundary layer, which is a region where the velocity varies from zero at the surface to a value, u_∞, associated with the flow.

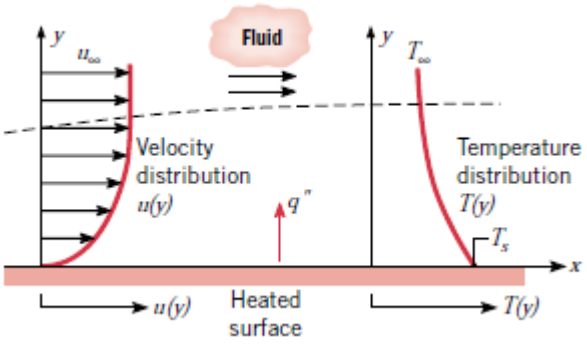


Figure 2-1: Boundary Layer Development in Convective Heat Transfer, as in [8]

If there is a difference between surface and fluid temperatures, there will also be a region within the fluid where the temperature varies from T_s at the surface and T_∞ in the outer flow. This region, the thermal boundary layer, can differ in size from the velocity boundary layer. Heat is always transferred from a higher-to a lower-temperature entity [9].

Within these boundary layers, the two mechanisms of convective heat transfer have varying effects on the overall heat transfer. The diffusion mechanism is dominant near the surface where the fluid velocity is low. At the surface, where the velocity boundary layer theory indicates a velocity of zero, heat is transferred only through diffusion [9]. As the velocity increases, so too does the contribution of bulk fluid motion to the heat transfer process.

Convection can be classified according to the nature of flow. When flow is caused by external means, such as a pump or fan, the resulting convection is referred to as forced convection. In contrast, for natural convection, the fluid motion originates from buoyancy forces generated by localised differences in density due to temperature variations [9].

The appropriate rate equation of convective heat transfer is, regardless of the type of convection, of the form:

$$q'' = h\Delta T \tag{2.19}$$

where q'', as in the previous sections, refers to the convective heat flux and h refers to the convective heat transfer coefficient (energy rate per area and temperature). The value of the convective heat transfer coefficient is dependent on the surface geometry, nature of the fluid motion, and various other thermodynamic and transport parameters. From the rate equation, it can be stated that the heat flux is proportional to the difference in temperatures [9].

To determine the convective heat transfer rate ($\dot{Q}$) the product of heat flux in (2.24) and the known area of heat transfer (A) is calculated [9]:

$$\dot{Q} = hA\Delta T \tag{2.20}$$

To determine the convective heat transfer coefficient, information regarding the flow and heat transfer surface is required [12].

2.1.7.2.1 Forced Convection

As mentioned above, forced convection is induced by external means such as a fan or pump. To determine the convective heat transfer in a forced convection scenario, several fluid and geometrical parameters are required [12].

The first step in forced convection calculations is to determine the Reynolds number of the flow, which is a dimensionless number that represents the ratio of inertial forces to viscous forces [12]. The Reynolds number can thus be determined through $Re = \frac{(\rho \cdot V \cdot L_c)}{\mu}$ where L_c is the characteristic length of the heat transfer surface. For a cylindrical pipe, this will be the diameter of the heat transfer surface [12].

The second step is to determine the Prandtl number for the fluid, a dimensionless number describes the ratio of momentum and thermal diffusivity in the fluid [12]. The Prandtl number is based on thermophysical properties of the fluid at the film temperature, T_f, where $T_f = \frac{T_s + T_\infty}{2}$. The Prandtl number can be determined through $Pr = \frac{c_p \cdot \mu}{k}$ where μ is the dynamic viscosity of the fluid [12].

The final step is to determine the Nusselt number, a dimensionless number that represents the ratio of convective to conductive heat transfer [12]. Laminar flow has a constant Nusselt number correlation whereas turbulent flow has several formulations in literature [12]. However, the Dittus-Boelter formulation is the preferred formulation [12].

The Dittus-Boelter formulation for turbulent flow is shown below:

$$\mathrm{Nu} = \frac{\mathrm{hL_c}}{\mathrm{k}} = 0.023 \cdot \mathrm{Re}^{0.8} \cdot \mathrm{Pr}^{\mathrm{n}} \tag{2.21}$$

Where $\mathrm{n} = 0.4$ is used heating of the fluid and $\mathrm{n} = 0.3$ for cooling. The equation in (2.21) can be rearranged to determine the convective heat transfer coefficient, h.

2.1.7.2.2 Natural Convection

To determine the convective heat transfer coefficient where natural convection is present, the Grashof number first need to be determined. The Grashof number is a dimensionless number that represents the ratio of buoyancy forces to viscous forces in a fluid [12]. It can be determined through:

$$\mathrm{Gr} = \frac{\mathrm{g} \cdot \beta \cdot (\mathrm{T_s} - \mathrm{T_\infty}) \cdot \mathrm{L_c^3}}{\nu^2} \tag{2.22}$$

Where $\beta\,[\mathrm{K^{-1}}]$ is the thermal expansion coefficient of the fluid at the film temperature $\mathrm{T_f}$. The characteristic length ($\mathrm{L_c\ m}$) is dependent on the geometry of the surface where the heat transfer occurs. The kinematic viscosity (ν) of the fluid is determined from known properties of the fluid at the film temperature.

With the Grashof number now known, the Rayleigh number can be determined. The Rayleigh number is a dimensionless number that represents the combined effects of buoyancy and thermal diffusion in a fluid [12]. The Rayleigh number can be determined through:

$$\mathrm{Ra} = \mathrm{Gr} \cdot \mathrm{Pr} \tag{2.23}$$

Use of the Rayleigh number to determine the convective heat transfer coefficient is done so through empirical correlations that is dependent on the geometry of the surface, as summarised in [12].

To determine the Nusselt number from the Rayleigh number on the surface of horizontal cylinder, the following equation can be used:

$$\mathrm{Nu} = \frac{\mathrm{h} \cdot \mathrm{L_c}}{\mathrm{k}} = \left\{ 0.6 + \frac{0.387 \cdot \mathrm{Ra_L^{\frac{1}{6}}}}{\left[1 + \left(\frac{0.559}{\mathrm{Pr}}\right)^{\frac{9}{16}}\right]^{\frac{8}{27}}} \right\}^2 \tag{2.24}$$

The equation above is valid for $\mathrm{Ra} \leq 10^{12}$.

The equation above can now be rearranged to determine the convective heat transfer coefficient for natural convection.

2.1.7.3 Radiation

Radiation refers to the energy emitted by matter that are at non-zero temperatures. In general, radiation is focused on solid surfaces; however, liquids and gases at non-zero temperatures also emit radiation [9]. The energy is transported by electromagnetic waves; therefore, while conductive and convective heat transfer requires a medium, radiation does not.

Consider a surface with a temperature of T_s. The rate of energy radiation per unit area, termed emissive power (E_b) is determined through the following expression:

$$E_b = \sigma T_s^4 \tag{2.25}$$

Note that the surface temperature T_s in equation (2.25) is in kelvin. The Stefan-Boltzmann constant (σ) has a value of $5.67 \times 10^{-8} \frac{W}{m^2 \cdot K^4}$. The emission from the expression in equation (2.25) is that of an ideal radiator, commonly referred to as a blackbody. The heat flux from an actual surface will be less under the same surface temperature and is defined by:

$$E = \varepsilon \sigma T_s^4 \tag{2.26}$$

The emissivity (ε) of a given surface is a measure of how efficiently the surface emits energy relative to an ideal radiator. Therefore, the value of emissivity is always between zero and one and is dependent on both the surface finish and material [9].

Radiation refers to the amount of energy emitted. Radiation may also be emitted to a surface and is referred to as irradiation. Part or all the radiation may be absorbed by the surface, thus increasing the thermal energy of the material. In the case of a small surface at temperature T_s that is surrounded by an isothermal surface at temperature T_{sur}, it can be derived that the irradiation (G) can be approximated by the emission of a blackbody, in which case $G = \sigma T_{sur}^4$. Assuming that it is a grey surface, where a surface has the same efficiency for absorption and emission, the radiative heat flux can be expressed as [9]:

$$q''_{rad} = \varepsilon \sigma (T_s^4 - T_{sur}^4) \tag{2.27}$$

To determine the rate of heat transfer through radiation $\dot{Q}_{rad}$, the product of the radiative heat flux (q''_{rad}) and the surface area A is calculated:

$$\dot{Q}_{rad} = \varepsilon \sigma A (T_s^4 - T_{sur}^4) \tag{2.28}$$

2.1.8 Thermal Resistance

From the rate equations in the previous section, for heat transfer with no internal energy generation and steady-state properties, an analogy can be illustrated. This is the analogy between the diffusion of heat and electrical charge. Upon defining resistance as the ratio of potential to transfer rate, which in electrical terms is $R = \frac{V}{I}$, it follows that thermal resistance for conductive, convective and radiative heat transfer is [9]:

$$R_{cond} = \frac{\Delta T}{\dot{Q}_x} = \frac{L}{kA} \tag{2.29}$$

$$R_{conv} = \frac{\Delta T}{\dot{Q}} = \frac{1}{hA} \tag{2.30}$$

$$R_{rad} = \frac{T_s - T_{sur}}{\dot{Q}_{rad}} = \frac{1}{A \cdot \varepsilon\sigma(T_s + T_{sur})(T_s^2 + T_{sur}^2)} = \frac{1}{A \cdot \varepsilon\sigma h_r} \tag{2.31}$$

These thermal resistances can in turn be used to create equivalent thermal circuits for more complex systems such as composite walls.

When the composite wall in Figure 2-2 is considered, the one-dimensional heat transfer rate can be expressed as:

$$\dot{Q}_x = \frac{T_{\infty,1} - T_{\infty,4}}{\sum R_t} \tag{2.32}$$

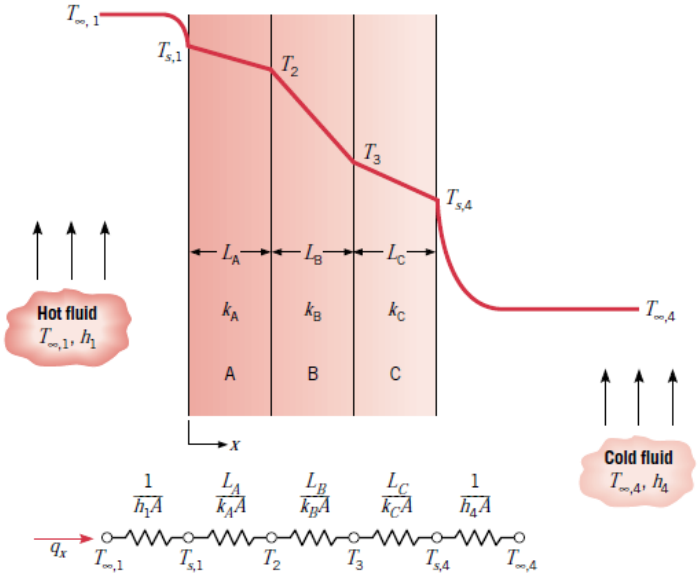


Figure 2-2: Heat Transfer Across Composite Wall as in [3]

In (2.32), $T_{\infty,1} - T_{\infty,4}$ is the temperature difference between the two fluids and $\sum R_t$ is a summation of all the relevant thermal resistances. Under steady-state conditions, the heat-transfer rate will

remain the same for each element. This leads to an alternative form of equation (2.32), where the driving potential is individually adjusted for each element [9]:

$$\dot{Q}_x = \frac{T_{\infty,1} - T_{s,1}}{\left(\frac{1}{h_1 A}\right)} = \frac{T_{s,1} - T_{s,2}}{\frac{L_A}{k_A A}} = \ \ldots \tag{2.33}$$

2.1.9 Overall heat transfer coefficient

An overall heat transfer coefficient, U, can be defined with:

$$\dot{Q} = UA\Delta T \tag{2.34}$$

Comparing (2.38) and (2.36), it is clear that the overall heat transfer coefficient is related to the total thermal resistance in the form of $UA = \frac{1}{\sum R_t}$ [9]. The following general expression can be stated:

$$R_{tot} = \sum R_t = \frac{\Delta T}{\dot{Q}} = \frac{1}{UA} \tag{2.35}$$

By assuming that surfaces are treated as isothermal or adiabatic based on their relation to the x-direction, a composite wall problem can be described with various series-parallel thermal resistance combinations [9]. Therefore, it is necessary to fully understand the analogy of thermal resistances to ensure their relevance to the heat transfer being modelled.

2.2 Systems and Devices Theory

The following section provides a brief overview of the typical components of the heat rejection process. This background is required to comprehend the rationale for several decisions made within the control philosophies and formulations in the chapters that follow.

2.2.1 Heat Rejection Process of the Metal Production Plant

Production processes, such as blast furnaces (BFs), basic oxygen furnaces (BOFs), and electric arc furnaces (EAFs), require heat to convert raw materials into workable products for downstream use. These processes also produce by-products in the form of high-temperature flue gases [3]. For example, the carbon-oxygen reaction within a BOF converter produces flue gas at temperatures ranging between 1200 ℃ and 1500 ℃ [4].

The high-temperature flue gas is typically cooled and cleaned before it is either released into the atmosphere through a flare or used in other processes on the Works. The flue gas temperature is reduced in a gas cooler, which is a component that forms part of a closed-loop cooling cycle and uses cooling water to transfer the heat from the flue gas. The heat transferred from the flue gas is controlled by adjusting the cooling water temperature and flow rate through the gas cooler.

The layout in Figure 1-1 shows that the cooling water is pumped to point 1, which is referred to as the gas cooler inlet. In the gas cooler, the cooling water transfers heat from the flue gas and exits at point 2. As noted earlier, the flue gas temperature and flow rates can fluctuate significantly, and such fluctuations are observed in the cooling water temperature at point 2. Note that the average temperature at point 2 for time t, $\overline{T}_2$, stays within the higher and lower temperature limits, denoted as $\overline{T}_2^H$ and $\overline{T}_2^L$, respectively.

The cooling water moves through an air-cooled heat exchanger at point 3, where the ambient air moves through the tube bundles and transfers heat from the cooling water. This is the conventional method for transferring heat from the cooling water [10].

However, with the increasing need for metal producers to remain competitive, the adoption of waste heat utilisation methods is becoming increasingly prevalent within production plants. In response to this transition, production facilities are continually exploring integrated heat-rejection processes that combine conventional heat removal and waste heat utilisation techniques [11].

In this system, a power generation cycle is introduced parallel to the air-cooled heat exchanger. Therefore, cooling water can also be distributed to the power generation system at point 4. The cooling water exiting both the power generation and air-cooled heat exchanger combines at point 5 before being pumped into the gas cooler.

To model the influence of control philosophies on this heat rejection system, each component needs to be represented with a model. This model needs to be formulated to react and perform as the current component. The components that need to be represented are the gas cooler, circulation pumps, the air-cooled heat exchanger (including the fans), the energy recovery process (including the turbine, pump and heat exchangers).

The rest of this section will provide the necessary theory and background for these components.

2.2.2 Gas Cooler

As mentioned in the previous section, the gas cooler is the heat exchanger that transfer thermal energy from the high temperature flue gas to the cooling water. It can thus be regarded as the heat source of the system.

To effectively control the flue gas temperature at the exit of the gas cooler, an acceptable range must first be established. The maximum temperature for the flue gas exiting the gas cooler can be based on downstream equipment requirements, such as a maximum temperature of 400 ℃ to protect the filters in the baghouse [5]. A lower temperature limit is also used to prevent acid dew point corrosion, with a specific value depending on the flue gas composition [6]. A sensible value for flue gas from fossil fuels with higher sulphur content ranges from 150 ℃ to 175 ℃ [7].

The heat transfer from flue gas to cooling water is influenced by the temperature and mass flow of both fluids [9]. Therefore, controlling the flow rate and temperature of the cooling water entering the gas cooler is critical to ensure that the gas cooler exit temperature is acceptable.

The flue gas flow rate and temperature entering the gas cooler are process-related and can, therefore, fluctuate significantly. A study by [8] used an EAF as a case study in which the available waste heat, calculated from the temperature and mass flow rate for the flue gas, ranged from 0 to 28 MW with an average of 8.8 MW.

2.2.3 Heat Exchangers

The process of thermal energy transfer between fluids at different temperatures separated by a wall is implemented by a device called a heat exchanger [9]. Equation (2.13) can be used to calculate the heat transfer rate to or from a fluid in the control volume. Since no work is done on the fluid in a heat exchanger, $\dot{W} = 0$, (2.16) is reduced to:

$$\dot{Q} = \dot{m}(h_{0e} - h_{0i}) \tag{2.36}$$

From (2.36) and the convective heat transfer section in 2.1.7, it follows that the rate of flow of a fluid influences the rate of heat transfer.

The equations in (2.13) and (2.36) quantifies the heat transferred to a fluid through means of fluid parameters and measurements. However, it does not define how the heat transfer rate is dictated by geometry or flow rates.

A concentric tube type heat exchanger with internal diameter D_i, external diameter D_o and length L is illustrated in Figure 2-3. The tube has no external or internal fins. The internal and external surfaces of the tube is the heat transfer areas. The heat transfer area is defined as $A = \pi DL$ with the appropriate diameter being used with calculating the internal and external area.

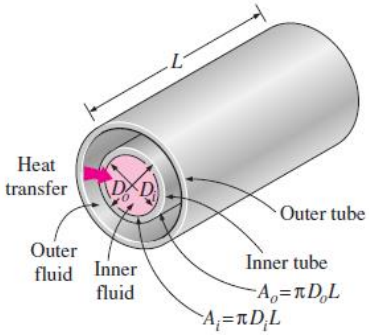


Figure 2-3: Concentric Tube Heat Exchanger, as in [2]

From this geometrical setup, it is clear that two fluids are separated by a wall with a thermal conductivity of k. Heat will first be transferred from the hot fluid to the wall through convection, through the wall with conduction and lastly to the cold fluid through means of convection [26].

Heat exchanger performance typically decreases over time as a result of fouling. Fouling is the accumulation of deposits on a heat transfer surface [26]. The increasing layer of deposits increases the resistance to heat transfer and thus needs to form part of the thermal resistance circuit. The value of the thermal resistance for fouling, is defined as:

$$R_{foul} = \frac{R_f}{A} \tag{2.37}$$

Where A is the applicable heat transfer area where fouling is present. The parameter R_f is referred to as the fouling factor and is dependent on various parameters, such as the fluid, temperature and velocities. Higher temperatures and lower velocities typically accelerate fouling [26]. There are also various forms of fouling, which include precipitation of solids, corrosion, chemical fouling, and biological fouling. Each form has unique mechanisms that accelerate or slows the rate of fouling.

For the heat transfer process in the heat exchanger illustrated in Figure 2-3, the thermal resistance circuit can now be completed, as shown in Figure 2-4. Note that the area A can differ for each resistance since A refers to the specific surface area where the resistance is relevant.

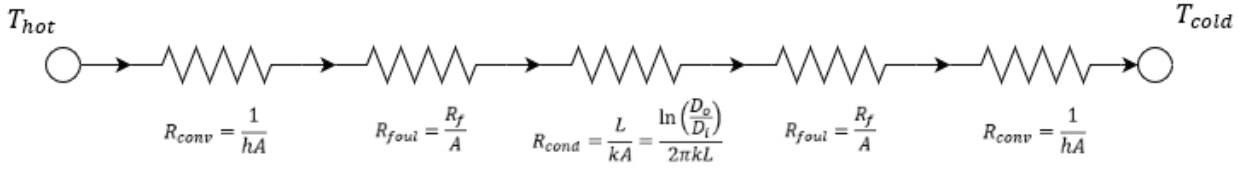


Figure 2-4: Thermal Resistance Circuit for Concentric Tube Heat Exchanger with Fouling

For the purpose of illustration, consider that the hot fluid is flowing in the annular region, and the cold fluid is within the tube. From (2.35), the overall heat transfer can be defined as:

$$\frac{1}{UA} = R_{tot} = \frac{1}{h_o A_o} + \frac{R_{f,o}}{A_o} + \frac{\ln\left(\frac{D_o}{D_i}\right)}{2\pi kL} + \frac{R_{f,i}}{A_i} + \frac{1}{h_i A_i} \tag{2.38}$$

Where the subscripts "i" and "o" refer to the parameters on the internal and external heat transfer surfaces respectively.

From (2.38) it is clear that an increase in the area of heat transfer will lead to a lower thermal resistance and thus an increased overall heat transfer coefficient. It is for this reason that extended surfaces are often incorporated into heat exchangers, typically in the form of fins. It can also be reasoned that the extended surface is applied to the fluid with a significantly lower

convection coefficient to prevent a high thermal resistance. However, the application of fins also has an efficiency, η_{fin}, that is based on the temperature distribution along the fin with isothermal fins being ideal. Short, high thermal conductivity fins can be deemed isothermal and thus $n_{fin} = 1$. The introduction of fins and fin efficiency will thus change the thermal resistance to convective heat transfer to:

$$R_{conv} = \frac{1}{h\eta_{fin}A_{tot}} \tag{2.39}$$

Where A_{tot} is the total heat transfer area, which is a summation of the area of the fins and the unfinned but exposed area of the tube. However, since the heat exchanger currently in question does not have finned areas, the thermal resistance to convective heat transfer will not need to be modified from its current state in (2.41).

The rate of heat transfer within the heat exchanger can be determined through [26]:

$$\dot{Q} = UA\Delta T_m \tag{2.40}$$

Where $\dot{Q}$ refers to rate of heat transfer within the heat exchanger and ΔT_m is defined as an appropriate average temperature between the two fluids [26]. Within this equation, the surface area A is constant, whilst the parameters of U and ΔT_m typically vary.

The overall heat transfer coefficient is typically used within an applicable method, such as the $\varepsilon - NTU$ and/or $LMTD$ methods to determine the rating or sizing requirements of a heat exchanger. Within the design process, where desirable temperatures and flows are known, these methods can be used to determine geometrical parameters. If a heat exchanger geometry has already been determined, these methods can be used to calculate heat transfer capabilities and thus suitability to the process requirement.

There are various types of heat exchangers. Two options can be identified for the heat-rejection process demonstrated in this study. The first is the use of air-cooled heat exchangers. In this type of heat exchanger, ambient air is forced through a tube bundle carrying high-temperature cooling fluid. Since the environment is used to lower the temperature of the cooling fluid, excess heat is removed from the control volume of the process. The second option is to use a heat exchanger to transfer excess heat from the cooling fluid to another fluid for further repurposing in other processes. In this type, the heat is not removed from the control volume and can still be utilised.

Since the highest priority is to ensure that the cooling fluid temperature reaches the setpoint, the heat exchangers that transfer heat to the environment must be sized to suitable dimensions to ensure that sufficient heat transfer can be achieved for the entire waste heat profile.

The forced draft of the air is generated by a pressuriser and uses electrical energy to remove heat from the system. Therefore, an air-cooled heat exchanger can be used to meet the basic requirements of cooling, even though it will negatively impact the cost of operation of the plant. Ideally, excess heat should be used to increase process efficiency and thus reduce the cost inputs of a production process.

2.2.4 Pumps and Fans

In this thesis, a mechanical device used to increase the dynamic pressure of a liquid or gas is referred to as either a fan or a pump. Typically pumps for liquid fluids, and fans for gaseous fluids. A pump or fan uses mechanical work to increase the flow pressure. According to [27], flow of air can be assumed incompressible for velocities up to 50 m/s and 1.2 kPa. The work required by both the pump and fans in this study can be thus calculated through (2.13), where $\Delta z = 0$ and $\dot{Q} = 0$ it results in [26]:

$$\dot{W}_p = \dot{m}(h_{0e} - h_{0i}) = \frac{\dot{m}\Delta P}{\rho} \tag{2.41}$$

where $\dot{W}_p$ is the work required at the shaft of the pressuriser, $\dot{m}$ and ρ is the mass flow and density of the fluid. The difference between the pressures of the fluid entering and exiting the pressuriser is denoted by ΔP.

An efficiency term, η, can be assigned to the mechanical and electrical losses to calculate the required work, $\dot{W}_e$:

$$\dot{W}_e = \frac{\dot{W}_p}{\eta} = \frac{\dot{m}\Delta P}{\rho\eta} \tag{2.42}$$

As stated in 2.2.2, the flow rate of the fluid has a clear influence on the rate of heat transfer achieved in a heat exchanger. Furthermore, it is mentioned that 0 that a fluctuating heat transfer requirement is expected for the cooling process in a metal production plant.

This section first demonstrates the common method of adjusting the flow rate of a fluid and the resulting heat transfer in a heat exchanger, followed by constraints for the operation of the turbine within the Rankine cycle.

Both the heat transfer processes used in the heat rejection process use pressurisers to control the heat transfer rates. Therefore, the heat rejection process requires electrical power to operate these pressurisers. Even though this demand will be offset by power generation in the Rankine cycle, minimising the power demand will have a positive impact on the efficiency of the system. Since the heat rejection process is operated continuously while the plant is in production, any increase in efficiency will become significant over time.

It is known that the dimensionless characteristics are constant for similar pressurisers [28]. The dimensionless characteristics consist of dimensionless flow (C_Q), head (C_H) and power (C_P). The dimensionless characteristics can be described by the following equations:

$$C_Q = \frac{Q}{N \cdot D^3} \tag{2.43a}$$

$$C_H = \frac{gH}{N^2 \cdot D^2} \tag{2.43b}$$

$$C_P = \frac{P}{\rho \cdot N^3 \cdot D^5} \tag{2.43c}$$

where Q is the flow in $\frac{m^3}{s}$, H is the head and D is impeller diameter both in m, power is denoted by P and is measured in watts (W) and the rotational speed, N, is measured in revolutions per minute (rpm). The density of the fluid is also represented by ρ ($\frac{kg}{m^3}$) with the acceleration of gravity, g, in $\frac{m}{s^2}$.

The affinity laws use the above equations to describe the behaviour of a pressuriser in terms of flow, head, and power when the speed or diameter is adjusted [28]. Since the cooling process in this study uses changes in speed to adjust the heat transfer, the affinity laws can be derived and presented in terms of rotational speed.

$$\frac{Q_1}{Q_2} = \frac{N_1}{N_2} \tag{2.44a}$$

$$\frac{H_1}{H_2} = \left(\frac{N_1}{N_2}\right)^2 \tag{2.44b}$$

$$\frac{P_1}{P_2} = \left(\frac{N_1}{N_2}\right)^3 \tag{2.44c}$$

Note that the equations in 2.44 assume that the pump maintains the same efficiency at different speeds [28]. It is implied that the error in behaviour prediction is relatively low when the difference in efficiency between the two speeds is also low. It is advised by [28] to use a model that estimates the change in efficiency to further enhance the accuracy of the affinity laws and the predicted operational cost savings.

The equations in 2.41 indicates that a change in flow is linear, while the power required is a cubic function of the speed ratio. Therefore, the flow rate adjustment ratio ($\frac{Q_1}{Q_2}$) can be cubed to obtain the required power adjustment ratio ($\frac{P_1}{P_2}$).

It also follows that there is potential for significant power savings by reducing the flow rate induced by a pressuriser to only the required value for sufficient heat transfer.

A device that regulates the speed and force of the rotational equipment is known as a variable speed drive [29], which is referred to as a VSD. It is also stated by [29] that the application of a VSD is the most effective energy-saving equipment for mechanical machines because the majority of electrical motors only operate at 100% speeds for short periods of time.

However, the term VSD is still broad and contains several subgroups. Mechanical VSDs include methods such as gearboxes and belt drives. These methods are known for their simplicity and low application cost. Electrical VSDs regulate power flow from the electrical supply to the motor [29].

With the use of a VSD to control the flow rate of a fluid, it is expected that the pressuriser and accompanying VSD selection will ensure a suitable operational range in which it will be controlled. However, [30] noted that the efficiency of electrical motors tends to decrease significantly below 50% speed. It follows that electrical motors with VSDs typically operate only at speeds greater than 50% of their normal operating speed.

2.2.5 Energy Recovery Process – Power Generation

Rankine and Brayton cycles are well-known processes that use energy to generate electrical power. The principle upon which these cycles generate power is to increase the fluid pressure and increase its temperature, after which energy is extracted when the fluid is expanded over a turbine. After expansion, the fluid is cooled. The main difference is that a Brayton cycle uses only fluid in a gaseous state, whereas the Rankine cycle's fluid has a vapour, two-phase, and liquid phase. The choice of the working fluid in both cycles typically depend on the heat source parameters, such as the temperature and flow rate.

The Rankine-based power generation cycle used within the heat rejection system is illustrated in Figure 2-5. Block 1 refers to the area in which heat is transferred from the high-temperature cooling liquid to the working fluid of the Rankine cycle process, which is contained in block 2.

Block 2 consists of a high-pressure working fluid in liquid form entering the preheater and moving thereafter to the superheater, where a phase change is expected. The high-pressure working fluid, which is now in the vapour phase, is expanded over a turbine connected to an electrical generator. At low pressures, there is still some usable thermal energy within the working fluid, which is expected to be in a two-phase state. This thermal energy is transferred to the recuperator before entering the condenser, where the working fluid is cooled to below saturation, thus changing to its liquid state. The working fluid in liquid form is pumped to a higher pressure, completing the cycle.

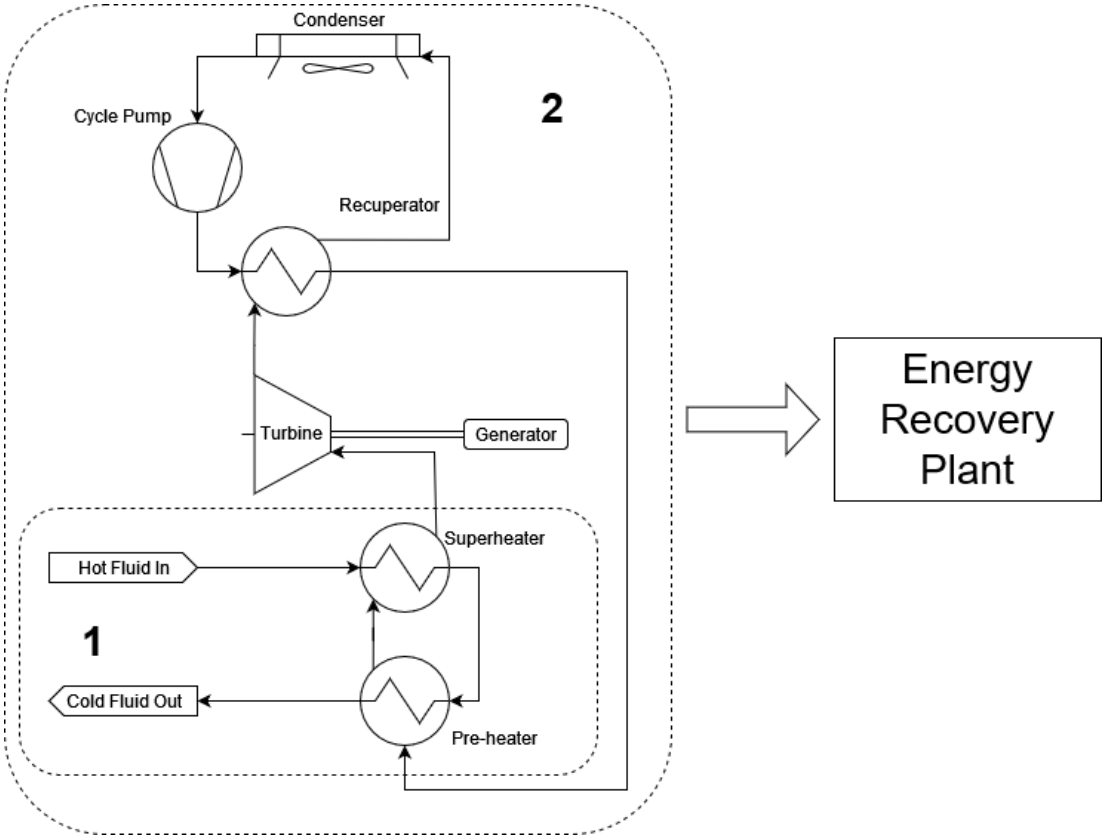


Figure 2-5: Rankine Cycle for Power Generation from Waste Heat Recovered

When it comes to power generation, an important parameter for continuous evaluation and improvement is efficiency. Efficiency is the conversion ratio of energy input to output. Therefore, the expected efficiency range significantly influences the procurement and control of energy recovery plants.

The Rankine cycle has considerably more mechanical and electrical equipment than air-cooled heat exchangers. This introduces the risk of an unplanned stoppage. An unplanned stoppage refers to any event that halts the power generation process, which cannot be predicted accurately.

What happens in a closed-loop heat-rejection cycle if all waste heat is assigned to a specific heat-transfer process that suddenly becomes unavailable when the plant is in production? Since minimal heat is rejected without stopping the flow of the cooling fluid, the temperature is expected to increase over time until it either moves out of the design envelope, or sufficient heat transfer is restored.

2.2.5.1 Turbines

A turbine is rotating equipment that extracts energy from a fluid. A fluid with high potential energy flows and expands over the blades connected to a rotor. This expansion is due to a drop in both the temperature and pressure because of energy transfer. The transferred energy is used to rotate

the rotor. Coupling the turbine to a generator result in the conversion of rotational energy into electrical power [25].

The conservation of energy in 2.13 can again be used to calculate the energy converted. No heat is added to the turbine, $\dot{Q} = 0$ and the difference in elevation over the control volume is assumed to be negligible, then:

$$\dot{W}_T = \dot{m}(h_{0e} - h_{0i}) \tag{2.44}$$

2.2.5.2 Turbine Trips and Controlled Startup

The turbine is designed to have a specified operational range, consisting of a minimum and maximum allowable flow threshold. A turbine may never be subjected to a flow below its minimum allowable limit, as such a scenario could result in detrimental vibrations and potentially cause significant damage to the turbine and associated components.

If the distributed flow associated with the power generation process falls below the specified limit, protective measures are initiated by closing the inlet valves to halt the incoming flow. This procedure, termed trip, is discussed in further detail in this thesis.

Additional protection measures are typically in place to ensure that a turbine cannot receive more than its maximum flow limit. This limits the power generation to the maximum design capacity.

In a report by [31], it is stated that any form of cycling, defined as the operation of electric generating units at varying load levels and trip occurrences, causes damage to the plant equipment. The damage is increased for high-temperature equipment due to the creep-fatigue interaction [31].

Thus, frequent start and stop sequences are detrimental to the power-generating components used in this study. Therefore, sufficient care should be taken in preventing frequent trips.

In addition, any rotating electrical equipment returning to operation needs to go through what is referred to as a “soft start” method. By gradually increasing the torque applied to the components, the lifespans of shafts, bearings, gears, and couplings are increased [32]. Therefore, the control philosophies in the chapters will not only need to address the requirement of a soft start but also ensure that adjustments made from one period to the next are controlled and gradual.

During a start procedure, as illustrated by Erhart [33], a leakage test is typically performed followed by heating the components. The working fluid is circulated while the turbine is bypassed. The turbine is bypassed until the evaporation pressure exceeds 3.5 bar, after which the control valve adjusts the flow to the turbine.

2.3 Control Philosophy and Methods

This section presents the literature on current control philosophies, with brief discussions of the reported results and evaluations. The relevant characteristics and environments of the control algorithms were also highlighted.

2.3.1 Heat Exchanger Efficiency Maximisation

This subsection presents the literature on the control strategies of heat exchangers within a network of heat transfer processes with the objective of minimising the electrical power requirement of the heat rejection cycle. The focus is on controlling the heat exchangers to achieve efficient heat transfer and minimise energy consumption.

A study by [30] examined several potential approaches for increased energy efficiency within a steel manufacturing facility, with a particular focus on cooling towers, where excess process heat is released into the environment. The original approach to the control is to run both cells of the cooling tower continuously, regardless of the environmental conditions or temperature of the cooling water. It is proposed to identify a suitable temperature zone for the water exiting the cooling tower and adjust either equipment or control based on the current exit temperature and its relation to the zone.

The first approach investigated is to keep the same control philosophy with only changes to blade angles every 6 months. During periods of low ambient temperature, the fan blade angle can be reduced to lower the power consumption of the cooling tower fans. This resulted in a 1.3% reduction in annual power consumption for the system [30].

The second approach is to always keep one fan in operation, with the second fan only being turned on or off depending on the temperature exiting the gas cooler. It is noted that during periods of low ambient temperature, the total time that the second fan is in operation is considerably less than for periods with high ambient temperature. This approach resulted in a 10% annual power consumption reduction [30].

The final approach is utilising variable-speed drives (VSDs) to control the fan speed. The control either increases or decreases the VSD setpoint based on the exit temperature of the water. This approach resulted in a year-round reduction of power consumption, totalling 35% of the original power consumption. It is noted that savings of the VSD approach is considerable, however significant investment costs accompany this saving should the required equipment not already be available [30].

The temperature zone proposed above is like the operational envelope that is required from the heat rejection system in this thesis. It is also noted that the current system does have VSDs fitted to the fans, providing the opportunity to make use of advanced fan speed control methods.

A study by [17] formulated a finned heat exchanger model approach that can be used to predict performance of an air-cooled heat exchanger at off-design conditions. The study used this model to determine the ideal air flow rate required as well as predicting the expected outlet temperature and performance losses due to fouling. The success of this study indicates that the air-cooled heat exchanger model can be used to determine the ideal flow rate of air across the tube bundles for a desired outlet temperature for the water.

2.3.2 Parallel Heat Recovery Operations with a Fluctuating Heat Source

The first section discussed the literature on the maximisation of energy efficiency for a heat transfer process requiring electrical power. This section shifts the focus to the control philosophies of an energy recovery system that has a fluctuating heat source profile.

Solutions to the challenges posed by a fluctuating heat source are grouped into two main categories: damping fluctuations and accommodation through stream control. Conventional stream control methods include bypassing the energy source and transferring excess thermal power to the ambient environment [34].

The study by Trafczynski et al. [35] attempted to maximise energy recovery between parallel branches of heat exchangers by actively adjusting the flow distribution between time periods. The purpose of the heat exchanger network in this study is the maximise the temperature of the cold streams passing through all the heat exchangers. A mathematical model of the heat exchanger network is built, including the relative performance and fouling of all heat exchangers and validated. The original control philosophy is referred to as a “constant split”, where the flow distribution between the branches is equal. Due to differences in heat exchanger conditions and design, this results in different outlet temperatures between the branches and thus there is potential to recover more energy depending on individual heat exchanger conditions.

The proposed strategy in this study is based on a “constant outlet temperature” philosophy. It is noted that the only parameter the control algorithm needs is the outlet temperature of each branch, with flow being adjusted accordingly until a constant outlet temperature is reached. The dataset used in this study has an available heat profile that fluctuated between 150 and 1100 kW. The proposed strategy resulted in a total energy recovery increase of 1.5%.

A study conducted by Vasičkaninová et al. [36] used fuzzy logic controllers to improve the energy efficiency of a small heat exchanger network. Within this heat exchanger network, the high-temperature fluid is distributed between two branches, which have a total of three identical heat exchangers. This resulted in a difference in the heat-transfer rate capability of the branches. None of the heat exchangers within the heat exchanger network can be used to generate electrical power. The efficiency is thus improved by minimising the coolant fluid flow induced by the pump while still transferring the required heat.

The energy recovery process in the studies did not generate any electrical power, unlike the system used in this thesis. However, this study illustrated the potential effect of a dynamic distribution of flow between branches of heat exchangers based on the heat exchanging ability of each branch.

2.3.3 Energy Recovery with a Fluctuating Waste Heat Profile

Recent waste heat recovery studies have focused on the organic Rankine cycle (ORC). The only difference in terms of process fundamentals between a traditional and an organic–Rankine cycle is that the working fluid is changed from water to an organic fluid. An ORC is suitable for heat source temperatures ranging from 50 ℃ to 280 ℃, and the temperature of the heat source is typically used in the selection of working fluid and design of the process components [37].

Heuristic control approaches for power generation systems with a fluctuating heat source are advised in the studies by Wang et al. [38] and Xu and Li [39]. Both studies focussed on the use of ORC systems for waste heat recovery for automotive systems. The intermittency and frequency of the heat source fluctuations in these studies resulted in poor performance from control methods that are process model informed. This is due to the computational requirements of the process model [38]. The use of machine learning methods is applied to determine the control adjustments required with less computational requirements. Both these studies noted success in terms of tracking errors and improving power generation, however, it is also noted that these systems were tested on historical datasets. It is stated by Xu and Li [39] that should a condition outside the learning dataset be experienced, errors of unpredictable magnitudes can be expected.

Waste heat recovery systems based on ORC processes are usually operated with two strategies: following the electric load (FEL) and following the waste heat (FWH) [40]. For the FEL strategy, the rotating speed of the generator, and therefore the turbine, is determined by the parameters of the electrical grid. This is also noted as a traditional approach for power-generating processes. This philosophy is difficult to follow with a fluctuating heat source. For an FWH strategy, the waste heat process aims to use the waste heat efficiently, while the process variables remain within operational levels. This approach results in electrical power generation following variations in the waste heat stream [40].

The study by Zhang et al. [40] also proposed the use of a constrained model predictive controller in a waste heat recovery process. In this study, constraints in terms of setpoints and controller outputs were applied to ensure that process variables remain in a safe operating zone [40]. The constrained model predictive control strategy is successful in keeping the process variables within safe operating limits despite fluctuations in exhaust gas, heat loads, and changes to set points. It is also noted that the energy conversion efficiency of the FWH strategy is higher than that of the

FEL strategy [40]. For a waste heat recovery maximisation objective, as in this thesis, an FWH-type approach must also be followed.

A study by Li et al. [41] also focused on an organic Rankine cycle (ORC) that operates under fluctuating and intermittent heat sources. In this study, several challenges posed by a fluctuating heat source is investigated with potential solutions identified. The challenges include the off-design inefficiency of systems and the need for strict operating restrictions for the sake of safety [41]. Potential issues that can occur from operating too far from design points include heat exchanger fouling, increased condensation pressures, corrosion and leakage, inconsistent dynamic responses and control failures. The turbines and pumps in the system will also be subject to its own inefficiency where at extreme conditions cavitation in the pumps and liquid droplets damage to the turbine blades can occur.

Current technical solutions for the fluctuation include thermal energy storage and stream control. It is stated that thermal energy storage systems based on sensible heat typically result in large systems and that a latent heat storage system has a narrow temperature operating range [41].

The system used in this thesis does not include a thermal energy storage, however it can potentially be investigated as an investment opportunity.

A study by Chowdhury et al. [42] presented two control strategies for a waste heat recovery system with a fluctuating heat source. The purpose of these strategies is to ensure that the conditions of the working fluid in the system remains in the operational range, thus avoiding critical conditions. In the first strategy, the evaporator outlet temperature is controlled by the flow rate of the working fluid and thus the operational speed of the cycle pump in the ORC. In this strategy, the turbine is allowed to turn freely. In the second strategy the evaporator outlet temperature is still controlled, but with the addition of a turbine output control as well. Since the mass flow rate of the working fluid not only influence the evaporator exit temperature but also the turbine output, the flow through the turbine and evaporator can potentially be different. This is achieved by installing a bypass line with a controller that determines the flow rate that will be passed to the turbine.

The study by [13] proposed three different operating philosophies for an ORC with a fluctuating heat source: constant vapor superheat operation, constant evaporation temperature and optimal evaporation temperature operation. For the constant vapor superheat operation, the cycle pump speed is adjusted while the speed of the turbine is kept constant. Note that to accommodate a fluctuating heat source, the superheat setpoint is set relatively high to ensure operational conditions in the cycle are maintained for all potential heat source fluctuation combinations in terms of flow and temperature. The constant evaporation temperature strategy is the addition of a pressure setpoint for the working fluid before the evaporator inlet, which is achieved by

regulating the turbine speed. In the third strategy, both the degree of superheat and evaporating pressure is regulated for maximum power generation [13].

The constant evaporation temperature is noted to be sensitive to a transient heat source and is only recommended when there is a strict constraint on vapor temperature and pressure. The third approach is recommended for a fluctuating heat source when observing power generation results.

In [43], a generalised predictive controller (GPC) is proposed for waste heat recovery. The GPC algorithm maintains the output of the plant at the required setpoints using a model-based approach. For each period, the operational parameters of the ORC are predicted, followed by solving an optimisation problem to determine the control adjustments. Thus, an accurate process model is required to ensure optimal control. However, the nonlinearity and dynamic nature of an ORC lead to a complex process model. Therefore, this study utilised a controlled autoregressive integrated moving average (CARIMA) model to predict the outputs of the ORC.

The study applied two control philosophies to the model. The first philosophy is to follow a given load demand and the second is to follow a given setpoint temperature for the working fluid exiting the evaporator [43]. No historical dataset or fluctuating heat source is used in this study even though the focus of the study is to ensure that the ORC parameters can be adjusted to maintain a desired setpoint should a disturbance in inlet conditions be observed.

A multivariable robust controller is designed for an ORC by [44]. It is stated that the simple structure and easily realisable controller do not require a precise mathematical model because the integral action compensates for unknown parameters of the process. The objective of this control strategy is to adjust the power generated to the changes in waste heat as soon as possible. This is performed while also regulating the vapour pressure and, thus, the degree of superheat of the organic fluid to maximise efficiency.

The controller is applied to a 100 kW waste heat recovery system that uses R245fa as the working fluid, after which two case studies are completed. The second case study is the most relevant because it is a disturbance rejection test in which the flow rates and temperatures of the waste heat stream are dynamically adjusted. The controller accurately tracks and adjusts the output power by adjusting the vapour pressure and degree of superheat of the organic fluid with operational constraints [44].

The studies of Zhang et al. [43] and Zhang et al. [44] show the ability of ORC control setpoints to be accurately followed for a given set of disturbances, with performance evaluations being done on the tracking ability of the system and its controller. In this thesis, performance evaluations for the PGEN component will be based on average power generation over the time horizon of a historical dataset.

A combined cycle generating power from thermal energy is investigated in the study by Fan et al. [45]. An ORC and supercritical CO_2 cycle (sCO_2) share a heat exchanger in an attempt to maximise energy recovery. The off-design behaviour of this combined cycle is analysed to develop improved control systems for both the individual cycles and the heat load distribution between the two branches. The objective of the control system is to always follow the thermal load. Thermal efficiency improvements of 1.09 to 3.36% is calculated for the combined ORC-sCO_2 cycle.

The study by Fan et al. [45] provides valuable insight into the potential of distributing flow between two or more branches for maximisation of power generation. However, in this study, no constraints were noted in terms of operational envelopes that need to be maintained. In addition, the off-design analysis only consisted of a relative heat load parameter and did not specify changes to flow rates or temperatures for the heat source. The use of a historical dataset is also not in the scope of the study. As a result, constrained start-up and trip scenarios for the power generation is not included for in the analysis.

It is noted in this study that adjusting the mass flow rate is the desired control strategy for the sCO_2 cycle since it is determined that the efficiency of the plant is not significantly influenced by adjustments. The preferred control strategy of the ORC is the same as the vapour-pressure control strategy in [13], [42] and [44]. The strategy of using variable speed to adjust the mass flow rate and vapour pressure provides significant flexibility due to the performance characteristics of the applied pumps and compressors.

The study by [46] proposed the use of a phase change material as thermal energy storage on the off-gas system of a steel plant. This study evaluated all proposed systems on a historical dataset and had a set of constraints for the cooling of the flue gas. All three systems evaluated in this thesis is a power generation system with no auxiliary cooling method should the power generation become unavailable. As such, the effect of a tripped and constrained restart procedure is not considered in the analysis of this study.

The current system used in this thesis does not have a thermal energy storage system, however, this study does provide valuable insights into the use of a thermal energy storage system for the dampening of fluctuations. This study also stated the need for more comprehensive analysis on waste heat recovery processes in the steel industry.

2.4 Identified Gap in Literature

From this section, it is clear that sufficient literature exists in terms of the control philosophies of single heat transfer processes, similar to the ACHX in the system. There is also literature on control philosophies when this heat transfer process is part of a power generation process.

Literature also exists on the optimal distribution of heat between multiple power generation processes in parallel.

None of the studies above addressed the need of the system in this thesis. The studies provided above did not make use of a historical dataset for performance evaluation, with fluctuating heat loads being demonstrated by either a set of off-design parameters or as a single disturbance to a evaluate dynamic responses.

Literature regarding control formulations for a combination of an air-cooled heat exchanger and the power generation process has not been identified. None of the processes in the literature section explicitly mentioned the need to mitigate the risk of an unplanned stoppage to ensure that an operational temperature envelope is always adhered to. Additional constraints in the form of equipment start-up delays are also not included.

However, these philosophies can potentially be used for the specific control of the ACHX and PGEN in the system, with the addition of constraints for maintaining the temperature envelope. Notable philosophies to be investigated for use in this thesis include the dynamic distribution of flow between the equipment to reach a desired objective [35] as well the adjustment of evaporating temperature and pressure to maximise the PGEN efficiency [13].

The absence of a suitable control philosophy for the objective of this thesis confirms the statement by Feng et al. [19] that there is an absence of comprehensive performance analyses on historical datasets. for waste heat recovery processes. It is also noted by Dal Magro [46] that the use of cost-effective waste heat recovery process in the steel manufacturing industry is hampered by the fluctuating heat source associated with the process.

A gap in the literature exists regarding a control formulation that enables the transfer of sufficient heat to maintain operational envelopes, even in the event of an unplanned stoppage. In addition, this control formulation must maximise energy recovery through the control of cooling water flow rates and distributions between the components. The flow rates and distributions need to be updated dynamically to due to the influence of changes in the heat source parameters.

2.5 Summary

The first section of this literature review chapter provides brief definitions and theories of the engineering fundamentals required to fully comprehend the content in the chapters to follow.

In the second section, a detailed description of all the components of the cooling cycle is provided. The background includes information on the heat exchangers, pumps, fans and energy recovery processes.

The third section focussed on relevant literature with regards to the control philosophies of the heat exchanger components and the system. It is noted that several of the control philosophies

can be used in combination to maximise power generation in the PGEN and ensure that heat transfer is efficient at the ACHX. The impact of dynamic distributions of flow between different heat exchanger branches are also discussed. However, it is noted that none of the control philosophies investigated is suitable for the system in this thesis, confirming literature that stated the need for further developments in this area.

The next chapter utilises the fundamentals supplied in this chapter to generate the layout, available heat profile, and heat transfer performance profile to be used in the chapters to follow in this thesis.

CHAPTER 3 PROCESS AND COMPONENT CONSIDERATIONS

The previous chapter discussed the fundamental working principles that are required to understand the heat transfer process and the control algorithms of this study. In this chapter the fluctuating waste heat profile will be shown along with more detail on the heat rejection process used to demonstrate the concepts and results of the contributions of this study.

3.1 Heat Rejection System

3.1.1 Layout

This section will illustrate a suitable layout of the heat rejection process that is designed to ensure that the cooling water is maintained within the required operational temperature envelope.

The steel production process produces a high temperature flue gas as byproduct and is regarded as the heat source to the heat rejection process. Cooling water is used in a heat exchanger referred to as a gas cooler to reduce the flue gas temperature. The cooling water is circulated in a closed loop, resulting in the need to remove sufficient heat from the cooling water before it enters the gas cooler.

The conventional heat rejection process layout is to make use of ACHX where the designed heat transfer capability is sufficient to achieve the maximum heat transfer rate expected [10]. The ACHX component can consist of multiple air-cooled heat exchangers connected in series and parallel from a cooling water flow perspective.

The heat removed from the cooling water through an ACHX is transferred to the environment and cannot be used to increase process efficiencies or generate electrical power. To remain competitive, metal producers need to identify and utilise waste streams to reduce production costs. This can be achieved by investing in a process that will facilitate the use of the current waste heat stream. One such process is a Rankine-cycle based process (PGEN) to convert the energy contained in the waste heat into electrical power.

Figure 3-1 depicts cooling water entering the heat rejection process. The heat and flow are distributed in a controlled manner between three streams. This distribution is calculated and adjusted by a control algorithm. After passing through each stream, flow collectively enters a tank at a temperature of T_{cw2} whereafter it is pumped to the gas-cooler.

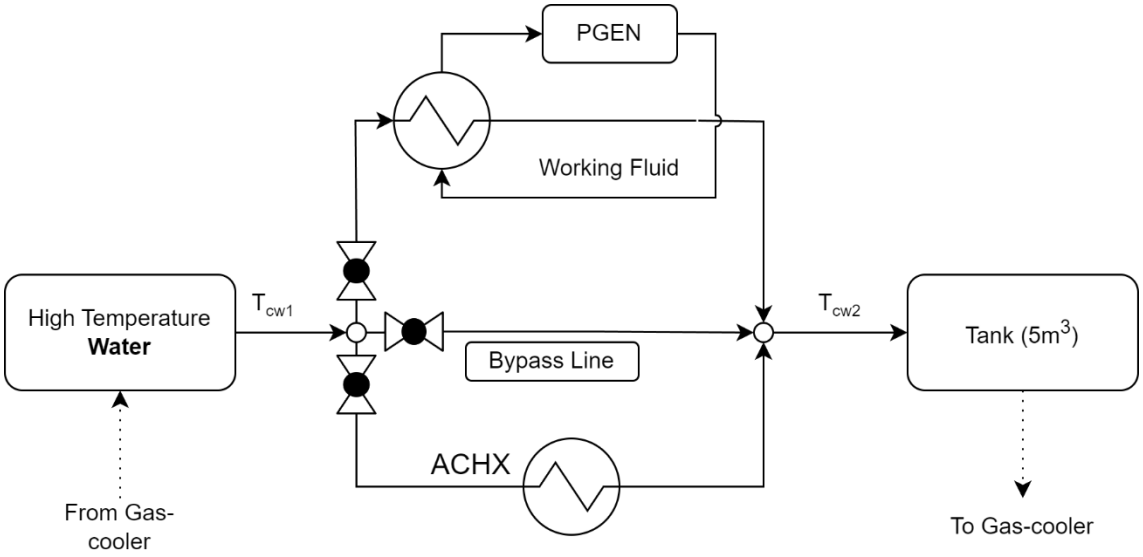


Figure 3-1: Detailed Layout of Heat Rejection Process

After distribution of the flow and heat to the PGEN and ACHX, internal control formulations will ensure that the temperature is achieved with maximum energy efficiency where possible. Note that flow can bypass both the ACHX and PGEN the bypass line (BP) can be used to minimise heat transfer when required. Therefore, this will typically be used in start-up conditions.

3.1.2 Control Requirements

The novel control formulation determining the flow distribution between the components have the objective of maximising the power generation while also adhering the process constraints given in sections to follow.

For the heat rejection cycle, the following conservation equations for heat and mass will apply:

$$\mathrm{Q_{hs}} = \mathrm{Q_P} + \mathrm{Q_A} + \mathrm{Q_{Res}} \tag{3.1}$$

$$\dot{\mathrm{m}}_{\mathrm{hs}} = \dot{\mathrm{m}}_{\mathrm{P}} + \dot{\mathrm{m}}_{\mathrm{A}} + \dot{\mathrm{m}}_{\mathrm{BP}} \tag{3.2}$$

Where $\mathrm{Q_{hs}}$ is the total available heat after the gas cooler and $\mathrm{Q_P}$ and $\mathrm{Q_A}$ is the heat to be removed from the flow distributed to the PGEN and ACHX respectively, in $[\mathrm{kJ}]$. The total mass flow of cooling water exiting the gas cooler is indicated with $\dot{\mathrm{m}}_{\mathrm{hs}}$ while the mass flow to the PGEN and ACHX is indicated by $\dot{\mathrm{m}}_{\mathrm{P}}$ and $\dot{\mathrm{m}}_{\mathrm{A}}$, in kg/s. The mass flow moving through the bypass line is indicated with $\dot{\mathrm{m}}_{\mathrm{BP}}$. Failing to remove $\mathrm{Q_{hs}}$ between the PGEN and ACHX components will result in the residual heat, $\mathrm{Q_{Res}} > 0$. This heat term is an indication of the difference between the temperature exiting the heat rejection cycle, $\mathrm{T_{cw2}}$℃, and the target temperature. The exit temperature can be calculated with an equation similar to (2.15):

$$\mathrm{Q_{Res}} = \dot{\mathrm{m}}_{\mathrm{hs}} \cdot \mathrm{C_p} \cdot (\mathrm{T_{cw2}} - \mathrm{T^{set}}) \tag{3.3}$$

It follows that in a scenario where sufficient heat transfer is done that $Q_{Res} = 0$, and, therefore, $T_{cw2} = T^{set}$. It also follows that when the $T_{cw2} > T^{set}$, not all the required heat is transferred while $T_{cw2} < T^{set}$ indicates that more than the required heat is transferred.

An unplanned stoppage for PGEN will result in a loss of heat transfer capacity to remove Q_P. This scenario will result in a need for ACHX to transfer more heat. If the ACHX cannot meet the entire heat transfer requirement, Q_T, it can be expected that $Q_{Res} > 0$, which will result in a temperature entering the gas cooler that is higher than the setpoint temperature. A higher value for T_{cw2} can still be acceptable as long as it is within the operational temperature envelope. An operational temperature envelope refers to the range of temperatures at which a system can function safely and effectively.

This section has provided the layout of the heat rejection system. The section to follow will provide more detail on the design and operational limits of the components within the heat rejection.

3.2 Gas-Cooler Operational Considerations

3.2.1 Flue Gas Temperature Envelope

The gas-cooler is a component that transfers heat from the flue gas with the objective of ensuring a suitable temperature for the flue gas conveyed to downstream processes. The material used in the piping of the gas-cooler is ASTM A106, a low-cost material similar to the material used in the electric arc furnace flue gas system used in the study by Gelfi et al. [47].

The transferred heat from the flue gas is typically referred to as waste heat. The temperature of the steel used to construct the gas cooler walls must be less than the design limit of 454 ℃ to reduce the risk of long-term overheating [48]. A lower temperature limit is also used to prevent acid dew-point corrosion, with a specific value depending on the composition of the flue gas [6]. The composition of the flue gas is expected to change throughout the metal production process, resulting in a variable acid dew-point temperature. However, for the purpose of this study, a fixed lower temperature limit is required.

The study by Gelfi et al. [47] analysed the failure of an electric arc furnace flue gas system on a steel production plant, in which it is found that the cooling water temperature is too low, resulting in acid condensation on the cooling ductwork. The study used the Verhoff equation to determine dew-point temperature based on water and SO_3 content of flue gas. The Verhoff equation is given as:

$$T_{DP} = \frac{1000}{1.7842 - 0.0269\log_{10}(P_{H_2O}) - 0.1029\log_{10}(P_{SO_3}) + 0.0329\log_{10}(P_{H_2O})\log_{10}(P_{SO_3})} \quad (3.4)$$

Where T_{DP} [K] is the acid dew point and P_{H_2O} and P_{SO_3}[atm] is the partial pressure [47].

For this study, historical data is analysed to determine the maximum concentration levels of the water vapour and SO_3. This is determined to be 8% and 10 ppm respectively. From equation (3.4), this results in an acid dew point temperature of ~119.6 ℃. A conservative safety margin of 50 ℃ is specified due to uninsulated downstream processes where further reduction in temperature can be expected. It results that the lower temperature limit of the flue gas in the gas-cooler is 150 ℃.

Furthermore, in the study by Gelfi et al. [47] it is stated that the presence of thick deposits unto to gas-cooler walls effectively insulates the pipework and thus maintains the material temperature close to that of the cooling water. It follows that the cooling water can also be assigned the same lower temperature limit at which it enters the gas cooler of 150 ℃. This corresponds with the plant used as a case study by Dal Magro [46].

3.2.2 Cooling Water Operational Envelope

The heat transfer between the flue gas and cooling water will vary with changes to temperatures and mass flows of both the flue gas and cooling water. The flue gas flow rate and temperature entering the gas cooler are not controllable since it is a direct result of the production process. In terms of the cooling water, the flow rate is controlled by the heat rejection process control algorithm. The cooling water temperature is controlled by adjusting the heat transferred from the cooling water through the ACHX and PGEN components.

The supplied design and operational parameters provided for the gas-cooler in this section are from an actual plant with additional information from relevant literature being used to ensure realistic parameters are assigned where required.

Table 3-1: Gas Cooler Design Parameters and Operational Envelope for Cooling Water

Node	Parameter	Unit	Value
-	Design UA	W/K	90 000
-	Maximum Pressure	bar	30
Exit of Gas Cooler	Upper Temperature	℃	210
	Lower Temperature	℃	150
Entry of Gas Cooler	Upper Threshold Temperature	℃	190
	Lower Threshold Temperature	℃	150
Cooling Water Flow	Maximum Flow Rate	m^3/h	450
	Design Flow Rate	m^3/h	288
	Minimum Flow Rate	m^3/h	20

The design flow rate and heat transfer capability of the gas cooler along with the operational temperature envelope for the gas cooler is provided in Table 3-1. The maximum achievable pressure within the system is also noted in this table.

The range of temperature values expected for the cooling water exiting the gas cooler is 150 ℃ to 210 ℃ according to historical data for this specific plant. The flue gas, as mentioned, is at a significantly higher temperature. It follows from the Carnot thermal efficiency that a higher power generation efficiency can be achieved should a higher heat source temperature be supplied. A higher heat source temperature to the PGEN can theoretically be achieved by reducing the flow rate of the cooling water through the gas cooler.

However, the maximum pressure of the cooling cycle in combination with water as the cooling fluid does not allow for a higher temperature. Higher temperatures will lead to phase changes within the gas cooler, which will significantly impact the heat transfer achieved. Loss of cooling in localised areas of the gas cooler can have potentially severe consequences. The mass flow rate of the cooling water through the gas cooler is thus adjusted to ensure that the cooling water temperature is maintained at least 20 ℃ below the boiling temperature at maximum pressure. Cooling water at 30 bar is expected to boil at 233.7 ℃ [23], indicating that the maximum temperature of cooling water exiting the gas cooler at 210 ℃ is within the allowed limits. The potential increase in thermal efficiencies as a result of higher temperature entering PGEN can, therefore, not be pursued.

The gas cooler design and process parameters are used to determine the operational envelope for the cooling water entering the gas cooler. The upper threshold value of 190 ℃ will, according to design calculations and flow rates, result in water exiting the gas cooler still within the upper temperature limit of 210 ℃. As mentioned in the previous section, a lower temperature limit of 150 ℃ for cooling water entering the gas cooler will prevent acid dewpoint corrosion on the gas cooler walls.

The multiple cooling water pump arrangement allows the system to operate in a flow rate range of between 20 and 450 m^3/h. Control of this flow rate is critical to achieve suitable temperatures of both fluids in the gas cooler while also attempting to recover the maximum waste heat from the flue gas. This is described in more detail in the next chapter. Note that the tank has a volume of 5 m^3, as shown in Figure 3-1. At the minimum cooling water flow rate, the longest volume replacement time can be determined as 15 min.

3.2.3 Fluctuating Waste Heat Profile

The operational temperature envelope of the flue gas is discussed in an earlier section. Failure to transfer sufficient heat will result in a material temperature above the upper limit of the operational envelope, which will negatively impact the reliability of the flue gas handling system.

However, transferring too much heat will result in a shell temperature below that of the acid dew point, which will also negatively impact the reliability and operational life of the flue gas handling system. An unreliable flue gas handling system is expected to impact the production process and, therefore, significant losses to the asset owner can be attached to operating outside the temperature envelope.

The flue gas in the gas-cooler is regarded as the heat source to the heat rejection process. The heat source, as discussed in previous chapters, has a fluctuating profile due to the inherent variations of the metals production process. From the conservation of energy and mass in a control volume, it follows that the combined ACHX and PGEN will also have a fluctuating heat transfer requirement. If the supplied thermal energy increases, the heat exchangers need to transfer more heat to ensure the conservation of energy within the control volume is respected.

It follows that the maximum and minimum temperature limit for the flue gas result in a maximum and minimum heat transfer requirement in both the gas-cooler and the heat rejection components. The equation in (2.19) can be used to determine the maximum and minimum waste heat to be transferred in both the gas-cooler and heat rejection components. Subscript changes result in equations (3.5) and (3.6).

$$\mathrm{Q_{max}} = \mathrm{m_{Tot}} c_p \left(\mathrm{T_f} - \mathrm{T^{LL}}\right) \tag{3.5}$$

$$\mathrm{Q_{min}} = \mathrm{m_{Tot}} c_p \left(\mathrm{T_f} - \mathrm{T^{UL}}\right) \tag{3.6}$$

Where $\mathrm{T^{UL}}$ and $\mathrm{T^{LL}}$ °C are the upper and lower limits of the applicable component's operational envelope and $\mathrm{m_{Tot}}$ is the total mass that moved through the component during the time interval. The maximum and minimum heat transferred is indicated with $\mathrm{Q_{max}}$ and $\mathrm{Q_{min}}$ J, respectively, and the temperature of the fluid entering the component is denoted by $\mathrm{T_f}$.

A historical dataset consisting of mass flow and temperatures for the flue gas is used to populate a waste heat profile over time, as in Figure 3-2. The historical dataset has a timeline of 83 days at 5 min intervals.

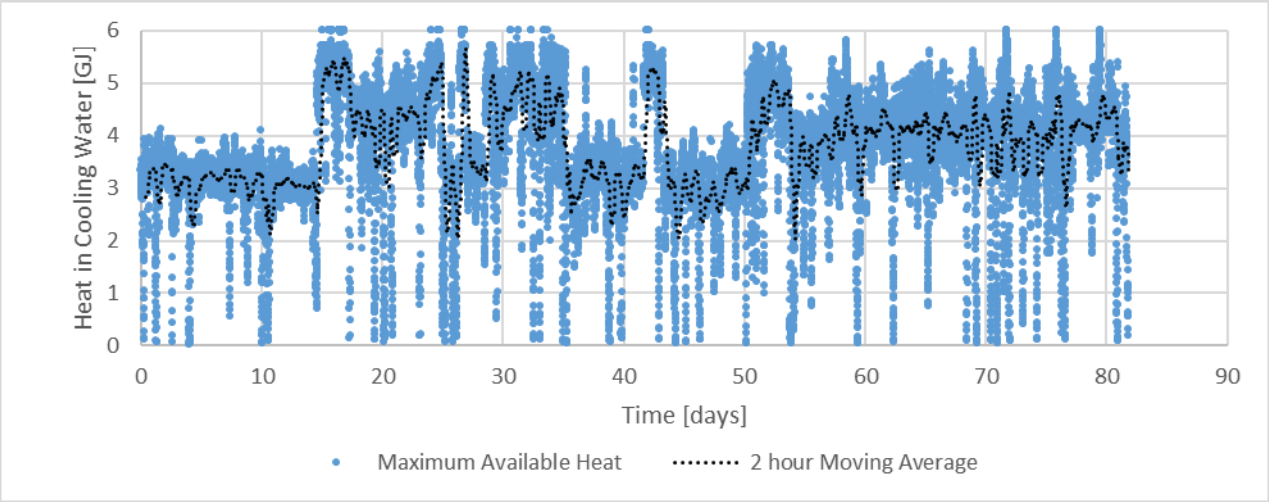


Figure 3-2: Representative Dataset of Waste Heat Over Time

Significant fluctuations are observed. These fluctuations can be attributed to the batch production approach used in the process. Time intervals where the available waste heat drops to zero indicate instances where none of the furnaces were in operation.

The maximum available heat is 6 GJ. Given the 5 min period, this results in an average heat transfer rate of 20 MW that need to be sustained to remove all the heat transferred from the flue gas in the gas cooler. Over the time horizon of the historical dataset, the total energy available in the flue gas is 88 806.5 GJ.

To illustrating the performance of the heat rejection system, a demonstrative dataset ranging 90 min are used, as shown in Figure 3-3. This dataset enables the demonstration of the adjustments to flow and heat distribution between the streams, including the influences on the temperature entering the gas cooler. It also enables the evaluation and demonstration of the inherent control philosophies under which the PGEN and ACHX operate.

The evaluation of power generation and other performance and risk parameters will still be evaluated through the use of the historical dataset in Figure 3-2.

Note that the maximum heat transfer requirement in the demonstrative dataset is 20 MW, indicating that both PGEN and ACHX are designed to receive and successfully transfer all of the waste heat.

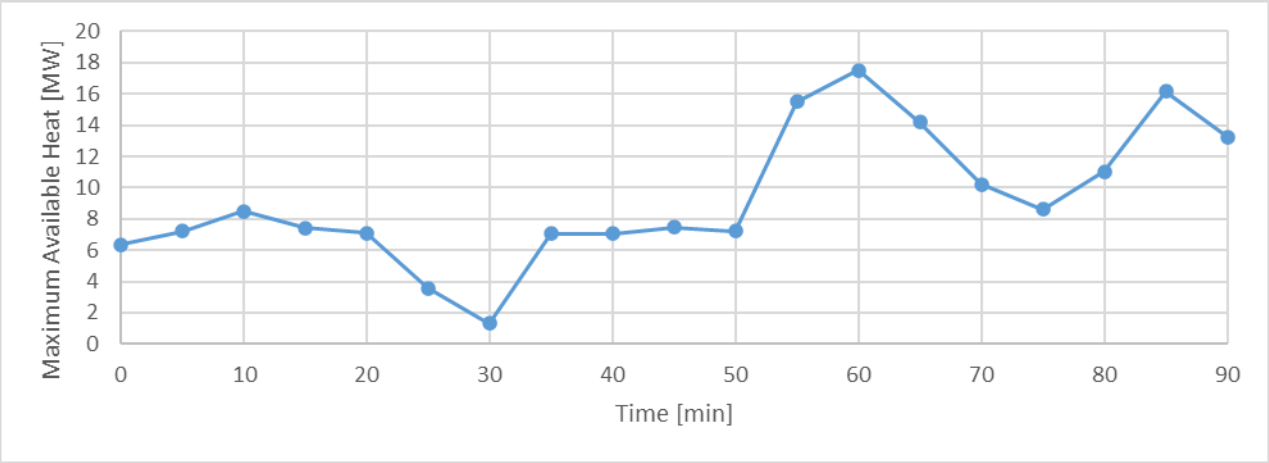


Figure 3-3: Demonstrative Waste Heat Dataset

Both the historical and demonstrative datasets can also be plotted with the applicable allowable heat transfer for any time period. The maximum and minimum allowable heat transfer during time periods can be determined by incorporating equation (3.5) and (3.6) as depicted in Figure 3-4.

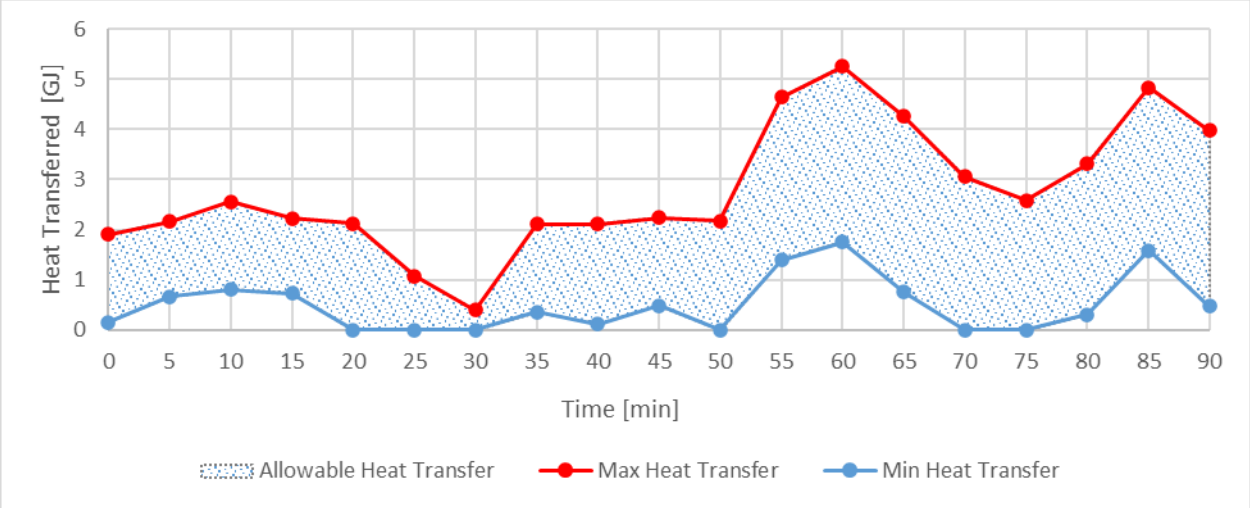


Figure 3-4: Maximum and Minimum Heat Transferred every Time Interval for the Demonstrative Dataset

From Figure 3-4 the maximum and minimum heat transferred during each time interval is supplied. Transferring heat outside this moving range will lead to breaching the operational envelope of the gas-cooler.

The total available heat from the flue gas over the 90 min is 55.11 GJ, which corresponds with an average allowable heat transfer rate of 9.67 MW. The time period of 20 to 30 min and 70 to 75 min is noted as periods where the flue gas temperature is such that no heat transfer is required to maintain the operational temperature envelope of the flue gas in the gas-cooler.

Note that the heat to be transferred from the cooling water by the PGEN and ACHX will differ from the waste heat figures illustrated above. This is due to the cooling water flow rate being influenced

by the cooling water temperature and, therefore, the heat transfer performance during the previous time interval.

3.3 Air Cooled Heat Exchanger Operational Considerations

The original plant is designed and built without any form of waste heat recovery considered. The ACHX is the original heat rejection equipment in the cooling system, with the waste heat being transferred to the environment through forced convection of ambient air.

This section will provide details on the installed ACHX along with an operational control philosophy to be used in the chapters to follow.

3.3.1 ACHX Original Design

The plant currently consists of two identical air-cooled heat exchangers, both capable of transferring heat at a rate of $10\ [\mathrm{MW}]$ resulting in a combined capability of $20\ [\mathrm{MW}]$. This collection of heat exchangers is referred to as ACHX in this thesis.

The original air-cooled heat exchanger design parameters are shown in Table 3-2 below.

Table 3-2: Design Parameters of an ACHX

Parameter	Unit	Value
Volume of Cooling Water	m^3	1.765
Fans per heat exchanger	-	2
Volume flow at full speed (per fan)	m^3/s	42
Static Pressure at full speed	Pa	265
Fan Diameter	m	3.048
Fan Speed Range min, max	RPM	155;333
Motor Power at Full Speed	kW	32.8
Tube Rows	-	6
Tubes per Row	-	43
Tube Internal Diameter	mm	31.75
Tube Thickness	mm	2.41
Tube Length	m	9.8
Tube Arrangement	-	Staggered
Tube Material	-	ASTM A179
Fin Density	/m	433
Fin Height	mm	16.2
Fin Thickness	mm	0.4
Fin Material	-	Aluminium

The parameters above are used in the determining a control philosophy for the ACHX based on both the cooling water flow rate and temperature. The model used in this control philosophy will also be used to determine the cooling water flow rate distribution between the ACHX and PGEN components.

3.3.2 ACHX Operational Model

Since the purpose of the ACHX is to transfer heat to the environment the fins and pipe surfaces are exposed to ambient air. Heat transfer will continue to occur between the cooling water and ambient air until both are at the same temperature. It follows that heat transfer in the ACHX should be expected even if none of the forced convection fans are in operation.

The resulting control philosophy needs to consider the heat transferred for both the ACHX with forced convection and without. By doing so, the potential for overcooling or unnecessary power consumption at the fans are limited.

3.3.2.1 Heat Transfer without Forced Convection

The study by Hahne and Zu [49] demonstrates a method where fin and tube diameters are used alongside material properties and operational temperatures to determine the natural convection heat transfer of air over the finned tubes. The final Nusselt number correlation of this study is;

$$\mathrm{Nu} = \frac{\mathrm{h} \cdot \mathrm{d_{eff}}}{\mathrm{k}} = 0.28 \cdot \left(\mathrm{Gr} \cdot \mathrm{Pr} \cdot \frac{\mathrm{b}}{\mathrm{d}}\right)^{\frac{1}{3}} \tag{3.7}$$

Where $\mathrm{Nu}, \mathrm{h}, \mathrm{k}$ is the Nusselt number, mean heat transfer coefficient and thermal conductivity of the shell respectively. The effective diameter, $\mathrm{d_{eff}}$, is described as $\mathrm{d} + \mathrm{f}$ where d is the diameter of the central tube and f is the height of the fin. The Prandtl number is denoted by Pr whilst b represents the distance between neighbouring fins. The Grashof number, Gr, approximates the ratio of buoyancy to viscous forces acting on a fluid and can be determined as follows:

$$\mathrm{Gr} = \frac{\beta \mathrm{g} \mathrm{d}_{\mathrm{eff}}^3 \Delta \mathrm{T}}{\mathrm{v}^2} \tag{3.8}$$

Where β denotes the coefficient of thermal expansion for the air and g is the gravitational acceleration. The kinematic viscosity is also indicated with v. For the final formulation in the study by Hahne and Zu [49], the temperature difference, $\Delta \mathrm{T}$, is determined by $\Delta \mathrm{T} = \mathrm{T_{tube}} - \mathrm{T_{ambient}}$.

All thermophysical parameters above are also determined at a reference temperature of $\frac{\mathrm{T_{tube}} - \mathrm{T_{ambient}}}{2}$. It follows that by changing the cooling water temperature, the expected convective heat transfer will also change. The experimental results in the study of Hahne and Zu [49] indicated that their results are to within 6% of the experimental results.

The current fouling condition of the heat exchanger can be used to determine the mean heat transfer coefficient through $h_f = \frac{1}{R_f + \left(\frac{1}{h}\right)}$ where $R_f \left[\frac{m^2 K}{W}\right]$ is the fouling factor. The mean heat transfer coefficient can be used to determine the heat transfer rate through $\dot{Q} = h_f A \Delta T$ where A is the total external heat transfer area. From the design parameters supplied in Table 3-2, the heat transfer area A can be determined as $5312.49\ [m^2]$ through:

$$A = A_{tube,exposed} + A_{fin} \tag{3.9}$$

$$A_{tube,exposed} = L_{tube,exposed} \cdot \pi \cdot (OD_{tube}) \cdot N_{tubes} \tag{3.10}$$

$$L_{tube,exposed} = L_{tube} - (\rho_{fin} \cdot L_{tube} \cdot t_{fin}) \tag{3.11}$$

$$A_{fin} = L_{tube} \cdot \rho_{fin} \cdot N_{tubes} \cdot [t_{fin} + 2\pi \cdot (r_{fin}^2 - r_{tube}^2) \tag{3.12}$$

By following the above method and varying the cooling water temperature in the air-cooled heat exchanger, the change in heat transfer can be predicted. The cooling water temperature is varied in the operational range from 150 ℃ to 210 ℃ for a constant mass flow rate. The results of this parametric study, along with a power curve correlation of the results, are given in Figure 3-5.

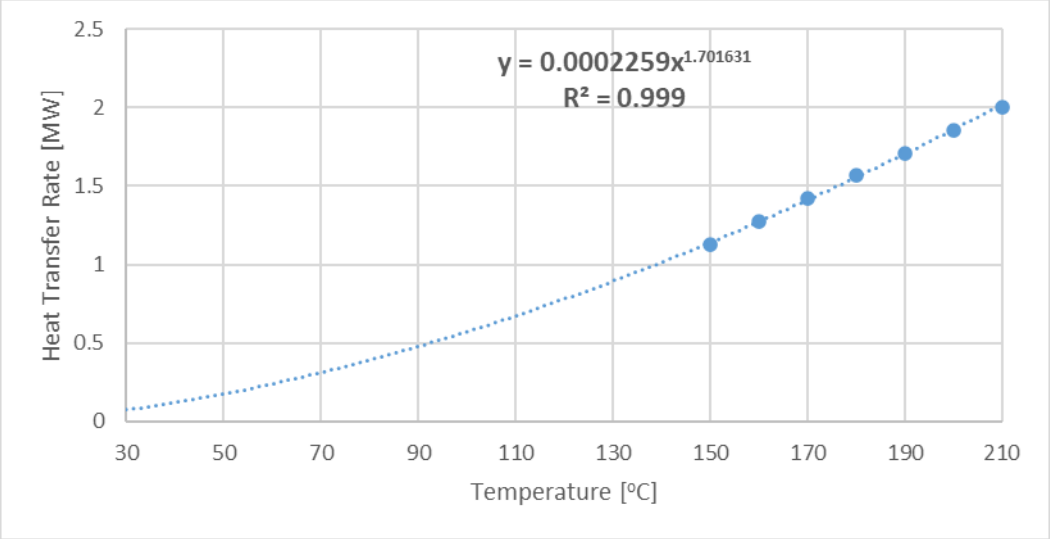


Figure 3-5: Heat Transfer Rate vs Cooling Water Temperature during Natural Convection per ACHX

By curve fitting a suitable equation, a heat transfer rate that is influenced by the cooling water temperature entering a non-operational ACHX can be determined and be used in the control philosophies to follow.

3.3.2.2 Heat Transfer with Forced Convection

The air-cooled heat exchangers used in this study has two identical fans installed in each. The purpose of these fans is to control the mass flow rate of the ambient air over the extended surfaces of the tube bundle and thus control the heat transfer rate.

A comprehensive heat exchanger model will enable the prediction of heat transfer performance based on variations in cooling water and ambient temperature and flows. The cooling water flow rate and temperature entering the ACHX cannot be adjusted from the heat exchanger control perspective. Therefore, to ensure sufficient heat is transferred, the fan speed and thus mass flow rate of the ambient air is adjusted.

The study by van Rooyen [17] is focussed on the performance prediction of finned-tube heat exchangers. The exact modelling approach is used in this thesis. The modelling approach applied to the ACHX in this thesis is supplied in Appendix A.

The cooling water flow rate and temperatures are varied in a parametric study along with controlling the mass flow rate of the air. A 3D surface of the predicted performance from this modelling approach, replicated in this study, is shown in Figure 3-6 for a fixed heat source temperature of 180 ℃.

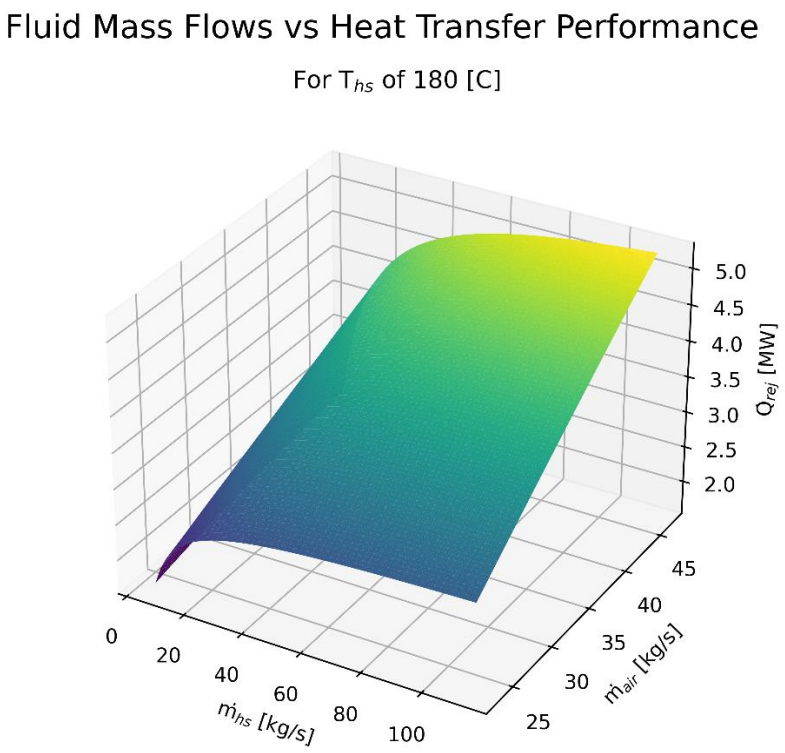


Figure 3-6: Fluid Mass Flows vs Predicted Heat Transfer Performance in the ACHX (Per Fan) for a Heat Source Temperature of 180 ℃

From Figure 3-6 it is clear than an increase in air mass flow increases the heat transferred from the cooling water. It is also observed that there is an increase in heat transfer if the mass flow rate of the cooling water is increased without adjustments to the air mass flow rate. Both of these phenomena are possible due to the large temperature gradient between the environment and the cooling water. The rate of heat transfer is thus dependent on both environmental and operational conditions.

The control of the air mass flow rate is done through variable speed drives on the fans and by the number of fans in operation. Therefore, by combining the above predicted performances for the ACHX into the current arrangement of two fans per bundle and two bundles in parallel, a control philosophy can be formulated. This control philosophy is able to determine the minimum required fans in operation as well the required operational speed of the fans.

3.3.2.3 Combined Operational Regime

By expanding the resulting heat transfer performance in Figure 3-6 with the predicted heat transfer when no fan is in operation, an informed decision can be made on when it is required to change the operational status of the first fan. This range can be seen in Figure 3-7.

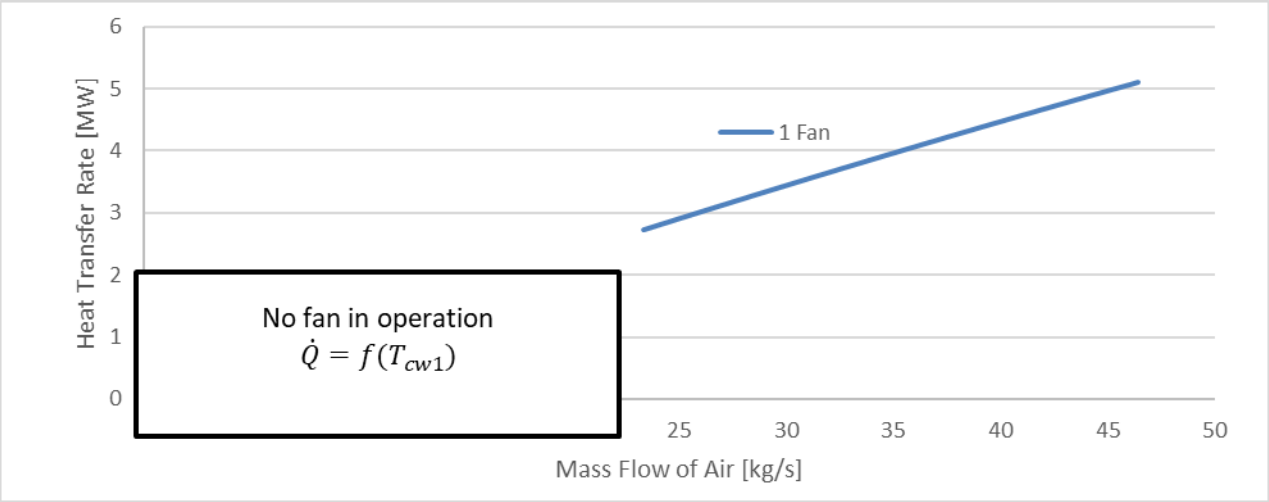


Figure 3-7: Combination of Forced and Natural Convection Heat Transfer in the ACHX

The maximum heat transfer rate expected due to natural convection in the air coolers, is 2 MW. Note that the minimum heat transfer rate that can be achieved by one operational fan is ~2.7 MW.

By further expanding the above figure for all four available operational fans, Figure 3-8 is populated. Note that in this figure it is assumed that all fans in operation will have the same rotational speeds as assigned by the control philosophy.

It can be concluded that the multiple fan ranges overlap in terms of predicted heat transfer rates. The control philosophy formulated from this information will have to decide between the number of fans not only based on the required heat transfer rate but also additional information such as the power consumption of the operational fans to achieve this heat transfer rate. Should the control philosophy need to decide between multiple valid options, the option with the least total power consumption needs to be identified.

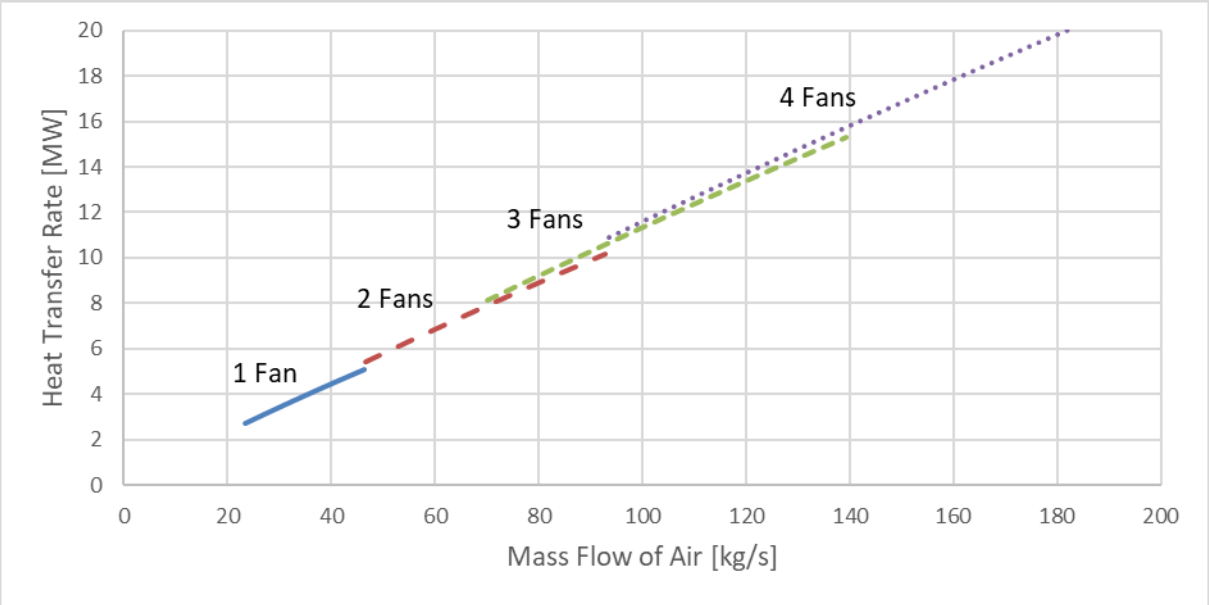


Figure 3-8: Heat Transfer Rate Range for the Four Fans in the ACHX

The formulation of this control philosophy forms is detailed in the next chapter.

3.4 Power Generation System Operational Considerations

The PGEN process converts the transferred heat to electrical power with the use of a Rankine cycle. This process has varying thermal efficiencies based on various parameters.

This section will demonstrate the model and approach used to predict the performance of the PGEN component with the aim of using the performance model in a control philosophy in future chapters.

3.4.1 PGEN Layout and Design Limitations

Before such a performance model can be formulated, an understanding of the general layout and limitations to the cycle is required.

3.4.1.1 PGEN Cycle Layout

The layout of the Rankine cycle, similar to the layout in Song et al. [50], is given in Figure 3-9. It basically consists of a pump, two heat exchangers to evaporate and condense the working fluid and a turbine connected to a generator.

The layout starts at the cycle pump that provides moves the working fluid at high pressure through the cycle. In the evaporating heat exchanger, heat is transferred from the cooling water to the working fluid at a controlled rate. The high pressure and superheated working fluid enter the turbine where it applies mechanical work over a turbine. The turbine is connected to a generator where the mechanical work is converted to electrical power. The low-pressure working fluid enters the condenser where ambient air is used to fully condense the working fluid.

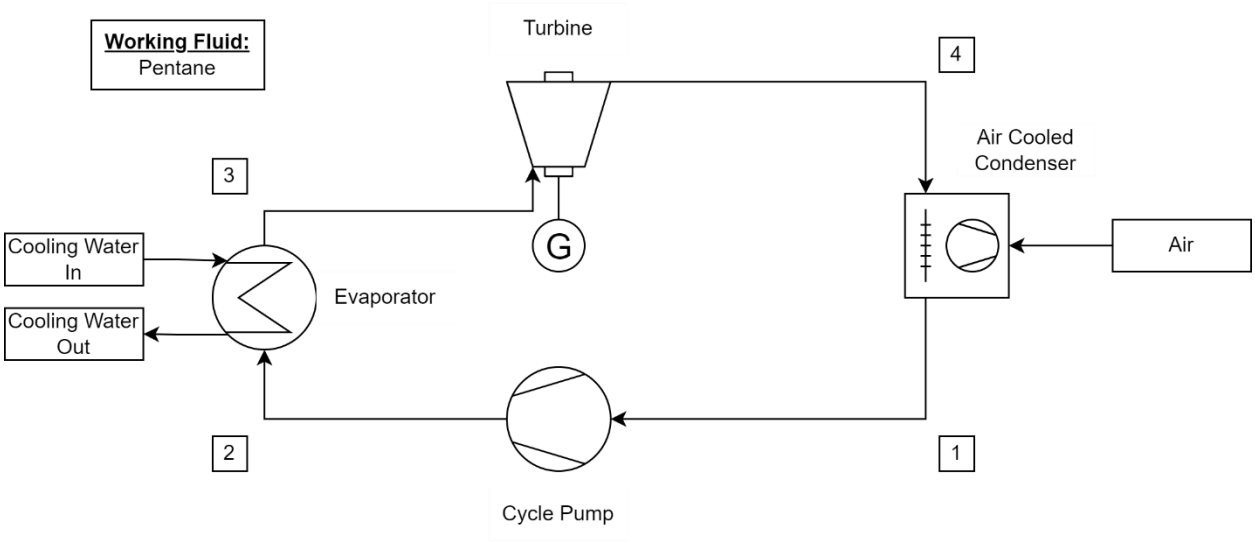


Figure 3-9: PGEN Component Layout

The working fluid is typically selected based on the heat source temperature. For the plant used in this study, the PGEN working fluid currently in use is Pentane. According to the study by Faghih and Pourshaghaghy [37], Pentane is designated as the optimum fluid for heat source temperatures ranging between 220 ℃ and 230 ℃.

3.4.1.2 Design and Operational Limitations

The design parameters used in the performance model for the PGEN is provided in Table 3-3.

The maximum heat that PGEN can transfer is 20 MW. The PGEN cycle has an organic fluid as the working fluid in the Rankine cycle. This type of cycle is commonly referred to as an organic Rankine cycle (ORC). According to a study by Tian and Shu [15], which summarised the differences between the steam and organic cycles in practice, indicated that an ORC is more flexible in terms of heat source fluctuations. An ORC already in operation can operate at partial load conditions of up to 10% [15]. This is used to limit the assigned heat transfer rate to a minimum of 2 MW for the PGEN.

The design efficiency of the pump is fixed at 0.85 - whilst the design inlet and outlet pressures are reported as 1.1 and 25 bar, respectively, in the design documents. The outlet pressure of the pump can also be adjusted by the PGEN control philosophy to be between 10 and 25 bar. The pump can deliver a maximum flow rate of 45 kg/s but has a design flow rate of 32 kg/s where the required pump power is 130 kW.

The turbine design point efficiency is also reported as 0.85 - along with a design point outlet pressure of 1.5 bar. The turbine efficiency is expected to vary in off-design conditions with changes in working fluid flow rate and density, which is described in the next section.

The evaporator has a relative pressure drop, at design conditions, between the inlet and outlet of 0.9 -. The minimum pinch point temperature achievable in the evaporator, T_{evap}^{PP}, is 10 ℃. For the design and off-design performance analysis, the cooling water will exit the evaporator at a temperature 150 ℃, which is the lower limit of the operational envelope as reported in an earlier section. In future chapters, this value is adjusted through the formulated control philosophies. The flow rate of both of the fluids entering the evaporator can be controlled to achieve a degree of superheat between 5 ℃ and 20 ℃ on the exit of the evaporator.

The condenser has a relative pressure drop, at design conditions, between the inlet and outlet of 20%. The cooling rate in the condenser is also controlled to the extent that the working fluid exits the condenser at 20 ℃ below the saturation temperature.

Table 3-3: PGEN Operational Limits and Design Parameters

Parameter	Limitation/Parameter	Unit
Assigned Heat Transfer	$2 \leq \dot{Q}_{PGEN} \leq 20$	MW
Pump		
Efficiency	$\eta_p = 0.85$	-
Inlet Temperature	$T_{p,i} = 35$	℃
Inlet Pressure	$P_{p,i} = 1.1$	bar
Outlet Pressure (design)	$P_{p,o} = 25$	bar
Outlet Pressure Range	$5 \leq P_{p,o} \leq 25$	bar
Maximum Flow Rate	$\dot{m}_{wf,max} = 45$	kg/s
Design Flow Rate	$\dot{m}_{wf,max} = 32$	kg/s
Pump Power at Design	$\dot{W}_{wf,p} = 130$	kW
Turbine		
Turbine Design Point Efficiency	$\eta_{t,des} = 0.85$	-
Outlet Pressure	$P_{t,o} = 1.5$	bar
Evaporator		
Relative Pressure Drop	$P_{e,o}/P_{e,i} = 0.9$	-
Pinch Point Temperature	$T_{evap}^{PP} \geq 10$	℃
Degree of Superheat for Working Fluid	$5 \leq T_{evap}^{*} \leq 20$	℃
Cooling Water Temperature Out Setpoint	$T_{hs,set} = 150$	℃
Design UA	$UA_{des} = 260\,000$	W/K
Condenser		
Relative Pressure Drop	$P_{c,o}/P_{c,i} = 0.8$	-
Degree of Subcooling for Working Fluid	$T_{cond}^{*} = 20$	℃
Cooling Water Circulation Pumps		
Efficiency	$\eta_{cwp} = 0.75$	-
Design Flow Rate	$\dot{m}_{des} = 80$	kg/s
Closed System Pressure Drop at $\dot{m}_{des}$	$\Delta P = 5$	bar

Should the flow to the PGEN at any stage be such that the PGEN can't operate within its heat transfer capability, a trip will occur to limit potential damage to process critical equipment such as turbines and pumps. A trip refers to any event where the PGEN does not transfer any heat from the cooling water and, therefore, also does not generate any power.

A trip occurrence is harmful to PGEN components, such as the turbine [25]. To ensure that frequent trips are avoided, a delay is typically introduced. This prevents start-up of the PGEN in operational conditions where the heat is not sufficient to maintain continuous operation.

3.4.2 PGEN Operational Performance Model

The waste heat profile illustrated in previous sections will result in a fluctuating heat source profile for the Rankine cycle. An off-design operational analysis needs to be considered with the formulation of a suitable control philosophy.

3.4.2.1 PGEN Component Models

Each component within the PGEN needs to have a mathematical representation in the comprehensive performance model of the PGEN. This will ensure that adjustments to controllable and non-controllable variables are accounted for.

Cycle Pump

The pump process from 1 to 2 in Figure 3-9 can be described by:

$$\dot{W}_p = \frac{\dot{m}_{wf} \cdot (h_{2s} - h_1)}{\eta_p} \tag{3.13}$$

Where the isentropic specific enthalpy of the working fluid after the compression through the pump and the inlet specific enthalpy of the working fluid is denoted by $h_{2s}\left[\frac{kJ}{kg}\right]$ and $h_1\ \left[\frac{kJ}{kg}\right]$, respectively. The mass flow of the working fluid is also represented with $\dot{m}_{wf}\ \left[\frac{kg}{s}\right]$.

The specific enthalpy on the inlet of the pump can be determined from the temperature and pressure of the working fluid. The entropy at the inlet can also be determined using the same inputs. The inlet entropy and outlet pressure can then be used to determine the isentropic specific enthalpy on the outlet.

Alternatively, if the required mass flow rate of the working fluid is known along with the required outlet pressure from the PGEN control philosophy, the following formula can be used:

$$\dot{W}_p = \frac{\dot{m}_{wf}}{\rho_{wf}} \cdot P_2 \cdot \frac{1}{\eta_p} \tag{3.14}$$

Where ρ_{wf} is the density of the working fluid and P_2 is the required outlet pressure of the cycle pump.

The design pressures and temperature for the working fluid are provided in Table 3-3.

Evaporator

The evaporator is the component between point 2 and 3 in Figure 3-9. Stated in Table 3-3, the pressure ratio between the inlet and the outlet of the evaporator, under design conditions, can be rearranged to:

$$P_3 = 0.9 \cdot P_2 \tag{3.15}$$

Note that the pressure P_2 is the outlet pressure of the cycle pump described above.

The heat transfer in the evaporator can be described with:

$$\dot{Q}_{evap} = \dot{m}_{wf} \cdot (h_3 - h_2) = \dot{m}_{hs} \cdot Cp_{hs} \cdot \left(T_{hs,i} - T_{hs,set}\right) = UA_t \cdot LMTD \tag{3.16}$$

Where Cp_{hs} and $\dot{m}$ are the average specific heat capacity for the cooling water and mass flow of each fluid as indicated with the subscripts, respectively. Since a phase change is expected for the working fluid the enthalpies at the inlet and outlet ($h_2, h_3 \left[\frac{J}{kg}\right]$), is used. The enthalpies are determined from temperature and pressure parameters. For the design analysis, it is assumed that the outlet temperature of the cooling water is the same as the target temperature, $T_{hs,set}$.

Since the mass flow of both the working fluid and heat source is expected to vary over time, the evaporator also needs to be analysed in off-design conditions. The approximation by Dal Magro [46] is used to adjust the overall heat transfer coefficient, UA based on differences between the current and design mass flows of both the cooling water and working fluid. The approximation is:

$$UA_t = UA_{des} \cdot \left(\frac{\dot{m}_{wf,t}}{\dot{m}_{wf,des}}\right)^{0.4} \cdot \left(\frac{\dot{m}_{hs,t}}{\dot{m}_{hs,des}}\right)^{0.4} \tag{3.17}$$

Where the subscript “des” indicates the design specification for the different parameters.

The temperature on the outlet of the evaporator, T_3, has, as shown in Table 3-3, a degree of superheat. The value of T_3 is determined by first determining the saturation temperature of the working fluid as shown in (3.17), where $X\,[-]$ represents the quality of the fluid. The temperature exiting the evaporator can then be determined with (3.18) by adding the degree of superheat.

$$T_{evap,sat} = f(X = 0, P_3) \tag{3.18}$$

$$T_3 = T_{evap,sat} + T^*_{evap} \tag{3.19}$$

Turbine

Work is done on the turbine through the movement of the working fluid moving through it from point 3 to 4. The mechanical power generated by the turbine can be determined through:

$$\dot{W}_t = \dot{m}_{wf}(h_3 - h_4) = \dot{m}_{wf}(h_3 - h_{4s}) \cdot \eta_t^* \tag{3.20}$$

Where $h_3 \left[\frac{kJ}{kg}\right]$ and $h_4 \left[\frac{kJ}{kg}\right]$ are the specific enthalpy of the working fluid entering and exiting the turbine. The specific enthalpy of the working fluid on the exit of the turbine for an isentropic expansion process is represented with $h_{4s} \left[\frac{kJ}{kg}\right]$. The efficiency of the turbine is represented with $n_t^* [-]$. At design conditions, $\eta_t^* = n_{t,des} = 0.85$ as stated in Table 3-3.

The turbine selection typically depends on the thermodynamic properties and flow rate of the fluid at the design point along with other factors such as power required and volumetric expansion ratio [51].

It follows that the turbine isentropic efficiency in off-design conditions is expected to change. The study by [51] included both a design and off-design performance analysis for a Rankine cycle that is supplied by a medium temperature heat source. The model used to determine the turbine efficiency in off-design conditions is used in this study.

The isentropic efficiency for the turbine in off-design conditions can be calculated through (3.21) [51].

$$\eta_t^* = \eta_{t,des} \cdot \sin\left[0.5\pi \left(\frac{\dot{m}_{off}\rho_{des}}{\dot{m}_{des}\rho_{off}}\right)^{0.1}\right] \tag{3.21}$$

Where η_t^* is the off-design turbine isentropic efficiency and ρ and $\dot{m}$ is the density and mass flow of the working fluid. The subscripts “des” and “off” refers to the design and off-design values, respectively.

Condenser

The condenser represents the part of the cycle between point 4 and 1. As stated in Table 3-3, the pressure ratio between the inlet and the outlet of the condenser, under design conditions, can be rearranged to:

$$P_1 = 0.8 \cdot P_4 \tag{3.22}$$

Note that the pressure P_4 is the outlet pressure of the turbine described above.

The heat transfer in the condenser can be described with:

$$\dot{Q}_{cond} = \dot{m}_{wf} \cdot (h_4 - h_1) \tag{3.23}$$

Where the inlet specific enthalpy, h_4, is the specific enthalpy on the outlet of the turbine as described above.

Cooling Water Circulation Pump

Additional equipment is fitted to the system that need to be accounted for when the determining the nett power generation from PGEN. The cooling water circulation pump power is drawn from the same source the PGEN supplies and is thus a consumer. Should the PGEN be unavailable with no power generation, then the nett power consumption is negative due to the pump power required to sustain the desired cooling water flow rate.

$$\dot{W}_{cwp} = \frac{\dot{m}_{cw} \cdot \Delta P}{\rho_{cw} \cdot \eta_{cwp}} \tag{3.24}$$

Note that the cooling water flow rate will influence the system pressure drop with an increase in flow rate expected to result in an increase in pressure drop across the system [12].

Thermal Efficiency:

The collective system model performance can be evaluated with the thermal efficiency. The thermal efficiency, η_{th}, is the ratio of the nett power generation, $\dot{W}_{nett} = \dot{W}_t - \dot{W}_p - \dot{W}_{cwp}$ [W], to the total heat supplied at the evaporator, $\dot{Q}_{evap}$ [W], as shown below;

$$\eta_{th} = \frac{\dot{W}_{nett}}{\dot{Q}_{evap}} \tag{3.25}$$

The efficiency can be influenced by various parameters, such as the heat source temperature and flow rate, the evaporating pressure and degree of superheat at the outlet of the evaporator.

3.4.2.2 PGEN Off-Design Operational Model Results

The above component models can be combined into a comprehensive model that will describe the performance of the PGEN. From Table 3-3 it is observed that the outlet pressure of the cycle pump and degree of superheat at the evaporator can be controlled within an allowable range for each. These adjustments will have an influence on the thermal efficiency and nett power generation of the cycle.

The purpose of this section is to illustrate the performance of the PGEN cycle over varying cooling water flow rates and temperature. A fixed outlet pressure and degree of superheat will, therefore, be assigned. In future chapters, these parameters, among others, is adjusted by the relevant control philosophy.

To illustrate the performance of the PGEN across varying heat source parameters, a 3D surface map is populated with the results of a parametric study. The models in 3.4.2.1 are used. The volume flow rate of the cooling water is varied between 5 and 115 kg/s whilst the temperature of the cooling water entering the evaporator is varied between 150 ℃ and 210 ℃.

The pressure for the working fluid entering the evaporator is set at 22.8 bar while the degree of superheat is maintained at 20 ℃. The results of this parametric study are illustrated in Figure 3-10 below.

From the figure it can be argued that an increase in mass flow and temperature typically increases the thermal efficiency of the system. A relatively small reduction in thermal efficiency for the PGEN is noted at the high end of both the mass flows and temperatures.

By accurately predicting the thermal efficiency and performance of the PGEN with varying heat source parameters, a control philosophy can now be formulated to maximise power generation.

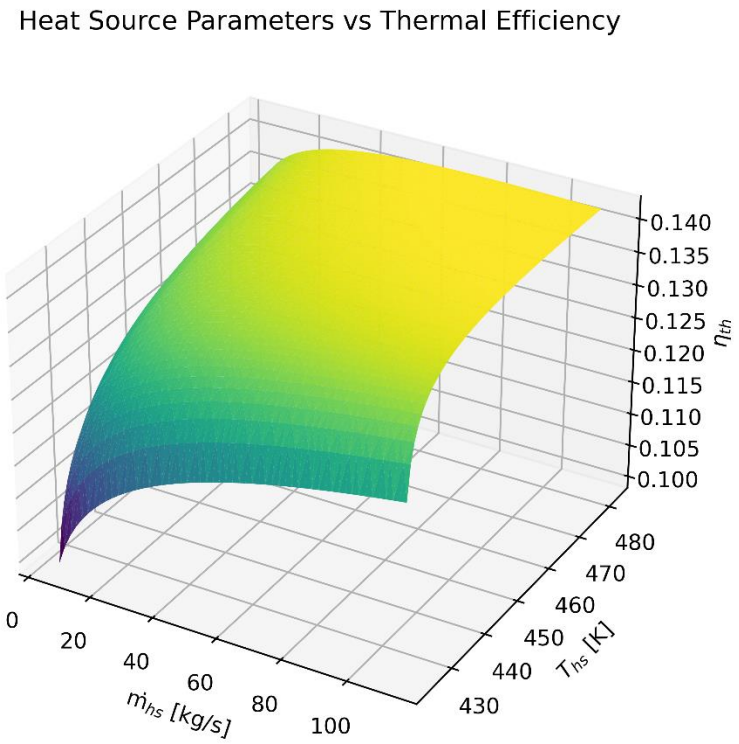


Figure 3-10: Thermal Efficiency vs Heat Source Parameters for $P_3 = 22.8$ bar and $T^*_{evap} = 20$ ℃

3.5 Heat Losses from Uninsulated Components

In the current system, there is uninsulated components between the outlets of the PGEN and ACHX components and the inlet of the gas cooler, as illustrated in Figure 3-11. The heat loss to the environment will result in a reduced temperature for the cooling water.

To ensure that the temperature entering the gas cooler, T_{cw2}, remains within the operational envelope, the temperature setpoint for the cooling water at both the PGEN and ACHX, T^{set}, needs to consider this reduction. It is thus necessary to accurately quantify the heat loss.

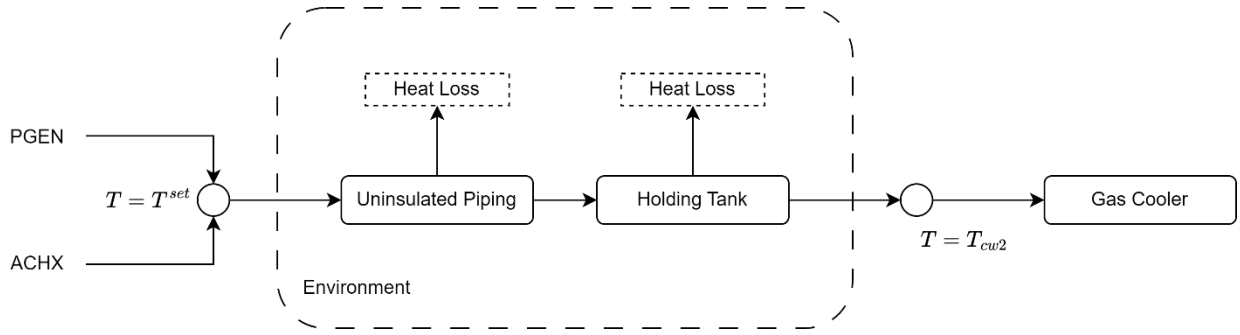


Figure 3-11: Heat Loss to the Environment Between PGEN, ACHX and the Gas Cooler

3.5.1 Details on Uninsulated Components

The theory of heat transfer mechanisms due to radiation, conduction and natural convection, which is used in this section, is supplied in Chapter 2.1.7. The properties of the uninsulated piping and tank before the gas cooler inlet are provided in Table 3-4.

Table 3-4: Uninsulated Components Between PGEN and ACHX and the Gas Cooler

Parameter	Value	Unit
Piping		
Exposed Length	30	m
Inner Diameter	0.33	m
Pipe Thickness	12.06	mm
Thermal Conductivity	58	
Emissivity	0.9	-
Holding Tank		
Volume	5	m^3
Diameter	1.6	m
Length	2.5	m
Thickness	40	mm
Thermal Conductivity	58	
Emissivity	0.3	-
Orientation (Direction of cylindrical axis)	Horizontal [1]	-

The total exposed length of the uninsulated pipes is 30 m, all with an outer diameter of 0.33 m. The pipe thickness is 12.06 mm, and the pipe material has a thermal conductivity of

[1] Required to assign characteristic length dimension and appropriate empirical formulations

63.9 $\left[{}^{\mathrm{W}}/_{\mathrm{m}^2 \cdot \mathrm{k}}\right]$. The pipe is also coated for visual identification amongst the other pipes in the vicinity, resulting in a surface emissivity of 0.9 -, which is in accordance with Table 1-6 in [12].

The tank has a volume of 5 m^3 with an inner diameter of 1.6 m and a length of 2.5 m. The thickness of the tank wall is 40 mm whereas the exposed surface is uncoated and has a surface emissivity of 0.3 -. Note that the orientation of the tank is that axial direction is horizontal. This information is required to correctly assign characteristic lengths as required in Chapter 2.1.7.

This section will demonstrate the effect that the cooling water temperature has on the heat loss from the system. The control philosophies in this thesis will use this section to determine a suitable setpoint temperature for the combined heat transfer process of the PGEN and ACHX.

3.5.2 Quantifying Heat Loss to the Environment

The approach to determine the heat loss from the uninsulated components are described concisely in this section. The approach with calculations is supplied in Appendix B.

3.5.2.1 Thermal resistance network

As stated in Chapter 2.1.8, the heat transfer mechanisms can be depicted as resistances, where equations (2.33-35) can be used to quantify the resistance to heat transfer. Using the resistance analogy, equation (2.35) can be used to determine the rate of heat transfer. The thermal resistance network for the heat loss from the piping are illustrated in Figure 3-12. The same layout can be used to describe the thermal resistance for heat loss from the tank.

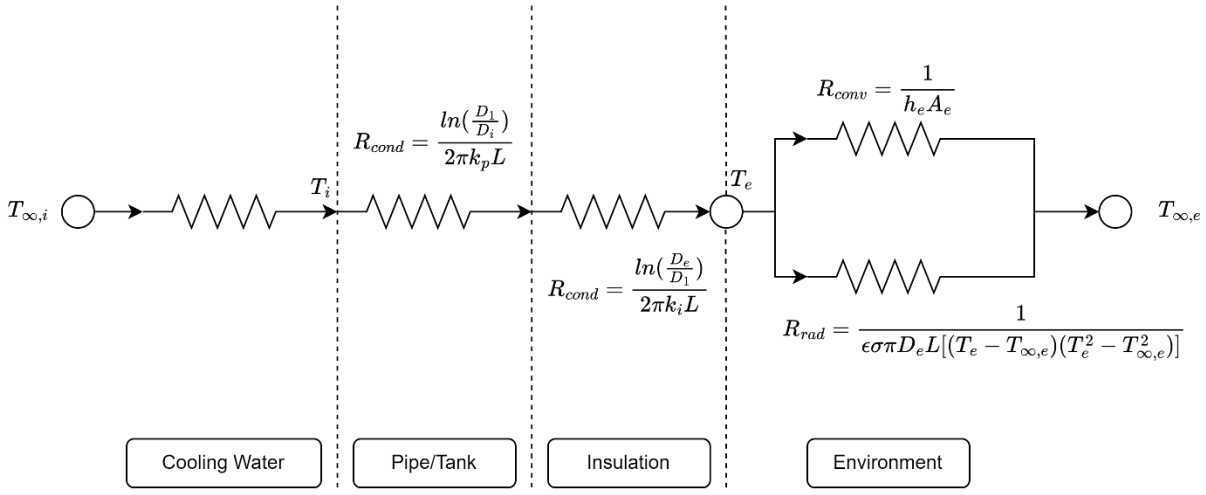


Figure 3-12: Thermal Resistance System for Heat Loss through Pipe and Tank

There is resistance to convective heat transfer from the cooling water to the inner surface of the pipe, whereafter there is a conductive heat transfer resistance through the pipe/tank material and any other materials until the exposed surface is reached. Note that for the currently uninsulated piping and tank in this system, this resistance is zero.

From the external surface the heat transfer resistance becomes parallel with one branch describing the convective heat transfer resistance due to natural convection whereas the other describes the radiative heat transfer resistance.

3.5.2.2 Assumptions

The Dittus-Boelter equation for determining the convective heat transfer properties of a fluid in a pipe are only valid for fully developed flow in a straight, smooth pipe where it assumes a uniform velocity profile [9]. Due to the absence of a comprehensive CFD model of the current tank system, the internal fluid dynamics and thus convective heat transfer coefficients cannot be accurately determined.

It is thus assumed that the internal convective heat transfer resistance for the tank is negligible. This results in the assumption that the internal surface temperature T_i is the same as the cooling water temperature and thus $T_i = T_{\infty,i}$.

3.5.2.3 Formulating the model

Through applying the principle of conservation of energy, with the assumptions made above, the following equation can be determined for the control volume illustrated in Figure 3-12:

$$\dot{Q}_{\infty,i}^{conv} = \dot{Q}^{cond} = \dot{Q}_{\infty,e}^{conv} + \dot{Q}^{rad} \tag{3.23}$$

By assigning the equations in (2.33–2.36) to equation (3.23), the following equations are obtained for the pipe and tank heat loss model:

$$\frac{2k\pi L(T_i - T_e)}{\ln\left(\frac{D_e}{D_i}\right)} = h_e A_e\left(T_{\infty,e} - T_e\right) + \frac{T_e - T_{\infty,e}}{\epsilon\sigma\pi D_e L\left(T_e + T_{\infty,e}\right)\left(T_e^2 + T_{\infty,e}^2\right)} \tag{3.24}$$

$$\frac{2k\pi L(T_i - T_e)}{\ln\left(\frac{D_e}{D_i}\right)} = h_i A_i\left(T_{\infty,i} - T_i\right) \tag{3.25}$$

With T_e and T_i the unknown external and internal surface temperatures respectively. The internal and external convection coefficients, h_i and h_e, are determined based on convective heat transfer theory provided in Chapter 2. The internal and external heat transfer area is denoted with A_i and A_e while the temperature of the cooling water and ambient air is denoted with $T_{\infty,i}$ and $T_{\infty,e}$ respectively. The geometrical properties of internal and external diameter and length are represented with D_i, D_e and L. The emissivity of the exposed surface is represented with ϵ while σ represents the Stefan-Boltzmann constant of $5.67 \times 10^{-8}\left[\frac{W}{m^2K^4}\right]$.

Note that equation (3.25) will not be used to determine the heat loss at the tank, only (3.25) will apply.

3.5.2.4 Iterative Solution

A demonstration of the iterative solution is supplied in Appendix B.

The equations of (3.24) and (3.25) are solved iteratively by assigning initial values and updating both ambient air and cooling water properties each iteration until convergence is achieved. After solving equation (3.24) and (3.25) for the piping system, the heat loss for the piping system is quantified. This heat loss is used to determine the temperature of the water entering the tank.

The equations of (3.24) is solved iteratively for the tank section by again assigning initial values and updating the ambient air properties each iteration until convergence is achieved. After a converged solution is obtained, the heat loss from the tank is quantified. The heat loss from the tank is used to determine the exit temperature of the cooling water. This exit temperature is the temperature at which the cooling water enters the gas cooler.

The model briefly discussed above and demonstrated in Appendix B is used to perform a parametric study. This parametric study can be used to illustrate the influence the setpoint temperature $\mathrm{T}^{\mathrm{set}}$ and mass flow rate $\dot{\mathrm{m}}_{\mathrm{hs}}$ of the cooling water has on the heat loss from the uninsulated components in the system.

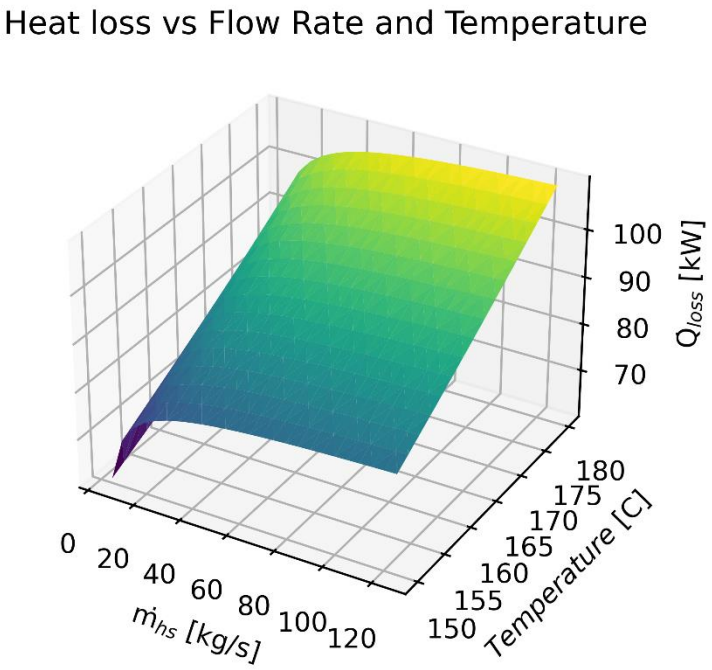


Figure 3-13: Heat Loss versus Temperature and Mass Flow Rate of Cooling Water

Note that as the temperature and mass flow rate increases, the heat loss from the uninsulated piping and tank also increases. The effect of the flow rate on the internal convection coefficient is also noted through the non-linearity with which the heat loss increases as the flow rate is increased.

This model can now be used to determine the required setpoint temperature, which is illustrated in the next chapter.

3.6 Unplanned trip events

The importance of the heat rejection process in the main production process has been described in detail in previous sections. The flue gas leaving the gas cooler needs to be within the safe operational temperature envelope. This is achieved by controlling the temperature and flow rate of the cooling water entering the gas cooler.

It is shown in earlier sections of this chapter that a loss in the heat rejection capacity of the cooling system can result in elevated temperature values for T_{cw2}, potentially cause the cooling water temperature to move outside the operational envelope. This increases the risk of disruptions to the production process.

An unplanned stoppage is an unexpected and sudden halt in the normal operation of a process that causes disruptions and potential production delays. For PGEN, this results in a loss of heat transfer capacity and power generation. To evaluate the performance of the control formulation adapting to sudden changes in the total heat transfer capability, an unplanned trip event for the PGEN is simulated at the same period for all control formulations.

An average mean time between failure (MBTF) for the PGEN used in this study indicates that no more than one unplanned event can be introduced for both profiles [52]. Trips due to low heat availability will also be included as discussed in the previous sections.

Since the heat source is fluctuating in nature, it can be argued that the impact of an unplanned trip on cooling water temperatures entering the gas cooler is dependent on the flow parameters and distribution at the time of the trip occurrence. It is, therefore, important to evaluate the impact of each trip event to ensure that the formulated control algorithm will result in sufficient heat transfer at all times.

It can be argued that an unplanned trip at peak heat transfer requirements is more difficult to adapt to for the formulated control philosophies. Since only one unplanned trip can be introduced for both the historical and demonstrative datasets, an unplanned trip will be forced at peak heat transfer requirements.

The historical dataset experienced an unplanned trip event at 26.75 days during a heat transfer requirement of 20 MW. For the demonstrative dataset, an unplanned event will occur at 60 min where the required heat transfer is at the peak of 20 MW.

3.7 Conclusion

This chapter provides a comprehensive summary of the cooling cycle layout. The need for stringent requirements from the control formulations are also briefly described. It is argued from conservation equations that any sudden unavailability of heat transfer capacity can result in elevated temperatures for the cooling water entering the gas cooler.

Operational temperature envelope and process limits are provided for both the flue gas and cooling water in the gas cooler. The fluctuating waste heat profile to be used in this thesis is also provided along with a brief description on how it is populated. A demonstrative dataset is also provided with the aim of illustrating changes in flow distributions and resulting temperatures for each control philosophy. The performance of the formulations in the chapters to follow will still be evaluated on the historical dataset.

The ACHX design parameters are provided along with suitable models to determine the heat transfer rate with or without forced convection. The models are used to populate a performance prediction that can be used by a control philosophy to determine the number of fans required along with the operational speed. The model can also be used to determine the required cooling water flow distribution when multiple heat rejecting components are considered.

The PGEN design parameters are also provided along with the operational limitations. Models are provided for each component within the PGEN cycle, after which a parametric study is completed for a given evaporating pressure and degree of superheat.

The model to determine the heat loss from the uninsulated components are also described and illustrated for the range of temperatures and mass flow rates expected in the system. This model will enable the adjustment of setpoint temperatures for the PGEN and ACHX to ensure that the operational envelope is maintained.

Lastly, the unplanned trip event is discussed. An unplanned trip needs to be forced at a peak heat transfer requirement to ensure that any formulated control philosophy can adapt to a sudden loss in heat transfer capability without causing the flue gas temperature to move out of the operational temperature envelope.

A summary of the progress made to the formulation of the novel control algorithms in this chapter are illustrated in Figure 3-14.

The fixed line blocks indicate the models/information supplied in this chapter. In this chapter, the focus is on the fluctuating waste heat profile together with the operational temperature envelope of the gas cooler. The models used to determine the ACHX and PGEN performance are also supplied along with a model that determines the heat loss from the uninsulated piping in the system.

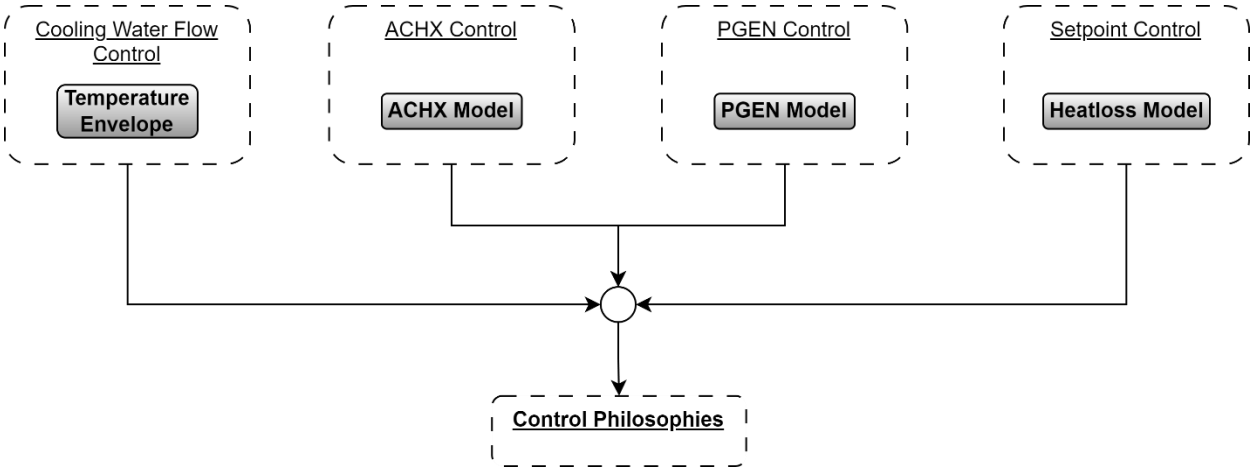


Figure 3-14: Progress to Control Algorithms after Chapter 3

In the next chapter, the performance models will be used to formulate control philosophies for both the PGEN and ACHX that controls the heat transfer internally. The operational envelope and heat loss models will also be used to determine suitable values for the setpoint parameters in the control algorithms.

Only after these formulations have been completed can a comprehensive control philosophy be formulated that manages the flow distributions and assigned heat transfer requirements.

CHAPTER 4 RECURRING COMPONENT CONTROL PHILOSOPHIES

This section demonstrates the formulation of the recuring control philosophies for the individual components that is used in control philosophies in later chapters.

4.1 Flue Gas Temperature Control Philosophy

The cooling water temperature entering the gas-cooler is a direct result of the heat rejection components, such as the PGEN and ACHX, attempting to remove all the absorbed heat from the cooling water. Failing to do so will result in higher temperatures for the cooling water which in turn influences the heat transfer rate obtained in the gas-cooler. Any change in the heat transfer rate can be rectified by altering the mass flow rate of the cooling water.

4.1.1 Cooling Water Flow Control (CWFC)

To ensure that the maximum heat is recovered from the flue gas, the control philosophy will need to react to the exiting flue gas temperature and adjust the cooling water flow rate accordingly. This control philosophy is illustrated in Figure 4-1.

This control philosophy is inherent to the plant design and operation and features as described below in all subsequent control philosophies unless changes to it are explicitly mentioned.

The time index for the formulation is given by $\mathrm{T} = \{1,2,\dots,|\mathrm{T}|\}$. The flow rate of the cooling water at time t, $\dot{\mathrm{m}}_{\mathrm{hs,t}}\,\mathrm{kg/s}$, is initialised as the flow rate at time $\mathrm{t}-1$, $\dot{\mathrm{m}}_{\mathrm{hs,t-1}}\,\mathrm{kg/s}$. The flue gas temperature at time $\mathrm{t}-1$, $\mathrm{T}_{\mathrm{fg,t-1}}$℃, is used to determine whether or not there is a need to adjust the flow rate and, if required, the magnitude of this adjustment. Additional input parameters to the control philosophy include the desired setpoint of the flue gas on the exit of the gas cooler, $\mathrm{T}_{\mathrm{fg}}^{\mathrm{set}}$℃, as well as the temperature interval, $\Delta\mathrm{T}_{\mathrm{fg}}$ ℃, that is used to determine a level of deviation from the set temperature. The flow rate adjustment, $\Delta\dot{\mathrm{m}}_{\mathrm{hs}}\,\mathrm{kg/s}$, represents a fixed magnitude by which the flow rate can be increased or decreased.

If the flue gas exit temperature is higher than the desired flue gas setpoint and the difference between $\mathrm{T}_{\mathrm{fg,t-1}}$ and $\mathrm{T}_{\mathrm{fg}}^{\mathrm{set}}$ is larger than $\Delta\mathrm{T}_{\mathrm{fg}}$, the outlet flue gas temperature is deemed too high. An increase in cooling water flow rate is required to increase the heat transferred from the flue gas. However, if the flue gas exit temperature is lower than the desired flue gas setpoint but the difference is still larger than $\Delta\mathrm{T}_{\mathrm{fg}}$, the outlet flue gas temperature is deemed too low and a decrease in cooling water flow rate is required to decrease the heat transferred from the flue gas. If the difference between the flue gas exit and setpoint temperature is below $\Delta\mathrm{T}_{\mathrm{fg}}$, no adjustment to the cooling water flow rate is required.

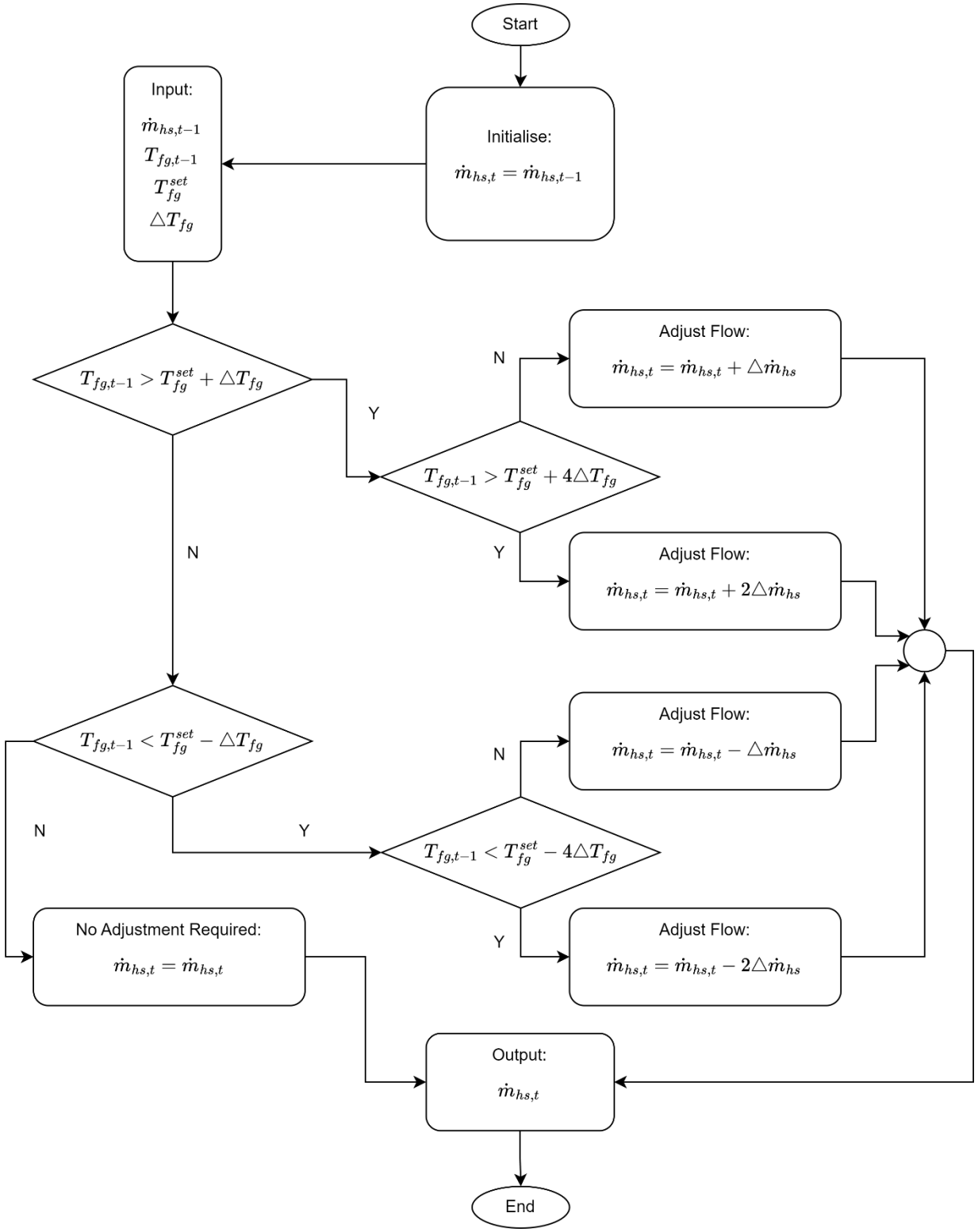


Figure 4-1: Cooling Water Flow Control Based on Flue Gas Temperature Exiting the Gas Cooler

If an increase in flow rate is required but the difference between T_{fg}^{set} and $T_{fg,t-1}$ is less than $4\Delta T_{fg}$ the flow rate is only increased by $\Delta \dot{m}_{hs}$. However, if the difference is more than $4\Delta T_{fg}$ then the cooling water flow rate is increased by $2\Delta \dot{m}_{hs}$. The same approach is followed if a decrease in flow rate is required.

4.1.2 CWFC Results on Demonstrative Dataset

The CWFC formulated in the previous section can now be applied to the demonstrative dataset to determine the cooling water flow rate and temperatures that will enter the PGEN and ACHX components.

Note that the operations of CWFC is inherent to the current Works philosophy and its actual operations can thus be investigated by evaluating the historical dataset, which is in the next section. No gas cooler model specific to this plant is currently available to determine the heat transfer efficiency and, therefore, the CWFC will not be adjusted in the novel algorithms unless explicitly stated.

For this demonstration, the values of $\Delta\dot{m}_{hs}$ and ΔT_{fg} are set at 5 kg/s and 5 ℃, respectively. It is also assumed that the cooling water entering the gas-cooler is at 150 ℃. The flue gas setpoint temperature is 210 ℃. A setpoint temperature too close to the upper or lower limit can potentially result in operation outside the temperature envelope, if the cooling water cannot adjust in time.

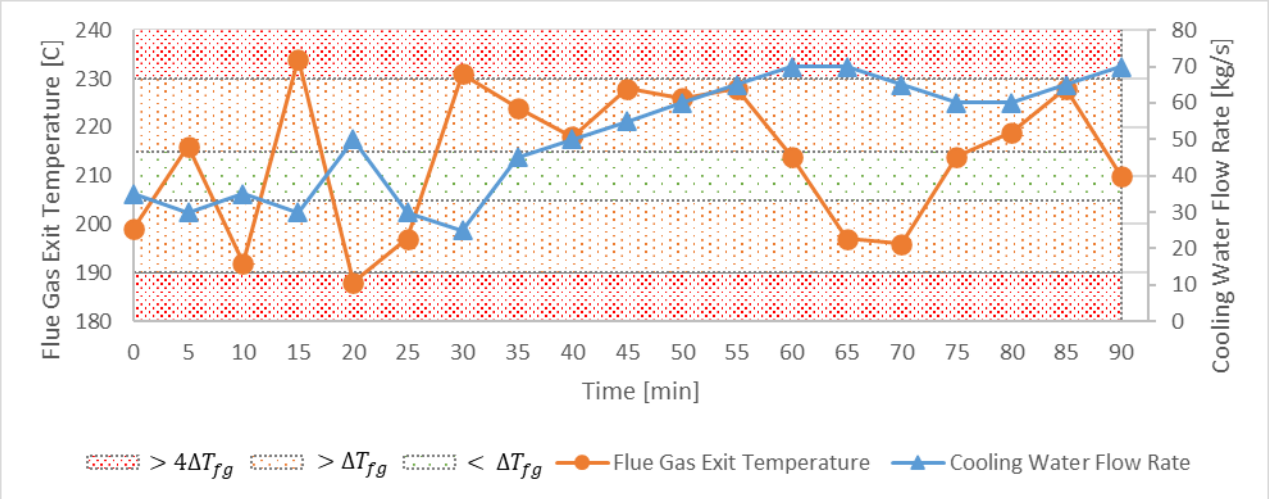


Figure 4-2: Cooling Water Flow Rate Adjustments through CWFC

The horizontal lines in Figure 4-2 indicate the thresholds that are used in CWFC to determine the change in flow rate required. It is clear that there is no change in flowrate at $t+1$ where the temperature is within 5 ℃ of 180 ℃ at time t. This is noted in the 60 – 65 min and 75 – 80 min periods, with the adjustment of cooling water flow made throughout the rest of the dataset since the temperature for all other time periods are outside the threshold of ΔT_{fg} from T_{fg}^{set}. At time 15,20 and 35 min, the flue gas exit temperature is more than the threshold of $4\Delta T_{fg}$ from T_{fg}^{set}. This results in a significant change in flow rate being made at 20,25 and 40 min to reduce the difference between the setpoint and actual flue gas exit temperature.

Note that in the time periods between 35 and 60 min, the cooling water flow rate increases gradually throughout all time periods since the flue gas exit temperature is above the 185 ℃

threshold. This is consistent with the increase in available waste heat noted in Figure 3-3 and Figure 3-4.

From the resulting cooling water flow in Figure 4-2, it is clear that CWFC can control the temperature of the flue gas to fluctuate within a given threshold around the desired setpoint for a given dataset. Suitable input parameters for ΔT_{fg} and T_{fg} will be specific to the production process. It is, therefore, expected that the input parameters of ΔT_{fg} and T_{fg} will be adjusted for in the historical dataset to always ensure compliance to the operational temperature envelope.

The temperature of the flue gas exiting the gas cooler indicates only the performance of the heat transfer process in terms of the operational temperature envelope. To evaluate the amount of heat transferred, the flow rate of the flue gas through the gas-cooler is considered.

The performance of CWFC is illustrated in Figure 4-3. The heat transferred to the cooling water is illustrated with the required ranges for the heat transfer, as shown in Figure 3-4.

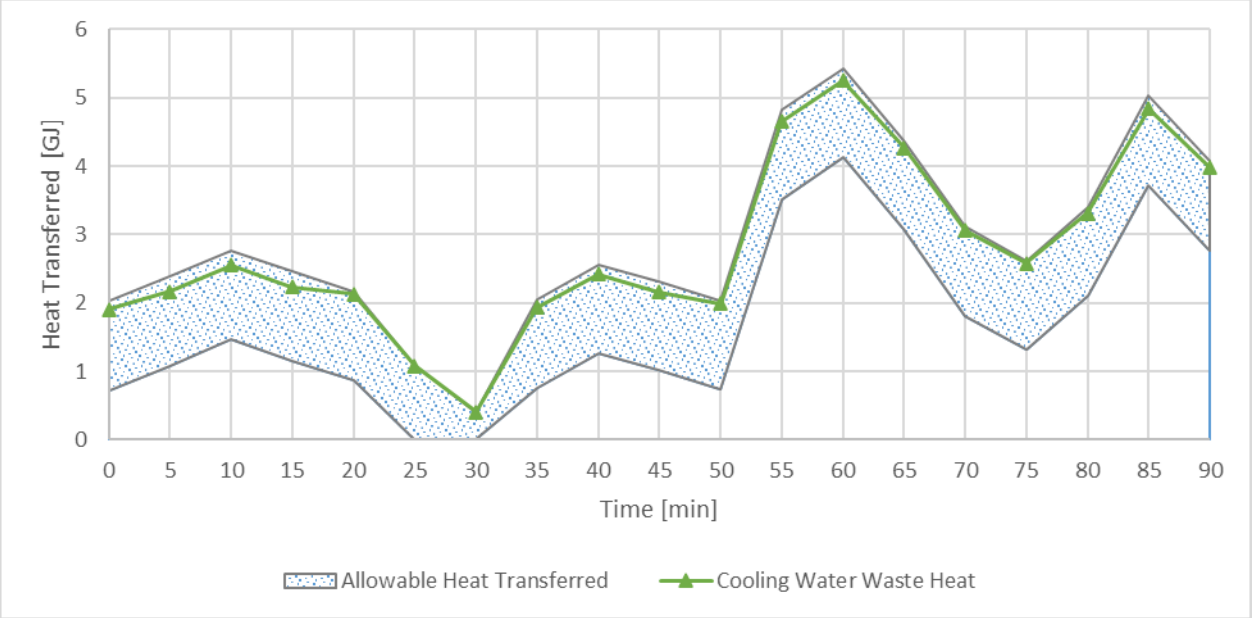


Figure 4-3: Heat Transferred in Gas Cooler at Time t for CWFC

The heat transferred during each time step is within the allowable range at all times. This can be expected, since the temperature of the flue gas exiting the gas cooler is shown to be within the operational temperature envelope in Figure 4-2.

The maximum heat transfer occurs at 60 min where a total of 5.25 GJ is transferred to the cooling water. The maximum available heat transfer at this time is 5.43 GJ. The total heat transferred to the cooling water over the 90 min is 52.88 GJ, which is 95.95% of the total available heat of 55.11 GJ, as noted in Chapter 3.2.3.

This difference in energy available and energy transferred is thermal energy that is wasted. This is a due to the reactive nature of the CWFC and can only be addressed by having a predictive capability in the control formulation and pro-actively adjusting the cooling water flow rate.

4.2 PGEN Control Philosophy

The PGEN component in the heat rejection cycle is described in the previous chapter. A surface graph is also supplied that shows the performance of the PGEN component for variations in cooling water flow rates and entering temperature. This graph is for a fixed outlet pressure of the cycle pump and degree of superheat on the evaporator exit. These two parameters have a significant influence on the thermal efficiency of the cycle [14]. This study is repeated to show the influence of both these parameters on the thermal efficiency in the sections below.

4.2.1 Changing the Outlet Pressure of the Cycle Pump

A change in outlet pressure at the cycle pump will result in changes to the pressure in the evaporator. A reduced pressure will result in a lower saturation temperature for the working fluid and, therefore, less heat will be required to reach the required degree of superheat on the evaporator outlet [23]. The opposite is also true for an increase in the outlet pressure.

The PGEN model formulated in Chapter 3.4.2 is used to illustrate the influence of the evaporating pressure on the thermal efficiency of the cycle. This is done by completing a parametric study where the evaporating pressure and heat source parameters are held constant while only the outlet pressure of the cycle pump is changed.

The results for a fixed cooling water flow rate of 60 kg/s and temperature of 200 ℃ is illustrated in Figure 4-4. The degree of superheat is also held constant at 10 ℃.

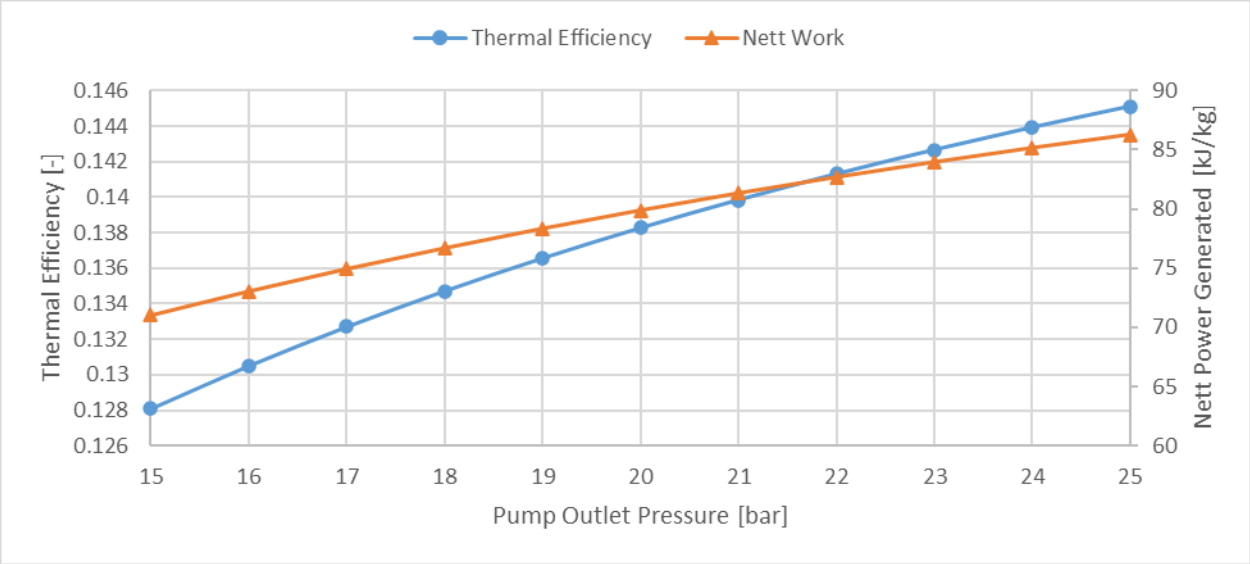


Figure 4-4: Thermal Efficiency of PGEN with a Varying P_3 at $T^*_{evap} = 10℃, \dot{m}_{hs} = 60\ \left[\frac{kg}{s}\right]$ and $T_{hs} = 200$ ℃

An increase in cycle pressure results in an increase in thermal efficiency for the cycle. The work done by the turbine per unit mass of working fluid also increases with an increase in pump outlet pressure. This corresponds with the study by Ata et al. [14].

4.2.2 Changing the Degree of Superheat on the Evaporator Exit

Lowering the required degree of superheat on the evaporator exit will result in a lower heat transfer requirement at the evaporator should the evaporating pressure be held constant [14]. Increasing the required degree of superheat will result in a higher heat transfer requirement under these conditions. Other cycle parameters such as the working fluid flow rate will need to adjust to maintain these parameters, which will have an influence on the overall cycle performance.

The PGEN model formulated in Chapter 3.4.2 is used to illustrate the influence of the degree of superheat on the thermal efficiency of the cycle. A parametric study is conducted where the pump outlet pressure and heat source parameters are held constant while only the degree of superheat at the evaporator is changed.

The results for a fixed cooling water flow rate of 60 $\left[\frac{\text{kg}}{\text{s}}\right]$ and temperature of 200 ℃ is illustrated in Figure 4-5. The pump outlet pressure is held constant at 20 $[\text{bar}]$.

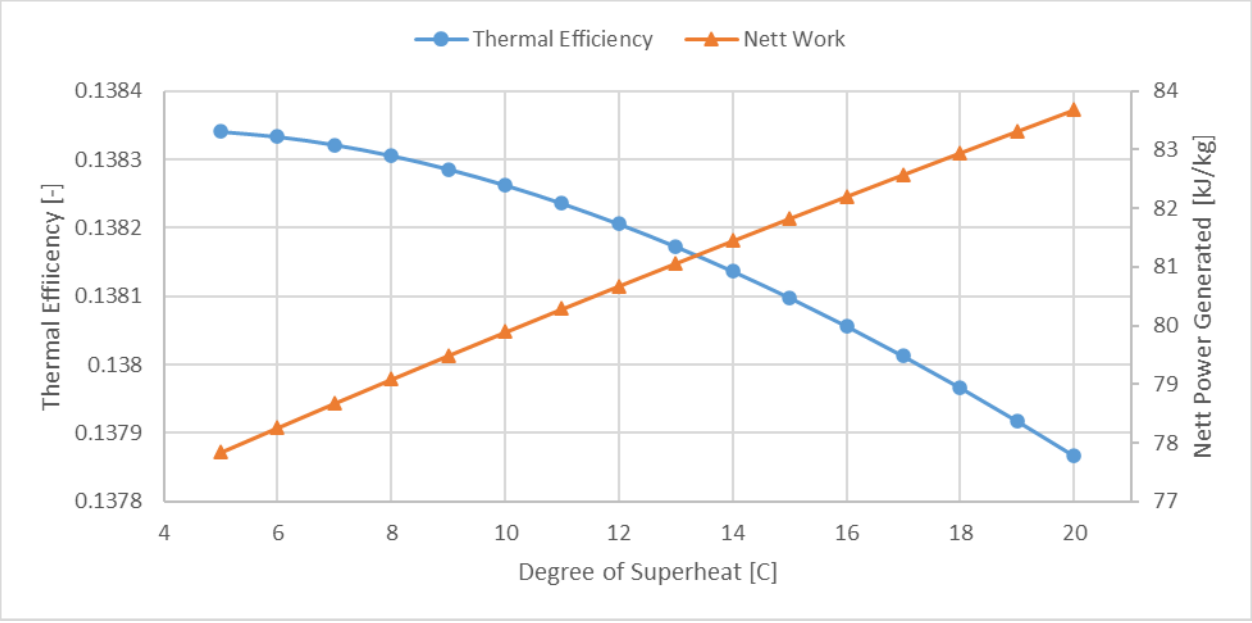


Figure 4-5: Efficiency of PGEN with varying T^{*}_{evap} at $P_{evap} = 20\ [\text{bar}], \dot{m}_{hs} = 60\ \left[\frac{\text{kg}}{\text{s}}\right], T_{hs} = 200$ ℃

An increase in the degree of superheat at the evaporator corresponds with a slight reduction in the thermal efficiency of the system. The increase in heat transfer required at the evaporator to maintain the degree of superheat also results in increased power generation per unit mass of working fluid. Both of these curves correspond with the study by [14].

4.2.3 Control Philosophy for Maximum Power Generation (PGCP)

The control philosophy in this section adjusts the cycle pump outlet pressure and degree of superheat to ensure that maximum thermal efficiency and thus power generation is achieved with the assigned cooling water flow rate and temperature. This control philosophy is referred to as Power Generation Control Philosophy (PGCP) and is illustrated in Figure 4-6.

The time index for the formulation is given by $T = \{1,2,\dots,|T|\}$. The cooling water at time t enters the PGEN at a temperature $T_{hs,t}$℃ and a mass flow rate of $\dot{m}_{hs,t}$ kg/s. The desired setpoint temperature for the cooling water leaving the PGEN cycle is also indicated and denoted as T_P^{set}℃. The required heat transfer rate, $\dot{Q}_P^*$ W, and total heat transfer over time t, Q_P^* J, is then calculated through equations similar to (3.3).

The pressure and degree of superheat in the evaporator at time t,$P_{evap,t}$ bar and $T_{evap,t}^*$℃, is initialised as the minimum of the allowable range, as indicated in Table 3-3. The calculated maximum power generated is also initialised as a zero value for comparison to further results.

The pressure and degree of superheat currently active is used to determine the desired evaporator exit temperature for the working fluid, $T_{wf,e} = T_3$. All the temperatures for the two fluids are known and thus the log mean difference in temperature ($LMTD$) is determined. Since there is a goal heat transfer rate at the evaporator, the desired UA_t can be determined after which the approximation of [46] is used to calculate the required mass flow rate for the working fluid, $m_{wf,t}$. This mass flow rate and evaporating pressure has a direct effect on the cycle pump power required and thus the nett power generation.

The PGEN model in 3.4.2 is then used to determine the predicted power generation, W_{nett} W, for the given cooling water parameters. If the evaporating pressure is still at the minimum, it is an indication that the degree of superheat is currently adjusted with the aim of maximising power generation. If the W_{nett} is more than W_{max}, then the degree of superheat value is stored as $T_{evap,max}^*$ ℃, after which it is increased within its range before the PGEN model is solved for again. If $W_{nett} < W_{max}$, then the stored values for degree of superheat and evaporating pressure are not updated. However, the degree of superheat is still increased to evaluate the entire allowable range.

After the allowable range for the degree of superheat has been evaluated, the evaporating pressure is iteratively increased. An increase in evaporating pressure also results in the resetting of the degree of superheat value, ensuring that the allowable range is tested again. This approach ensures that the entire allowable range of degree of superheat and evaporating pressure is evaluated before the values that will result in maximum power generation is identified.

The code for PGCP used in this study is provided in Appendix C.

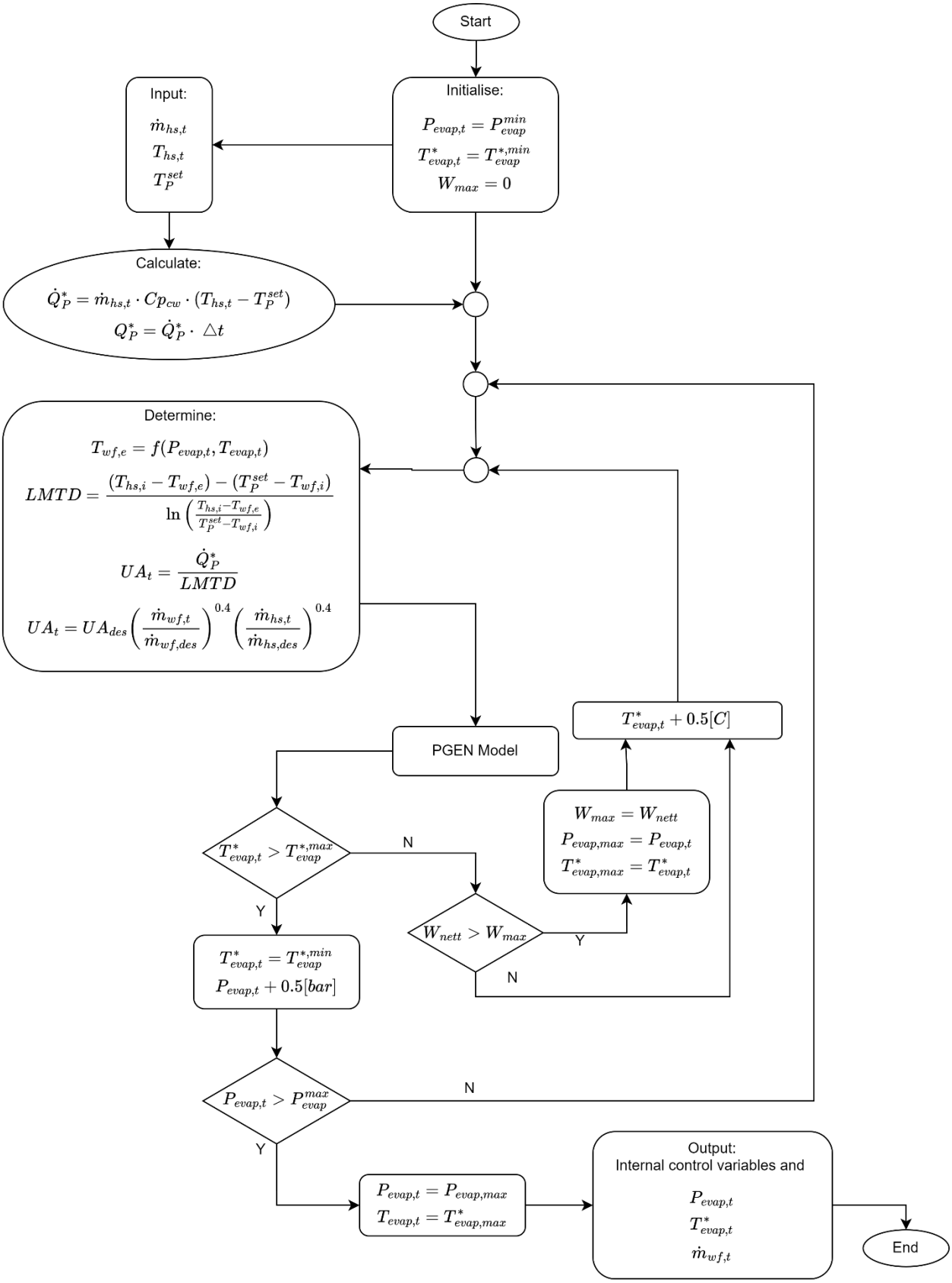


Figure 4-6: PGEN Control Philosophy (PGCP)

4.2.4 PGCP Results on Demonstrative Dataset

To illustrate the adjustment and performance changes of the control philosophy in this section, the demonstrative dataset is used. For the purpose of illustrating the performance of the PGCP, it is assumed that all the cooling water flow is directed to the PGEN component. The setpoint for cooling water return temperature is T_P^{set} =150 ℃.

Note that $T_P^{set} = T^{LL}$, since the PGEN and ACHX control philosophies are currently demonstrated separately. The outlet temperature of ACHX and heat losses to the environment, therefore, do not influence the control of PGEN for the purpose of this demonstration.

A section of the temperature and flowrate of the cooling water with the control philosophy results are given in Table 4-1 below. Graphs illustrating the PGEN operations for the timeline from $0 \leq t \leq 90$ min follow the table.

The results section of Table 4-1 reports the average heat transfer rate in the evaporator, where heat is removed from the cooling water, for time t. The desired evaporating pressure and temperature where maximum power generation is achieved are also displayed along with the mass flow rate for the working fluid during time t. The thermal efficiency and nett power generation for time t is also reported.

Table 4-1: Results for PGCP on Demonstrative Dataset

Demonstrative Dataset			**Results**					
$\mathbf{t}$	$\dot{\mathbf{m}}_{\mathbf{hs}}$ $\mathbf{kg/s}$	$\mathbf{T_{hs}}$ ℃	$\dot{\mathbf{Q}}_{\mathbf{evap}}$ $[\mathbf{MW}]$	$\mathbf{P_{evap}}$ $[\mathbf{bar}]$	$\mathbf{T^*_{evap}}$ ℃	$\dot{\mathbf{m}}_{\mathbf{wf}}$ $\mathbf{kg/s}$	$\boldsymbol{\eta}_{\mathbf{th}}$ $[-]$	$\dot{\mathbf{W}}_{\mathbf{nett}}$ $[\mathbf{MW}]$
0	35	193.5	6.355	18	17	10.911	13.22	0.840
5	30	207.7	7.213	19	19	12.160	13.60	0.981
10	35	208.3	8.510	18	20	14.403	14.22	1.210
⋮	⋮	⋮	⋮	⋮	⋮	⋮	⋮	⋮
80	60	194.1	11.026	19	8	19.652	14.92	1.645
85	65	209.5	16.137	21	5	28.577	15.41	2.487
90	70	195.4	13.257	20	5	23.7025	15.18	2.013

The first parameter to be evaluated is the power generated with the formulated control philosophy, as shown in Figure 4-7. The power generation with this philosophy is compared to a control philosophy where the evaporating pressure and degree of superheat is held fixed at 15 [bar] and 15 ℃, respectively. These values are selected as they ensure a valid solution for all entries in the demonstrative dataset, given the process constraints in Table 3-3.

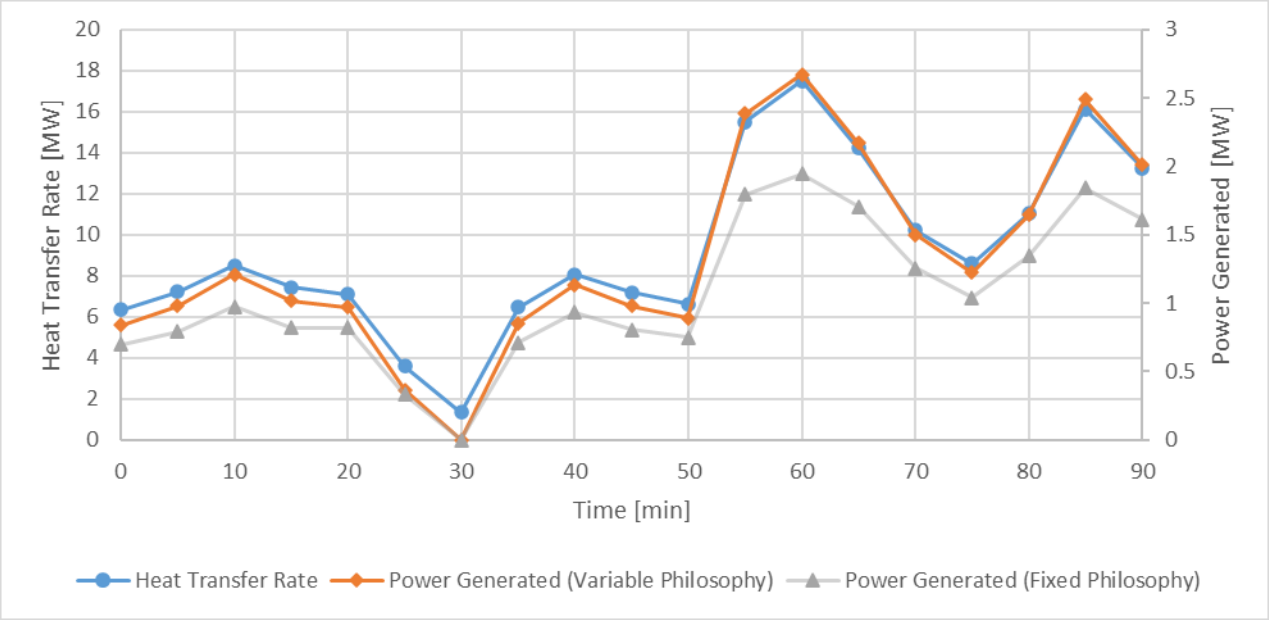


Figure 4-7: Power Generation Comparison of PGCP to Fixed Philosophy on Demonstrative Dataset

The average power generation for the fixed philosophy is 1.102 [MW], whereas the use of PGCP results in a 21.04 % increase at 1.334 [MW]. Note that this improvement in power generation is obtained without any changes to the heat transfer from the cooling water heat source. These improvements are attributed to the adjustment of the degree of superheat and the evaporating pressure of the working fluid within the PGEN component.

Lower heat transfer rate requirements result in a smaller difference between the performance of the compared control philosophies. This can be attributed to the lower temperature and/or mass flow rate of the cooling water requiring a reduction in evaporating pressure and degree of superheat to ensure that process constraints are adhered to.

To confirm this, Figure 4-8 illustrates the evaporating pressure and degree of superheat over time. Note the reduction in evaporating pressure between 15 and 30 min, which corresponds with the reduction in required heat transfer rate, as shown in Figure 4-7.

At 60 min, the power generation is at the maximum and an increase from the previous time interval, but the required degree of superheat is reduced to reach maximum thermal efficiency in the cycle. This can be attributed to the influence the evaporating pressure and degree of

superheat has on other cycle parameters, which include the working fluid mass flow rate, the required power at the pump, and turbine efficiencies.

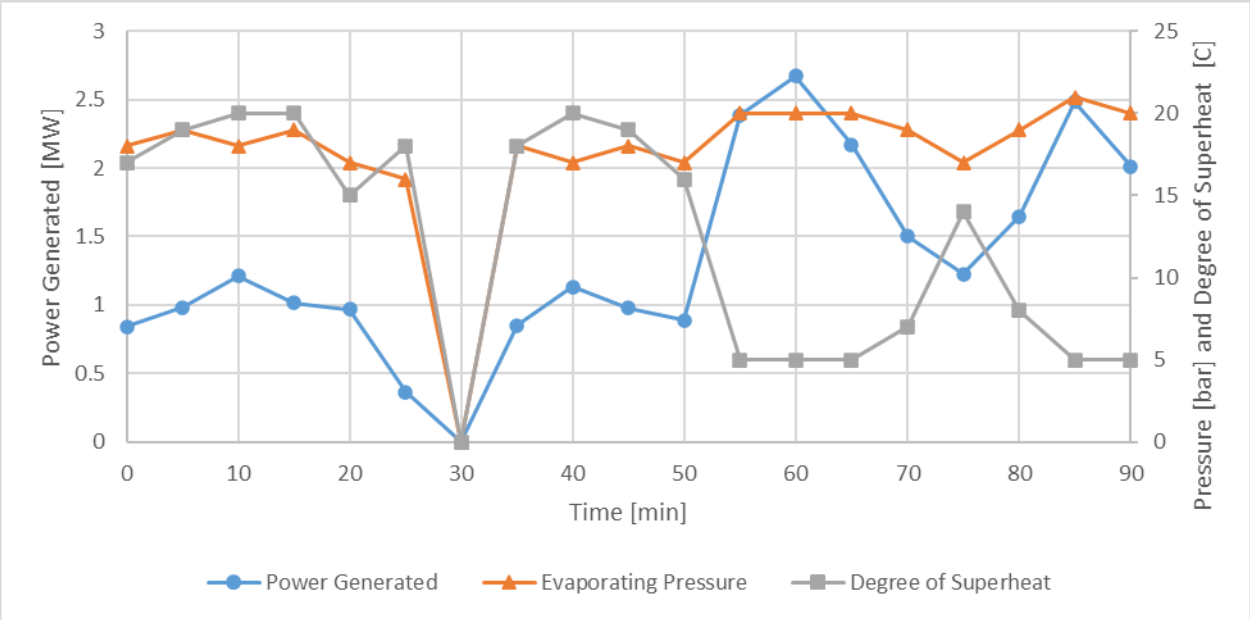


Figure 4-8: Evaporating Pressure and Degree of Superheat Variation for PGCP on Demonstrative Dataset

This section illustrates the PGCP, a control philosophy that is used to control the evaporating pressure and degree of superheat in the PGEN component for the novel formulations in this thesis.

It is shown that the PGCP delivers increased power generation at the supplied cooling water flow rate and temperature compared to a fixed parameter control philosophy. The approach and results obtained correlates with the approach and conclusions of Ata et al. [14] and Hu et al. [16].

4.3 ACHX Control Philosophy

As noted earlier in this thesis, the ACHX is the original method of transferring heat from the cooling water. This section describes the control philosophy of the ACHX along with any assumptions made. The main deliverables for the ACHX control philosophy are to determine the required number of fans as well as their operational speed.

4.3.1 Control Philosophy for Efficient Heat Transfer (ACCP)

The control philosophy in this section adjusts the number of and rotational speeds of the fans within the ACHX to ensure that the desired heat transfer rate is achieved. This control philosophy is referred to as Air Cooler Control Philosophy (ACCP) and is illustrated in Figure 4-9.

The time index for the formulation is given by $\mathrm{T} = \{1,2,\ldots,|\mathrm{T}|\}$. The cooling water at time t enters the ACHX at a temperature of $\mathrm{T}_{\mathrm{hs,t}}$℃ and a mass flow rate of $\dot{\mathrm{m}}_{\mathrm{hs,t}}[\mathrm{kg/s}]$. The desired setpoint temperature for the cooling water leaving the ACHX is also an input parameter and denoted as

T_A^{set}°C. The maximum number of fans us denoted with n_{max}, while the rotational speed range of fans is represented with $[\omega_{min}, \omega_{max}]$.

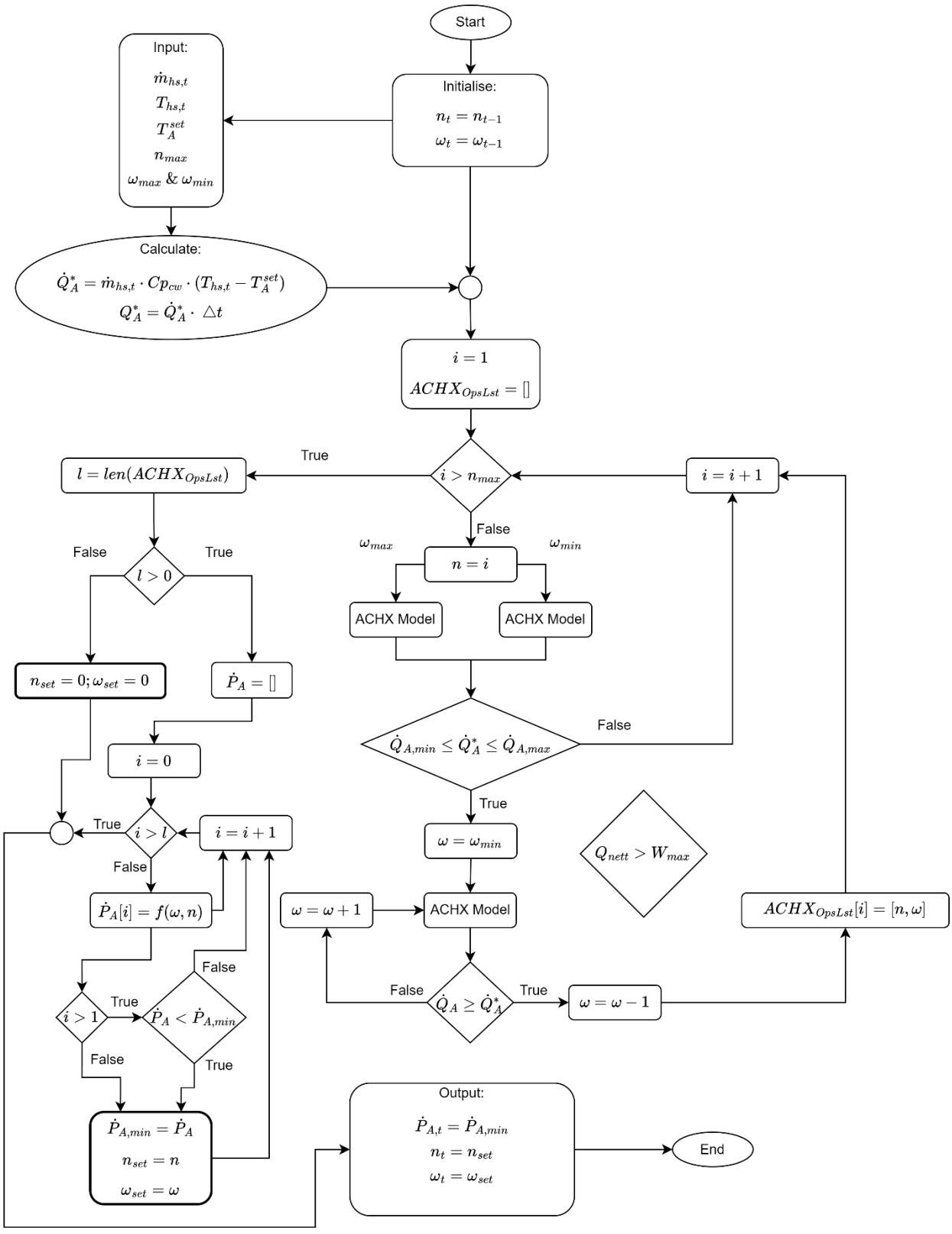


Figure 4-9: ACHX Control Philosophy (ACCP)

The required heat transfer rate, $\dot{Q}_A^*$ [W], and the total heat transfer over time t, Q_A^*[J] are then calculated through equations similar to (3.3).

The number of fans, n, and rotational speed, ω, at time t is initialised as the same values of the previous time step, $t-1$. An iterative process is then started with in iterator $i=1$ and an empty list of potential operating points for the ACHX, $ACHX_{OpsLst}$. The number of fans operational, n, is set equal to the iterator, i, after which the minimum and maximum rotational speeds of the fans are used to determine the range of heat transfer rates the ACHX can be adjusted to for the specific number of fans in operation, $[\dot{Q}_{A,min}, \dot{Q}_{A,max}]$. This is done through application of the ACHX model demonstrated in Chapter 3.3.2. If the required heat transfer rate is not in this range, then the control philosophy adds another fan until this value is either true or the iterative process has reached the maximum number of fans.

However, if the required heat transfer is in this range, further calculations are required. The rotational speed is set to the minimum speed and then the ACHX model is used to determine the expected heat transfer rate. If the calculated heat transfer rate of n fans with a speed of ω are lower than the required heat transfer rate, $\dot{Q}_A^*$, then the rotational speed is increased, and the calculation is repeated. Should the calculated heat transfer rate be larger than the required heat transfer rate, the control philosophy then removes the previous speed adjustment to ensure that the assigned parameters do not have a heat transfer rate above that which is required. This ensures that the difference between the calculated and required heat transfer is at a minimum, without the ACHX having a heat transfer rate that is too high. After this process, n and ω is appended to the list of viable operating points and thus $ACHX_{OpsLst}[i] = [n, \omega]$.

After reaching this maximum number of fans, the list of $ACHX_{OpsLst}$ should consist of all the potential operating points that the ACCP can decide on. The purpose of this study is to maximise power generation and any power consumption by the ACHX fans will be reduce the nett power generated. It follows that ACCP should determine the operating point in the list of viable options that deliver suitable heat transfer rates but at the minimum power consumption.

The length of the options list is first determined. If the list is empty, then there are no viable options, and the heat transfer rate required is low enough that natural convection will deliver suitable heat transfer rates. Note that the ACHX is suitably sized for the maximum heat transfer rate required for the system and thus the list will not be empty due to the heat transfer rate being above the maximum heat transfer rate of the ACHX.

The ACCP then loops through the list of viable options. The first option is used to determine the power consumption from $\dot{P}_A[i] = f(\omega.n)$ where f is a function unique to the motor and fan assembly

of the ACHX. The first option result for $\dot{P}_A$ is assigned as the minimum. The $\dot{P}_A$ of every option in this list is then calculated and compared to the currently assigned minimum. If an option is determined to have a lower power consumption value, then this option replaces the current option.

After iterating through the entire list, the current setpoint options are determined to be the option that draws the minimum power of all the viable options and is thus assigned to the output values of the ACCP. Note that both the setpoint temperature and desired heat transfer rates are provided and determined without any influence from the PGEN philosophy and can thus be regarded as independent of the PGEN operation.

The code used to simulate the performance of the ACCP is provided in Appendix D.

4.3.2 ACCP Results on Demonstrative Dataset

To illustrate the adjustment and performance changes of the ACCP control philosophy described in this section, the demonstrative dataset is used. For illustrating the performance of the ACCP, it is assumed that all the cooling water flow is directed to the ACHX component. The setpoint for cooling water return temperature is T_{set} =150 ℃. The maximum number of fans in operation, is n_{max} =4, while the rotational speed range is $[\omega_{min}, \omega_{max}]$ =155, 333 as set out in the design parameters given in Table 3-2.

Note that $T_{set} = T^{LL}$, since the PGEN and ACHX are currently controlled separately. The outlet temperature of ACHX, therefore, does not currently influence the control of PGEN, and vice versa. By using $T_{set} = T^{LL}$, the cooling water entering the gas cooler, as illustrated in Figure 3-1, T_{cw2}, will be at or above T^{LL}.

A section of the temperature and flowrate of the cooling water with the control philosophy results are given in Table 4-2 below to illustrate the decision-making process of the ACCP. Graphs illustrating the ACHX operations for the timeline $0 \leq t \leq 90$ min follow the table.

The results section of Table 4-2 reports the minimum and maximum heat transfer rate achievable for every number of fans in operation. Note that these values differ for each period because of heat source parameters on the heat transfer rate in the ACHX.

At $t = 70$ min, the ACCP determines that either three or four fans can be in operation and achieve the required heat transfer rate. Both options are simulated to determine the required speed along with the power consumption of the operational fans. During this period, the ACCP determines that four operational fans will consume less power to achieve the required heat transfer rate. The ACCP then reports only the required number of operational fans as well as the desired rotational speed to the heat rejection system.

Table 4-2: Section of Results for ACCP on Demonstrative Dataset

Demonstrative Dataset				Results				
t	$\dot{m}_{hs,t}$ kg/s	$T_{hs,t}$ $℃$	$\dot{Q}_A^*$ $[MW]$	n_{fans} $[-]$	$\dot{Q}_{min}^*$ $[MW]$	$\dot{Q}_{max}^*$ $[MW]$	Speed $[RPM]$	$\dot{W}_{A,t}$ $[kW]$
⋮	⋮	⋮	⋮	⋮	⋮	⋮	⋮	⋮
70	65	187.64	10.204	1	2.846	5.331	-	-
				2	5.391	9.614	-	-
				3	7.686	13.143	239	79.91
				4	9.767	16.087	178	79.35
⋮	⋮	⋮	⋮	⋮	⋮	⋮	⋮	⋮

The heat transfer rate of the ACHX under control of the ACCP for the demonstrative dataset is illustrated with an additional line indicating the number of fans in operation in Figure 4-10. The allowable heat transfer range is also displayed. At $t = 30$ min, ACCP determines that no fans are required, and that natural convection will ensure the average heat transfer rate for the period is within the suitable range such that the returning cooling water temperature is within the operational temperature envelope.

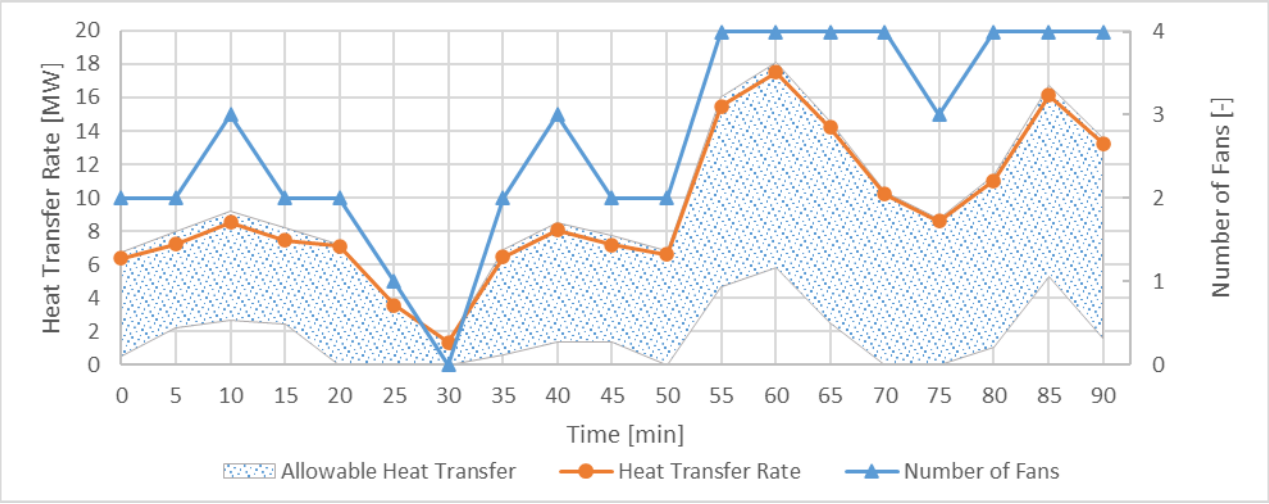


Figure 4-10: Heat Transfer Achieved in ACHX under ACCP on Demonstrative Dataset

From this figure it is shown that ACCP increases the number of fans in operation as the required heat transfer increases. However, controlling the rotational speed of all the fans is critical to ensure that the operational temperature envelope is maintained. From $t = 55 - 70$ min there are four fans in operation with an increasing heat transfer rate requirement.

The line indicating the number of fans in operation in Figure 4-10 is changed to show the operational fan speeds, resulting in Figure 4-11. For t = 35 – 70 min there are four fans in operation, and, from the figure it, is clear that an increase in heat transfer requirement results in an increase in fan operational speed.

Note that at t =75 min, where the number of required fans in operation reduced to three, a corresponding increase in fan speed is determined to ensure that sufficient heat transfer is maintained.

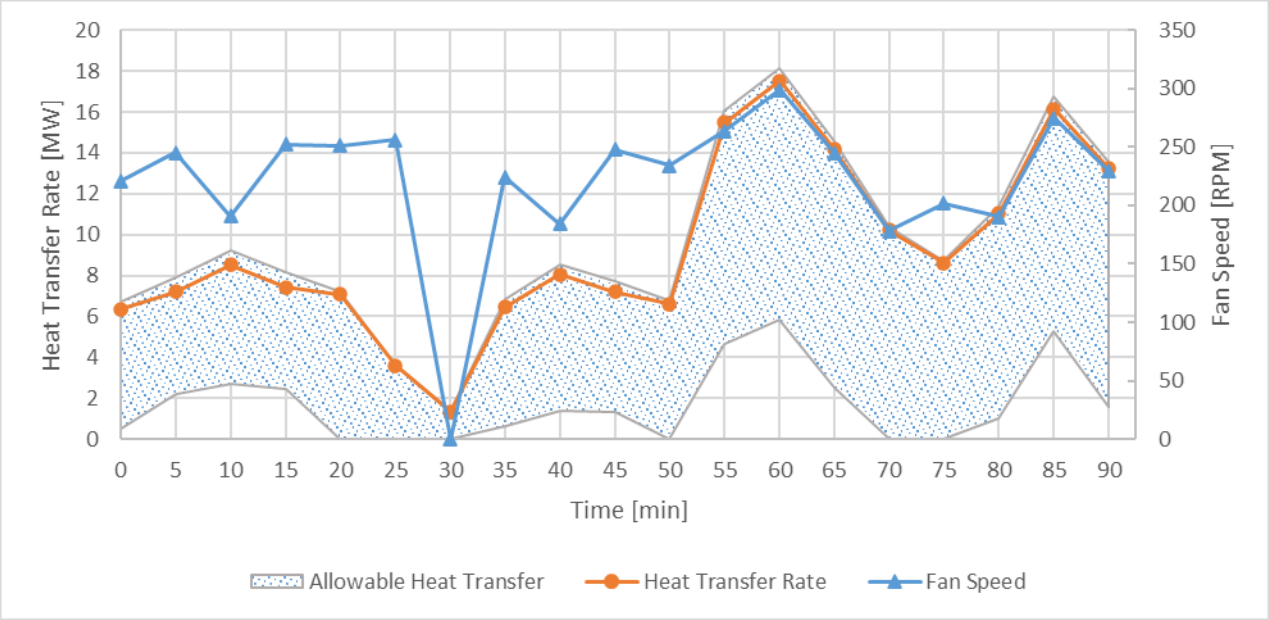


Figure 4-11: Fan Operational Speed Assigned by ACCP on Demonstrative Dataset

This section illustrates the ACCP, a control philosophy that is used to control number of and rotational speeds of the fans in ACHX for the novel formulations in this thesis. The decision-making process showed ensures that, should the ACCP have more than one viable operating point, the operating point consuming the minimum power relative to the other options is selected.

4.4 Setpoint Temperature Control Model

In Chapter 3 it is noted that heat transfer to the environment is expected at the uninsulated components between the heat exchangers of PGEN and ACHX and the gas cooler. The heat transfer is expected to result in a decrease in the temperature of the cooling water entering the gas cooler.

It is critical to determine and compensate for this reduction in temperature to ensure that the cooling water entering the gas cooler is within the operational temperature envelope. By quantifying the expected temperature reduction, the setpoint temperature for the cooling water exiting both the PGEN and ACHX can be adjusted accordingly.

This section describes the control philosophy that the heat rejection control algorithm uses to determine a suitable setpoint temperature for the cooling water exiting the ACHX and PGEN components.

4.4.1 Control Philosophy for Temperature Setpoint Determination (TSD)

The control philosophy in this section adjusts the setpoint provided to the ACHX and PGEN to ensure that, if the setpoint temperature is met, that the cooling water entering the gas cooler will be within the operational envelope. This control philosophy is referred to as Temperature Setpoint Determination (TSD) and is illustrated in Figure 4-12.

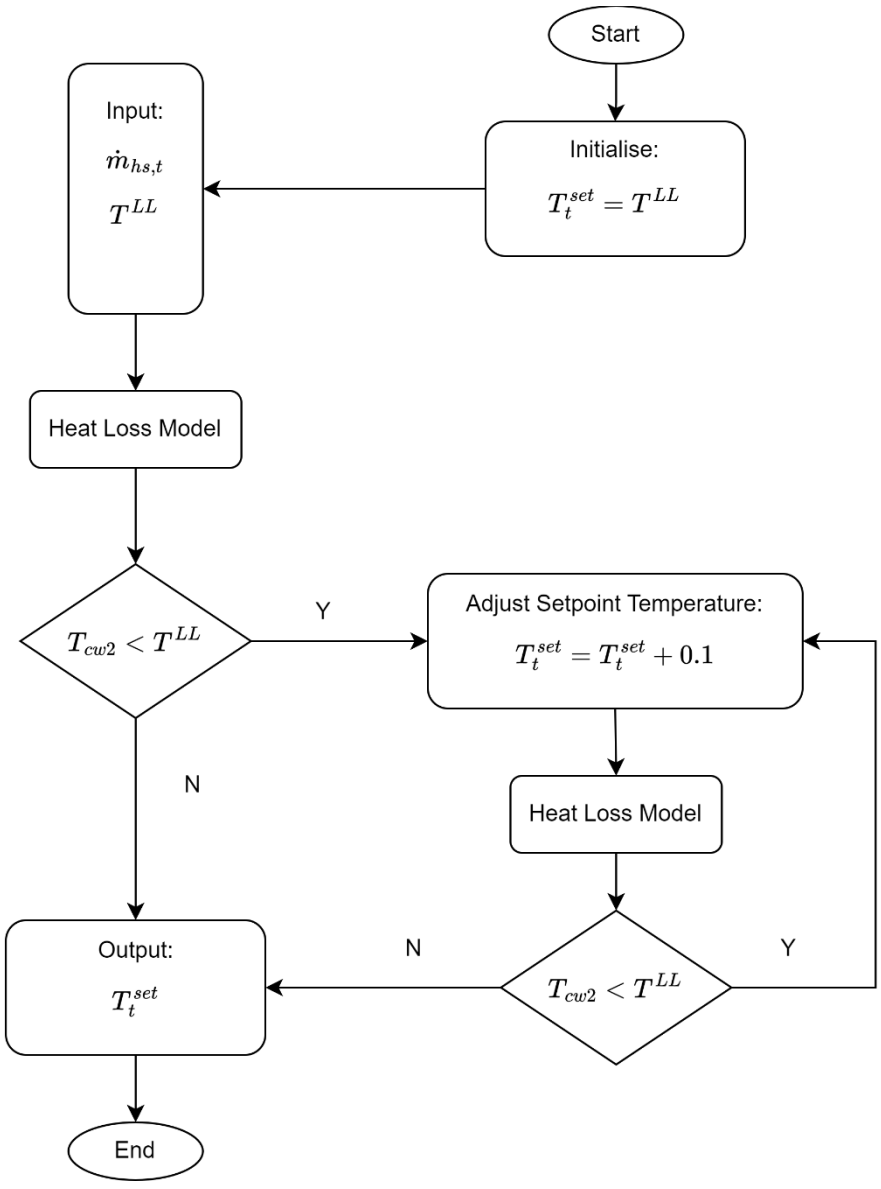


Figure 4-12: Temperature Setpoint Control Philosophy (TSD)

The time index for the formulation is given by $\mathrm{T} = \{1,2,\ldots,|\mathrm{T}|\}$. The cooling water at time t enters the uninsulated components at a temperature of $\mathrm{T}_{\mathrm{t}}^{\mathrm{set}}{}^{\circ}\mathrm{C}$, as is the goal exit temperature assigned to PGEN and ACHX at time t. The cooling water flows at a rate of $\dot{\mathrm{m}}_{\mathrm{hs,t}}[\mathrm{kg/s}]$.

The control model then uses the heat loss model described in Chapter 3.5 to determine the expected temperature of the cooling water entering the gas cooler, denoted in Chapter 3 as T_{cw2}. If this temperature is below the lower limit of the operational envelope, T^{LL}, then the setpoint is increased.

This process is repeated until the expected value of T_{cw2} is within the operational envelope. The setpoint that results in maintaining the operational envelope is then delivered as an output to be used as the setpoint for PGEN and ACHX.

The control philosophies of both the ACHX and PGEN ensure that their respective exit setpoint temperatures is determined and assigned in such a way that ensures $T_{cw2} > T_t^{set}$. It follows that $T_{P,t}^{set}$ can be lower than T_t^{set}, as long as $\dot{Q}_{P,t} + \dot{Q}_{A,t} \leq \dot{Q}_{T,t}$.

The script used for TSD is provided in Appendix E.

4.4.2 TSD Results on Demonstrative Dataset

The demonstrative dataset is used to illustrate the changes in T^{set} over time under the TSD described in this section. The geometrical layout and thermal properties of both the piping and tank components are provided in Table 3-4.

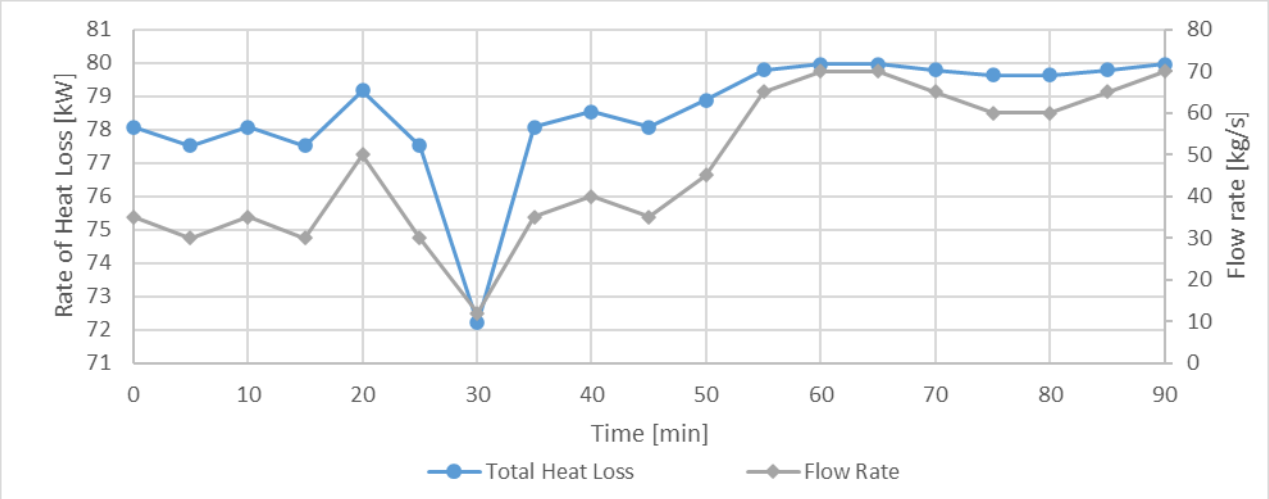


Figure 4-13: Rate of Heat Loss from Uninsulated Components over Time for Demonstrative Dataset

The heat loss rate from the uninsulated components over the time horizon of the demonstrative dataset is illustrated in Figure 4-13. The uninsulated components have definite fluctuations in the determined heat loss that are due to the changes in flow rate and thus the velocity and internal convection coefficient of the cooling water.

The total heat loss rate from the system is illustrated in Figure 4-14 along with the desired setpoint temperature required to ensure that the operational envelope is maintained. From the figure it can be noted that the setpoint temperature can still be increased during time periods where the estimated heat loss is relatively low. This is clear throughout the demonstrative dataset. This is

due to the flow rate dependency of heat transfer calculations for both determining convective heat transfer coefficients as well as the expected temperature reduction of the cooling water.

As an example of this, consider t =30 min where the estimated heat loss is the lowest of the time horizon, however, the setpoint temperature is also the highest. The flow rate at t =30 min is also at its lowest point. It follows from $\dot{Q} = \dot{m}C_p\Delta T$ that a higher temperature difference can be expected if the flow rate is reduced with only relatively small changes to $\dot{Q}$.

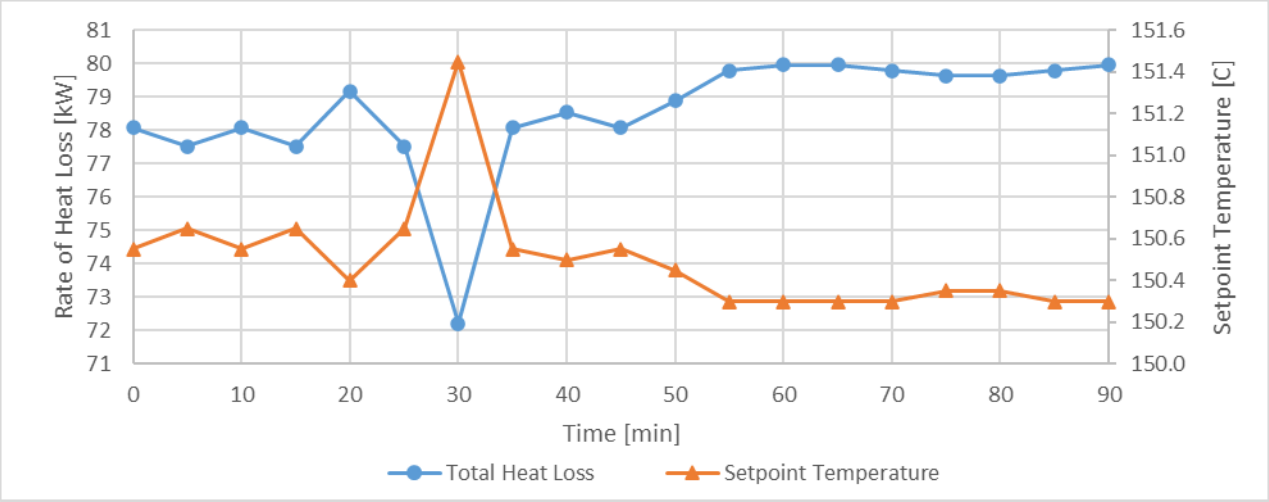


Figure 4-14: Total Heat Loss Rate and Setpoint Temperature over Time for Demonstrative Dataset

This section describes and illustrates the TSD model and how it is used in this thesis to ensure that the operational envelope is maintained. The TSD model can provide a suitable setpoint temperature for the relevant components under the control algorithms of this study.

4.5 Summary and Conclusion

In Chapter 4.1, the control philosophy that is used to control the cooling water flow rate to the gas cooler is described and illustrated on the demonstrative dataset. It is shown that the current reactive philosophy can maintain the flue gas temperature within the operational envelope.

In Chapter 4.2, the control philosophy of the PGEN is described and illustrated on the demonstrative dataset along with details on the internally controlled parameters to maximise efficiency within the component constraints. It is shown that the PGCP, through adjustments to the evaporating pressure and degree of superheat of the working fluid, increases the average power generation by 4.58%, compared to a control philosophy that has fixed parameters.

In Chapter 4.3, the control philosophy of the ACHX is described and illustrated on the demonstrative dataset. It is shown that the ACCP adjusts both the number of and rotational speeds of the fans in the ACHX to maintain a suitable heat transfer rate. This is done while minimising the power consumption by selecting the desired operational point from a list of viable operating points after calculating the estimated power consumption of each.

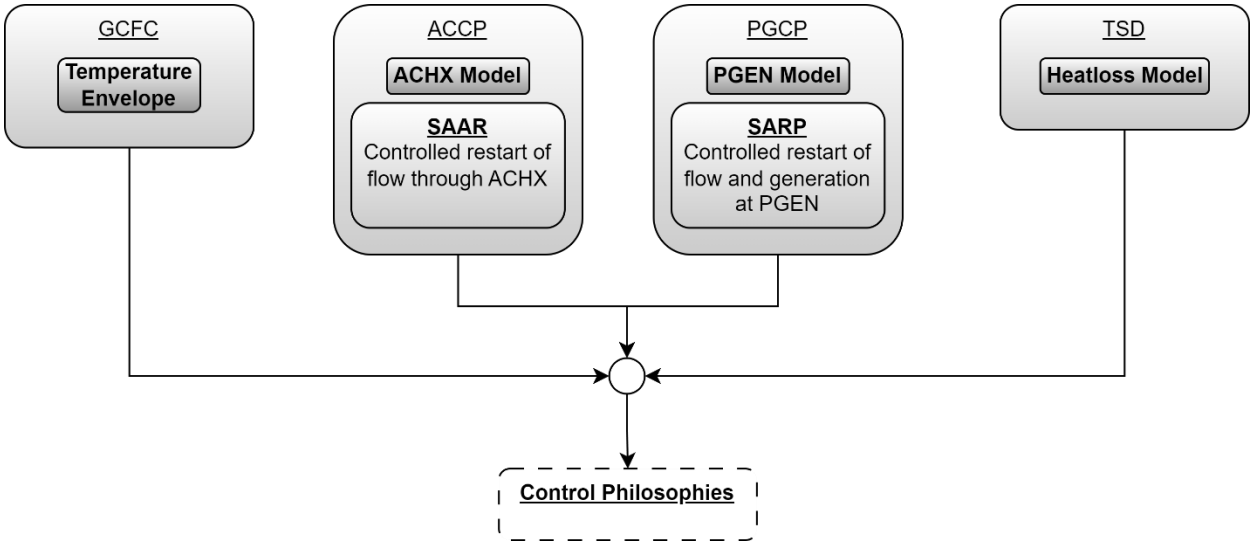


Figure 4-15: Summary of Control Philosophies Demonstrated in Chapter 4

Note that in both Chapters 4.2 and 4.3, the setpoints of PGCP and ACCP are set at the same value. This is due to the independent nature of each control philosophy where the control philosophy of each is not influenced by the operation of the other.

In Chapter 4.4, the control philosophy that determines a suitable setpoint temperature for use in both PGEN and ACCP is described. This philosophy considers the expected heat loss from the system based on current system geometry as well as flow properties of the cooling water. This setpoint temperature will ensure that, even though a section of the system is uninsulated, the temperature of the cooling water entering the gas cooler is within the operational envelope.

A summary of the control philosophy layout of this chapter is illustrated in Figure 4-15. The control algorithms and models demonstrated after this chapter are shaded. Future algorithms and dependencies are indicated with dashed lines.

CHAPTER 5 THE WORKS PHILOSOPHY

In Chapter 3 the models that predict the performance of the PGEN, ACHX as well as a model that determines the uncontrolled heat loss to the environment is illustrated. In Chapter 4 these models are used to formulate individual control philosophies for the cooling water flow rate, PGEN and ACHX as well as a model that determines the required setpoint of the cooling water exiting the PGEN and ACHX.

This section demonstrates the formulation of the current Works' Philosophy (WP) that aims to maximise power generation while ensuring that the temperature entering the gas cooler is maintained within a suitable range while the production process is in operation.

This chapter starts with the illustration of repeatable sub-models that are used to ensure sustained operations and concludes with the formulation and results of the WP on both the demonstrative and historical datasets.

5.1 Sub-algorithms for Sustained Operations

The PGEN and ACHX each have design and operational constraints that need to be accounted for in the formulation in this thesis. During time periods of low heat availability, the current Works Philosophy and future philosophies must attempt to sustain the operations of the PGEN and ACHX as far as possible whilst maintaining the operational envelope.

Failing to maintain operation of the PGEN and ACHX results in the execution of restart procedures that is expected to have a temporary impact on the heat transfer capacity and power generation of the heat rejection system.

The need for a minimum flow through the ACHX as well as the conditions under which the PGEN and ACHX will be bypassed in the system is provided in this section along with the relevant restart procedure. Including this in the control modelling enables to evaluation and analysis of the control philosophy under a fluctuating heat source.

5.1.1 Heat Flow From ACHX with No Operational Fans

As mentioned previously, the ACHX is the initial method of transferring heat from the cooling water before the addition of a PGEN. It follows that the ACHX geometry and piping are designed with maximum flow of the heat rejection system already taken into consideration. All the cooling water of the heat rejection system can, therefore, be distributed to the ACHX.

It is shown in Chapter 3.3.2.1 that the convection of ambient air over the finned tubes of the ACHX will result in heat transfer even when no fan is in operation. This is due to the temperature difference in the ACHX and the ambient air.

Consider a scenario where the ACHX is isolated with no mass flow entering or leaving the domain and no fan in operation. It follows from the heat transfer mechanisms described in Chapter 2.1 that heat transfer will occur if there is a difference in temperature between two points. Thus, the natural convection heat transfer will occur until the temperature of the fluid inside the ACHX is the same as the ambient air. After sufficient time, the cooling water in this component can thus be below the operational temperature envelope of the gas cooler. This can potentially result in operation outside the temperature envelope when the flow through the ACHX is restored due to PGEN unavailability or significant changes in heat transfer requirements.

The rate of heat transfer from the stagnant water, $\dot{Q}_A^*$ MW, in the ACHX is illustrated by the power curve approximated in Figure 3-5,where it is a function of the stagnant water temperature, T_{cw}^* ℃. This curve is given by equation (5.1).

$$\dot{Q}_A^* = 0.0002259 \cdot T_{cw}^{*\,1.701631} \tag{5.1}$$

The internal volume of a heat exchanger is $1.765\ m^3$ as noted in Table 3-2, thus the ACHX has a total volume of $3.530\ m^3$ for the ACHX. Since the volume of the stagnant water is known, the temperature of the stagnant water can be plotted over time. To illustrate the rate of heat loss from the stagnant water over time, it is assumed that the initial temperature of the water is 210 ℃.

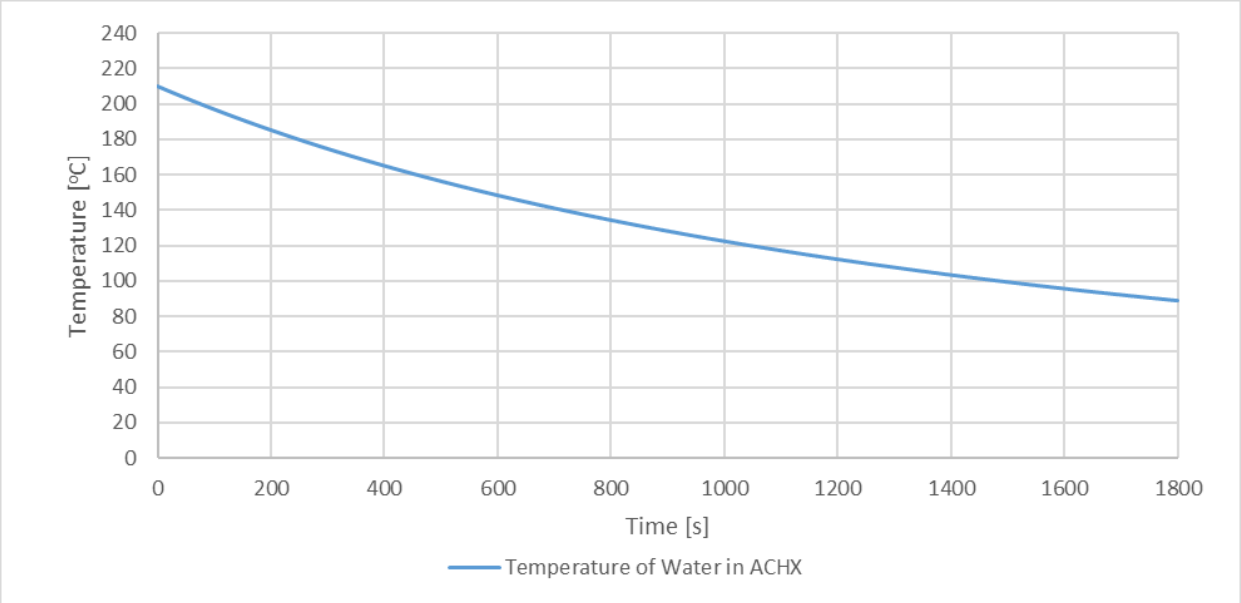


Figure 5-1: Temperature of Stagnant Cooling Water in ACHX over time for $T_0 = 210$ ℃

The temperature of the stagnant cooling water in the ACHX are illustrated in Figure 5-1. Note that after 30 min no flow through the ACHX domain, the internal fluid temperature has reduced to ~85 ℃. The cooling water flow rate ranges from $20 - 450\ m^3/h$, thus replacing this volume of $3.530\ m^3$ will take at least 28 s when the flow rate is at the maximum. This indicates that temperature below the operational envelope will enter the gas cooler for at least 28 s.

A minimum flow of cooling water will, therefore, need to be designated to the ACHX to ensure that the operational envelope is maintained, even if the PGEN becomes unavailable. The approaches to determining the minimum flow will be discussed and illustrated in this and future chapters.

5.1.2 Bypass Flow and Restart of flow through ACHX

It is known that there are time periods where the thermal load available from the cooling water is lower than the expected heat transfer from the ACHX, even with no fans in operation:

$$\dot{Q}^{0}_{A,t} > \dot{m}_{hs,t} Cp_{cw} \cdot \left(T_{hs,t} - T^{set}_{t}\right) \tag{5.2}$$

This section will describe the approach used to ensure that the temperature envelope is maintained.

5.1.2.1 Bypassing Flow to Maintain Operational Envelope

Assume that in this low heat condition, all the cooling water is distributed to the ACHX with no flow going to PGEN. It then follows that:

$$\dot{m}_{A,t} Cp_{cw} \cdot \left(T_{hs,t} - T^{set}_{A,t}\right) > \dot{m}_{hs,t} Cp_{cw} \cdot \left(T_{hs,t} - T^{set}_{t}\right)$$

$$T_{hs,t} - T^{set}_{A,t} > T_{hs,t} - T^{set}_{t}$$

$$T^{set}_{A,t} < T^{set}_{t}$$

From the definition of $T^{set}_{A,t}$ it is known that this is not allowed and will result in cooling water entering the gas cooler below the operational envelope. Note that water exiting the gas cooler is such that $T_{hs,t} > T^{set}_{t}$ and, therefore, the heat rejection system is still in operation under the control algorithms in this thesis.

To ensure the operational envelope is maintained, a bypass line is used. The flow rate through this bypass is referred to as $\dot{m}_{BP,t}$ kg/s. The bypass line is an insulated pipeline, in parallel with the PGEN and ACHX components, as shown in Figure 3-1. From the mass conservation in equation (3.2) it can be stated that all the cooling water will move through the bypass line if the mass flow through PGEN and ACHX is zero.

As an example to this approach, assume an average cooling water flow for time t of $\dot{m}_{hs,t} = 22$ kg/s at an average temperature of $T_{hs,t}$ =158 ℃ entering the heat rejection system. The TSD algorithm is used to determine a setpoint temperature T^{set}_{t} =150.98 ℃. This results in a total heat availability of 191.1 MJ, which is the equivalent of an average heat transfer rate of 637 kW.

The equation in (5.1) then determines that an ACHX with zero operational fans will still result in a heat transfer rate of 1.25 MW. If all water is passed through the ACHX, it can be expected that the operational envelope will not be maintained since $\mathrm{Q}_{\mathrm{A,t}}^{0} > \dot{\mathrm{Q}}_{\mathrm{hs,t}}$.

The solution proposed in this section is to bypass all the cooling water flow, $\dot{\mathrm{m}}_{\mathrm{BP,t}} = \dot{\mathrm{m}}_{\mathrm{hs,t}}$. In doing so, the cooling water experiences only the heat loss from the uninsulated piping and tank, resulting in a cooling water temperature entering the gas cooler of 157.02 ℃.

5.1.2.2 Restarting the ACHX

It is shown in Chapter 3.3.2.1 that the convection of ambient air over the finned tubes of the ACHX will result in heat transfer even when no fan is in operation. This is due to the temperature difference in the ACHX and the ambient air.

Consider a scenario where the ACHX is isolated with no mass flow entering or leaving the domain and no fan in operation. It follows from the heat transfer mechanisms described in Chapter 2.1 that heat transfer will occur if there is a difference in temperature between two points. Thus, the natural convection heat transfer will occur until the temperature of the fluid inside the ACHX is the same as the ambient air. After sufficient time, the cooling water in this component can thus be below the operational temperature envelope of the gas cooler. This can potentially result in operation outside the temperature envelope when the flow through the ACHX is restored due to PGEN unavailability or significant changes in heat transfer requirements.

To ensure that the volume of water in the ACHX does not enter the gas cooler below the temperature limit of the operational envelope, a restart procedure for the ACHX is required. In this procedure, the flow distribution between the ACHX and bypass line is determined in such a way that ensures $\mathrm{T}_{\mathrm{cw2}} > \mathrm{T}_{\mathrm{t}}^{\mathrm{set}}$.

The procedure of restarting the flow through the ACHX is shown in Figure 5-2 below. A brief demonstration of this process is provided below.

As a demonstration, assume that the internal temperature of the ACHX is $\mathrm{T}_{\mathrm{Ai,t}} = 100\ ℃$ when sufficient heat and flow is available to restart the flow distribution to the ACHX with $\dot{\mathrm{Q}}_{\mathrm{hs,t}} = 5.9\ \mathrm{MW}$ and $\dot{\mathrm{m}}_{\mathrm{hs,t}} = 60\ \mathrm{kg/s}$. The setpoint temperature determined by TSD for this flow is $\mathrm{T}_{\mathrm{t}}^{\mathrm{set}} = 150.36\ ℃$.

There are $3530\ \mathrm{kg}$ of water in the ACHX system. It thus follows that if all the flow were to be distributed to the ACHX, the gas cooler would receive water outside the operational envelope for $\frac{3530\ \mathrm{kg}}{60\frac{\mathrm{kg}}{\mathrm{s}}} = 59\ \mathrm{s}$ of the 5 min period.

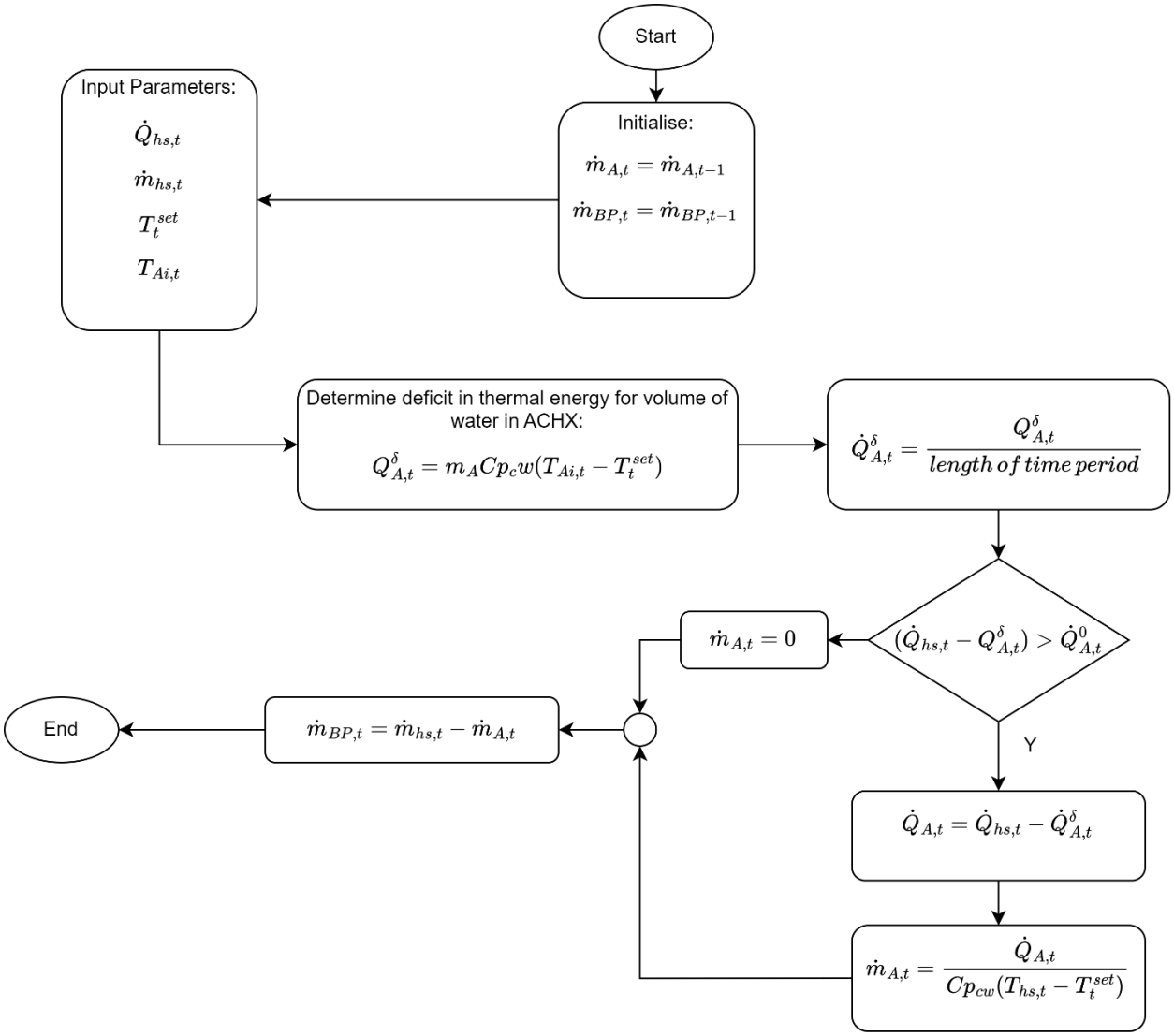


Figure 5-2: Restarting Flow through the ACHX

This is addressed by bypassing a fraction of the cooling water flow to ensure that the point at which the bypass line and ACHX exit combines has a sufficiently high temperature such that $\mathrm{T_{cw2}} \geq \mathrm{T_t^{set}}$. This guarantees that the operational envelope is maintained.

Since the cooling water temperature is $50\ ℃$ below the setpoint, there is a deficit in thermal energy of $736\ \mathrm{MJ}$ to the setpoint temperature. Using equation (3.1), it can be argued that the system be controlled such that $\mathrm{Q_{Res}}$ is $736\ \mathrm{MJ}$ at minimum.

To ensure that $\mathrm{Q_{Res}}$ is at least minimum, the heat transferred by the ACHX needs to be, on average, at least $\frac{736}{5 \cdot 60} = 2.45\ \mathrm{MW}$ less than the available heat transfer rate from the cooling water. This results in a heat transfer rate in the ACHX of $3.45\ \mathrm{MW}$ With the required heat transfer rate now known, the flow distribution can be determined to ensure that $\mathrm{T_{A,t}^{set}} \geq \mathrm{T_t^{set}}$.

This results in $\dot{m}_{A,t}$= 34.95 kg/s for $T_{A,t}^{set} = T_t^{set}$. From equation (3.2), it follows that the bypass line has a flow rate of $\dot{m}_{BP,t}$= 25.05 kg/s

This algorithm is referred to as Sub-Algorithm ACHX Restart, shortened as SAAR.

5.1.3 Tripped PGEN Scenario

Flow through the ACHX is required to ensure that the cooling water operational envelope is maintained when other heat rejection processes become unavailable. Being the only other heat rejection process, it is expected that this scenario will occur when the PGEN enters a tripped state. During a tripped state, the PGEN will not be available for any heat transfer from the cooling water, and as such the ACHX will need to transfer the required heat.

This section will briefly describe the approach of including a tripped PGEN scenario in the modelling of all future control philosophies in this thesis.

5.1.3.1 Cold and Warm Start Procedures

As noted in Chapter 2 and from Lecompte et al. [8] and Cocco et al. [53], the cycle on which the PGEN is based can operate down to 10% of their nominal load. This correlates with the constraints of the PGEN provided in Table 3-3. If the designated flow to the PGEN is such that the available heat is below the reported threshold, the PGEN will enter a tripped state due to low heat availability.

A tripped PGEN will still experience heat transfer to the environment. The working fluid, as described in Chapter 3, is superheated prior to entering the turbine and sub-cooled after exiting the condenser. Through this heat loss, it can thus be expected that the working fluid in the superheater section of the evaporator component will, after sufficient time, condense to a two-phase and ultimately liquid state. The time required for this to happen will depend on the rate of heat loss as well as the time the PGEN system does not receive any heat from the cooling water.

The time that elapses while a PGEN is in a tripped state will, therefore, typically determine the required start procedure. The start procedures typically fall into two categories, namely “cold” and “warm” start procedures [53]. During a cold start the heat exchangers and other components are outside operational envelopes and is heated to operational conditions.

The study by Cocco et al. [53] analysed a system where a cold start is classified as a start procedure that commences after the system had a stop period of longer than two days. Any period shorter than two days justifies the use of a warm start procedure. The PGEN manufacturers for the system analysed by Cocco et al. [53] indicated that for a cold start, the system requires 25% if the nominal thermal load for a continuous period of two hours. For a warm start, the 25% of the nominal thermal load is only required for 30 min. No electrical power is generated during a start procedure [53].

Since no power is generated during both warm and cold start procedures, approaches to reduce the number of trips from low heat availability need to be investigated. The study by Lecompte et al. [8] indicates that a thermal buffer with either a steam or thermal oil loop can be used to reduce the number of trips. However, the current infrastructure does not have the required infrastructure for this type of mitigation.

It is required that the control philosophy applied considers the delay as currently specified by the PGEN manufacturers until the PGEN can be operational.

5.1.3.2 Time Delay and Start Procedures for PGEN

As mentioned in Chapter 2, the required delay is influenced by the dynamic response of the system to meet operational requirements, such as the minimum evaporating pressure and a fixed elapsed time parameter in [33]. Since a dynamic response model of the PGEN is not within the scope of this thesis, a time-based delay is applied. It is thus assumed that the system measurements during a start procedure allow for a return to operation after the required time has elapsed.

The PGEN manufacturers in this study indicate a 20 min delay for a warm start procedure where the required continuous thermal load to the evaporator is 4 MW, which is 20% of the design load. Any start procedure commencing where the PGEN is non-operational for less than 12 hours is regarded as a warm start. Alternatively, a cold start procedure is applied. A cold start procedure requires a continuous thermal load of 4 MW for a minimum period of 180 min before power generation can occur.

Time representative parameters t_t^{sp} and t_t^0 min is introduced along with binary parameters $\delta_{P,t}$ and $\delta_{\dot{Q}}$. The values of t_t^{sp} and t_t^0 indicate the time elapsed in the start procedure and the total elapsed time that the PGEN system has been unavailable, respectively. The binary parameters of $\delta_{P,t}$ and $\delta_{\dot{Q}}$ indicate whether the PGEN is available for power generation and heat transfer from the cooling water, respectively.

The algorithm governing the start procedure is provided in Figure 5-3. The first step after initialisation of the algorithm, is to determine the available rate of heat transfer to the PGEN. This is done through using the heat source and minimum ACHX flow rates as well as the heat source and PGEN setpoint temperatures. If the available rate of heat transfer to the PGEN is less than the specified 4 MW, the parameter tracking the elapsed time of the start procedure, resets to zero. However, if there is sufficient heat, the time elapsed from $t-1$ to t is added to t_t^{sp}.

The total elapsed time since the PGEN became unavailable is then used to determine whether a cold or warm start procedure is required. Note that the tracked elapsed time in the start procedure is used to ensure that the algorithm does not change from a warm to a cold start procedure while

the warm procedure is being followed by adding the elapsed procedure time to the limit. If the elapsed procedure time is equal to or greater than the delay time applied, the binary variables of both $\delta_{P,t}$ and $\delta_{\dot{Q}}$ are set to one, indicating that the PGEN system can transfer heat from the cooling water while also generating electrical power. If not, then only the value of $\delta_{\dot{Q}}$ becomes one, indicating that the PGEN can transfer heat from the cooling water without power generation.

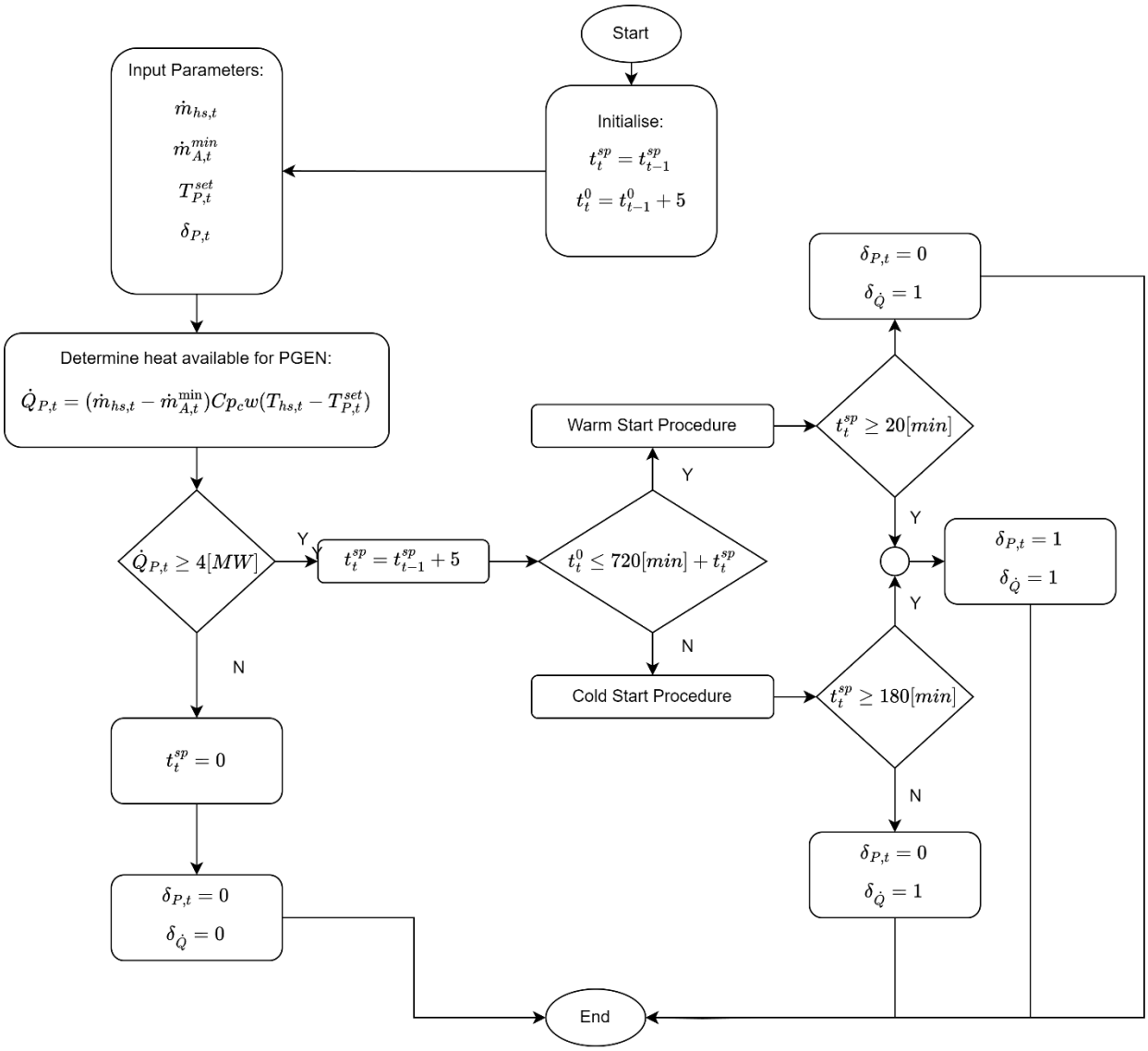


Figure 5-3: Time Delay in Start Procedure of PGEN

Note that in the algorithm illustration, the required thermal load of 4 MW and the time representative parameters are set as constants. This indicates that these values are fixed as per the PGEN design and the control philosophies in this and future chapters will not be able to adjust these values.

The results of the time delay described in this section of the chapter is illustrated and discussed in the next section. All the required models and algorithms to formulate the current Works Philosophy have now been provided and discussed.

This algorithm is referred to as Sub-Algorithm PGEN Restart, shortened to SAPR.

5.2 Formulation of the Works Philosophy (WP)

The sub-algorithms provided above are used to ensure that the trip and restart of flow through the PGEN and ACHX is accurately accounted for during the execution of WP. The formulation of the WP is provided in this section of the chapter.

The flow diagram of the WP is provided in Figure 5-4.

For a cooling cycle that comprises of both PGEN and ACHX, the objective should be to distribute the heat in such a way that maximum power is generated while ensuring that sufficient cooling is always taking place, even during an unplanned trip event. Maximising the power generation directly results in less electrical power demand from a power utility and, therefore, a reduction in plant expenditure.

In the formulation below, $\mathrm{T}\,(℃)$, $\mathrm{Q}\,(\mathrm{J})$, $\dot{\mathrm{Q}}\,(\mathrm{W})$ and $\dot{\mathrm{m}}\,(\mathrm{kg/s})$ represent temperature, heat, heat transfer rate and mass flow respectively with sub-and superscripts used to identify specific parameters and values.

The time index for the formulation is given by $\mathrm{T} = \{1,2,\dots,|\mathrm{T}|\}$. The difference in time between t and $\mathrm{t}+1$ is constant and indicated by $\Delta\mathrm{t}$. The cooling water exits the heat gas cooler at a temperature $\mathrm{T}_{\mathrm{hs,t}}$ (℃) and a mass flow rate of $\dot{\mathrm{m}}_{\mathrm{hs,t}}$ (kg/s). At time t, the TSD uses the predicted heat loss in the system to determine the desired temperature of the cooling water exiting both the PGEN and ACHX components, $\mathrm{T}_{\mathrm{t}}^{\mathrm{set}}$ (℃). The average of the available heat transfer rate at time t, $\dot{\mathrm{Q}}_{\mathrm{hs,t}}$ (W), and the available heat over time t, $\mathrm{Q}_{\mathrm{hs,t}}$ (J) is then calculated through equations similar to (3.3).

The first decision made in WP is whether to bypass all the flow. This is done by first the ACHX model to determine the predicted heat transfer rate and heat transferred over time t for the ACHX with zero fans in operation. This prediction is made through the approximated model discussed in Chapter 3.3.2.1 and denoted as $\dot{\mathrm{Q}}_{\mathrm{A,t}}^{0}$ (W) and $\mathrm{Q}_{\mathrm{A,t}}^{0}$ (J) respectively. If the predicted heat transfer over time t for a non-operational ACHX is more than the available heat, $\mathrm{Q}_{\mathrm{A,t}}^{0} \geq \mathrm{Q}_{\mathrm{hs,t}}$,then all the flow needs to be bypassed. It follows that the flow through the PGEN and ACHX components are zero, $\dot{\mathrm{m}}_{\mathrm{P,t}} = \dot{\mathrm{m}}_{\mathrm{A,t}} = 0$, and the flow through the bypass line is $\dot{\mathrm{m}}_{\mathrm{BP,t}} = \dot{\mathrm{m}}_{\mathrm{hs,t}}$. This is to minimise the heat transferred with PGEN and ACHX, $\mathrm{Q}_{\mathrm{P,t}} = \mathrm{Q}_{\mathrm{A,t}} = 0$, and thus maintaining the operational envelope. Through this decision, equation (3.1) will simplify to:

$$\mathrm{Q}_{\mathrm{hs}} = \mathrm{Q}_{\mathrm{Res}} \tag{5.3}$$

Since $\mathrm{Q}_{\mathrm{hs,t}}$ and thus $\mathrm{Q}_{\mathrm{Res}} > 0$, it is ensured that the operational envelope is maintained.

If not all the flow needs to be bypassed, the next step is to determine whether the ACHX is able to maintain the operational envelope. This is done by evaluating whether there is cooling water distributed to the ACHX and what the internal cooling water temperature is in the previous period. These parameters are provided and denoted with $\dot{m}_{A,t-1}$ and $T_{Ai,t-1}$.

If $\dot{m}_{A,t-1}$ is zero and $T_{Ai,t-1} < T_t^{set}$, it follows that the ACHX had stagnant water during the previous period that is below the allowable minimum temperature for cooling water entering the gas cooler. The operational envelope will, therefore, not be maintained should all the flow be distributed to ACHX. However, should no flow be distributed to the ACHX, the internal temperature will lower further with no heat being transferred in the system. Therefore, to ensure that ACHX can safely return to operation, a flow distribution between the ACHX and the bypass line is determined.

The mass of the water in the ACHX, m_A, as well as the internal temperature $T_{Ai,t}$ is used to determine the required distribution through SAAR (Chapter 0). This sub-algorithm ensure that the flow is distributed in such a way that the operational envelope is maintained through the mixing of the sub-cooled water from the ACHX and the higher temperature water from the bypass line. SAAR thus provides a $\dot{m}_{BP,t}$ and $\dot{m}_{A,t}$ where $\dot{m}_{hs,t} = \dot{m}_{BP,t} + \dot{m}_{A,t}$. Note that during this operational regime, there is no objective for heat transfer. No fans will be operational in this time period and thus $Q_{A,t} = Q_{A,t}^0$ and $\dot{Q}_{A,t} = \dot{Q}_{A,t}^0$.

If $\dot{m}_{A,t-1}$ is zero but $T_{Ai,t-1} \geq T_t^{set}$ then it follows that the internal temperature of the ACHX is such that all the flow can be distributed to the ACHX without risk of breaching the operational temperature envelope. The normal operation of the ACHX in the heat rejection system can thus be resumed.

The normal operation of the ACHX under the control of WP is to distribute a fixed fraction of the total flow to the ACHX. This fraction is denoted with α – where $\dot{m}_{A,t} = \alpha \cdot \dot{m}_{hs,t}$. Due to the requirement of maintaining flow through the ACHX it can be stated that $0 < \alpha \leq 1$. The flow distributed to the ACHX is to ensure that there is a continuous flow through the ACHX, mitigating the risk of not maintaining the operational envelope should PGEN become unavailable. For $\alpha = 1$, all flow is distributed to the ACHX.

The setpoint temperatures of both the ACHX and PGEN, denoted as T_P^{set} and T_A^{set}, respectively, are then set at the same temperature of T_t^{set}, as is done in Trafczynski et al. [35]. The Works follows this approach due to historical reliability and control concerns of the PGEN. These concerns resulted in the decision to run both the ACHX and PGEN as independent processes.

The available flow and thermal load for the PGEN is thus $\dot{m}_{P,t} = \dot{m}_{hs,t} \cdot (1 - \alpha)$ and $\dot{Q}_{P,t} = \dot{m}_{P,t} \cdot Cp_{cw} \cdot (T_{hs,t} - T_{P,t}^{set})$, respectively.

For WP to determine and assign the required flow and thermal load objective, the current PGEN operational regime needs to be considered in combination with the available heat. The binary parameters of $\delta_{\dot{Q}}$ and $\delta_{P,t}$ are, therefore, introduced, where a value of one indicates that the PGEN can transfer heat and that the PGEN can generate power, respectively. Note that $\delta_{\dot{Q}} \geq \delta_{P,t}$, indicating that heat can be transferred at PGEN without power generation and that power can only be generated if heat is transferred.

If the available heat is such that the average thermal load that can be assigned to the PGEN during t is less than the lower design limit of $\dot{Q}_P^{min}$, then the values of $\delta_{\dot{Q}}$ and $\delta_{P,t}$ is zero. If the available thermal load is within the design limits of PGEN, then WP first determines if the PGEN is in operation at $t-1$. If not, then SAPR (Chapter 5.1.3) is used to initiate and control the PGEN restart procedure. As mentioned in Chapter 5.1.3, a warm or cold start procedure is assigned and managed by SAPR depending on the time elapsed while PGEN is out of operation. During the start procedure, the PGEN can be used to transfer heat from the cooling water without any power generation, thus $\delta_{\dot{Q}} = 1$ and $\delta_{P,t} = 0$. The final step of the restart procedures is the same for the normal operation of the PGEN where both heat transfer and power generation takes place and thus $\delta_{\dot{Q}} = 1$ and $\delta_{P,t} = 1$.

The binary parameters can now be used to determine the flow and thermal load assigned to the PGEN. If $\delta_{\dot{Q}} = 0$ and $\delta_{P,t} = 0$ then the PGEN is unavailable for both heat transfer and power generation and thus all flow and thermal load is distributed to the ACHX. However, if $\delta_{\dot{Q}} = 1$ and $\delta_{P,t} = 0$ then PGEN is currently in the process of returning to operation, as dictated by SAPR. During this process, flow can thus be distributed to the PGEN and thus $\alpha < 1$. The thermal load that must be assigned to the PGEN is, as discussed in Chapter 5.1.3, 20% of the design thermal load $\dot{Q}_{P,t} = \dot{Q}_P^{max} \cdot 20\%$. Note that in SAPR, both binary parameters change to zero and the startup procedure will restart if the thermal load to the PGEN is below the 20% requirement.

Finally, if $\delta_{\dot{Q}} = 1$ and $\delta_{P,t} = 1$ then the PGEN is in normal operating mode and the WP can distribute thermal load to the PGEN to generate electrical power.

The temperature setpoints for the PGEN and ACHX as well as the distribution of flow between the PGEN, ACHX and BP has been determined. The assigned mass flows and determined setpoints will now be used by the control philosophy to continuously adjust controllable equipment such as valves and fans to ensure that the flow and temperature setpoints are reached. From $\dot{Q} = \dot{m} \cdot Cp \cdot \Delta T$ it can be stated that if these setpoints are reached, the assigned thermal loads are also reached.

A sample script of WP is provided in Appendix F.

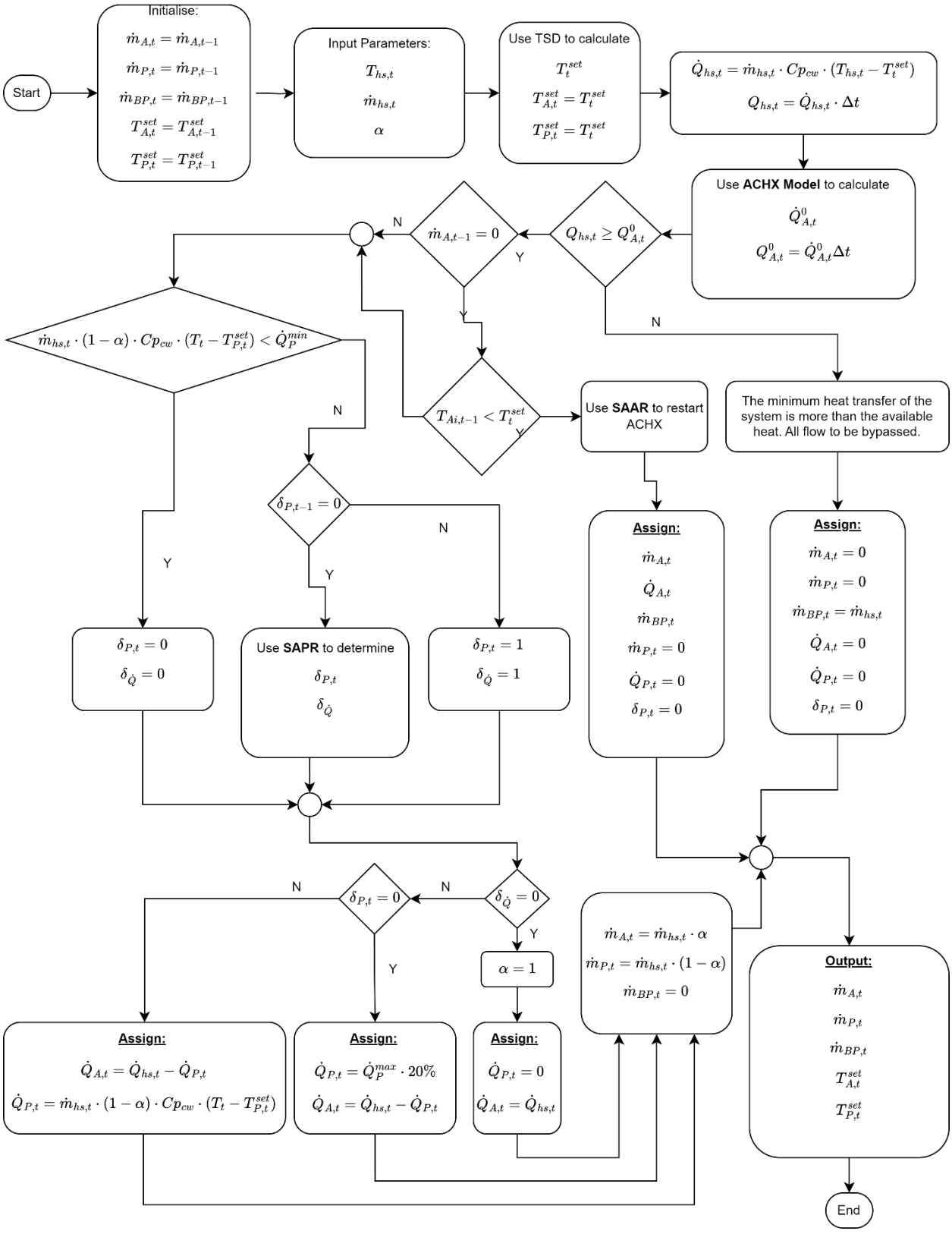


Figure 5-4: Flow Diagram of WP

5.3 Performance Evaluation of WP

To evaluate the operation of WP, two datasets are used. The first dataset demonstrates the typical operation of ACHX and PGEN on a smaller timeframe where changes in operational modes are clearly identifiable.

This historical dataset is then used to evaluate the average performance of the PGEN and ACHX processes over a longer period of time. Sections of the performance on the historical dataset will also be illustrated where required.

5.3.1 Demonstrative Dataset

To demonstrate the behaviour of WP, the plant parameters set out in Table 3-1, Table 3-2 and Table 3-3 be used with additional parameters being supplied where required.

The average minimum cooling water temperature entering the gas cooler is set as $\overline{T}^{LL}$ =150 ℃ as in Table 3-1. PGEN has a lower heat limit of $\dot{Q}_P^{min}$ =2 MW and a maximum thermal load of $\dot{Q}_P^{max}$ =20 MW. The cold and warm start procedure parameters for PGEN are as set out in Chapter 5.1.3. The value of α =0.25 as per the current Works' Philosophy.

5.3.1.1 Results for Distribution of Flow and Heat

The setpoint temperature for both the ACHX and PGEN are the same, as described in the formulation above. The setpoint temperature for the system with a demonstrative dataset has, therefore, already been illustrated in Figure 4-14.

The total heat transferred every time period is illustrated in Figure 5-5 along with the heat transferred by the PGEN and ACHX individually.

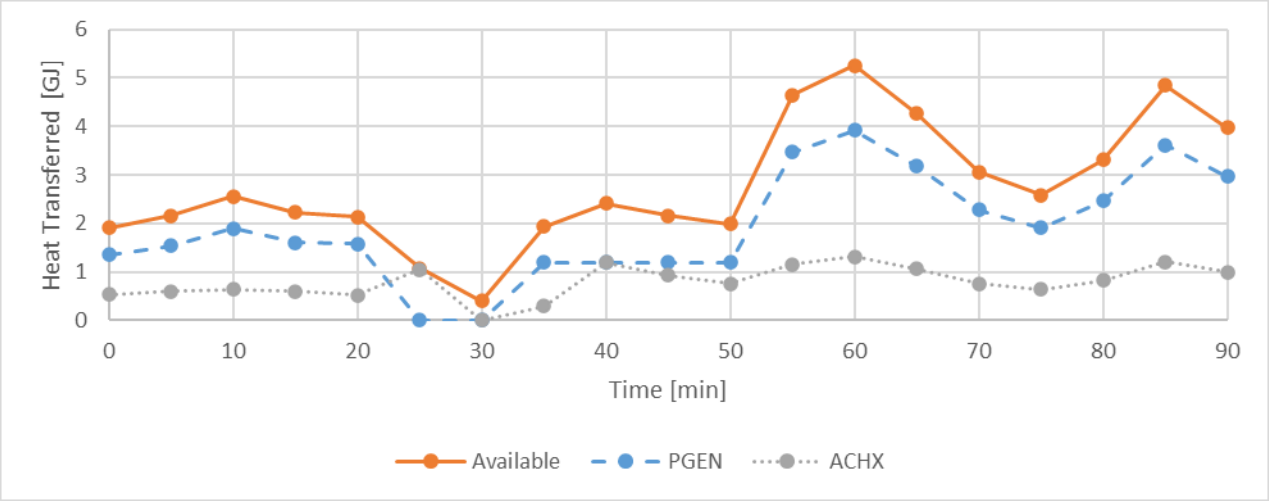


Figure 5-5: Heat Transferred by ACHX and PGEN for WP on a Demonstrative Dataset

From this figure, it can be noted that at 25 min the available heat after the minimum heat transfer through ACHX is observed is such that PGEN enters a tripped state. Note that all the available heat is thus transferred by ACHX to ensure that the temperature setpoint is reached.

The available heat at 30 min is not sufficient to initiate the restart procedure of the PGEN and thus all the heat is again transferred by the ACHX. However, at 35 min there is sufficient heat for the restart procedure of the PGEN to commence; thus, a fixed value of heat is transferred from 35 to 50 min, during which the ACHX transfers the rest of the available heat. At 55 min the restart procedure of the PGEN has been completed and the heat transferred by the PGEN can be increased along with a restart of the electrical power generation process.

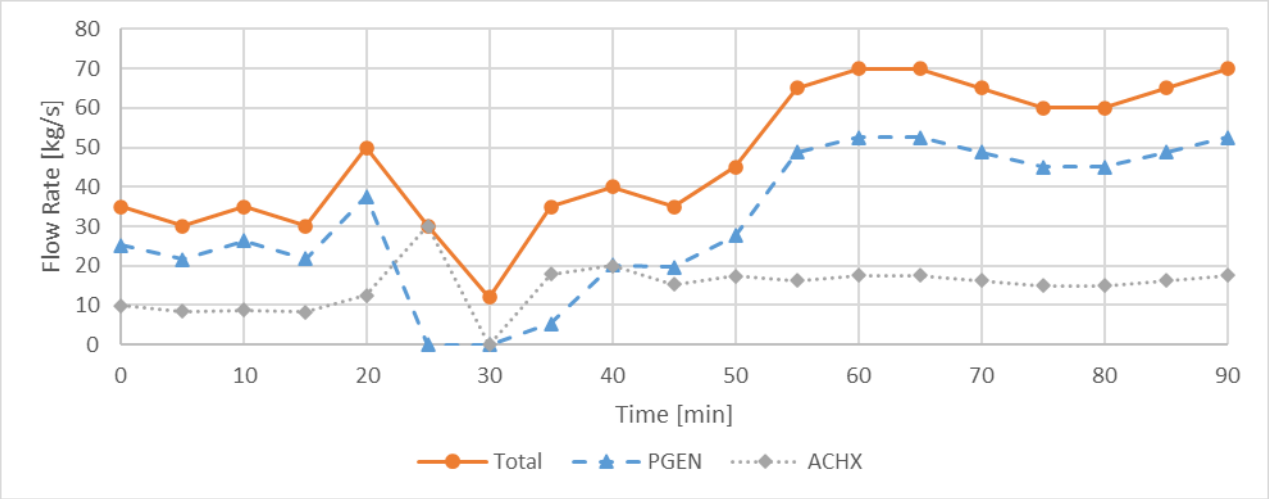


Figure 5-6: Flow Distribution between ACHX and PGEN

The flow distribution between the ACHX and PGEN is illustrated in Figure 5-6. The effect of the fixed ratio of flow distribution philosophy is clearly noted during the times that both the PGEN and ACHX transfers heat under normal operating conditions. However, during the restart procedure of the PGEN from 35 to 50 min, the flow distribution is determined based on the setpoint temperature and the heat transfer requirement at the PGEN, currently a constant 4 MW.

5.3.1.2 Results for ACHX and PGEN Operation

The operational settings of the ACHX during the demonstrative dataset is illustrated in Figure 5-7. Firstly, note that a single fan only became operational at 25 min. This is due to the average heat transfer rate of the ACHX with no operational fans being sufficient to remove the required heat to meet the setpoint temperature.

The single fan becomes operational from 35 to 70 min. The required operational speed of the fan is also illustrated on the secondary axis. The timeframe where the required operational speed of the fan at the ACHX is at its highest also corresponds to the timeframe of highest available heat transfer, even though the PGEN is in operation.

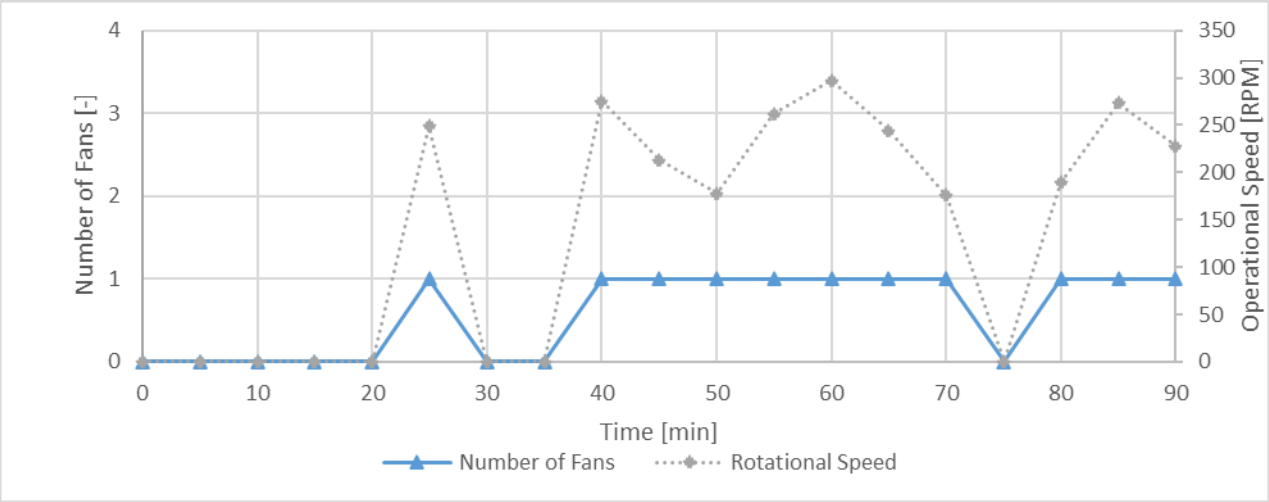


Figure 5-7: ACHX Operational Settings for WP on Demonstrative Dataset

Due to the independent operation of the PGEN and ACHX, it can be noted that even though the PGEN has returned to operation at 55 min, fans are still in operation. This is to remove the required heat to ensure that the setpoint temperature for the ACHX is met. The demonstrative dataset time horizon does not allow the simulation of an ACHX with no flow and the subsequent monitoring of the internal temperature with the purpose of restarting the flow through it in a controlled manner (Chapter 5.1.2.2). This will thus be illustrated on the historical dataset.

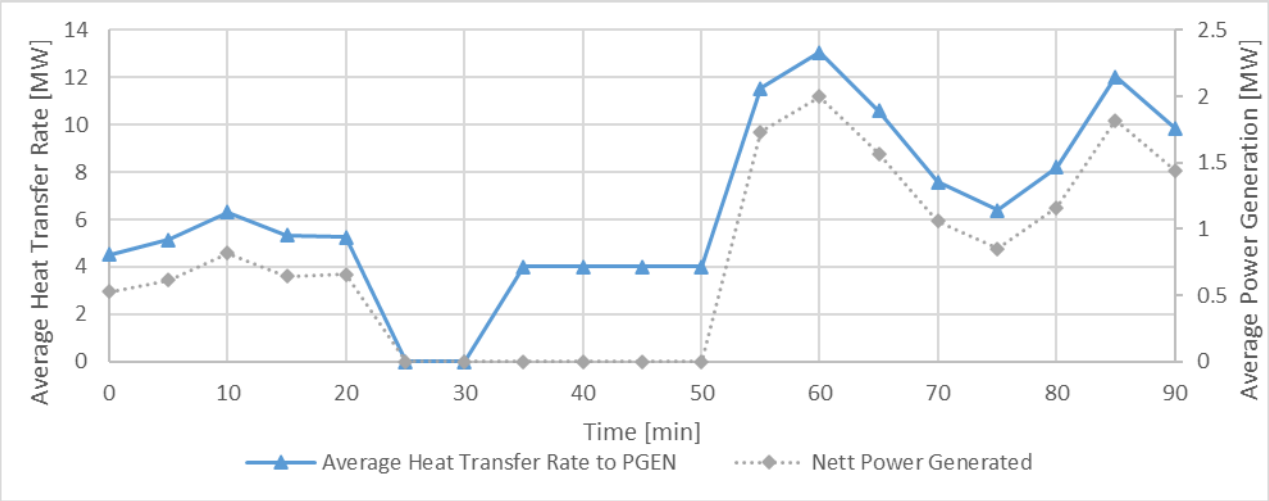


Figure 5-8: Power Generation by PGEN for WP on Demonstrative Dataset

The average heat transfer rate at the PGEN along with the nett power generation is illustrated in Figure 5-8. During the restart phase, no power is generated, as dictated by the controlled restart philosophy of the PGEN.

A total of 36.57 GJ is transferred to the PGEN at an average heat transfer rate in the evaporator component of 6.415 MW. This is 69.74% of the total available heat. The average power generation while the PGEN is in operation 1.145 MW, resulting in an average of 0.784 MW over the time horizon of the demonstrative dataset.

An average for the thermal efficiency, weighted by power generation, also indicate a value of 14.16%. An illustration of how the thermal efficiency vary over the time horizon is provided in Figure 5-9.

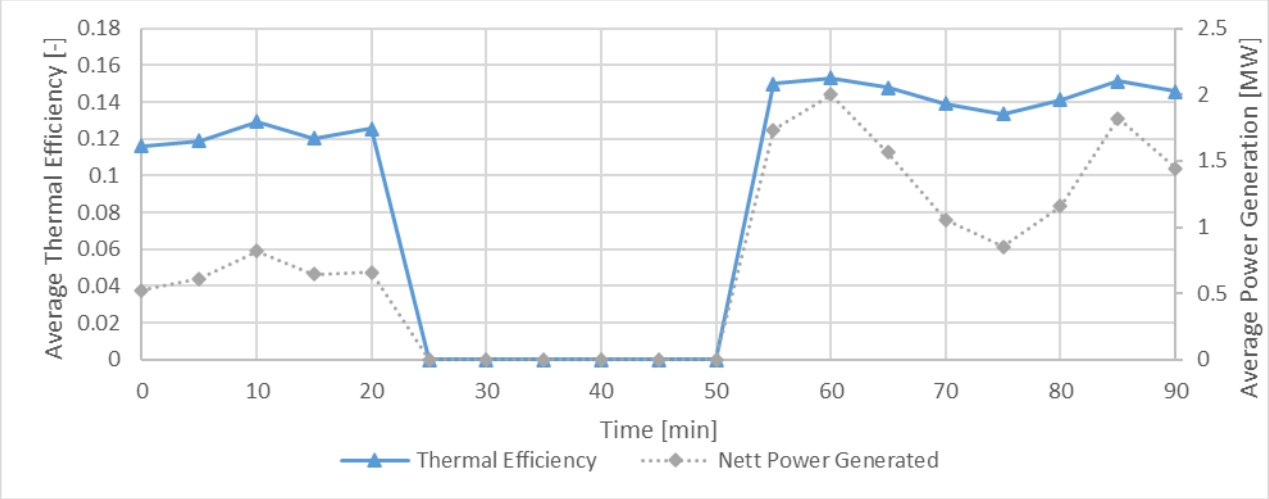


Figure 5-9: Efficiency over Time for PGEN with WP on Demonstrative Dataset

As noted in Chapter 4.2, the PGEN control philosophy adjusts the evaporating pressure and degree of superheat achieved in the PGEN cycle to maximise power generation. The reasoning behind these adjustments has been provided earlier in this thesis. The adjustments the PGEN control philosophy makes to these parameters are illustrated in Figure 5-10.

Note that during the restart procedure a fixed evaporating pressure and degree of superheat is maintained by the PGEN control philosophy. Since no power generation is allowed during this procedure the control philosophy does not attempt to adjust these parameters since there is no power generation objective.

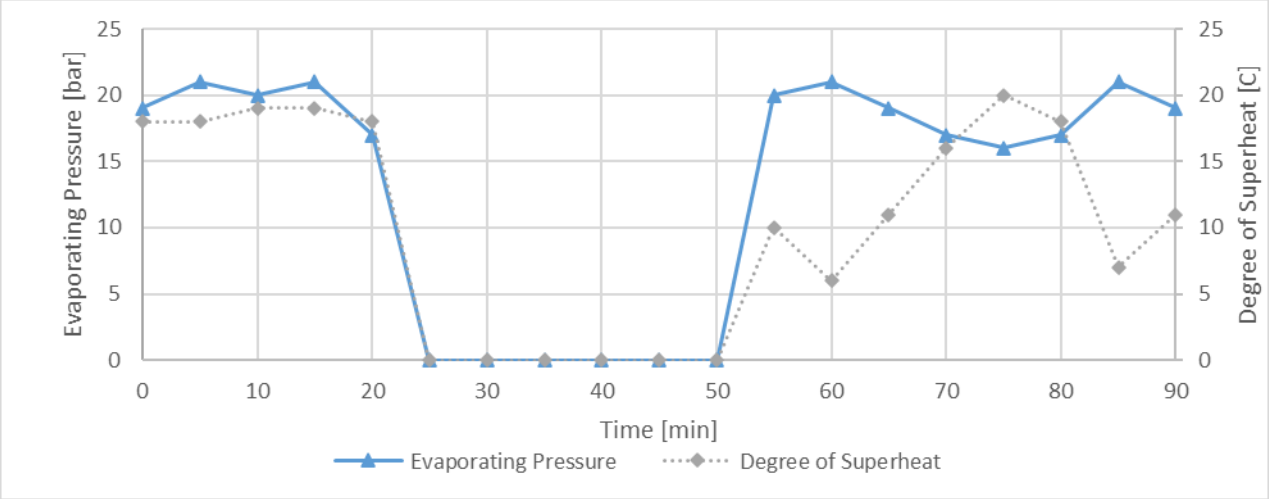


Figure 5-10: PGEN Settings for WP on Demonstrative Dataset

From the above results on the demonstrative dataset, the WP and sub-models work as expected. The simulation process can thus be followed on the historical dataset to determine the expected performance of the ACHX and PGEN under the control of the WP.

5.3.2 Historical Dataset

To evaluate the behaviour of WP, the plant parameters set out in Table 3-1, Table 3-2 and Table 3-3 are used with additional parameters being supplied where required.

The average minimum cooling water temperature entering the gas cooler is set as $\overline{T}^{LL}$ =150 ℃ as in Table 3-1. PGEN has a lower heat limit of $\dot{Q}_P^{min}$ =2 MW and a maximum thermal load of $\dot{Q}_P^{max}$ =20 MW. The cold and warm start procedure parameters for PGEN are as set out in Chapter 5.1.3. The value of $\alpha = 0.25$ as per the current Works' Philosophy.

5.3.2.1 Demonstration of SAAR

The first section of results illustrated is the performance of SAAR, where flow through the ACHX must be restarted in a controlled manner to ensure that the cooling water temperature entering the gas cooler remains within the operational envelope.

This is illustrated in Figure 5-11. At 335 min all the flow is bypassed due to low heat availability in the cooling water. This approach is maintained until 360 min where only a controlled fraction of the water is passed through the ACHX, and the rest is bypassed. This is as per the SAAR approach where the flow moving through the bypass line is used to ensure that the temperature at point 5 in Figure 1-1 is always within the operational envelope.

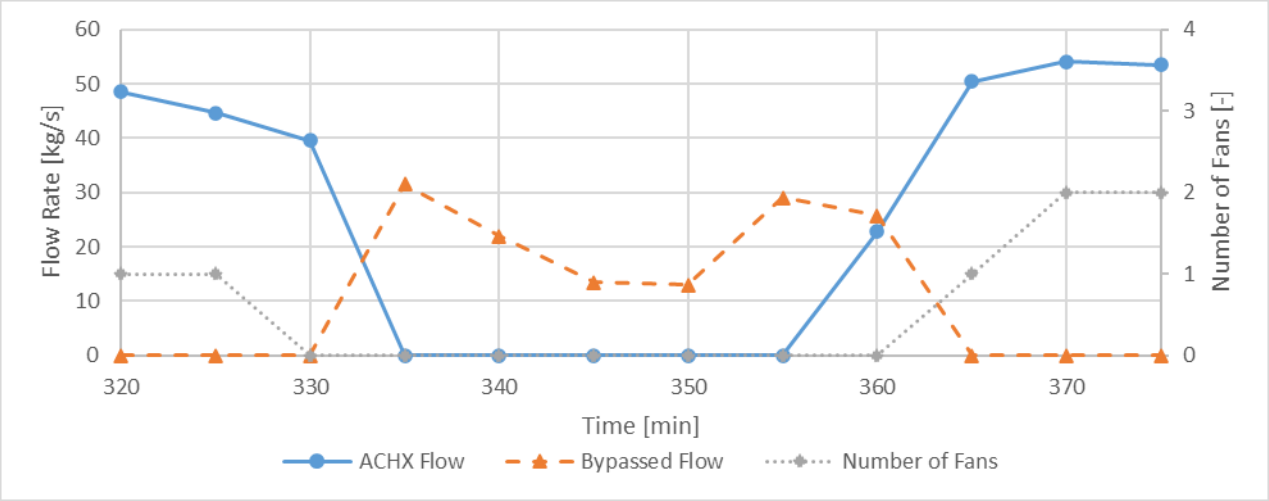


Figure 5-11: Demonstration of SAAR in Historical Dataset

With the internal temperature being restored to within the operational envelope at 355 min, normal operation resumes at 360 min. This is as expected with the SAAR philosophy. It is thus accepted that the SAAR sub-model works as intended on the historical dataset with no required adjustments identified.

5.3.2.2 Unplanned Trip of PGEN

It is stated in Chapter 3.6 that 1 unplanned trip event for the PGEN will occur during the historical dataset as per the expected reliability. It is required that the heat rejection system maintain the operational envelope, even when an unplanned trip event is triggered. Failure to maintain the operational envelope renders the control philosophy invalid for use.

An unplanned trip event is forced at 38 520 min in the historical dataset, with a downtime of 60 min. The response of the system is illustrated in Figure 5-12. Note that the control philosophy of WP makes no adjustment to flow distributions or temperature setpoints in anticipation for this trip. As stated earlier in this chapter, it is expected that maintaining a minimum flow rate through the ACHX will ensure compliance to the operational envelope.

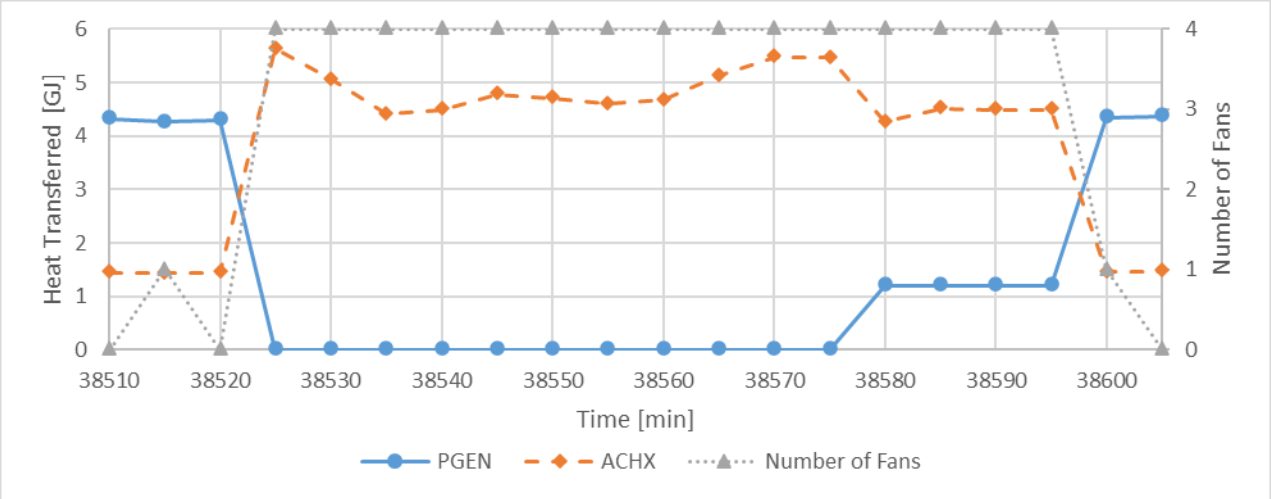


Figure 5-12: Unplanned Trip Response of WP

During the period with the unplanned trip event, all the heat is transferred by the ACHX, with an increase in fan usage from 1 to 4. Hereafter the ACHX is controlled for 60 min as if there is no PGEN available. Due to the high heat availability during this trip event, the PGEN can complete the warm restart procedure in the first attempt, after which the heat transfer to the PGEN is increased again.

SAPR works as intended, not only during low heat availability times as shown in the previous section, but also during periods of high heat availability with unplanned trip events.

5.3.2.3 Summary of Performance Results

The section below summarises the performance of the system over the historical dataset under the control of WP. Performance parameters monitored that has not been defined yet is the electrical power generation by PGEN, $W_{P,t}$ (W) and the energy recovery efficiency $\eta_{ER} = \sum W_{P,t} / \sum Q_{fg,t}$. The energy recovery efficiency is the ratio of the electrical power generated by PGEN to the total energy available in the flue gas, stated as 88 806.5 GJ in Chapter 3.

Table 5-1: Summary of Performance Evaluation for WP

Parameter	WP	Unit
Time $\overline{T_5} < 150\,℃$	0	min
% of time PGEN is in operation	95.9	%
Heat transferred by Gas Cooler	81 914.9	GJ
% of Total Heat in Flue Gas	92.24	%
Heat transferred by PGEN	60 889.85	GJ
% of Total Heat in Cooling Water	74.33	%
Average heat transfer rate at PGEN	8.61	MW
Average power generation	1.231	MW
Weighted average η_{th}	14.39	%
Energy Recovery Efficiency	9.40	%

The gas cooler operational envelope is maintained throughout the time horizon of the historical dataset while the PGEN is in operation for 95.9% of the time. The current approach to cooling water flow resulted in 81 914.9 GJ of available heat in the cooling water, which is 92.24% of the available heat in the flue gas. The total heat transferred by the PGEN evaporator is 60 889.85 GJ, which is 74.33% of the total heat available in the cooling water in the historical dataset.

The average heat transfer rate at the evaporator of the PGEN is also determined to be 8.612 MW, resulting in an average power generation of 1.231 MW over the time horizon. The thermal efficiency of the PGEN is weighted according to the power generated and this resulted in 14.39%. The energy recovery efficiency, described above, resulted in a value of 10.55%.

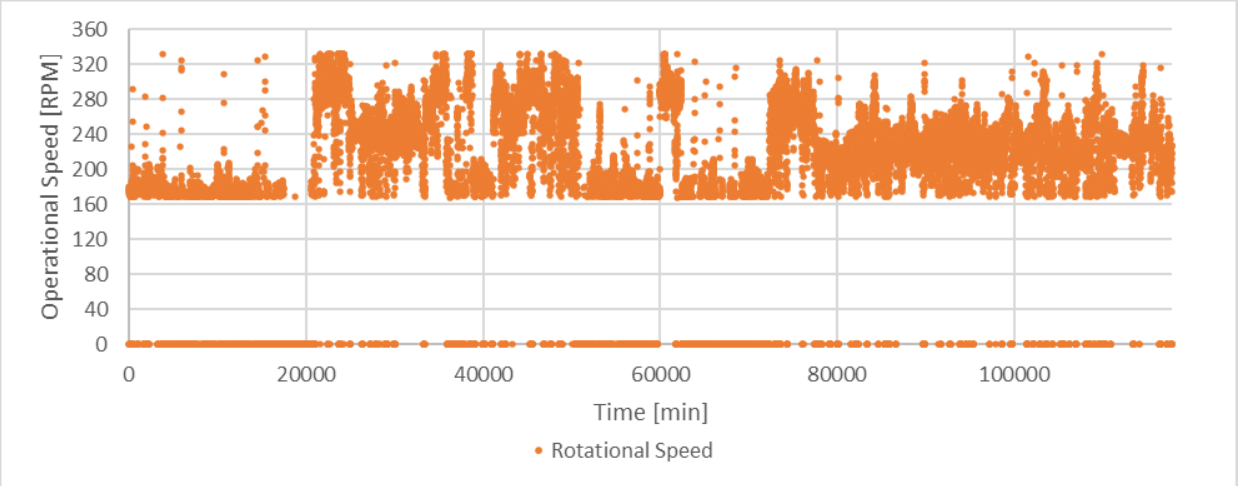


Figure 5-13: Operational Speed of Fans over Time Horizon of Historical Dataset

The operational speed of the fans is illustrated in Figure 5-13. It can be noted that there are several time periods where there are no fans in operation. The minimum and maximum operational speeds of the fans are also adhered to, as stated in Table 3-2.

In addition to the ACHX being controlled to meet fluctuating heat transfer demands, the PGEN is also operated under the PGCP. As the fluctuation in heat source properties results in off-design operation of the PGEN, some variation in thermal efficiency can be expected.

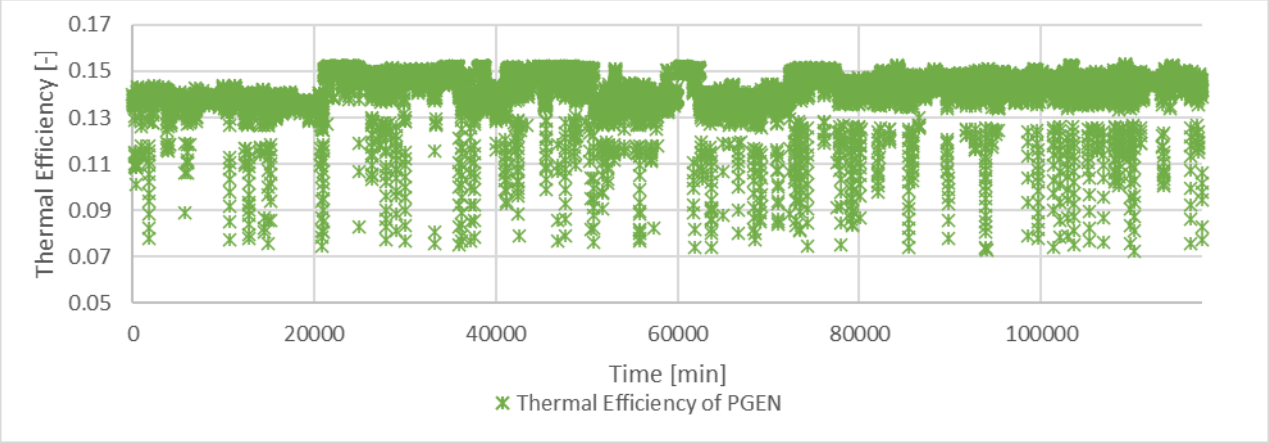


Figure 5-14: Thermal Efficiency of PGEN over time horizon of Historical Dataset

The resulting thermal efficiency over the time horizon of the historical dataset is illustrated in Figure 5-14. A maximum and minimum thermal efficiency of 15.31 and 7.25% is noted, respectively.

The resultant temperatures at point 5 in Figure 1-1 is also illustrated in Figure 5-15, along with the allowable limits. The temperature is close to the lower limit for most of the time periods, as per the philosophy approach to maximise energy recovery from the cooling water. Note that the operational envelope is maintained.

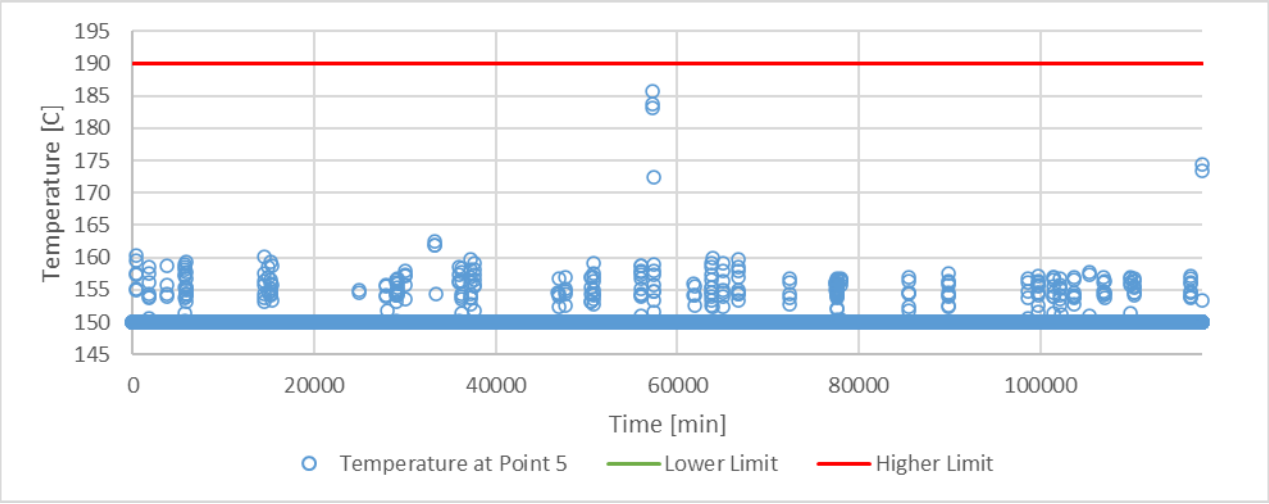


Figure 5-15: Temperature at Point 5 with WP

5.3.3 Adjustment to Ratio

The fixed value of α is shown to be sufficient to ensure the gas cooler operational envelope is maintained. However, a fixed value for flow distribution under fluctuating cooling water parameters after the gas cooler is not determined with maximum power generation as the objective. This section will briefly summarise the results and compare it to the WP for $\alpha = 0.25$ in Table 5-1.

An identical simulation approach to that done in this chapter is followed such as unplanned trips and component parameters, with the only parameter that is adjusted being the flow distribution ratio of α. Values of 0.2 and 0.3 for α is modelled.

The result of this comparison is provided in Table 5-2. It is shown that all three values of α delivers acceptable performance in terms of maintaining the temperature envelope at point 5. The percentage of time that the PGEN is in operation is also similar with 95.9% for both α =0.2 and 0.25 and 95.8% when α =0.3. The percentage of available heat transferred by the PGEN is a maximum of 79.232% at α =0.2 and a minimum of 69.383% at α =0.3. This is to be expected with the independent operation and thus fixed flow distribution ratio and identical setpoint temperature between the ACHX and PGEN.

The average heat transfer rate at the PGEN evaporator is a maximum of 9.18 MW when α =0.2, this also results in the highest average power generation of 1.326 MW.

Table 5-2: Comparison of performance for different α parameters under WP

	Value of α			
Parameter	**0.20**	**0.25**	**0.30**	**Unit**
Time $\overline{T}_5 < 150$ ℃	0	0	0	min
% of time PGEN is in operation	95.9	95.9	95.8	%
Heat transferred by PGEN	64 891.44	60 889.85	56 834.92	GJ
% of Total Heat	79.22	74.33	69.38	%
Average heat transfer rate at PGEN	9.18	8.61	8.04	MW
Average power generation	1.326	1.231	1.134	MW
Weighted average η_{th}	14.32	14.39	14.21	%
Energy Recovery Efficiency	10.21	9.40	8.66	%

The energy recovery efficiency is also noted to be at a maximum at $\alpha = 0.2$ with 10.21% while the minimum is reported at $\alpha = 0.3$ with a value of 8.66%. This indicates that there is potential for improvement in the power generation performance of the system if the ratio of flow distribution were to change or even be dynamically adapted every timestep.

5.4 Conclusion

This chapter illustrated the formulation and performance of the WP on a historical dataset. The first section of the chapter provided two sub-algorithms that must always be present and unchanged the control philosophy.

The first sub-algorithm ensures that the control philosophy maintains the temperature envelope in low heat conditions where flow through the ACHX need to be bypassed. This sub-algorithm ensures this by restoring the flow through the ACHX by managing the flow distribution between the bypass and ACHX until no flow is bypassed.

The second sub-algorithm ensures that a PGEN process in a tripped state is monitored and restarted in a controlled procedure, depending on the time it is offline. Both the hot and cold restart procedures include the monitoring of the time delay until sufficient heat is available. A fixed amount of heat is then used per timestep for a required amount of time until the system is deemed warm enough to restart the power generation. Once the power generation is restarted, the limit to heat transferred at the PGEN is also removed.

The chapter then provides the formulation of the current used Works Philosophy. In summary, this philosophy operates the PGEN and ACHX as independent processes with a fixed ratio of flow distribution between them. The independent approach also results in the setpoint temperatures of both processes being set high enough to ensure that the operational envelope is maintained even if one of the systems should become unavailable. The current works philosophy distributes 25% of the flow the ACHX under normal operation.

In addition to the performance evaluation, a tripped state is also forced during a high heat availability period to evaluate both the restart procedure and the ability to maintain the operational envelope. The WP is successful in maintaining the operational envelope.

The WP approach on the historical dataset resulted in a PGEN that is operational 95.9% of the time, transferring 74.33% of the available heat from the cooling water. The average power generation for the PGEN is determined to be 1.231 MW with a weighted thermal efficiency of 14.39%. The energy recovery ratio is also determined to be 9.40%.

The final section of this chapter re-evaluated WP with different flow distribution ratios. It is observed that a higher flow to the PGEN results in higher power generation when the setpoint temperature of both the PGEN and ACHX is set to be the same. There is thus potential for improvement of the power generation performance of the system without negatively impacting the operational envelope.

An illustrative summary of the Works Philosophy and its communication with the different process models is provided in the figure below. Note that the gas cooler temperature control is currently inherently part of the dataset and not adjusted as per the WP.

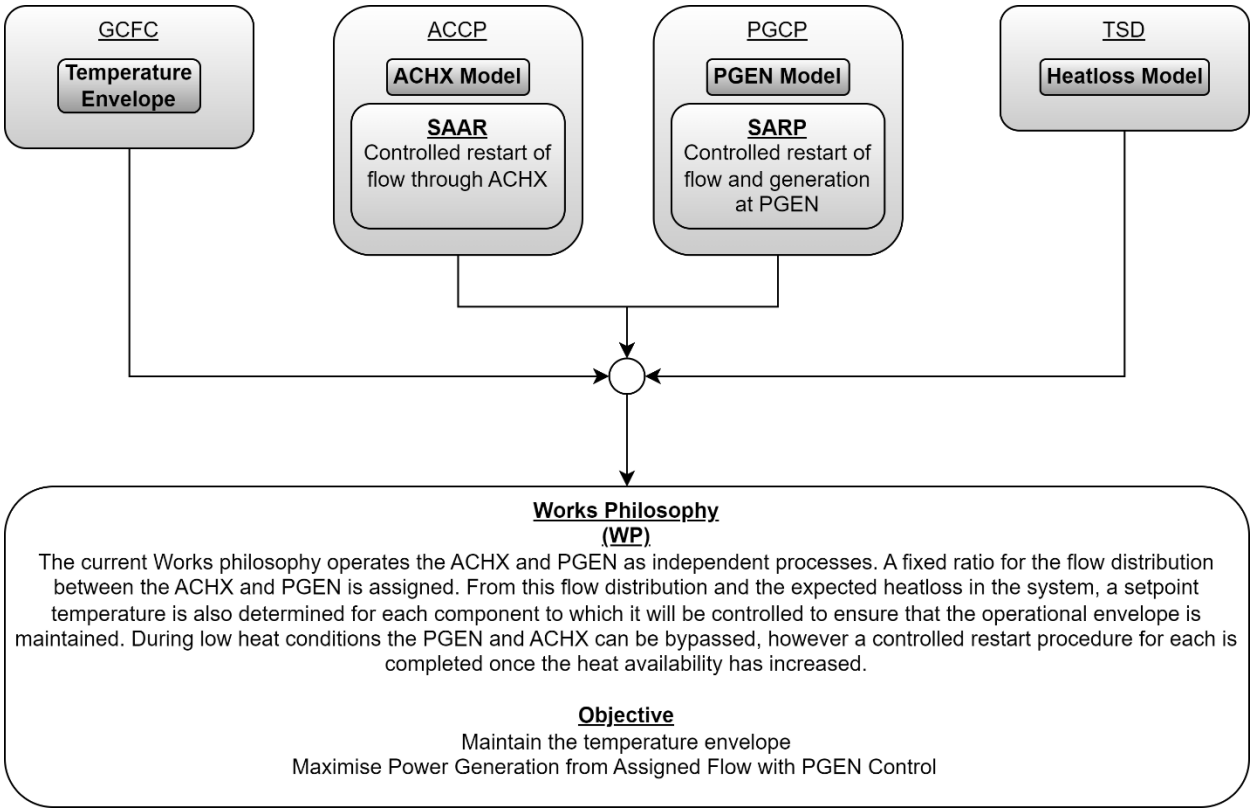


Figure 5-16: Summary of Control Philosophies of WP after Conclusion of Chapter 5.

CHAPTER 6 DISCRETE ADJUSTMENT TO DISTRIBUTION

It is shown in the previous chapter that operating the PGEN and ACHX as independent processes with a fixed ratio of flow distribution is sufficient to maintain the operational envelope. However, it is also shown that the current ratio of flow distribution does not maximise power generation.

This chapter will attempt to improve on the power generation performance of WP while still maintaining the operational envelope.

6.1 Approach Changes from WP

The fluctuating heat source results in off-design operation of all the components in the system. It is noted in the previous chapter that the current WP is to operate the PGEN and ACHX as independent systems. Combine this with the fixed ratio of distribution between the two components and the results is that both the ACHX and PGEN having the same setpoint temperature.

The same setpoint temperature and a fixed flow distribution ratio results in the heat transfer distribution between the ACHX and PGEN also being having a fixed ratio. With a fluctuating heat source, it is expected that this does not result in maximum power generation.

Due to off-design effects in terms of heat transfer, turbine and pump performance a fluctuating heat source has, it is expected that maximum power generation point is dynamic across the time horizon. The flow distribution and setpoint temperature that results in maximum power generation be determined every time the heat source has a change in parameters.

It follows that to attempt maximum power generation with the available heat, the operation of PGEN and ACHX need to be approached as a singular system. This will allow for the dynamic adjustment of flow distribution ratios and the assignment of different setpoint temperatures to these components, all based on the current heat source conditions and the heat transfer availability in the system. This is referred to as the Discrete Adjustment to Distribution Philosophy (DADP).

The first step toward this dynamic adjustment is the addition of sub-algorithms that can determine the allowable distribution rates at every time step based on the heat source parameters.

6.2 Additional Sub-Algorithms for Sustained Operation

The previous chapters sub-algorithms are still valid for this philosophy. As stated above, a sub-algorithm is required that uses the current heat source parameters and determines the allowable distribution ratio between the ACHX and PGEN. This section will provide the formulation and testing of this sub-algorithm.

6.2.1 Minimum and Maximum Cooling Water Flow through ACHX

Before the improved control philosophy for the distribution of flow between ACHX and PGEN can be formulated and demonstrated, the minimum cooling water flow rate through the ACHX need to be established. All future control philosophies formulated in this thesis will consider this range when determining the required distribution between the ACHX and PGEN.

6.2.1.1 Change in Minimum Flow Approach for DADP

The WP is the current Works philosophy, and, therefore, the minimum flow assigned to the ACHX represents the approach followed at present. The current approach to determine the minimum flow to be assigned to the ACHX is illustrated in Figure 6-1.

The minimum flow that needs to be assigned to the ACHX at time t, $\dot{m}_{A,t}^{min}$ kg/s, is determined using the total cooling water mass flow, $\dot{m}_{hs,t}$, the cooling water temperature, $T_{hs,t}$, as well as the setpoint temperature $T_{A,t}^{set}$ for the ACHX system.

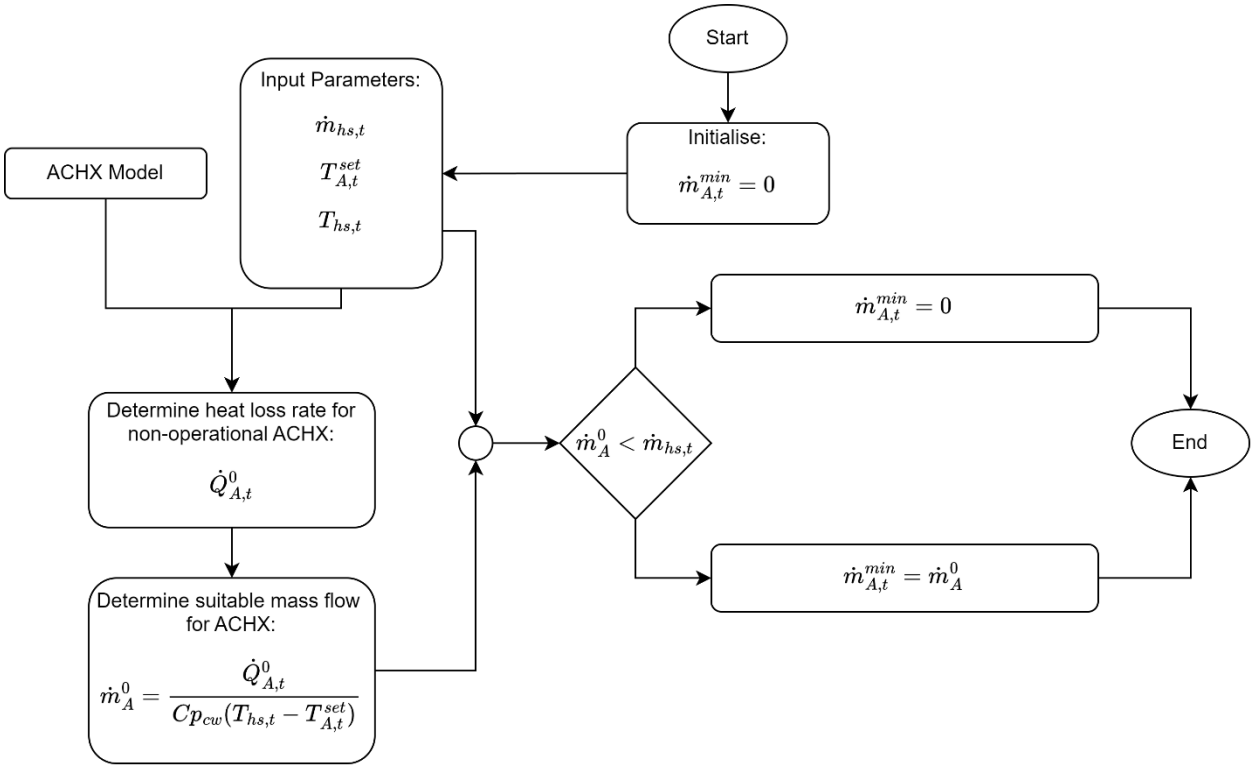


Figure 6-1: Minimum Flow Assignment to ACHX through WCP (SAMF)

The ACHX model, discussed in Chapter 3, is used to determine the heat transfer rate to the environment, $\dot{Q}_{A,t}^{0}$ (W) for a non-operational ACHX. This heat transfer rate is then used to determine the required flow rate $\dot{m}_A^0$ that will ensure the returning cooling water temperature is above the setpoint, $T_{cw2} > T_{A,t}^{set}$. Note that as $\dot{m}_A^0$ is increased, a lower temperature difference in the cooling water can be expected for the same heat transfer rate.

Thus, if $\dot{m}_A^0 > \dot{m}_{hs,t}$ it indicates that there is not sufficient heat in the cooling water to maintain the operating envelope and thus the philosophy from Chapter 5.1.2.1 is used where the ACHX is bypassed and then restarted in a controlled manner.

However, if $\dot{m}_A^0 < \dot{m}_{hs,t}$ it indicates that there is sufficient heat that the if the minimum flow is to be sent to the ACHX, the operational envelope is maintained on the lower limit. As mentioned earlier, an increase to this minimum flow without increasing the heat transfer rate through the fans will result in a lower temperature difference and thus $T_{cw2} > T_{A,t}^{set}$ is maintained.

6.2.1.2 Minimum flow through ACHX for Demonstrative Dataset

To illustrate how the minimum flow through the ACHX is determined, the control philosophy illustrated in Figure 6-1 is applied to the demonstrative dataset, provided in Figure 3-3.

For this demonstration the setpoint temperature T_t^{set} is determined through the heat loss algorithm illustrated in Chapter 4.4. It is also considered that the PGEN can become unavailable at any time and, therefore, the setpoint temperature for the ACHX needs to be larger or equal to the setpoint for the system and thus $T_{A,t}^{set} \geq T_t^{set}$. For this demonstration $T_{A,t}^{set} = T_t^{set}$.

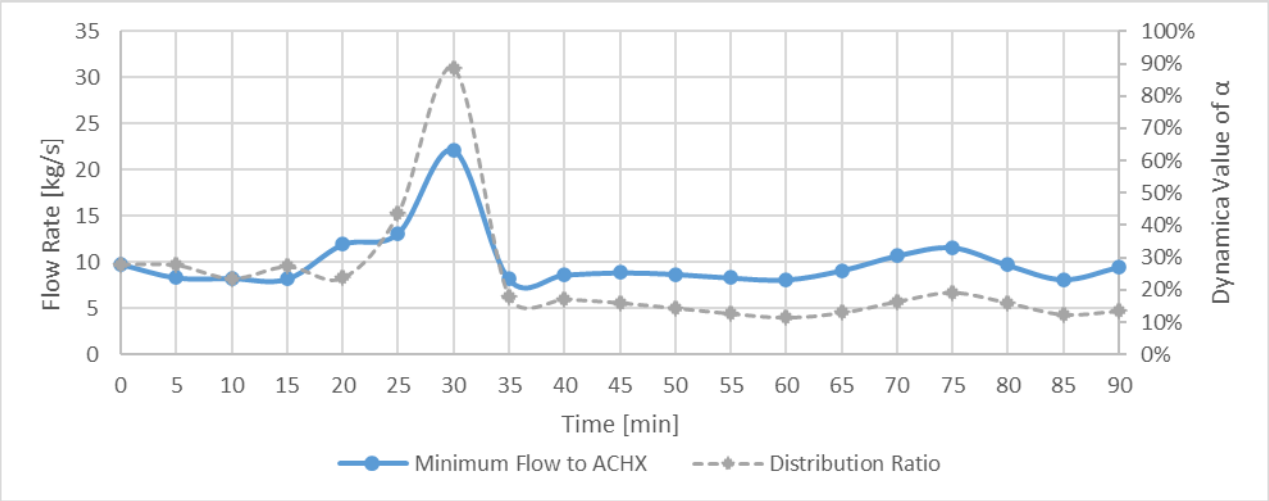


Figure 6-2: Minimum Flow through ACHX for Demonstrative Dataset

The minimum flow to the ACHX is shown on the primary axis in Figure 6-2 along with the relative value of α over time. The definition of a is maintained from the previous chapter.

Note that at $t = 30$ min almost 90% of the flow is required to flow to the ACHX. However, from $t = 35$ min a maximum flow distribution ratio of 20% is noted. The rest of the cooling water can be distributed to the PGEN for power generation without any added risk of breaching the operational envelope.

The next section will focus on how much of the remaining available flow must be distributed to the PGEN for maximum power generation.

6.3 Nett Power Generation vs Flow Distributed to PGEN

As mentioned above, it is shown in the previous chapter that a fixed flow distribution of $\alpha = 0.25$ does not maximise power generation. A reduction in the value α resulted in a higher flow rate being distributed to the PGEN and since the setpoint temperatures of both the PGEN and ACHX were set to be equal, this also resulted in more heat being transferred at the PGEN. This in turn resulted in an increase of the average power generation and energy recovery efficiencies.

Before the conclusion is made that for maximum power generation the maximum flow needs to be distributed to the PGEN, the current process and component constraints need to be considered.

The PGEN performance is dependent on the flow and temperature of the cooling water entering the evaporator. With fluctuating parameters, it is to be expected that the evaporator is operating in off-design conditions, as discussed in Chapter 3.4.2.1. The efficiency of heat transfer is thus impacted by these fluctuations. To meet the setpoint temperature for the cooling water exiting the PGEN, the working fluid flow rate and evaporating pressure is adjusted which in turn influences the pump power required.

To evaluate the influence that the flow rate of cooling water to the PGEN evaporator has on the power generation performance, a case study is completed in the next section.

6.3.1 Case study for PGEN Flow Distribution Calculation

For this case study, the cooling water flow rate and temperature entering the heat rejection system is kept constant. The minimum flow required to the ACHX is determined. The flow distributed to the PGEN will then be adjusted iteratively between the allowable flow range. The allowable cooling water flow to PGEN ranges from all the residual flow, $\dot{m}_{hs,t} - \dot{m}_{A,t}^{min}$, to zero.

For the case study, cooling water exits the gas cooler at 190 ℃ at a flow rate of 36 kg/s. This results in a required average heat transfer rate of 6 MW or a total heat transfer of 1.8 GJ over a 5 min period.

The first step is to determine the average minimum heat transfer rate expected over 5 min for an ACHX with no operational fans, which is 1.704 MW. It follows that an average of 8.296 MW or 2.489 GJ can be transferred by the evaporator of the PGEN.

The second step of the case study is thus to determine the minimum flow to ACHX. The value of $\dot{m}_{A,t}^{min}$ is determined to be 10.217 kg/s. This indicates that the flow that can be distributed to PGEN ranges from $0 \leq \dot{m}_{P,t} \leq 25.783$ kg/s.

At each iteration, the PGCP is used to determine the evaporating pressure and degree of superheat that will result in maximum power generation. The evaporating pressure and degree of

superheat allowable ranges are still the same as the limitations provided in Table 3-3. The maximum flow rate achievable for the working fluid through the cycle pump is also unchanged. The shaft power required is also determined from the equation in (3.14).

The PGCP has been described in detail in Chapter 4.2 and will not be restated in this section. Should a distributed flow rate result in invalid operational parameters for the PGEN then it is removed from the results dataset.

The case study is repeated for three other flow rate and cooling water temperature combinations. The second combination has a cooling water temperature of 200 ℃ and a flow rate of 28.8 kg/s while the third combination has cooling water temperature of 210 ℃ and a flow rate of 24 kg/s. The last combination is for cooling water temperature of 180 ℃ at a flow rate of 48 kg/s. All the combinations result in a required average heat transfer rate of 6 MW or a total of 1.8 GJ over the 5 min period.

The results of this case study are provided in Figure 6-3 where the nett power generation is plotted versus the cooling water flow to PGEN for several inlet temperatures.

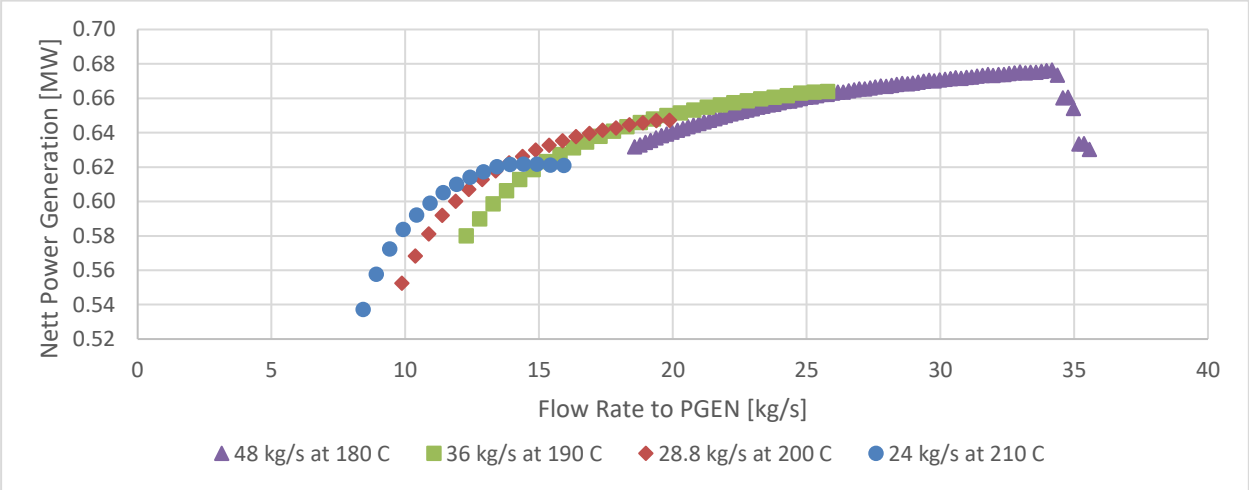


Figure 6-3: Nett Power Generation vs Cooling Water Flow Rate to PGEN

From the results it is noted that for two of the four case studies, the cooling water mass flow where the maximum power generation is observed is not at the maximum mass flow rate. For the combination with the lowest flow rate, there is a relatively small decrease in power generation as the flow rate is increased. On the opposite end, for the 48 kg/s and 180 ℃, there is a significant reduction in power generation after the flow rate to the PGEN is increased beyond 34.8 kg/s.

It follows that to achieve maximum power generation during all periods in the time horizon, the control philosophy needs to consider that curves like Figure 6-3 exists. The control philosophy must thus be able to find the maximum power generation point for the specific heat source parameter of the current period to reach the objective.

6.3.2 Bisection Method

To find this maximum power generation point, several numerical analysis methods can be used. The bisection method is a simple method where the root of an equation can be identified [54]. In this method an interval that contains the root of the equation is divided in two. The half that contains the root is identified after which the process is repeated until the root is identified [54].

The algorithm to find the root of an equation is given below:

Table 6-1: The Bisection Method Algorithm

	Step
1	Identify two numbers, a and b, where the function has different signs
2	Define the midpoint, $c = \frac{(a+b)}{2}$ and $f(c)$
3	Determine if the root exists I. $f(a)f(c) < 0$ then $r\epsilon(a, c)$ or II. $f(b)f(c) < 0$ then $r\epsilon(c, b)$
4	Choose the desired interval between (i) and (ii)
5	Repeat until maximum iterations or desired accuracy is reached

Note that the method above cannot be applied as stated above due to the absence of a curve fit for the power generation versus cooling water flow rate to PGEN. Had this been available, the derivative of this curve could be used where an identified root would indicate a turning point and a potential maximum point.

This method can be modified to find the maximum on the curves shown in Figure 6-3. The modified algorithm is shown in Table 6-2. The modified algorithm starts with identifying the minimum and maximum flow rate that can enter the PGEN and still deliver a valid operational point. The midpoint between these limits is identified after which the power generation is determined at the limits and the midpoint.

The trend is then evaluated from the minimum to the midpoint, referred to as the left direction, and from the midpoint to the maximum, referred to as the right direction. By analysing the trends, a decision can be made in which direction the flow rate must be adjusted to reach maximum power generation.

If the trend to the left of the midpoint is positive while the trend to the right is negative, it can indicate that the maximum is close to the midpoint and thus both the minimum and maximum flow rates can be brought closer to the midpoint. If both the trends are positive, the midpoint needs to move closer to the maximum and, therefore, the minimum flow is increased. If the trend to the left

is negative, it indicates that the midpoint needs to move to the left, thus decreasing the maximum flow rate. The above decision-making process is provided in Table 6-2.

This algorithm is repeated until the maximum number of iterations, or the desired accuracy is reached. The final midpoint is then reported and assigned to the control philosophy.

Table 6-2: Modified Bisection Method Algorithm for use in DADP (BM-PGEN)

	Step
1	Identify the maximum and minimum flow rate to the PGEN, a and b.
2	Define the midpoint, $c = \frac{(a+b)}{2}$ and determine the power generation at c; $W_{P,t}(c)$
3	Determine the power generation at the maximum and minimum flow, $W_{P,t}(a)$ and $W_{P,t}(b)$
4	Determine the trends between the midpoint and the maximum and minimum flows: I. $m_r = \frac{W_{P,t}(a)-W_{P,t}(c)}{a-c}$ II. $m_l = \frac{W_{P,t}(c)-W_{P,t}(b)}{c-b}$
5	Update the interval accordingly: I. $m_r < 0$ and $m_l > 0$ then $b = \frac{b+c}{2}$ and $a = \frac{(a+c)}{2}$ II. $m_r > 0$ and $m_l > 0$ then $b = c$ III. $m_l < 0$ then $a = c$
6	Repeat steps 2 to 5 until maximum iterations or desired accuracy is reached.

6.4 Formulation of the Discrete Adjustment to Distribution (DADP)

The sub-algorithms provided in earlier chapters are used to ensure that the trip and restart of flow through the PGEN and ACHX is accurately accounted for during the execution of DADP. IN addition, the bisection method above is used to maximise the power generation whenever there is sufficient heat to do so. The formulation of the DADP is provided in this section of the chapter.

An illustration of the logic of DADP is illustrated in Figure 6-4.

The notation in the formulation below is consistent with the formulation of WP where T (℃), Q (J), $\dot{Q}$ (W) and $\dot{m}$ (kg/s) represent temperature, heat, heat transfer rate and mass flow respectively with sub-and superscripts used to identify specific parameters and values.

The time index for the formulation is given by $T = \{1,2,\dots,|T|\}$. The difference in time between t and $t+1$ is constant and indicated by Δt. The cooling water exits the heat gas cooler at a temperature $T_{hs,t}$ (℃) and a mass flow rate of $\dot{m}_{hs,t}$ (kg/s). At time t, the TSD uses the predicted heat loss in the system to determine the desired temperature of the cooling water at the combined flow point at the exit of both the PGEN and ACHX components, T_t^{set} (℃). The average of the

available heat transfer rate at time t, $\dot{Q}_{hs,t}$ (W), and the available heat over time t, $Q_{hs,t}$ (J) is then calculated through equations similar to (3.3).

The first decision made in DADP is whether to bypass all the flow. This is done by first the ACHX model to determine the predicted heat transfer rate and heat transferred over time t for the ACHX with zero fans in operation. This prediction is made through the approximated model discussed in Chapter 3.3.2.1 and denoted as $\dot{Q}^0_{A,t}$ W and $Q^0_{A,t}$ (J) respectively. The SAMF algorithm then determines the minimum flow rate such that a heat transfer of $Q^0_{A,t}$ will result in $T^{set}_{A,t} = T^{set}_t$. Thus, the minimum flow through a ACHX with zero operational fans that can guarantee the temperature envelope is maintained.

If the predicted heat transfer over time t for a non-operational ACHX is more than the available heat, $Q^0_{A,t} \geq Q_{hs,t}$,then all the flow needs to be bypassed. It follows that the flow through the PGEN and ACHX components are zero, $\dot{m}_{P,t} = \dot{m}_{A,t} = 0$, and the flow through the bypass line is $\dot{m}_{BP,t} = \dot{m}_{hs,t}$. This is to minimise the heat transferred with PGEN and ACHX, $Q_{P,t} = Q_{A,t} = 0$, and thus maintaining the operational envelope. Through this decision, equation (3.1) will simplify to:

$$Q_{hs} = Q_{Res}$$

Since $Q_{hs,t}$ and thus $Q_{Res} > 0$, it is ensured that the operational envelope is maintained.

If not all the flow needs to be bypassed, the next step is to determine whether the ACHX is able to maintain the operational envelope. This is done by evaluating whether there is cooling water distributed to the ACHX and what the internal cooling water temperature is in the previous period. These parameters are provided and denoted with $\dot{m}_{A,t-1}$ and $T_{Ai,t-1}$.

If $\dot{m}_{A,t-1}$ is zero and $T_{Ai,t-1} < T^{set}_t$, it follows that the ACHX had stagnant water during the previous period that is below the allowable minimum temperature for cooling water entering the gas cooler. The operational envelope would, therefore, not be maintained should all the flow be distributed to ACHX. However, should no flow be distributed to the ACHX, the internal temperature will lower further with no heat being transferred in the system. Therefore, to ensure that ACHX can safely return to operation, a flow distribution between the ACHX and the bypass line is determined.

The mass of the water in the ACHX, m_A, as well as the internal temperature $T_{Ai,t}$ is used to determine the required distribution through SAAR (Chapter 5.1.2.2). This sub-algorithm ensure that the flow is distributed in such a way that the operational envelope is maintained through the mixing of the sub-cooled water from the ACHX and the higher temperature water from the bypass line. SAAR thus provides a $\dot{m}_{BP,t}$ and $\dot{m}_{A,t}$ where $\dot{m}_{hs,t} = \dot{m}_{BP,t} + \dot{m}_{A,t}$. Note that during this operational regime, there is no objective for heat transfer. No fans are operational in this period and thus $Q_{A,t} = Q^0_{A,t}$ and $\dot{Q}_{A,t} = \dot{Q}^0_{A,t}$.

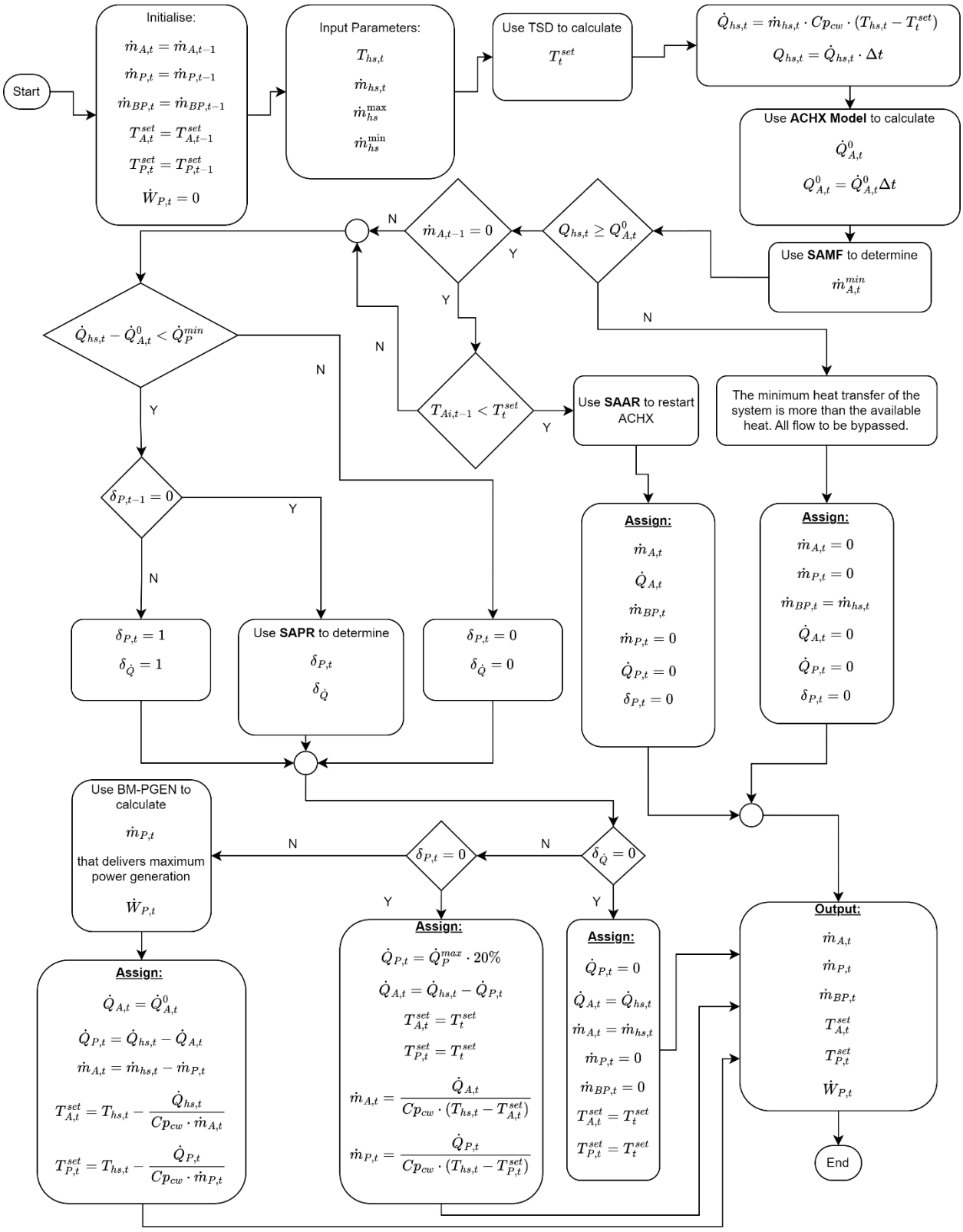


Figure 6-4: Flow Diagram of DADP

If $\dot{m}_{A,t-1}$ is zero but $T_{Ai,t-1} \geq T^{set}_t$ then it follows that the internal temperature of the ACHX is such that all the flow can be distributed to the ACHX without risk of breaching the operational

temperature envelope. The normal operation of the ACHX in the heat rejection system can thus be resumed.

The normal operation of the ACHX under the control of DADP is to distribute only the minimum flow to the ACHX such that $T_{A,t}^{set} = T_t^{set}$ is achieved without the operation of a fan. The flow distributed to the ACHX is to ensure that there is a continuous flow through the ACHX, mitigating the risk of not maintaining the operational envelope should PGEN become unavailable.

The rest of the flow is available for distribution to PGEN. However, before the distribution to PGEN can be determined, the operational status of the PGEN at time t needs to be considered. The maximum flow and thermal load to the PGEN is thus $\dot{m}_{hs,t} - \dot{m}_{A,t}^{min}$ and $\dot{Q}_{hs,t} - \dot{Q}_{A,t}^{0}$, respectively.

The binary parameters of $\delta_{\dot{Q}}$ and $\delta_{P,t}$ are used with the same definition as in WP, where a value of one indicates that the PGEN can transfer heat and that the PGEN can generate power, respectively. Note that $\delta_{\dot{Q}} \geq \delta_{P,t}$, indicating that heat can be transferred at PGEN without power generation and that power can only be generated if heat is transferred.

If the available heat is such that the average thermal load that can be assigned to the PGEN during t is less than the lower design limit of $\dot{Q}_P^{min}$, then the values of $\delta_{\dot{Q}}$ and $\delta_{P,t}$ is zero. If the available thermal load is within the design limits of PGEN, then DADP first determines if the PGEN is in operation at $t-1$. If not, then SAPR (Chapter 5.1.3) is used to initiate and control the PGEN restart procedure. As mentioned in Chapter 5.1.3, a warm or cold start procedure is assigned and managed by SAPR depending on the time elapsed while PGEN is out of operation. During the start procedure, the PGEN can be used to transfer heat from the cooling water without any power generation, thus $\delta_{\dot{Q}} = 1$ and $\delta_{P,t} = 0$.

The final step of the restart procedures is the same for the normal operation of the PGEN where both heat transfer and power generation takes place and thus $\delta_{\dot{Q}} = 1$ and $\delta_{P,t} = 1$. The binary parameters can now be used to determine the flow and thermal load assigned to the PGEN. If $\delta_{\dot{Q}} = 0$ and $\delta_{P,t} = 0$ then the PGEN is unavailable for both heat transfer and power generation and thus all flow and thermal load is distributed to the ACHX. However, if $\delta_{\dot{Q}} = 1$ and $\delta_{P,t} = 0$ then PGEN is currently in the process of returning to operation, as dictated by SAPR.

During this process, flow can thus be distributed to the PGEN. In this scenario, the thermal load is 20% of the maximum heat transfer capacity of the PGEN.

Note that in SAPR, both binary parameters change to zero and the startup procedure will restart if the thermal load to the PGEN is below the 20% requirement.

Finally, if $\delta_{\dot{Q}} = 1$ and $\delta_{P,t} = 1$ then the PGEN is in normal operating mode and the DADP can distribute thermal load to the PGEN to generate electrical power. This is also where the most significant difference between the DADP and WP is introduced.

The bisection method BM-PGEN, described in Chapter 6.3.2, is used to iteratively find the flow distribution to PGEN that is expected to deliver maximum power generation while transferring all the available heat in the cooling water. Once the desired value of $\dot{m}_{P,t}$ is determined, the residual of the flow is assigned to the ACHX. Note that the expected power generation is also reported with $\dot{W}_{P,t}$.

A sample script of DADP is provided in Appendix G.

The desired heat transfer between the PGEN and ACHX as well as the distribution of flow between the PGEN, ACHX and BP (where relevant) has now been determined for all the possible operational regimes of the system. The final requirement is to determine the desired setpoints of each component that is used by the control philosophy to continuously adjust controllable equipment such as valves and fans to ensure that the flow and temperature setpoints are reached. From $\dot{Q} = \dot{m} \cdot Cp \cdot \Delta T$ it can be stated that if these temperature setpoints are reached, the assigned thermal loads and desired total heat transfer is also reached.

6.5 Performance Evaluation of the DADP

To evaluate the operation of DADP, two datasets are used. The first dataset demonstrates the typical operation of ACHX and PGEN on a smaller timeframe where changes in operational modes are clearly identifiable.

The historical dataset is then used to evaluate the average performance of the PGEN and ACHX processes over a longer period of time. Sections of the performance on the historical dataset will also be illustrated where required.

The performance of the DADP relative to WP will also be illustrated and noted where relevant.

6.5.1 Demonstrative Dataset

To demonstrate the behaviour of DADP, the plant parameters set out in Table 3-1, Table 3-2 and Table 3-3 be used with additional parameters being supplied where required.

The average minimum cooling water temperature entering the gas cooler is set as $\overline{T}^{LL}$ =150 ℃ as in Table 3-1. PGEN has a lower heat limit of $\dot{Q}_P^{min}$ = 2 MW and a maximum thermal load of $\dot{Q}_P^{max}$ = 20 MW. The cold and warm start procedure parameters for PGEN are as set out in Chapter 5.1.3.

6.5.1.1 Results for Distribution of Flow and Heat

The flow distribution between the ACHX and PGEN are determined every period according to the DADP. The distribution determined by the DADP is illustrated in Figure 6-5. The dynamic difference in flow distribution can be observed under the normal operation from time 0 to 20 min and again from 55 to 90 min.

From the observed flow rates, it is also clear that the PGEN repeated the trip occurrence and subsequent restart observed from 25 to 50 min in WP.

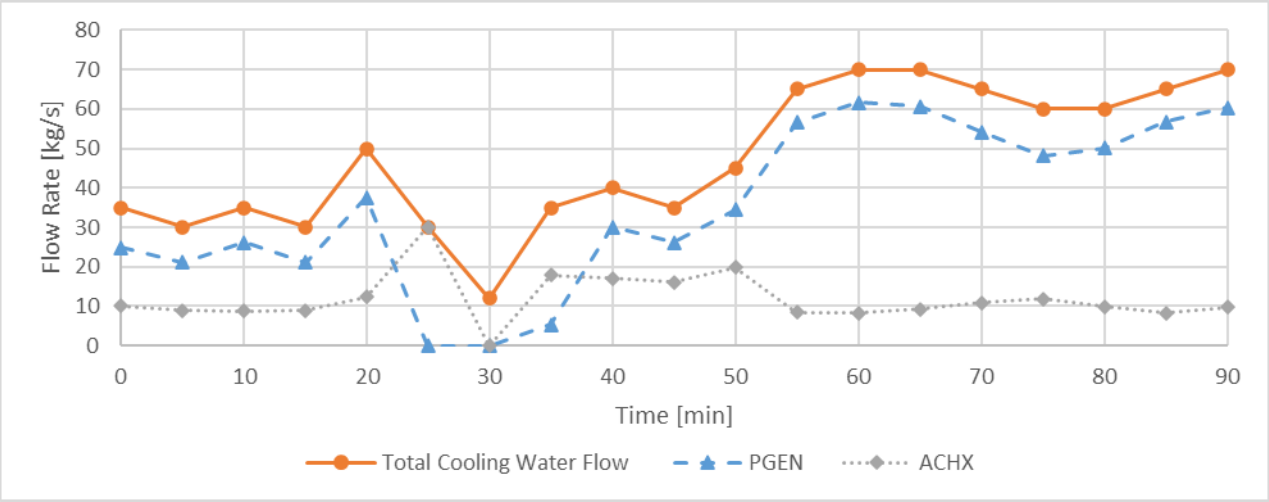


Figure 6-5: Flow Distribution between ACHX and PGEN under DADP

The flow distributed to the PGEN under the DADP is compared to the same parameter under the WP in Figure 6-6. At time 0 to 20 min that the DADP assigned lower flow rates to PGEN compared to WP. During the restart procedure at 35–50 min more flow is distributed to the PGEN under the DADP.

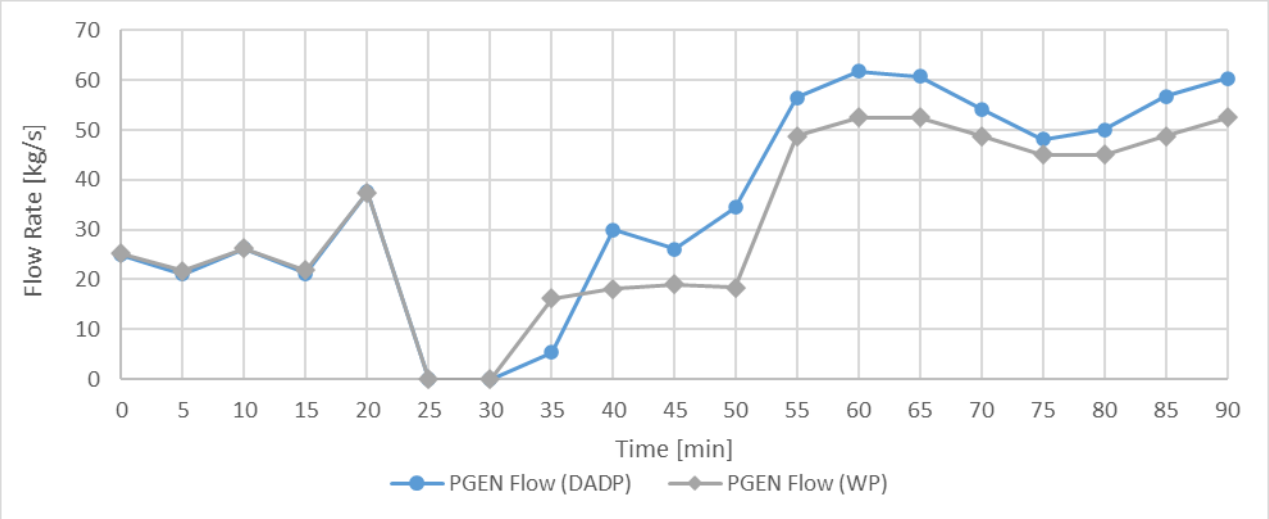


Figure 6-6: Comparison of PGEN Cooling Water Flow under DADP and WP

This change in flow distribution is attributed to the objective of DADP to maximise power generation with the change in approach to not operate the PGEN and ACHX as independent processes. This allows the PGEN to potentially transfer more heat by having a lower temperature setpoint for the cooling water exiting the evaporator.

The setpoint temperature for both components under DADP is based on the flow and desired heat distribution. A comparison between the setpoint temperature and average heat transfer rates assigned to the PGEN is illustrated in Figure 6-7.

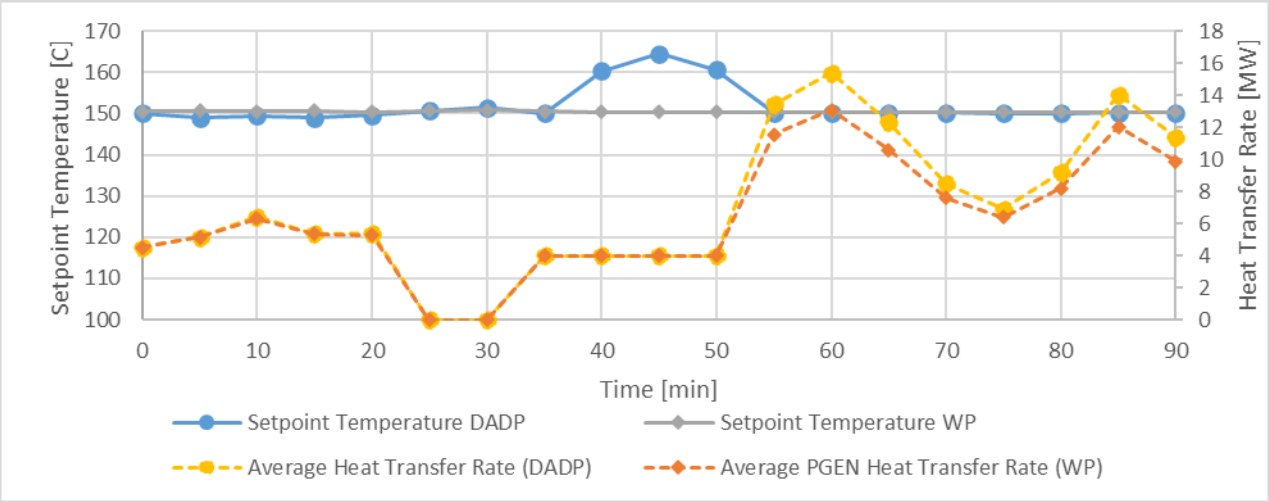


Figure 6-7: Setpoint Temperature and Average Heat Transfer Comparison between DADP and WP

For the period where comparatively lower flow rate is distributed to the PGEN under DADP, it is also noted that the temperature setpoint is lower than the WP temperature setpoint. The average heat transfer rate to the PGEN between DADP and WP thus has an insignificant difference from 0–20 min. During the restart procedure, the setpoint temperature of the cooling water is increased to be above the lower limit of the operational envelope. This is due to the observed increase in cooling water flow the PGEN during this period, as noted in Figure 6-5.

Once the PGEN is in normal operation after 55 min, the temperature setpoint is reduced again. In this section of the demonstrative dataset, it can be observed that there is an increase in average heat transfer for the PGEN between DADP and WP.

The combination of determined flow rates and setpoint temperatures during all times of normal operation are a result of the approach followed to reach maximum power generation efficiency.

6.5.1.2 Results for ACHX and PGEN Operation

The operational settings of the ACHX during the demonstrative dataset is illustrated in Figure 6-8. Firstly, note that a single fan only became operational at 25 min. This is due to the average heat transfer rate of the ACHX with no operational fans being sufficient to remove the required heat to meet the setpoint temperature.

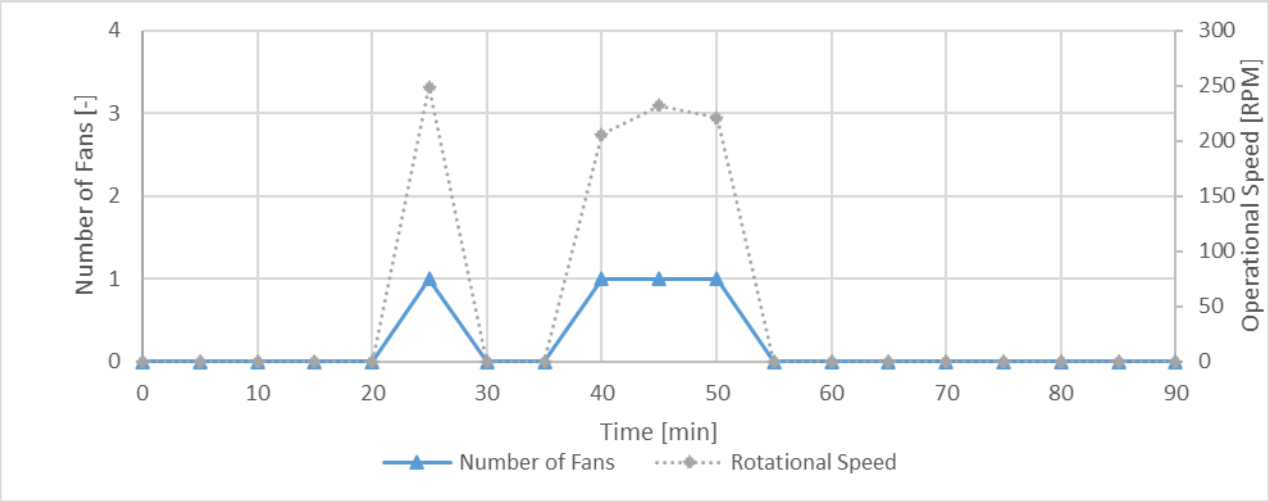


Figure 6-8: ACHX Operational Settings for WP on Demonstrative Dataset

More fans become operational from 35–65 min with 3 the maximum number of fans in operation at 45–50 min. The required operational speeds of the fans are also illustrated on the secondary axis. The timeframe where the required number of operational fans at the ACHX is at its highest also corresponds to the timeframe the PGEN is out of operation or in a controlled startup sequence.

The above-mentioned results are the same as for the WP. However, since the approach in DADP is to remove the independent operation of the PGEN and ACHX, it can be noted that when the PGEN returned to operation at 55 min, no fans are in operation. Under WP, fans were required to reach the desired setpoint temperature. This is due to reduction in required heat transfer by the ACHX under the DADP from 55–90 min.

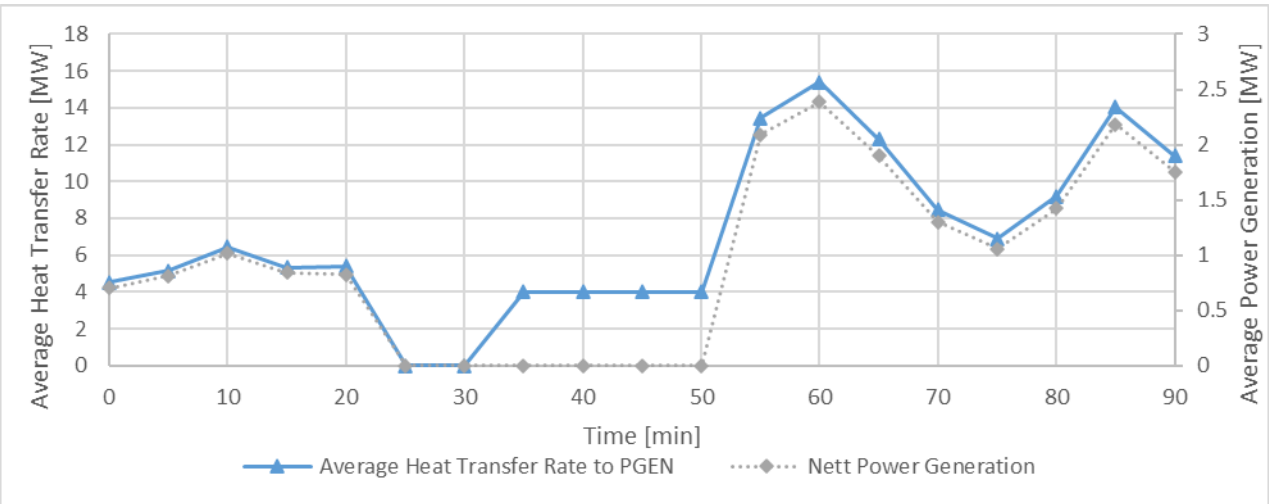


Figure 6-9: Power Generation by PGEN for WP on Demonstrative Dataset

The average heat transfer rate at the PGEN along with the nett power generation is illustrated in Figure 6-9. During the restart phase, it is observed that no power is generated, as dictated by the controlled restart philosophy of the PGEN.

The total heat transferred to the PGEN increased from 36.56 GJ under the WP to 40.18 GJ under DADP at an average heat transfer rate in the evaporator component of 7.050 MW. This is a 9.91% increase and amounts to 72.2% of the total available heat. The average power generation while the PGEN is in operation 1.316 MW, resulting in an average of 0.900 MW over the time horizon of the demonstrative dataset.

An average for the thermal efficiency, weighted by power generation, also indicate an average thermal efficiency of 14.58 %. An illustration of how the thermal efficiency vary over the time horizon is provided in Figure 6-10 along with the performance results for WP.

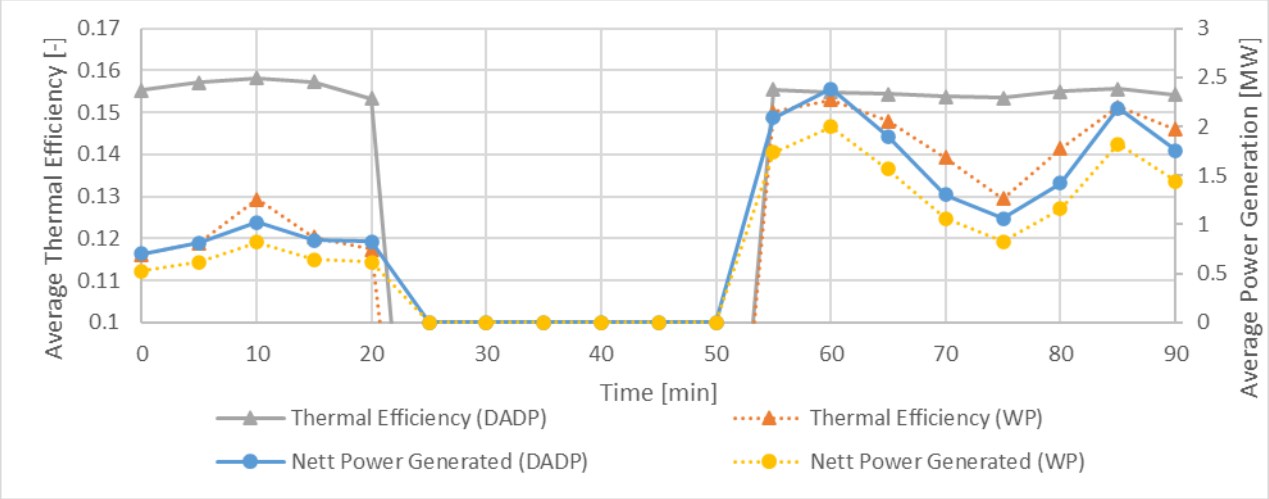


Figure 6-10: PGEN Efficiency Comparison between DADP and WP on Demonstrative Dataset

As noted in the previous section, DADP distributed less cooling water to the PGEN at 0–20 min, however it is stated that the setpoint temperature is relatively lower than under the WP. This resulted in an insignificant difference between the heat transferred for WP and DADP, as illustrated in Figure 6-7. It is stated that this is the result of the power generation maximisation approach by DADP. In Figure 6-10, this is further demonstrated by the noted increase in both thermal efficiency and power generation for the same period.

It is also observed that for all other periods, the power generation improved from WP to DADP. This is a direct result of the DADP iteratively determining the flow distribution that will result in viable operational regimes and maximum power generation from the total cooling water flow.

6.5.2 Historical Dataset

The previous section illustrated the differences between DADP and WP on a demonstrative dataset. The sub-algorithms of SAAR, SAPR and the reaction to the forced trip remains consistent with WP. The next section will show, in addition to performance, adherence to the operational envelope.

6.5.2.1 Performance and Operational Parameters on the Historical Dataset

The operational speed of the fans is illustrated in Figure 6-11. It can be noted that there are several time periods where there are no fans in operation. In addition, comparison to Figure 5-13 shows a significant reduction in the operation of fans in the ACHX, indicating that less heat is transferred by the ACHX.

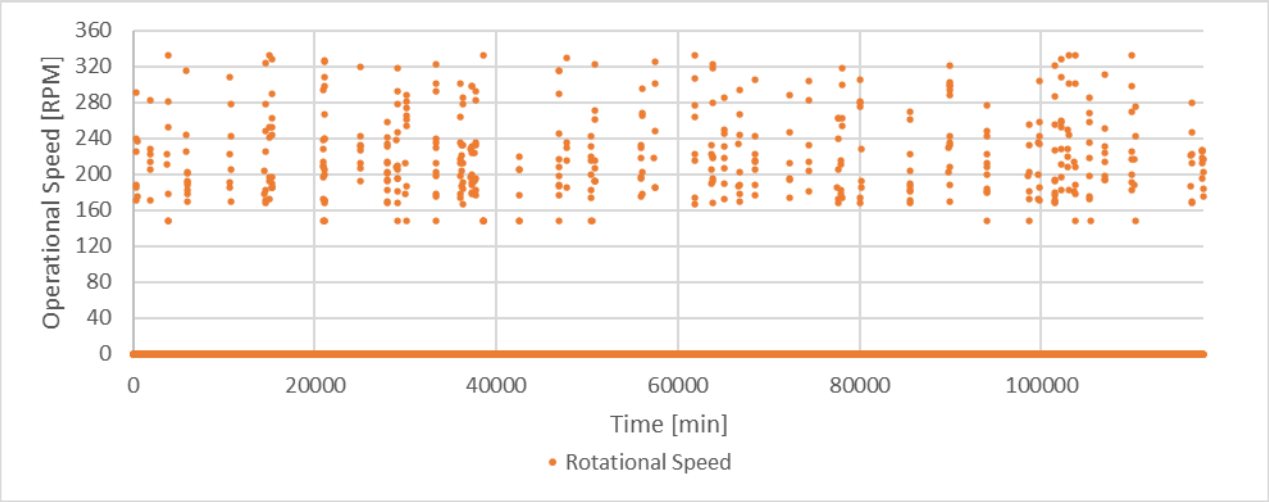


Figure 6-11: Operational Speed of Fans over Time Horizon of Historical Dataset

In addition to the ACHX being controlled to meet fluctuating heat transfer demands, the PGEN is still operated under the PGCP where the evaporating pressure and degree of superheat is adjusted to maximise power generation from the assigned flow. In addition, DADP determines at the flow distributed to the PGEN to further increase the power generated.

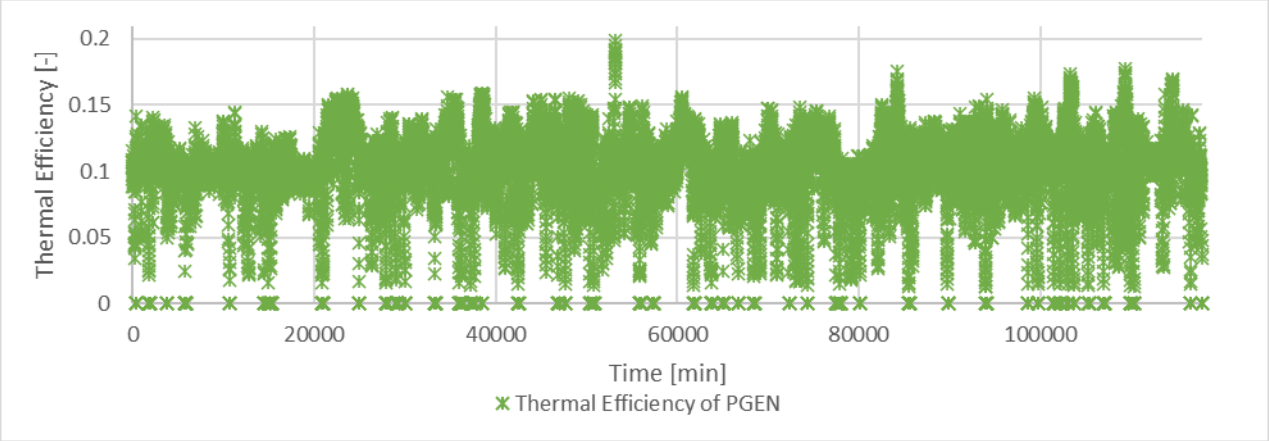


Figure 6-12: Thermal Efficiency of PGEN over Time Horizon of Historical Dataset

The resulting thermal efficiency over the time horizon of the historical dataset is illustrated in Figure 6-12. A maximum and minimum thermal efficiency of 19.89 and 12.99% is observed, respectively.

The resultant temperatures at point 5 in Figure 1-1 is also illustrated in Figure 6-13, along with the allowable limits. It is once again noted that the temperature is close to the lower limit for most of the time periods, as per the philosophy approach to maximise energy recovery from the cooling water. Note that the operational envelope is maintained with a minimum and maximum temperature of 150 ℃ and 185.7 ℃.

The high temperature is noted during periods of low flow where the available heat in the cooling water is such that both the ACHX and PGEN is bypassed.

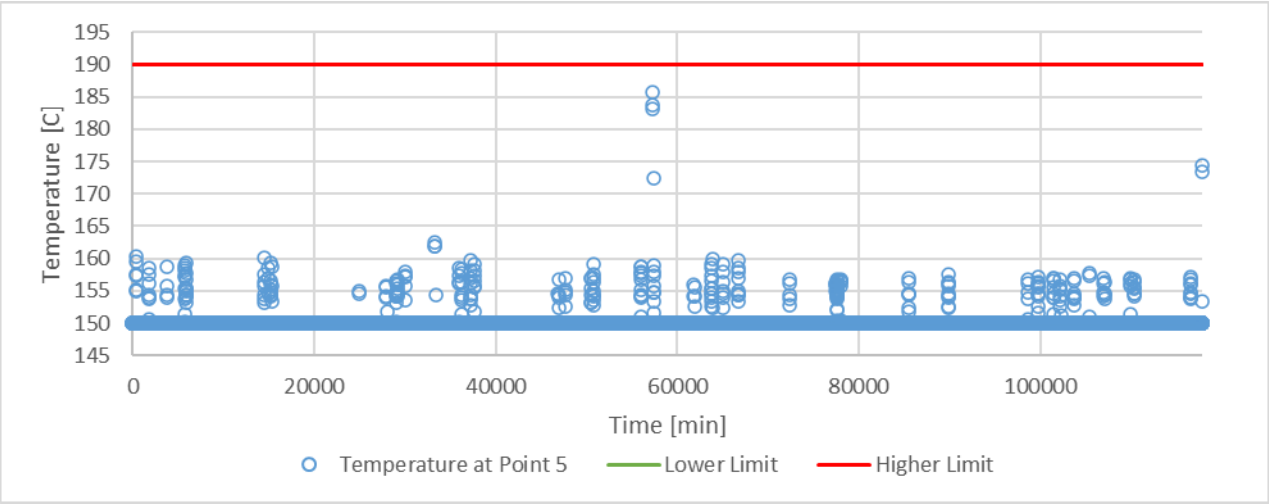


Figure 6-13: Temperature at point 5 with DADP

The operational envelope is not breached. This is as expected since there is no change to the approach in WP that guarantees the operational envelope. The SAAR is still in use, controlling both the bypass of flow during low heat conditions and the controlled startup of ACHX should the internal temperature of the ACHX reduce to outside the operational envelope.

6.5.2.2 Comparison between DADP and WP

The performance of the DADP will now be compared to the results of the system under WP in the previous chapter. A summary of these results is provided in Table 6-3.

The gas cooler operational envelope is still maintained throughout the time horizon of the historical dataset while the PGEN is in operation for 95.9% of the time. This is the same as for WP. The total heat transferred by the PGEN evaporator, however, increased from 60 889.85 GJ to 70 107.61 GJ which is 85.59% of the total heat available in the cooling water in the historical dataset. Note that since the total cooling water flow rate of the system is not adjusted, and no change is observed in the amount of heat absorbed from the flue gas, with only 92.24% of the available heat in the flue gas being transferred.

The average heat transfer rate at the evaporator of the PGEN also increased from 8.612 MW under WP to 9.915 MW. This resulted in an increase of 20.63% on the average power generation,

increasing from 1.231 MW to 1.485 MW over the time horizon. The thermal efficiency of the PGEN is weighted according to the power generated and this increased from 14.39% to 15.05%.

The energy recovery efficiency resulted in a value of 11.34%, increasing from a value of 9.40%. This indicates that the eventual power generation from the system is 11.34% of the available energy in the cooling water.

Table 6-3: Comparison of Performance between WP and DADP

Parameter	**DADP**	**WP**	**Unit**
Time $\overline{T}_5 < 150$ ℃	0	0	min
Minimum $\overline{T}_5$	150.00	150.00	℃
Maximum $\overline{T}_5$	185.74	185.74	℃
% of time PGEN is in operation	95.9	95.9	%
Heat transferred by Gas Cooler	81 914.9	81 914.9	GJ
% of Total Heat in Flue Gas	92.24	92.24	%
Heat transferred by PGEN	70 107.61	60 889.85	GJ
% of Total Heat	85.586	74.333	%
Average heat transfer rate at PGEN	9.916	8.612	MW
Average power generation	1.485	1.231	MW
Weighted average η_{th}	15.06	14.39	%
Energy Recovery Efficiency	11.34	9.40	%

6.5.2.3 Comparison to Maximum flow to PGEN Philosophy

As noted in Chapter 6.3, a philosophy where the minimum flow allowed is provided to the ACHX while the residual flow can all be used for power generation, will not necessarily result in maximum power generation. This is based on the current PGEN model being used, including the turbine efficiency curve and limitations on the evaporator of the PGEN.

A comparison of the performance between such a maximum flow philosophy and DADP is provided in Table 6-4 below.

The time the PGEN is in operation and the heat transferred by the PGEN evaporator are the same between the maximum flow philosophy and DADP. This is as expected since DADP can potentially result in not only a lower flow rate of cooling water to the PGEN, but also a lower setpoint temperature to ensure the same amount of heat is transferred to the PGEN from the cooling water.

The average power generation of 1.485 MW for DADP over the time horizon is 3.8% higher than maximum flow philosophy**.** The weighted thermal efficiency of the PGEN also resulted in 15.06%, compared to 14.52% for the maximum flow philosophy. The energy recovery efficiency also has a relatively small difference where the DADP has a value of 11.34%, compared to a value 10.93% for the maximum flow philosophy.

Table 6-4: Comparison of Performance Evaluation between Maximum Flow Philosophy and DADP

Parameter	**Max Flow**	**DADP**	**Unit**
Time $\overline{T}_5 < 150$ ℃	0	0	min
Minimum $\overline{T}_5$	150.00	150.00	℃
Maximum $\overline{T}_5$	185.74	185.74	℃
% of time PGEN is in operation	95.9	95.9	%
Heat transferred by PGEN	70 107.61	70 107.61	GJ
% of Total Heat	85.586	85.586	%
Average heat transfer rate at PGEN	9.916	9.916	MW
Average power generation	1.431	1.485	MW
Weighted average η_{th}	14.52	15.06	%
Energy Recovery Efficiency	10.93	11.34	%

The above table indicates that the DADP is successful in not only maintaining the operational envelope, but also determining the flow distribution that will result in maximum power generation from the available heat in the cooling water. From the above set of results, it is clear that providing the maximum flow to the PGEN did not result in the maximum power generation over the time horizon of the historical dataset.

6.6 Conclusion

This chapter illustrated the formulation and performance of the DADP on a historical dataset. The first section of the chapter provided a summary of the change in approach required to improve on the performance of WP.

The chapter then provided another sub-algorithm, referred to as SAMF, that is used to determine a minimum flow to the ACHX. The residual of the flow is thus available and can be assigned to the PGEN.

The next section in this chapter then provides insight into the off-design performance of the components in the PGEN. A case study is then completed where the cooling water flow is compared to the power generation for several heat source parameters. It is shown that at off-design conditions, the maximum flow of cooling water to the PGEN does not result in maximum

power generation. This can be attributed to the PGEN cycle pump work required and the off-design performance of the PGEN turbine. A customised bisection method is then introduced that can be used to identify the flow distribution to the PGEN that will result in maximum power generation.

The chapter then provides the formulation for the Discrete Adjustment to Distribution Philosophy. In summary, under normal operation this philosophy firstly determines the minimum flow required by the ACHX after which the desired cooling water distribution to the PGEN is determined using the above-mentioned bisection method. The required heat transfer at the PGEN is also determined after all losses through an ACHX with no operational fans and uninsulated components are calculated. After the flow and heat distributions have been determined, the specific setpoint temperatures for both the PGEN and ACHX is determined.

In summary, the WP of the previous chapter aimed to maximise power generation with the assigned cooling water flow by adjusting the evaporating pressure and degree of superheat in the PGEN. The assigned cooling water flow is based on a fixed distribution ratio. The DADP aims to further improve on this power generation by adjusting the flow of cooling water distributed to the PGEN.

The DADP approach on the historical dataset resulted in a PGEN that is operational 95.9% of the time, transferring 85.59% of the available heat from the cooling water, an increase from 74.33% under WP. The average power generation for the PGEN is determined to be 1.485 MW, compared to 1.231 MW under WP. The DADP also delivered a weighted thermal efficiency of 15.05%. The energy recovery ratio is also determined to be 11.34%, which is also increased from 9.40% under WP.

Note that since the total cooling water flow rate of the system is not adjusted, and no change is observed in the amount of heat absorbed from the flue gas, with only 92.24% of the available heat in the flue gas being transferred. This can potentially be improved on.

The DADP is then compared to a philosophy where all the available flow is assigned to the PGEN after compensating for the minimum flow required at the ACHX. The results indicate that the maximum flow to PGEN philosophy will result in an average reduction of 0.054 MW in power generation, reducing the weighted thermal efficiency and energy recovery ratio to 14.52% and 10.93% respectively.

In addition to the above performance evaluations, a tripped state is also forced during the same high heat availability period as is done in the previous chapter to evaluate whether the operational envelope is maintained. No changes to the restart procedures are made in the formulation and thus both the restart procedure and the ability to maintain the operational envelope is consistent with WP. The DADP is thus successful in maintaining the operational envelope.

An illustrative summary of the DADP and its communication with the different process models is provided in the figure below.

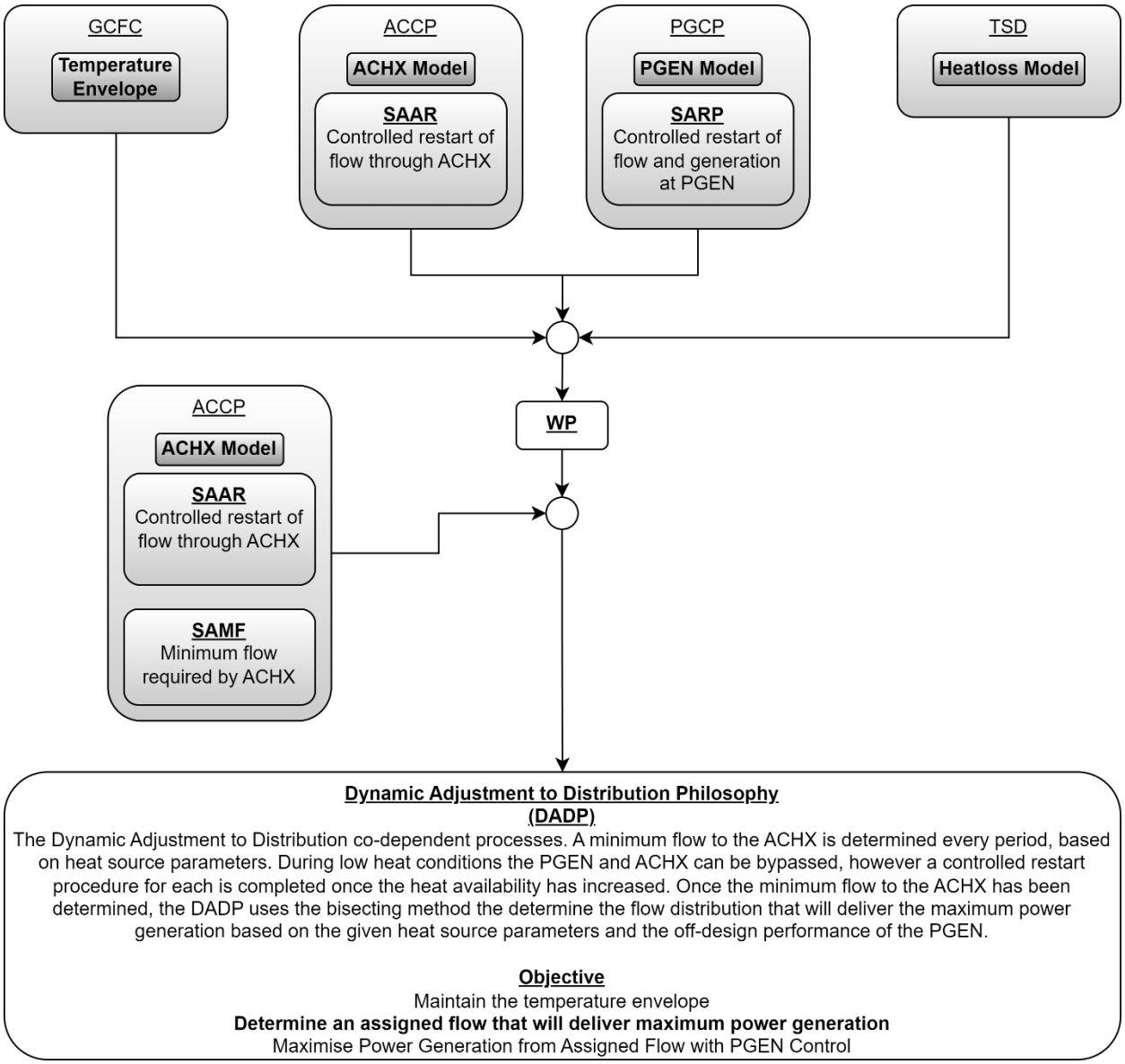


Figure 6-14: Summary of DADP after Conclusion of Chapter 6.

CHAPTER 7 DISCRETE ADJUSTMENT TO FLOW

The DADP improves on WP by adjusting the flow distribution between the ACHX and PGEN with the objective of maximum power generation. This approach ensures maximum power generation from the energy within the cooling water that exits the gas cooler.

This chapter will attempt to improve on the power generation performance of DADP while still maintaining the operational envelope.

7.1 Approach Changes from DADP

7.1.1 Maximising Energy Recovered from Flue Gas

The use PGCP in DADP and WP ensures that maximum power generation is achieved with the cooling water that is distributed to the PGEN. In DADP, the cooling water flow distribution is changed from a fixed to a variable ratio approach. The range of allowable distribution ratios are based on the cooling water parameters exiting the gas cooler. The bisection method in DADP then determines the ideal distribution ratio that will deliver maximum power generation.

This approach thus ensures that maximum power generation is achieved from the thermal energy in the cooling water exiting the gas cooler. However, it is known that the current approach of the cooling water flow control (CWFC) is reactive to the exiting gas temperature.

The current setpoint that CWFC attempts to maintain is 180 ℃. This resulted in the average exit temperature of the gas cooler ranging between 160 ℃ and 350 ℃, as shown in Figure 7-1.

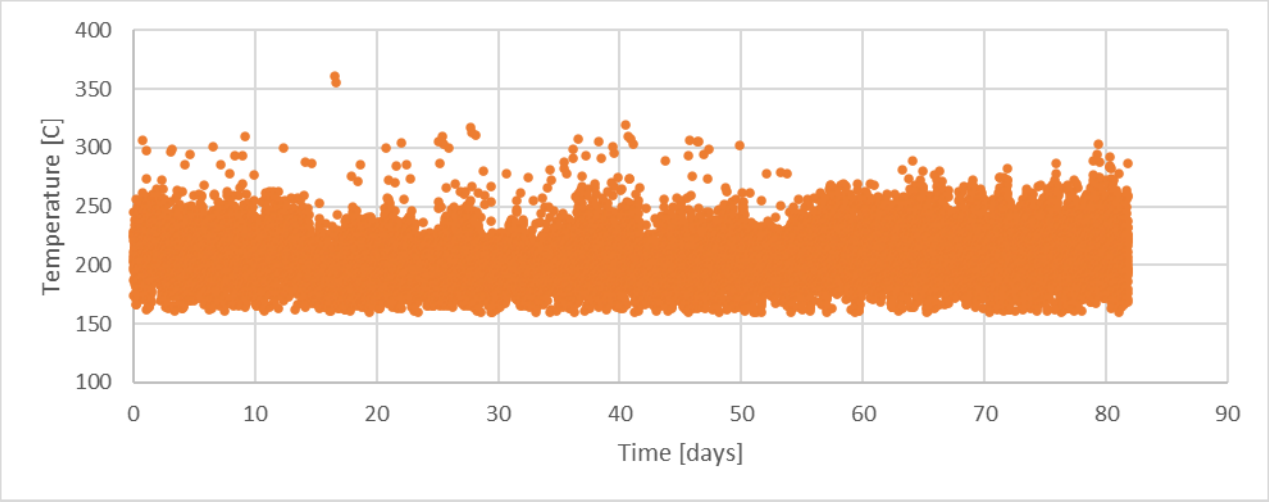


Figure 7-1: Exit Temperature of Flue Gas at the Gas Cooler for CFWC

The lower limit of the operational envelope for the gas is at 150 ℃ to prevent acid dewpoint being reached. As indicated by the study of Gelfi et al. [47] in Chapter 3.2.1 and 3.2.2, the build-up of material on the gas cooler walls typically result in stagnant or low velocity gas on these wall

surfaces. It follows that the gas in these areas must not reach dewpoint temperature and thus this dictated the minimum parameter of the operational envelope of the cooling water.

However, for a realistic model of the gas cooler, a setpoint temperature for the exiting flue gas cannot be the same or lower as the entering cooling water temperature. This is discussed in the next section. If the cooling water flow control model is capable of faster adjustments using a process model, the setpoint of the flue gas exit temperature can be adjusted to be a 10 ℃ difference to the cooling water entering the gas cooler. If the setpoint of 150 ℃ is achieved for the heat rejection system, this results in a setpoint of 160 ℃ for the exit temperature of the gas.

From the results in Figure 7-1, it follows from $Q = m \cdot Cp \cdot \Delta T$ that there is more thermal energy to be safely extracted from the flue gas. Considering the 5 min period and the constant gas mass flow rate, the amount of residual heat in the gas can be determined from the elevated temperatures. This is illustrated in Figure 7-2, which also includes a 2-hour moving average of the residual heat.

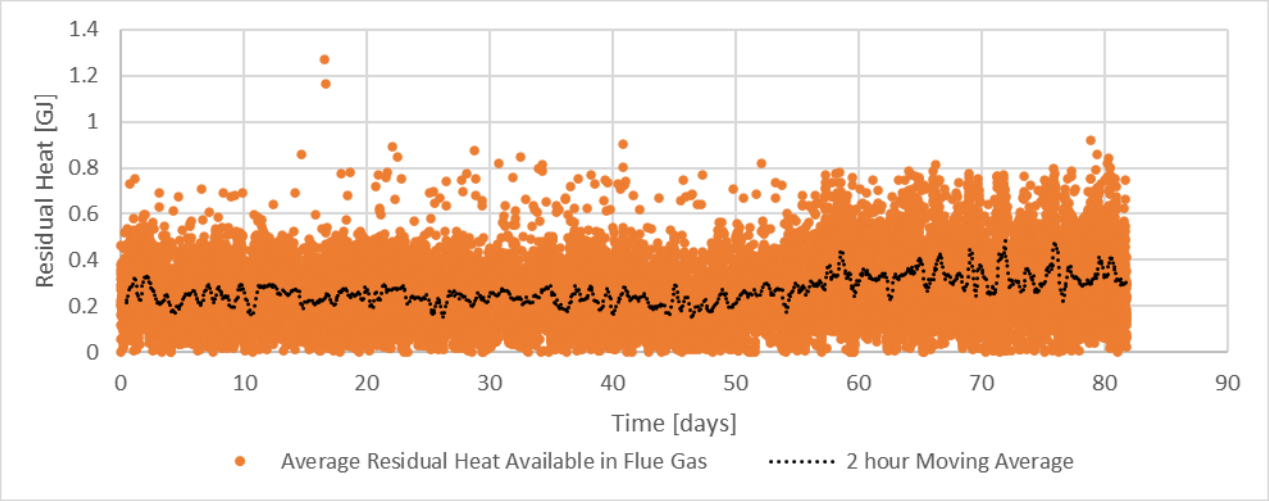


Figure 7-2: Residual Heat in Flue Gas with CWFC

From the figure above it is clear that the average residual heat range between 0.2 and 0.4 GJ over a two-hour period with an average of 0.27 GJ over the time horizon of the historical dataset. Given that the average heat available in the cooling water is 3.80 GJ, this indicates that, on average, the heat availability in the cooling water can be increased by 7.1%.

7.1.2 Minimise Power Consumption from Cooling Water Pumps

The previous section focused on transferring the maximum available heat from the flue gas. However, to achieve this an increase in cooling water flow rate is required. This results in an increased in power consumption from the electric motor-driven pumps. It is shown in Chapter 3.4.2.1 that the shaft power required is dependent on the flow rate and differential pressure.

It is also shown in the performance results of WP and DADP that there are several scenarios where the PGEN is not generating any power or transferring any heat from the cooling water. These scenarios include low heat availability periods and restart procedures.

Increasing the cooling water flow rate to reduce the flue gas to the minimum of the operational envelope will lead to an increase in available energy in the cooling water. However, this may still result in insufficient energy to sustain power generation. The increase in thermal energy will have to be transferred to the environment through the ACHX with no benefit of power generation. A required increase in operational fans and thus power consumption will also be observed in some scenarios.

It follows that during the periods where PGEN is unavailable the cooling water flow rate can be reduced to minimise the required power consumption from pumps and fans to transfer the heat.

7.2 Flow influences on Gas Cooler Heat Transfer

As mentioned in Chapter 4.1, the CWFC does not make use of process model to adjust the cooling water flow rate and instead makes adjustment in reaction to the gas cooler flue gas exit temperature.

7.2.1 Simplified Gas Cooler Model

To determine the required cooling water flow rate that will transfer the required heat from the flue gas, a gas cooler model is required. The model is able to determine not only the required flow rate but also the gas cooler exit temperature of the cooling water at the calculated flow rate.

The current heat transferred during a period can be determined through:

$$\mathrm{Q_{hs}} = \mathrm{m_{hs}} \cdot \mathrm{Cp_{hs}} \cdot (\mathrm{T_{hs}} - \mathrm{T_1^{set}}) \tag{7.1}$$

Where $\mathrm{T_1^{set}}$ refers to the setpoint temperature at point 1 as indicated by Figure 1-1 and $\mathrm{T_{hs}}$ is the temperature of the cooling water exiting the gas cooler. Note that the cooling water is referred to as the heat source for the control philosophies, thus the use of “hs” for the cooling water.

The residual heat in the flue gas, $\mathrm{Q_{fg}^{res}}$, can be determined with:

$$\mathrm{Q_{fg}^{res}} = \mathrm{m_{fg}} \cdot \mathrm{Cp_{fg}} \cdot \left(\mathrm{T_{fg}} - \mathrm{T_{fg}^{set}}\right) \tag{7.2}$$

With $\mathrm{T_{fg}}$ the exit temperature and $\mathrm{T_{fg}^{set}}$ as the setpoint temperature of the flue gas temperature control. The current heat transferred and residual heat in the gas can thus be summed to determine the maximum heat available from the flue gas. Assuming that the temperatures and flow rate are measured and updated every second, the maximum allowable heat transfer rate can be determined:

$$\dot{Q}_{hs,max} = \frac{\left(Q_{hs} + Q_{fg}^{res}\right)}{\Delta t} \tag{7.3}$$

The current heat transfer rate in a heat exchanger can be used determined the value of T_{fg}^{*} with:

$$\dot{Q}_{hs} = \dot{m}_{fg} \cdot C_{fg} \cdot \left(\mathbf{T_{fg}^{*}} - T_{fg}\right) \tag{7.4}$$

With the T_{fg}^{*} the calculated flue gas temperature entering the gas cooler, hench the superscript "*". Now that the flue gas temperature entering the gas cooler has been determined, the $\epsilon - NTU$ method can be used to determine the desired cooling water flow rate.

The heat exchanger performance needs to be formulated as a function of the controlled cooling water flow rate. This allows the use of the formulation to determine the expected heat transfer for a range of cooling water flow rate.

As stated in earlier chapters, the UA represents the performance and is referred to as the overall heat transfer coefficient of the gas cooler. The value of UA at off-design conditions are typically determined with a heat exchanger model. Due to the absence of a detailed gas cooler design model for the current Works, published literature is used. The gas cooler is modelled as a simple counter current heat exchanger and, therefore, the approximation by Dal Magro [46] can thus be used:

$$UA = UA_{des} \cdot \left(\frac{\dot{m}_{cw}}{\dot{m}_{cw,des}}\right)^{0.4} \cdot \left(\frac{\dot{m}_{fg}}{\dot{m}_{fg,des}}\right)^{0.4} \tag{7.5}$$

Where the flow rate of cooling water at time t, referred to as the heat source for the control philosophies, are denoted with $\dot{m}_{hs}$. An additional subscript of "des" indicates the design flow rate as indicated in Table 3-1.

The required number of thermal units (NTU) for the heat exchanger is then used to determine the desired UA of the gas cooler.

$$NTU = \frac{UA}{C_{min}} \tag{7.6}$$

Before the number of thermal units (NTU) can be determined, the C_{min} value first need to be calculated. This can be done with the equations in (7.7) to (7.11) below. In this step, the ratio of heat transfer rate capacities of the two fluids are determined.

$$C_{fg} = \dot{m}_{fg} \cdot Cp_{fg} \tag{7.7}$$

$$C_{hs} = \dot{m}_{hs} \cdot Cp_{hs} \tag{7.8}$$

$$C_{min} = \min (C_{fg}, C_{hs}) \tag{7.9}$$

$$C_{max} = \max (C_{fg}, C_{hs}) \tag{7.10}$$

$$C_r = \frac{C_{min}}{C_{max}} \tag{7.11}$$

Note that the specific heat value of the flue gas is a function of the composition and temperature. The average temperature of the flue gas is used for this calculation and thus updated accordingly with every change in measured temperature.

Once the value for NTU, C_{min} and C_r is known, the heat exchanger effectiveness, ϵ, is determined with the effectiveness formula for a counter current heat exchanger, as in (7.12)

$$\epsilon = \frac{1 - e^{-NTU \cdot (1 - C_r)}}{1 - C_r e^{-NTU \cdot (1 - C_r)}} \tag{7.12}$$

The effectiveness can now be used to determine the expected heat transfer rate for a controlled cooling water flow rate at a given flue gas temperature and flow rate entering the gas cooler. This is done through (7.13) as stated by Cengel et al. [12].

$$\dot{Q}_{hs} = \epsilon \cdot C_{min} \cdot (T_{fg}^{*} - T_1^{set}) \tag{7.13}$$

The expected heat transfer rate is then used to determine the temperatures of both the cooling water and flue gas exiting the gas cooler through (7.14) and (7.15).

$$T_{fg} = T_{fg}^{*} - \frac{\dot{Q}_{hs}}{\dot{m}_{fg} \cdot C_{fg}} \tag{7.14}$$

$$T_{hs} = T_1^{set} + \frac{\dot{Q}_{hs}}{\dot{m}_{hs} \cdot C_{hs}} \tag{7.15}$$

Only at this stage of calculation can it be determined whether the cooling water flow rate will result in a breach of the operational envelope of either fluid. The values of (7.14) and (7.15) can now be used to filter and determine an allowable cooling water flow rate range.

7.2.2 Case Study for Cooling Water Flow Control

A case study is conducted to assist with the formulation of an improved cooling water flow control algorithm. For this purpose, the flue gas temperature entering the gas cooler is set to a fixed value of T_{fg}^{*} =950 ℃ and the flow rate it set at $\dot{m}_{fg}$ = 20 kg/s. The minimum allowable flue gas temperature is set at T_{fg} =180 ℃.

The cooling water flow rate of the current Works can range between 5 and 120 kg/s. It follows from (7.2) and (7.3) that there are 15.198 MJ of heat that can be transferred every second.

The calculations in Chapter 7.2.1 are repeated for the cooling water flow range. The flow range is adjusted in steps of 5 kg/s between cases.

Table 7-1: Selection of Results for Flow Control Case Study

#	$\dot{m}_{hs}$ kg/s	UA [W/K]	C_r −	Q_{hs} [MJ]	T_{fg} ℃	T_{hs}℃
1	120	70 565	0.0394	15.302	~~174.8~~	180.6
2	115	69 374	0.0411	15.270	~~176.4~~	181.8
3	110	68 151	0.0430	15.236	~~178.2~~	183.2
4	105	66 895	0.0451	15.198	180.1	184.7
	⋮	⋮	⋮	⋮	⋮	⋮
13	60	53 478	0.0789	14.585	211.2	208.3
14	55	51 649	0.0861	14.461	217.44	~~213.1~~
	⋮	⋮	⋮	⋮	⋮	⋮
22	20	34 461	0.2367	12.400	321.8	~~298.7~~
23	15	30 715	0.3156	11.611	~~361.8~~	~~335.6~~
24	10	26 167	0.4734	10.370	~~424.7~~	~~398.7~~
25	5	19 793	0.9468	8.012	~~544.1~~	~~534.3~~

From the results in Table 7-1, it is clear that operating at the maximum and minimum ends of the cooling water flow range will result in breaching of the operational envelope. For case 1–3, where the flow range is varied between 110–120 kg/s, the flue gas temperature is below the minimum of 180 ℃. For case 23–25, where the flow rate is varied between 5–15 kg/s, the flue gas temperature exiting the gas cooler is above the maximum temperature limit of 350 ℃. Note that for cases 14–25, the cooling water exiting the gas cooler is also above the maximum of 210 ℃. It follows that only cases 4 to 13 has a cooling water flow rate that will result in the operational envelope being maintained.

The step between flow rates can be adjusted to the minimum achievable on the water flow control to achieve values closer to the operational envelope limits. The maximum cooling water flow rate is determined to be 105.2 kg/s, delivering a flue gas temperature of 180 ℃ whereas the minimum cooling water flow rate of 16.3 kg/s will result in a cooling water exit temperature of 210 ℃. This allowable range can now be used by the control philosophy to determine the required flow.

7.3 Formulation of the Cooling Water Flow Range (CWFR) Algorithm

This section will focus on using the above calculations to improve the control of the cooling water flow rate based on the current operating regime of the ACHX and PGEN.

The calculations done in the previous section is used to determine the influence of changes to the cooling water flow rate on both the temperature of the flue gas and cooling water exiting the gas cooler. A minimum and maximum flow of cooling water can thus be determined and provided to the control philosophy for further processing, this is done by the below algorithm referred to as Cooling Water Flow Range (CWFR).

An illustration of the algorithm is provided in Figure 7-3.

Note that, in addition to the cooling water flow and temperature, the flue gas setpoint and inlet temperature is provided as input. This is determined by the algorithm in the previous section.

The first step is to assign the cooling water flow rate equal to the minimum flow rate possible with the circulation pumps, $\dot{m}_{hs} = \dot{m}_{hs}^{min}$. The cooling water flow rate is thus not equal to the maximum possible, and thus the UA of the system is determined at this flow rate. After determining the UA, the values of C_{min}, C_{max} and C_r are calculated. The number of thermal units, NTU, are then calculated followed by the determination of the heat exchanger effectiveness, ϵ.

The effectiveness at this flow rate is then used to determine the heat transferred per second, $\dot{Q}_{hs}$, after which the exit temperatures of the flue gas and cooling water is determined, T_{fg} and T_{hs} respectively. If the exiting flue gas temperature is higher than the upper limit of the operational envelope,T_{fg}^{UL}, then then flow rate is increased by the indicated step change, $\dot{m}_{step}$, and the process is repeated. This process is repeated until a flow rate is determined that provides an allowable value for the exit temperature of the flue gas.

After a suitable value for T_{fg} has been obtained, the algorithm also confirms that the exit temperature of the cooling water, T_{hs}, is below the upper limit of the operational envelope, T_{hs}^{UL}. If not, then the flow rate is still increased by the indicated step change. From the above process flow rates below the current value will breach either of the fluids upper limit. It follows that once both these conditions are satisfied; the minimum flow rate of the cooling water can be updated to the current flow rate and thus $\dot{m}_{hs}^{min} = \dot{m}_{hs}$.

The flue gas exit temperature is now measured against the lower limit of the operational envelope, T_{fg}^{LL}. If the lower limit has not been breached, then the flow rate is increased until the condition is satisfied. Once the condition has been satisfied it indicates that the more heat is transferred at the current flow than what is allowed and thus the flow rate adjustment is reversed. The updated flow rate is now assigned to the maximum flow rate of the cooling water and thus $\dot{m}_{hs}^{max} = \dot{m}_{hs}$.

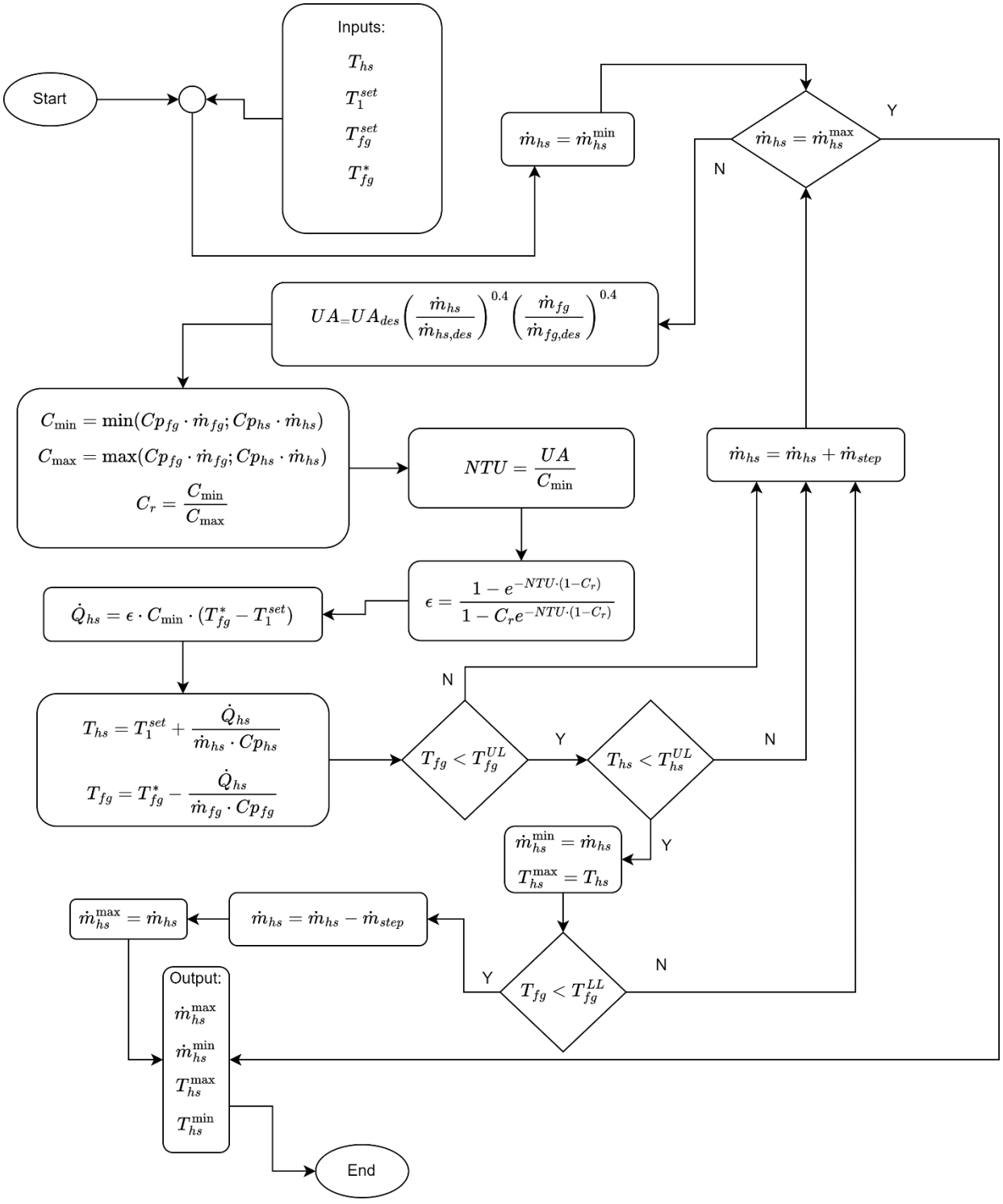


Figure 7-3: Cooling Water Flow Range (CWFR) for Operational Envelope in Gas Cooler

This algorithm provides a minimum and maximum flow rate that will result in maintaining the operational envelope. The control philosophy in this chapter can now use this range to determine the cooling water flow rate that will result in maximum power generation.

The script for the CWFR is provided in Appendix H.

7.4 Formulation of the Discrete Adjustment to Flow Philosophy (DAFP)

The sub-algorithms provided in earlier chapters are used to ensure that the trip and restart of flow through the PGEN and ACHX is accurately accounted for during the execution of DAFP. The bisection method, BM-PGEN, is also used to determine the flow distribution that will result in maximum power generation whenever there is sufficient heat to do so. The formulation of the DAFP is provided in this section of the chapter.

A demonstration of the logic of DAFP is illustrated in Figure 7-4.

The notation in the formulation below is consistent with the formulation of DADP where $\mathrm{T}℃$, $\mathrm{Q}\ [\mathrm{J}]$, $\dot{\mathrm{Q}}\ [\mathrm{W}]$ and $\dot{\mathrm{m}}\ [\mathrm{kg/s}]$ represent temperature, heat, heat transfer rate and mass flow respectively with sub-and superscripts used to identify specific parameters and values.

The time index for the formulation is given by $\mathrm{T} = \{1,2,\dots,|\mathrm{T}|\}$. The difference in time between t and $\mathrm{t}+1$ is constant and indicated by $\Delta\mathrm{t}$. The cooling water exits the heat gas cooler at a temperature $\mathrm{T}_{\mathrm{hs,t}}$ ℃ and a mass flow rate of $\dot{\mathrm{m}}_{\mathrm{hs,t}}$ kg/s.

The first step of DAFP is to receive the maximum and minimum flow of the cooling water at time t, $\dot{\mathrm{m}}_{\mathrm{hs,t}}^{\mathrm{max}}$ and $\dot{\mathrm{m}}_{\mathrm{hs,t}}^{\mathrm{min}}$ respectively. This range is provided by the algorithm in Chapter 7.3. Thereafter, a midpoint of this range is determined, $\dot{\mathrm{m}}_{\mathrm{hs,t}}^{\mathrm{mid}}$. The UA, $\mathrm{C}_{\mathrm{min}}$, $\mathrm{C}_{\mathrm{max}}$, C_{r}, NTU and ϵ values are then calculated with a similar approach to that of Chapter 7.3. The heat transferred per second for the midpoint flow is then calculated after which the flue gas and cooling water exit temperatures are predicted should the cooling water through the gas cooler be adjusted to the midpoint. There is now a minimum, maximum and midpoint cooling water flow and temperature, all sustaining the operational envelope.

The DADP from Chapter 6.4 is then used to determine the expectant nett power generation should the cooling water exit the gas cooler at these properties. The trends between the midpoint and maximum and minimum flows, Δ_{U} and Δ_{L} respectively, are evaluated to determine the range where maximum power generation potential is. A modified Bisection method, like in Chapter 6.3.2 is then used to determine adjustments to the maximum and minimum cooling water flow until convergence is achieved. Evaluating the trends can result in three scenarios:

I. $\Delta_{\mathrm{L}} > 0$ and $\Delta_{\mathrm{U}} > 0$: Both trends indicate that a potential maximum generation is at a flow higher than the current midpoint cooling water flow rate.
II. $\Delta_{\mathrm{L}} > 0$ and $\Delta_{\mathrm{U}} < 0$: Both trends indicate that a potential maximum generation is near the midpoint flow and the range can thus be reduced around the midpoint.
III. $\Delta_{\mathrm{L}} < 0$ and $\Delta_{\mathrm{U}} < 0$: Both trends indicate that increased power generation is at a flow lower than the current midpoint.

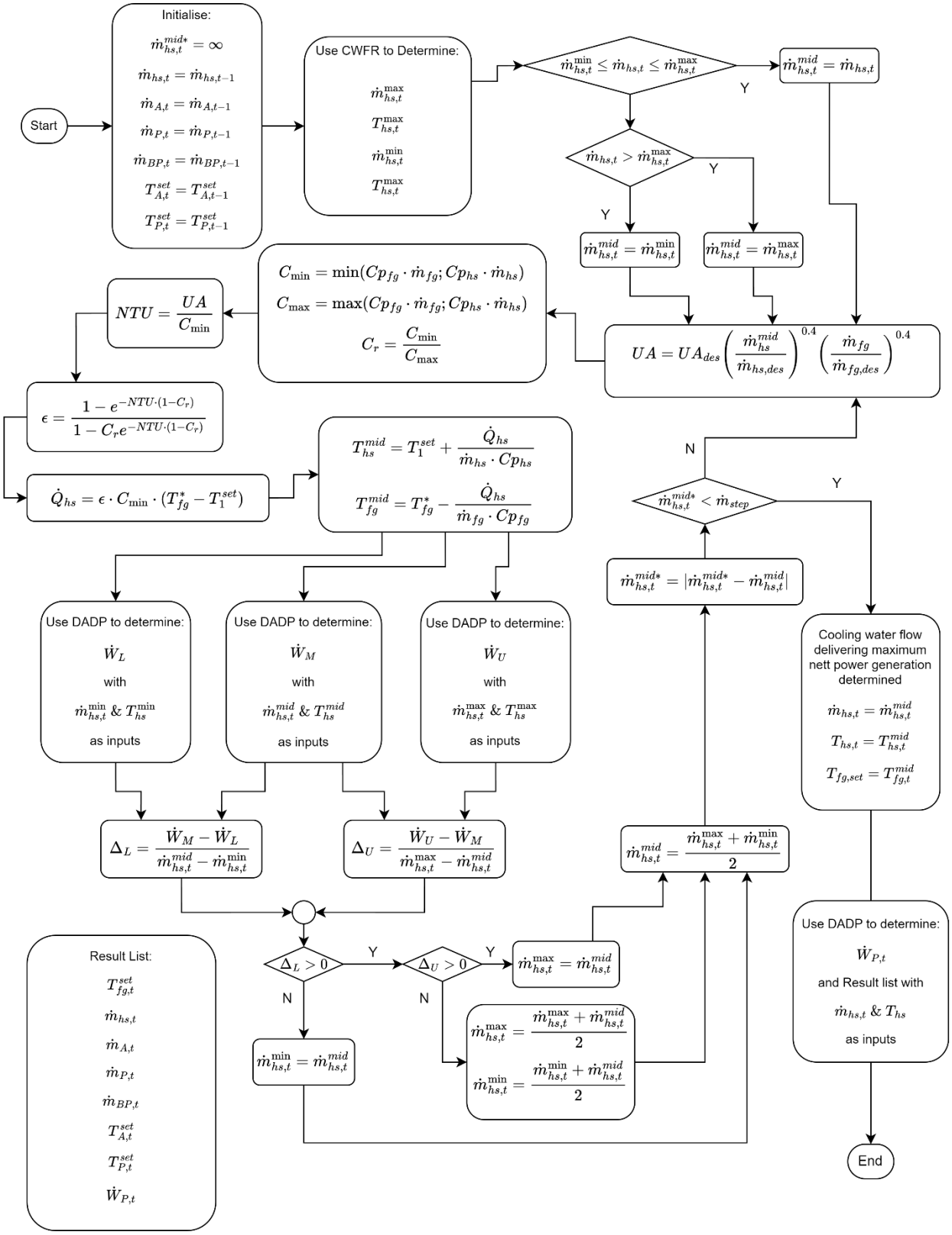


Figure 7-4: Flow Diagram of DAFP

The maximum and minimum cooling water flow rate is then adjusted according to the decision making set out in the above scenarios after which the midpoint flow is recalculated. This process

is repeated until the convergence is achieved. Convergence is measured by the step in the cooling water midpoint flow rate at each iteration.

Note that, due to DADP and component models, the nett power generation of a system with an offline PGEN is negative. This is due to power consumption from the circulating cooling water pumps and ACHX fan operation. The approach above can thus still be followed since the minimum power consumption is identified if all the power generation values are negative.

The desired cooling water flow rate through the gas cooler is now determined along with the expected heat transferred every second, the flue gas exit temperature and the temperature of the cooling water that will enter the ACHX and PGEN section. Thus, from here an unchanged DADP can be used to further determine the required flow distribution and temperature setpoints between the ACHX and PGEN.

A sample script for DAFP is provided in Appendix I.

The heat transferred from the flue gas has now been adjusted for maximum power generation or minimum power consumption, where applicable. The desired heat transfer between the PGEN and ACHX as well as the distribution of flow between the PGEN, ACHX and BP (where relevant) has now been determined for all the possible operational regimes of the system. The final requirement is to determine the desired setpoints of each component that will be used by the control philosophy to continuously adjust controllable equipment such as valves and fans to ensure that the flow and temperature setpoints are reached. From $\dot{Q} = \dot{m} \cdot Cp \cdot \Delta T$ it can be stated that if these temperature setpoints are reached, the assigned thermal loads and desired total heat transfer is also reached.

7.5 Performance Evaluation of the DAFP

To evaluate the operation of DAFP, the two datasets are used. The performance of the DAFP relative to WP and DADP will also be illustrated and noted where relevant.

7.5.1 Demonstrative Dataset

To demonstrate the behaviour of DAFP, the plant parameters set out in Table 3-1, Table 3-2 and Table 3-3 be used with additional parameters being supplied where required.

The average minimum cooling water temperature entering the gas cooler is set as $\overline{T}^{LL}$ =150 ℃ as in Table 3-1. PGEN has a lower heat limit of $\dot{Q}_P^{min}$ =2 MW and a maximum thermal load of $\dot{Q}_P^{max}$ =20 MW. The cold and warm start procedure parameters for PGEN are as set out in Chapter 5.1.3. The lower and upper limit of the flue gas operational envelope is set at $\overline{T}_{fg}^{min} = \max[\overline{T}^{LL} + 10; \overline{T}_1 + 10]$ and $\overline{T}_{fg}^{max} = 350$ ℃.

7.5.1.1 Operational Status of Components

The DAFP adjusts the flow through the gas cooler to either minimise power consumption or maximise power generation, depending on the operational status of the components in the system. Therefore, it is first required to evaluate the operational status of the components at each period. This is done by evaluating the values of δ_P and $\delta_{\dot{Q}}$ over the time horizon. An illustration of these values is provided in Figure 7-5.

The PGEN is fully operational, transferring both heat from the cooling water and generating power, from 0–25 min. At 30 min, the PGEN enters a tripped state. In this state, the PGEN is not allowed to transfer heat and thus also not generate power. For 35–50 min, the PGEN is in a warm restart procedure where a required amount of heat is transferred for certain time. Note that the PGEN trips one period later compared to DADP.

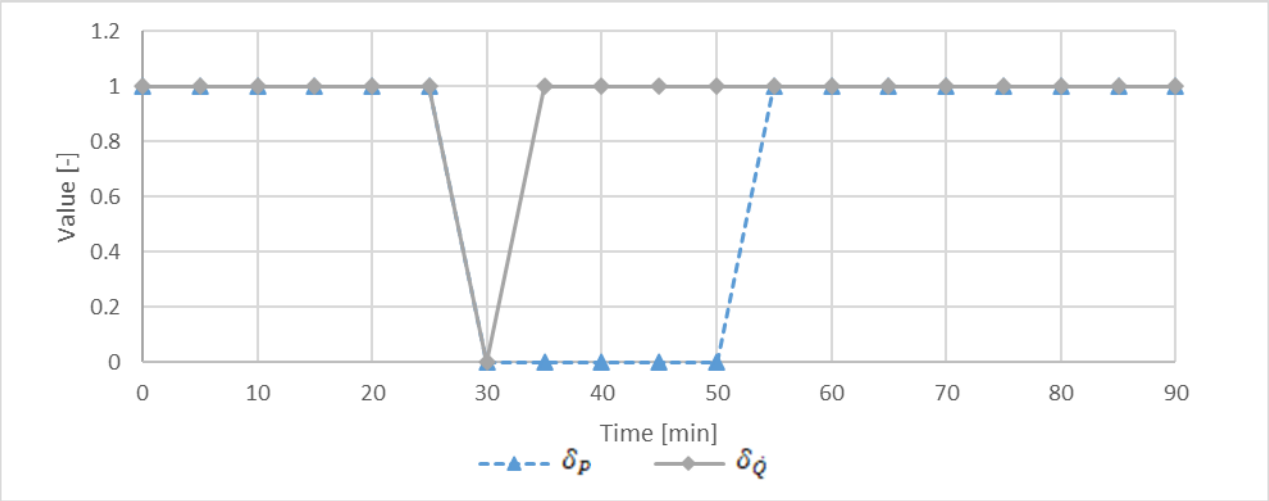


Figure 7-5: Operational Status of Components with DAFP in Demonstrative Dataset

After 55 min, the warm restart procedure is completed and the heat transfer restriction at the PGEN is removed, and the unit is also allowed to generate power with the transferred heat.

7.5.1.2 Flow and Temperature Adjustments

The first step in the DAFP is to determine the allowable heat transfer and the associated cooling water flow rate for these heat transfers. The DAFP then iterates through the allowable flow rates and assigns a flow rate that will result in either maximum power generation or minimum power consumption. The resulting impact on cooling water temperature is provided in Figure 7-6.

In this figure, it is shown that the flue gas exit temperature for DAFP is at the minimum of the operational envelope for 0–25 min and 55–90 min. This indicates that the cooling water flow rate is increased to the maximum of the allowable flow range while the PGEN is in operation, as is noted in the previous figure.

At time 30 to 50 min, the flue gas temperature increased along with the cooling water temperature. During this period, the cooling water flow is reduced to the minimum allowed. The cooling water temperature increased to the maximum limit of 210 ℃. Comparatively, the flue gas temperature is not near the upper limit of 350 ℃, indicating that the allowable flow range in this time zone is constrained by the cooling water exit temperature.

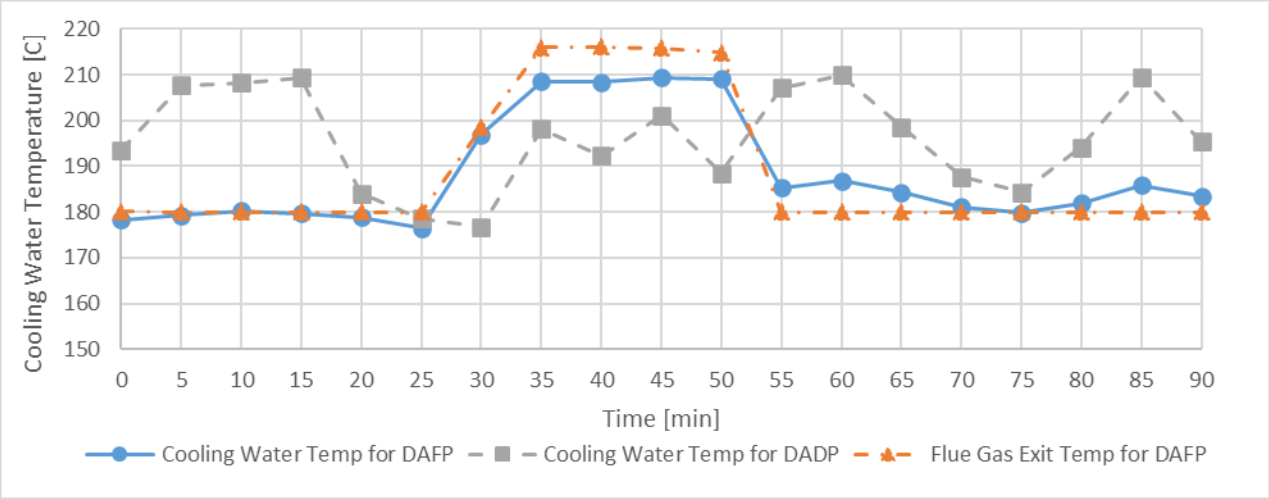


Figure 7-6: $T_{hs,t}$ Comparison between DADP and DAFP and T_{fg} for DAFP

It is noted that the PGEN is in a warm restart procedure from 35–50 min. It follows that the DAFP attempted to only transfer the required heat from the flue gas to sustain the PGEN heat transfer requirement in the restart procedure of SAPR. However, the cooling water temperature exiting the gas cooler prevented DAFP from reducing the heat transfer any further.

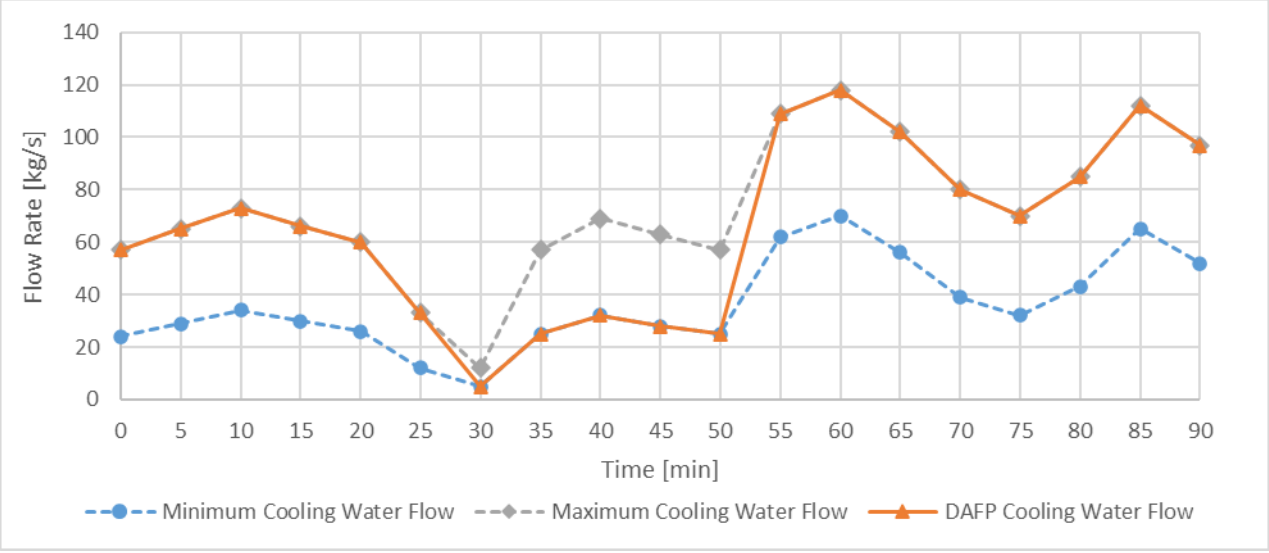


Figure 7-7: Allowable Cooling Water Flow Rate in DAFP

The results for the allowable cooling water flow range are provided in Figure 7-7 along with the desired cooling water flow rate for DAFP. While the PGEN is online, the DAFP maximises power generation by transferring all the allowable heat from the flue gas. Note that the approach in DAFP

is not to assign the maximum flow rate and instead iteratively determine the flow rate that will deliver maximum power generation.

During the times that PGEN are offline, the DAFP minimises power consumption by reducing the flow rate to the minimum allowed. This reduces the energy required to pump the cooling water while maintaining both the flue gas and cooling water operational envelope. The available heat in the cooling water exiting the gas cooler between DAFP and DADP is compared in Figure 7-8. Note that for the periods where the PGEN is operational ($\delta_P = 1$), more heat is available in the cooling water with DAFP compared to DADP. The opposite is true for periods where the PGEN is non-operational. A relative comparison is also shown on Figure 7-8 to emphasise the difference.

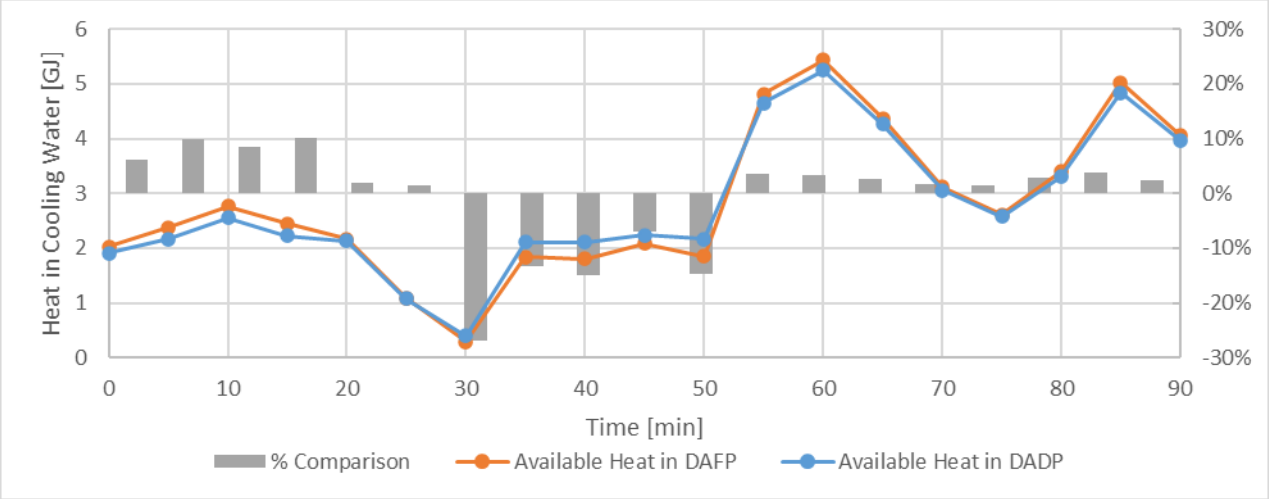


Figure 7-8: Available Heat Comparison between DAFP and DADP

The flow distribution between ACHX and PGEN is still dictated by the same approach as in DADP where the PGEN flow is determined that will deliver the highest power generation. This approach remains unchanged. Minor differences between the results of DADP in Figure 6-5 and DAFP in Figure 7-9 are noted. This is mainly due to the difference in cooling water flow rate which in turn adjust the range of flow that can be distribution to the PGEN.

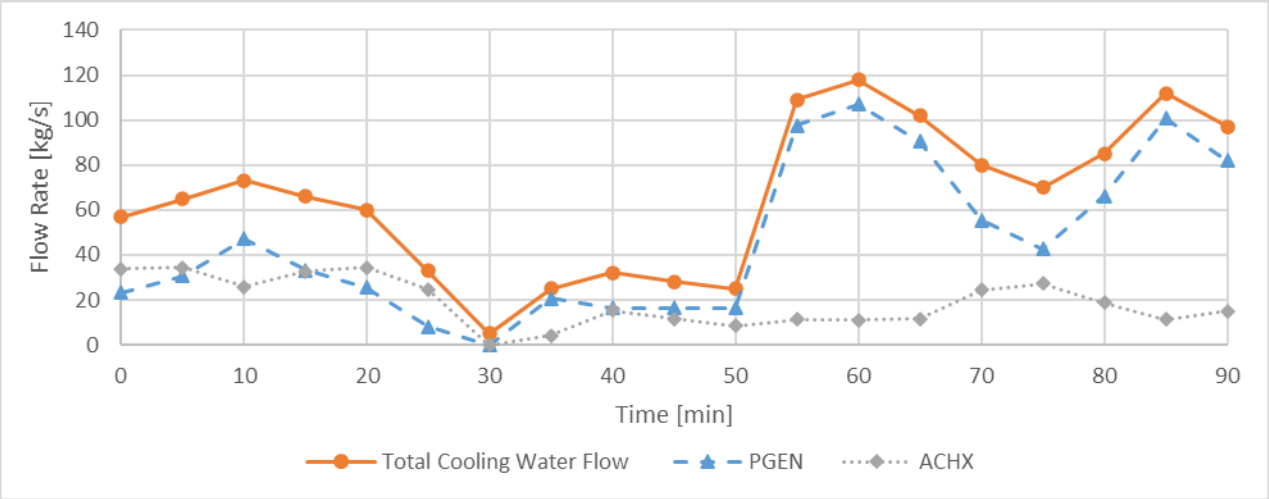


Figure 7-9: Flow Distribution between ACHX and PGEN for DAFP

7.5.1.3 Nett Power Generation

The purpose of DAFP is to improve on the nett power generation of DADP by adjusting the cooling water flow rate. To evaluate whether this is successful, a comparison of the nett power generation between DAFP and DADP is illustrated in Figure 7-10. To emphasise the relative changes in performance, an additional indicator is introduced that illustrates the percentage of power generation change observed. It is noted that the DAFP improves on the power generation performance of DADP in every period that the PGEN is operational. It follows that the DAFP is successful in achieving the objective of maximising power generation by adjusting the flow of cooling water throughout the system.

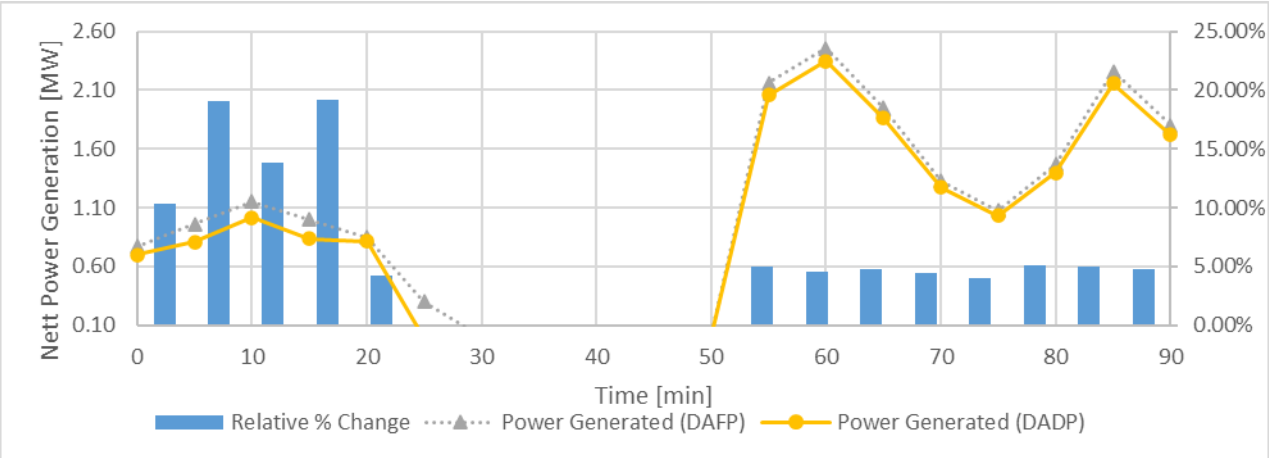


Figure 7-10: Comparison of Nett Power Generation for DADP and DAFP

7.5.1.4 Summary of Demonstrative Dataset Results

The demonstrative dataset has been used from Chapter 5-7 to illustrate the differences in performance between the control philosophies and ensuring that all sub-algorithms operate as required. The table below is a summary of the results between the different philosophies.

Table 7-2: Comparison of DAFP, DADP and WP on Demonstrative Dataset

Parameter	DAFP	DADP	WP	Unit
Available Heat in Cooling Water	53 681	52 567	52 567	MJ
Heat transferred by PGEN	43 567	40 185	36 566	MJ
% of Total Heat	81.16	76.43	69.55	%
Average heat transfer rate at PGEN	7.64	7.05	6.42	MW
Average power generation	1.028	0.962	0.868	MW
Weighted average η_{th}	15.12	15.52	15.58	%

The available heat in the cooling water remains constant from WP to DADP, since no cooling water flow rate adjustments were made. The DAFP then adjusted the flow rate such that more heat is available in the cooling water.

This then resulted in more heat being transferred to the PGEN with DAFP transferring 81.16% of the available heat to the PGEN. The PGEN under DAFP also resulted in the highest average power generation figure with a value of 1.028 MW. Note that this achieved even though the weighted average thermal efficiency of the system reduced from DADP to DAFP. This is a result of the approach to maximise power generation. If maximum efficiency is the objective, the thermal efficiency would have increased at the expense of power generation performance.

7.5.2 Historical Dataset

The previous section illustrated the differences between DAFP and DADP on a demonstrative dataset. The sub-algorithms of SAAR, SAPR and the reaction to the trip remains consistent with WP. The difference in cooling water flow rate is observed between the two philosophies. The performance of the PGEN and ACHX under the adjusted cooling water flow rate is compared in this section.

7.5.2.1 Performance and Operational Parameters on Historical Dataset

Several comparisons can be made between the results of the DAFP and DADP on the historical dataset. As mentioned earlier in this chapter, the only difference between the DAFP and DADP is that the DAFP adjusts the cooling water flow rate for maximum power generation. The same approach is followed when the philosophy needs to determine the desired distribution between the PGEN and ACHX.

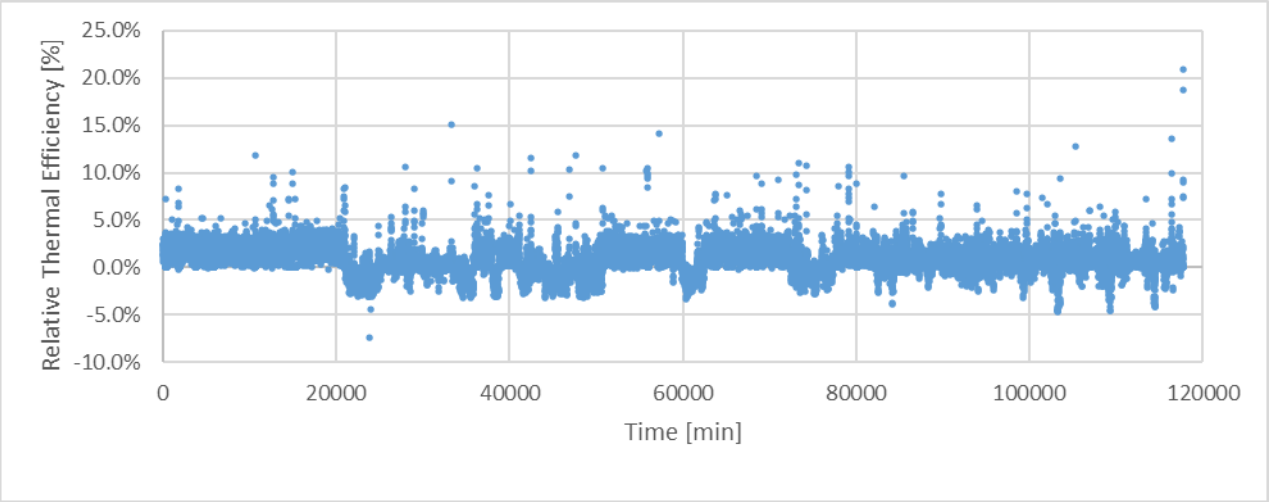


Figure 7-11: Relative Changes in Thermal Efficiency from DADP to DAFP

Thus, the PGEN performance and efficiency can be evaluated. The relative increase or decrease in thermal efficiency in the power generation of PGEN is illustrated in Figure 7-11. From this figure it is observed that there are several periods in the historical dataset where the efficiency of the PGEN component reduces from DADP to DAFP. This indicates that the DAFP does not attempt to maximise thermal efficiency but rather power generation. To ensure that the power generation is improved, even when the thermal efficiency reduced, a similar figure for nett power generation increases is populated, as in Figure 7-12.

Note that the nett power generation in the PGEN model includes the power consumed by the PGEN cycle pump and the cooling water circulation pumps. Thus, increasing the flow rate of the cooling water increases the power consumption as noted in Chapter 3.4.2.1. The DAFP evaluates if this increase in power consumption will benefit the nett power generation.

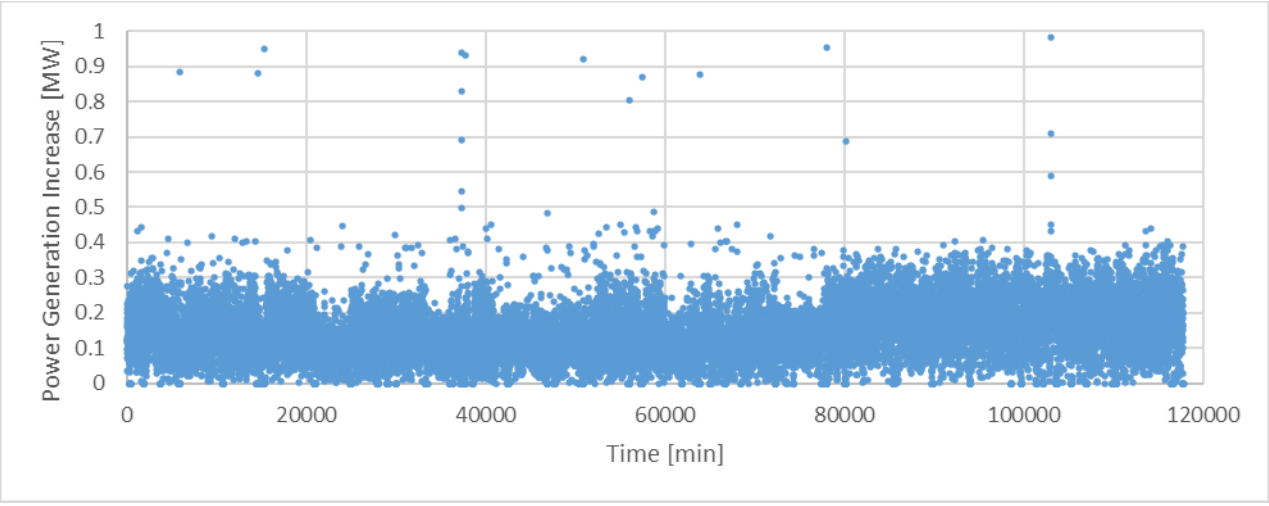


Figure 7-12: Increase in Power Generation from DADP to DAFP

From this figure there are no periods where the power generation is reduced. It follows that the DAFP would only adjust the cooling water flow rate if the nett power generation benefits from the

change. The DAFP is thus successful in its objective to maximise nett power generation by adjusting the flow of the cooling water throughout the system.

7.5.2.2 Comparison to DADP

The performance of the DAFP will now be compared to the results of the system under DADP and WP in the previous chapters. A summary of these results is provided in Table 7-3.

The gas cooler operational envelope is still maintained throughout the time horizon of the historical dataset while the PGEN is in operation for 96.2% of the time. This is longer than for DADP and WP. This can be attributed to more heat being transferred from the flue gas, resulting less trips or shorter delays before startup procedures are initiated. The adjustment in cooling water flow rate increased the energy transferred from the flue gas to 88 238.2 GJ which is 99.36% of the available energy over the time horizon. The difference is due to periods where the PGEN is non-operational and the energy transfer and power consumption in the system is minimised. The number of trips reduced from 52 in DADP to 51 in DAFP while the average amount of time between a trip and completion of a restart procedure reduced from 122 min for DADP to 114 min for DAFP.

In addition, the total heat transferred by the PGEN evaporator increased from 70 107.61 GJ to 76 687.30 GJ which is 86.91% of the total heat available in the cooling water in the historical dataset.

Table 7-3: Comparison of Performance between DAFP, DADP and WP

Parameter	DAFP	DADP	WP	Unit
Time $\overline{T_5} < 150$ ℃	0	0	0	min
Minimum $\overline{T_5}$	150	150.00	150.00	℃
Maximum $\overline{T_5}$	185.74	185.74	185.74	℃
% of time PGEN is in operation	96.2	95.9	95.9	%
Heat transferred by Gas Cooler	88 238.2	81 914.9	81 914.9	GJ
% of Total Heat in Flue Gas	99.36	92.24	92.24	%
Heat transferred by PGEN	76 687.30	70 107.61	60 889.85	GJ
% of Total Heat	86.909	85.586	74.333	%
Average heat transfer rate at PGEN	10.846	9.916	8.612	MW
Average power generation	1.615	1.485	1.231	MW
Weighted average η_{th}	14.96	15.06	14.39	%
Energy Recovery Efficiency	12.38	11.34	9.40	%

The average heat transfer rate at the evaporator of the PGEN also increased from 9.916 MW under DADP to 10.846 MW with DAFP. This resulted in an increase of 8.8% on the average power

generation, increasing from 1.485 MW to 1.615 MW over the time horizon. The weighted thermal efficiency of the PGEN decreased from 15.05% to 14.96%. It follows that the cooling water flow rate in the system is adjusted to generate more power even though it is at a lower efficiency.

The energy recovery efficiency resulted in a value of 12.38%, increasing from a value of 11.34%.

The number of trips the PGEN experiences reduced from 52 to 51 with the time between a trip and restart also reducing from 122 min to 114 min with DAFP. This is due to the energy recovery maximisation approach where the cooling water flow rate is adjusted to the point where PGEN operation or restart procedures can be maintained or restart earlier.

7.6 Conclusion

This chapter illustrated the formulation and performance of the DAFP on a historical dataset. The first section of the chapter provided a summary of the change in approach required to improve on the performance of DADP.

The approach changes can be summarised as determining the allowable range of the cooling water flow rate and then using the operational status of the PGEN and expected nett power generation to decide on flow rate adjustments. The chapter then provided a simplified gas cooler model to evaluate the difference in heat transfer performance that can be expected with adjustments to the cooling water flow rate. A case study is completed to show the impact that the flow rate adjustments will have on the flue gas and cooling water exit temperature as well as the heat transferred between the fluids. A formulation of the sub-algorithm that determines the allowable range for the cooling water is then provided.

The Discrete Adjustment to Flow Philosophy is then formulated. The DAFP uses the above sub-algorithm and a modified bisection method to determine the flow rate that will deliver the maximum power generation. Three initial guess values for the flow rate are determined in the allowable range and assigned after which the gas cooler model determines the flue gas exit and cooling water exit temperature. No other changes are made from DADP and thus the same approach follows as for DADP. Once the nett power generation at these guess values are determined, then the bisection method is implemented to find the cooling water flow rate that will deliver the maximum nett power generation. Note that for a period where PGEN is offline, the nett power generation is maximised for the cooling water flow rate that will require the least power at the circulation pump.

A summary of the evolution from DADP to DAFP is provided in the figure below.

In summary, the WP aimed to maximise power generation with the assigned cooling water flow by adjusting the evaporating pressure and degree of superheat in the PGEN. The assigned cooling water flow is based on a fixed distribution ratio. The DADP then improved on this power

generation by adjusting the flow of cooling water distributed to the PGEN. The DAFP provides further improvement by using the operational status of the PGEN and a gas cooler model to maximise power generation or minimise power consumption.

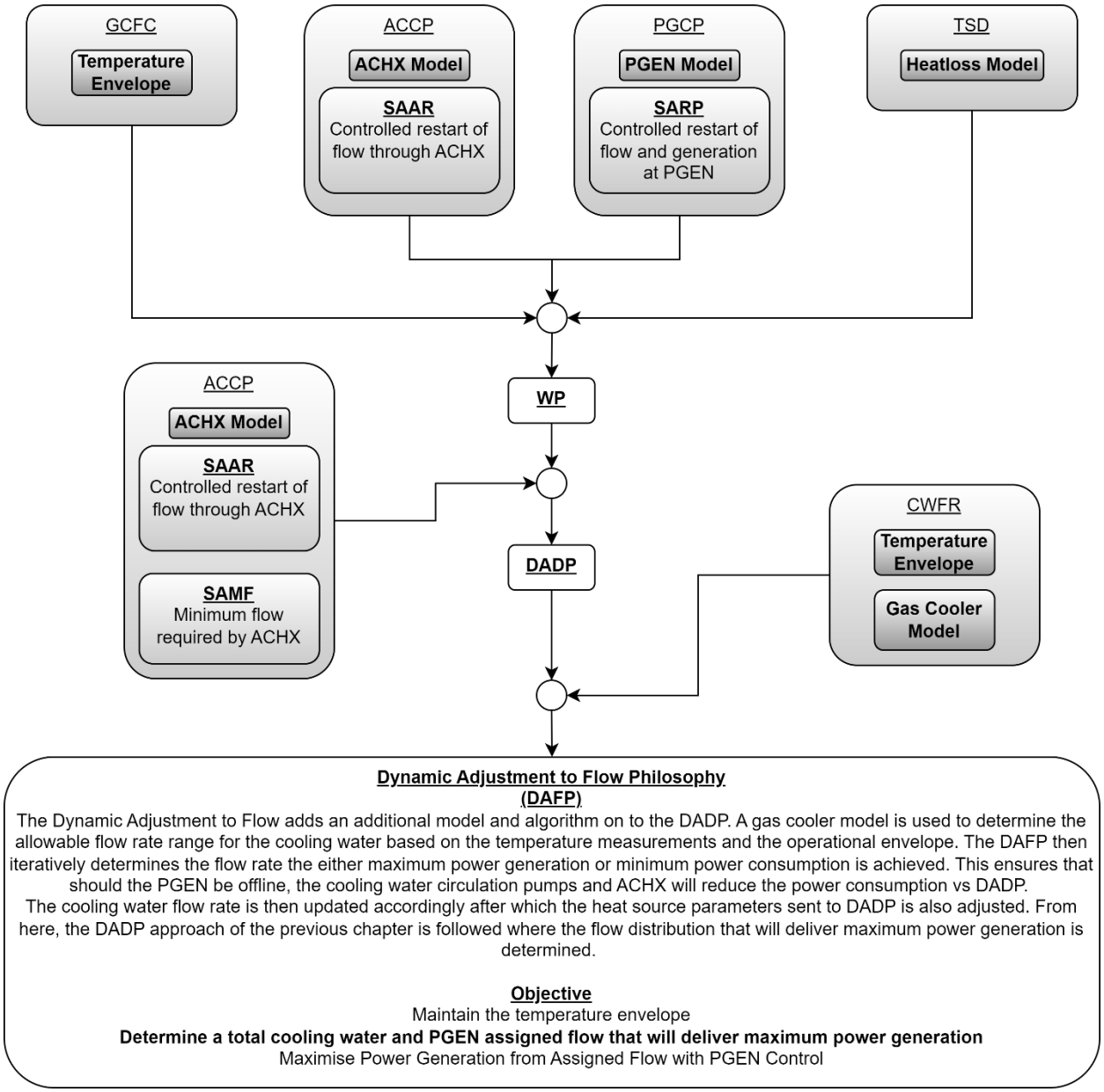


Figure 7-13: Summary of DAFP after Conclusion of Chapter 7.

The DAFP approach on the historical dataset resulted in a PGEN that is operational 96.2% of the time, transferring 86.91% of the available heat from the cooling water, an increase from 85.59% under DADP. The average power generation for the PGEN is determined to be 1.615 MW, compared to 1.485 MW under DADP. The DAFP also resulted in a weighted thermal efficiency of 14.96%. The energy recovery ratio is also determined to be 12.34%, which also increased from 11.34% under DADP.

The number of trips the PGEN experiences reduced from 52 to 51 with the time between a trip and restart also reducing from 122 min to 114 min with DAFP. This is due to the energy recovery maximisation approach where the cooling water flow rate is adjusted to the point where PGEN operation or restart procedures can be maintained or restart earlier.

CHAPTER 8 POTENTIAL SYSTEM IMPROVEMENTS

The DAFP, formulated in the previous chapter, improved on the power generation performance of the system while still maintain the operational envelope for the current system. The DAFP includes the adjustment of cooling water flow rates, the adjustment of cooling water flow distribution and PGEN operational parameters to deliver the maximum power generation.

The current system consists of a PGEN and no thermal energy storage systems (TESS). In this chapter, the DAFP is modified to investigate the potential performance improvements for the addition of a TESS.

8.1 Addition of a TESS

It is noted during the DAFP that the PGEN experienced 51 trips under DAFP with an average delay of 114 min between the trip event and restarting power generation. This can be attributed to the significant fluctuations mentioned and illustrated in Chapter 3.2.3.

8.1.1 Updated System Layout with TESS

The system used in this study does not have any form of TESS and thus the philosophies in earlier chapters addressed the need to adapt both the PGEN and ACHX to meet the fluctuating heat transfer demands. The fluctuating heat availability resulted in several trips for the PGEN followed by constrained restart procedures where no power is generated. This results in the ACHX transferring the heat to the environment, with no benefit to the system owner. It is stated by Dal Magro [46] that the fluctuating nature of waste heat in the steel industry need to be dampened in order to deploy affordable energy recovery systems.

Dal Magro [46] attempted to develop such a technology, using phase-change materials as a TESS to dampen the fluctuations observed in the flue gas cooling system. The plant effectively uses the latent heat of a material during the phase change process to store energy. Several processes were identified for a latent heat TESS, one of which is the waste heat to power generation on an electric arc furnace. There are thus similarities between the system by [46] and the system used in this study.

It follows that a similar TESS can be added to the current system. Applying a TESS model to the DAFP and then simulating the historical dataset allows for the evaluation of performance changes that can be expected. It allows for the determination of realistic returns for the investment such a system will require.

The system layout of Figure 1-1 is configured to include a TESS between the gas cooler outlet and node where the flow is distributed between the ACHX and PGEN, as illustrated in Figure 8-1. The cooling water will exit the gas cooler at point 2, and then based on the TESS parameters,

heat will be transferred between the TESS and cooling water, resulting in a different temperature at point 2*.

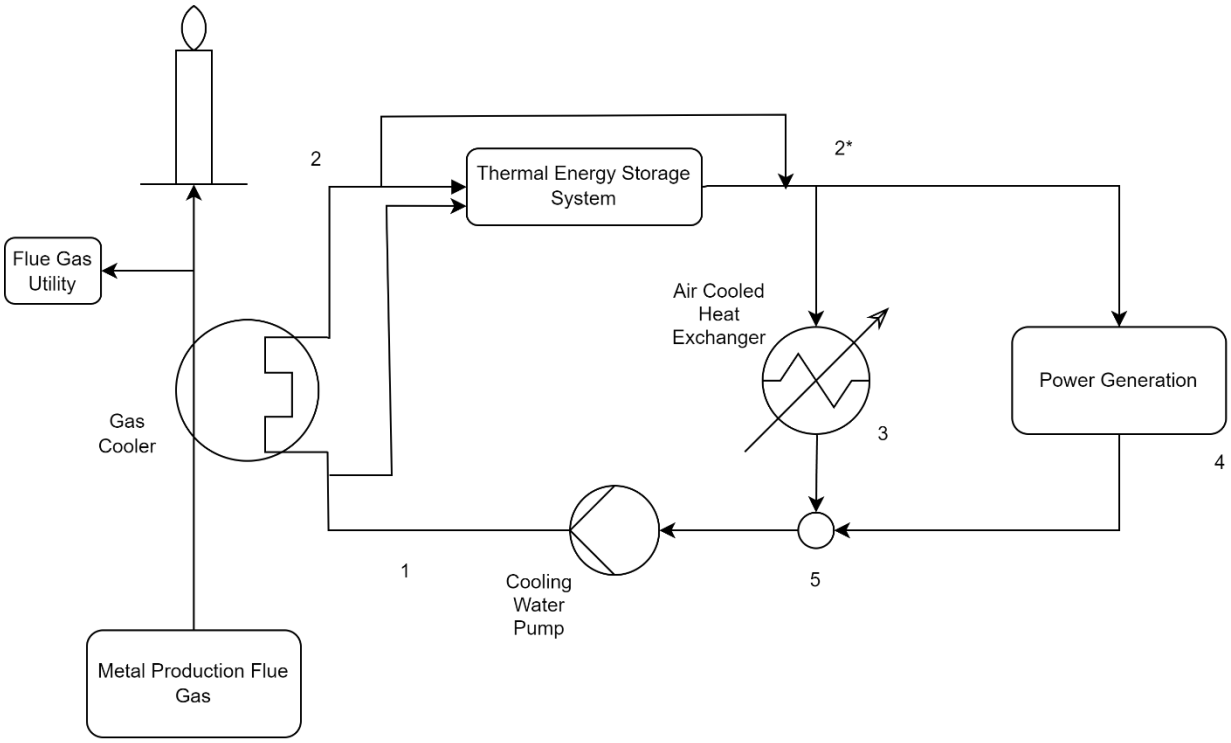


Figure 8-1: Layout of Heat Rejection System with Addition of a TESS

Note that both the gas cooler and TESS can be bypassed depending on heat availability in the flue gas and cooling water, respectively.

8.1.2 TESS Parameters

The design of an optimised TESS is not part of the scope of this study. However, the impact of a suitable TESS needs to be evaluated. Thus, the design parameters for the TESS used in this study will be based on suitable values from either published literature or the historical dataset.

The design parameters for the TESS are provided in Table 8-1.

The TESS applied in this system will also be based on a phase change type TESS. The desired temperature at which material changes phase needs to be determined. From heat transfer theory provided in Chapter 2-5, heat is transferred from the higher temperature medium to the lower temperature medium. Thus, if the value at which the TESS stores latent heat, T_{TESS}, is more than the average cooling water temperature then it follows that the cooling water will transfer heat to the TESS for most of the time horizon. Thus, such a setup will result in increased storing of thermal energy but reduced usage of the stored energy.

Conversely, if the temperature at which the TESS stores latent heat is less than the average cooling water temperature, then the TESS will transfer more heat to the cooling water for most of

the time horizon. Such a setup will result in increased usage of the stored thermal heat but reduced storing or “charging” of the TESS.

Table 8-1: TESS Design Parameters

Parameter	Value	Unit
Type	Phase-change	-
Melting Temperature of Phase Change Material	180	℃
Maximum Temperature Increase with TESS Heat Exchanger	15	℃
Total Thermal Energy Capacity	15	MW.h
	54	GJ
Energy Density	335	MJ/m^3

The cooling water temperatures for each of the 51 trip events are populated in Figure 8-2. Of the 51 events, only 2 of the events occurred when the cooling water temperature is higher than 170 ℃ for the cooling water exiting the gas cooler. Since the pinch point noted in Table 3-1 is 15 ℃, it follows that by choosing a material with a phase change occurring at 180 ℃ can potentially prevent or delay 49 trip events, depending on TESS capacity.

The cooling water temperature exiting the gas cooler under DAFP control is sorted in three groups in Figure 8-3. Cooling water below 180 ℃ can flow through the TESS to absorb heat from whereas cooling water above 180 ℃ can be used to transfer heat to the TESS.

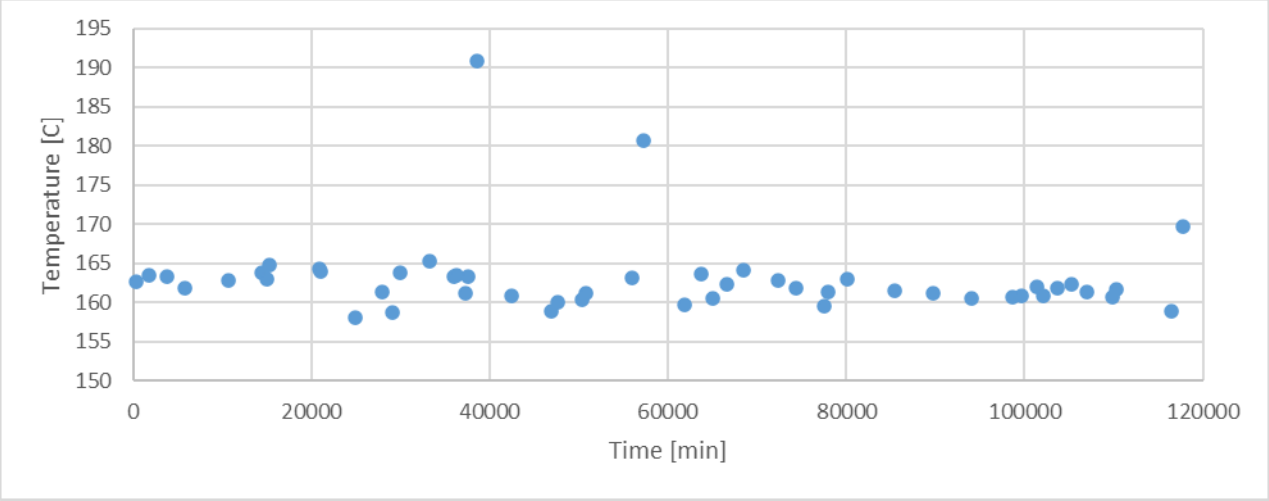


Figure 8-2: Temperature at which PGEN tripped for DAFP

The next design parameter provided is the energy density of the TESS. The energy density is set as 335 MJ/m^3, a realistic value for a TESS of this temperature and type according to [55]. It follows

from the capacity rating that the storage consists of a volume of 160 m^3. Heat fluxes for the TESS walls, floors and roof were assumed to be the consistent with the system evaluated in [56] with 160 W/m^2 for the roof and walls and 92 W/m^2 for the floor. Based on a storage vessel with a height of 3.2 m and a diameter of 8 m, a required volume of 160 m^3 will be reached, albeit with a heat loss rate of 25.53 kW. Over a 24-hour period, this equals 2.21 GJ which is 4.1% of the capacity of the TESS.

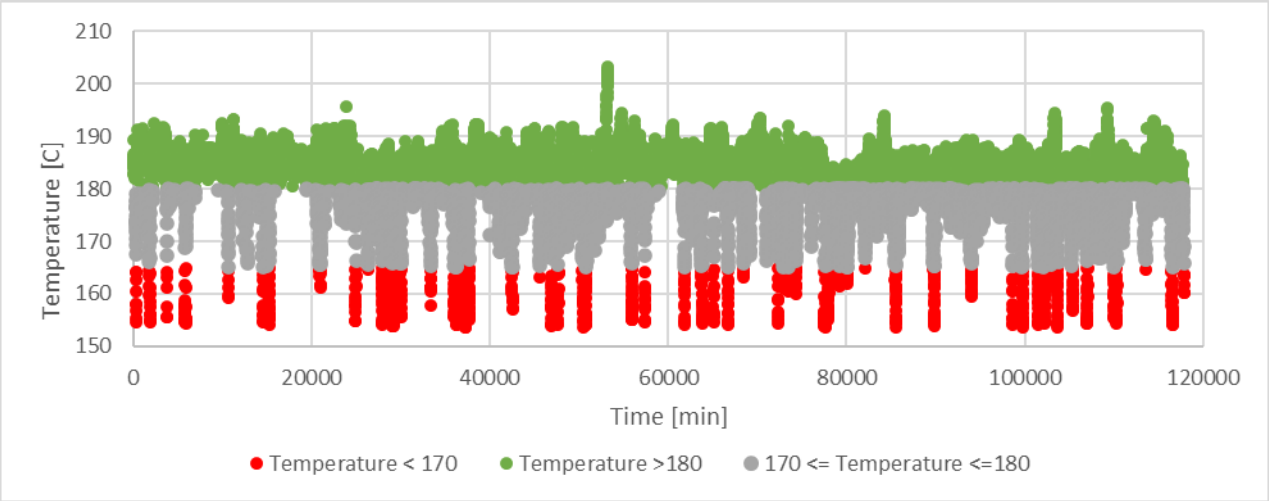


Figure 8-3: Temperature of Cooling Water exiting Gas Cooler for DAFP

8.2 Adjustments to DAFP

The previous section provided the basic TESS parameters that is considered in the evaluation of power generation performance should an investment into a suitably sized storage system be made. In this section, the additional considerations are provided in terms of the TESS control algorithm as well as any required changes to the DAFP.

8.2.1 TESS Control Algorithm (TCA)

Due to the location of the TESS in the heat rejection system, the cooling water parameters measured at the exit of the gas cooler need to be considered. This section will describe the use of these measurements to either charge or discharge the TESS with thermal energy.

An illustration of the control algorithm is provided in Figure 8-4.

As an initial step, the energy being charged and discharged at time t is initialised as $Q_{charge} = Q_{discharge} = 0$ J. The energy that is added to the cooling water that bypassed the gas cooler is also initialised as $Q_{add} = 0$ J. The estimated energy loss for the period is provided as an input, $Q_{TESS,t}^{loss}$ J along with the measured flow rate, temperature and available heat of the cooling water.

A setpoint energy requirement is also introduced as Q_{hs}^{req} J and is the desired minimum available heat in the cooling water. As a first step, the available heat is compared to the setpoint energy

requirement. If $\mathrm{Q_{hs,t}} > \mathrm{Q_{hs,t}^{req}}$, then it follows that heat transfer to the cooling water is not required. Since heat transfer can only occur between two mediums with different temperatures, the second decision to be made in the algorithm is whether heat can be transferred to or from the TESS.

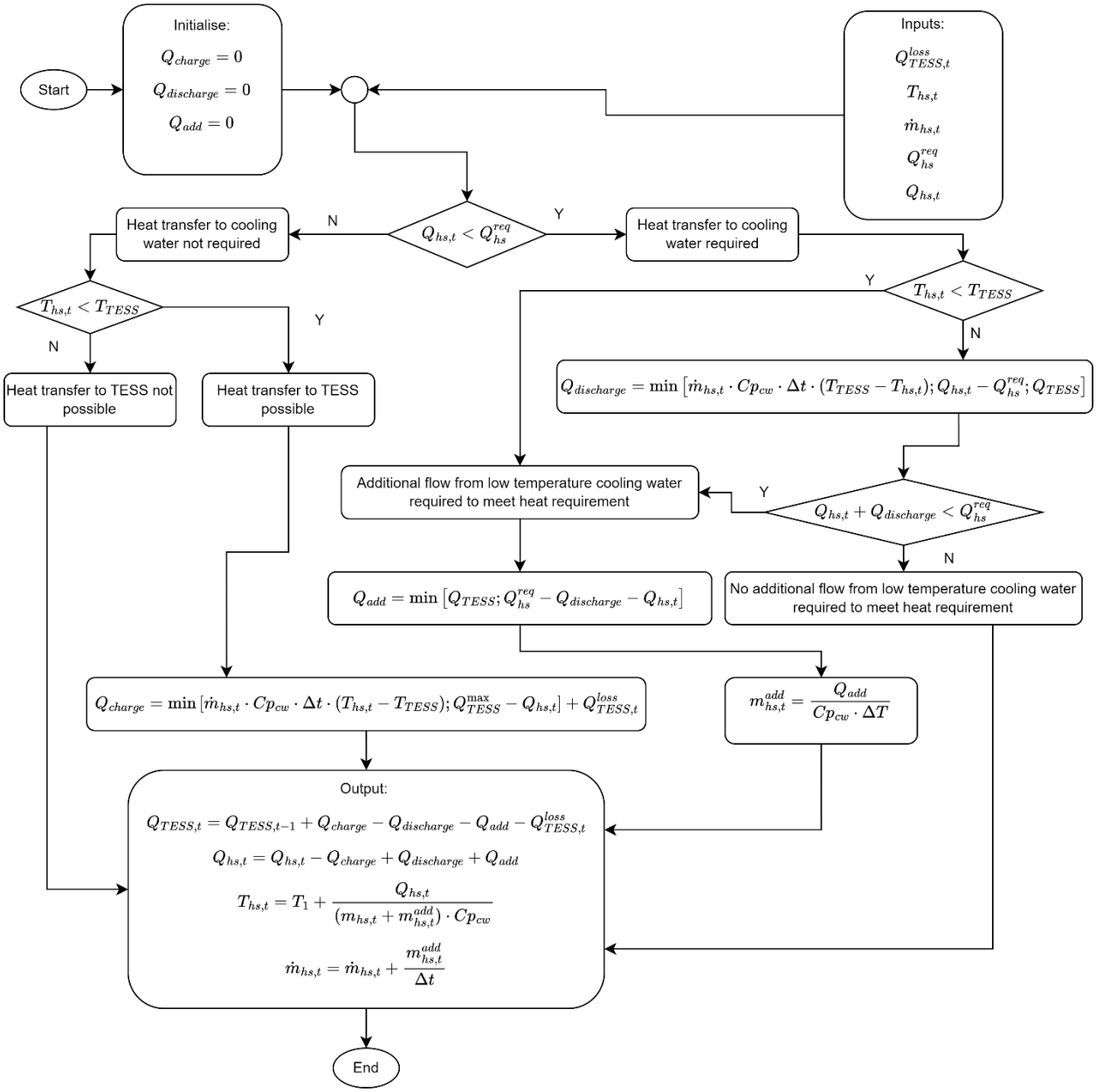


Figure 8-4: TESS Control Algorithm (TCA) to Adjust Cooling Water Temperature entering DAFP

For $\mathrm{Q_{hs,t}} > \mathrm{Q_{hs}^{req}}$ and $\mathrm{T_{hs,t}} < \mathrm{T_{TESS}}$ it indicates that there is sufficient heat for the cooling water requirement however the temperature prevents heat transfer from the cooling water to the TESS. Since $\mathrm{Q_{charge}} = \mathrm{Q_{discharge}} = \mathrm{Q_{add}} = 0$ it follows that the cooling water properties entering the ACHX and PGEN sections are unchanged from the exit of the gas cooler. However, if $\mathrm{Q_{hs,t}} > \mathrm{Q_{hs}^{req}}$ but $\mathrm{T_{hs,t}} > \mathrm{T_{TESS}}$ then it follows that there is potential for energy transfer from the cooling water to the gas cooler, referred to as “charging”. The amount of energy transferred is limited by the

minimum between the energy contained in the temperature difference between the mediums and the amount of energy required to reach full capacity for the TESS.

Alternatively, if $Q_{hs,t} < Q_{hs}^{req}$ and $T_{hs} > T_{TESS}$ it follows that additional energy is required however the temperature of the cooling water exiting the gas cooler is too high to allow heat transfer from the TESS to the cooling water. In this scenario, additional cooling water is circulated at the low temperature of T_1 and passed through the TESS to absorb heat. Note that the additional cooling water flow bypasses the gas cooler to ensure the operational envelope is maintained.

The heat transferred to the additional cooling water stream, Q_{add}, is limited between the available energy in the TESS, Q_{TESS}, and the difference between the available and required thermal energy. After determining the heat transferred to the additional cooling water stream, the additional cooling water stream flow rate is determined. This is done by assuming a temperature difference, $\Delta T℃$ for the additional cooling water stream. Once both streams combine after the TESS, both mass flow rates and available energy is combined.

The only other potential scenario is for $Q_{hs,t} < Q_{hs}^{req}$ and $T_{hs} < T_{TESS}$. In this situation, the cooling water flow rate can absorb thermal energy from the TESS. The energy discharged from the TESS is limited by the available energy in the TESS, the difference in energy required and available as well as the energy contained in the maximum possible cooling water temperature difference. Should the energy discharged not be sufficient, flow in the additional cooling water stream is required. Once both streams combine after the TESS, both mass flow rates and available energy is combined.

The flow rates and energy content of the cooling water entering the ACHX and PGEN is thus potentially different from the parameters exiting the gas cooler. The DAFP model requires flow rate and temperature of the cooling water and thus, after updating the available heat and flow rate parameters, an equivalent temperature is determined at point T_2^*.

The current TESS energy content level is updated by adding the charging, discharging, additional cooling water stream and energy loss values for time t to the previous energy content level.

8.2.2 Evaluation on Demonstrative Dataset

To illustrate the performance of the TESS in the system the demonstrative dataset results from DAFP is used. For this demonstration, the minimum heat requirement is set to $Q_{hs}^{req} = 1.86$ GJ, which is the equivalent of an average heat transfer rate of 6.2 MW for the 5 min period. The TESS consists of a capacity of Q_{TESS} =54 GJ and the maximum temperature difference obtainable for the cooling water is 15 ℃ with a phase change material temperature at 180 ℃.

Note that for the purpose of this section DAFP is not applied. The flows observed can, therefore, change when the demonstrative dataset is evaluated in the next section.

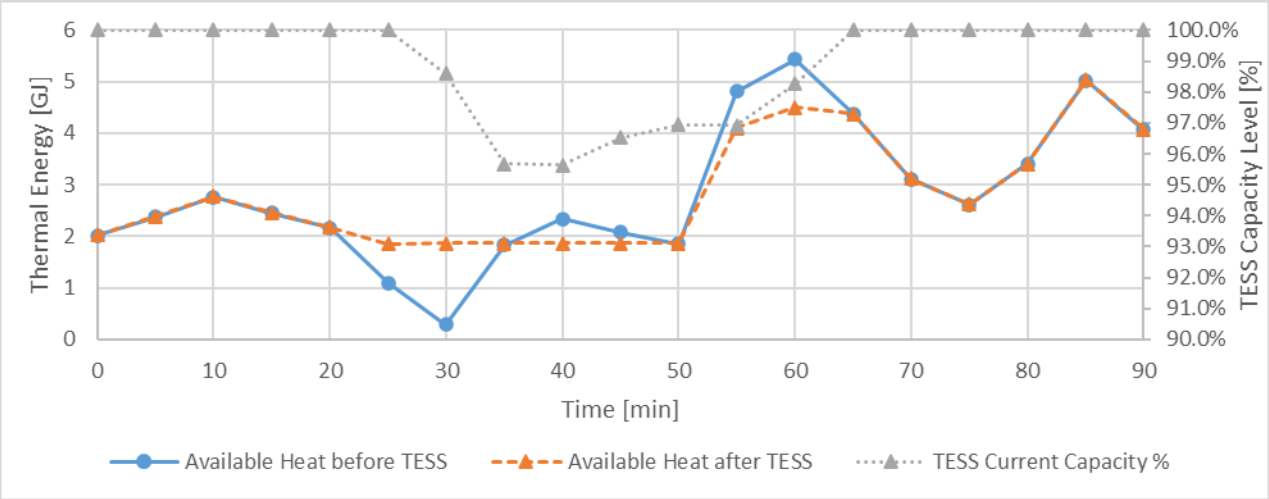


Figure 8-5: Heat Availability in Cooling Water Before and After TESS

The heat availability before and after the TESS is illustrated in Figure 8-5, along with the TESS heat capacity as a percentage of the maximum. At time 25–30 min, heat is transferred from the TESS to the cooling water since the available heat after the TESS is observed to be higher. In the period 40–65 min, heat is transferred from the cooling water to the TESS with the heat availability after the TESS observed to be lower. The charging and discharging of the TESS are also confirmed in the trend of the capacity % of the TESS.

In terms of the heat availability with charging and discharging, note that the availability of heat in the cooling water remains at the 1.86 GJ requirement for the period 25–50 min. Thereafter, a significant increase in heat availability is observed. However, not all the available heat is used to charge the TESS. This is due to the TESS charging algorithm described in the previous section where the heat transferred to the TESS is constrained by either the temperature difference between the cooling water and phase change material or the capacity of the TESS. Since the TESS capacity only reached 100% at 65 min, it can be concluded that the constraint for the charging phase in 55–60 min is due to temperature.

Note in Figure 8-6 that the discharging phase from 25–35 min, the additional flow stream is activated. The temperatures of the cooling water at the reduced flow rates are too high to have heat transferred from the TESS. Thus, the additional flow stream is used where water at T_1 is used to absorb energy from the TESS. The additional flow stream is determined by using the required energy that needs be transferred to meet the minimum requirement and the assumed temperature difference obtainable in the heat exchanger.

Once both flow streams combine at point 2*, the conservation of mass and energy will ensure that the minimum energy requirement for the ACHX and PGEN combination of systems are met.

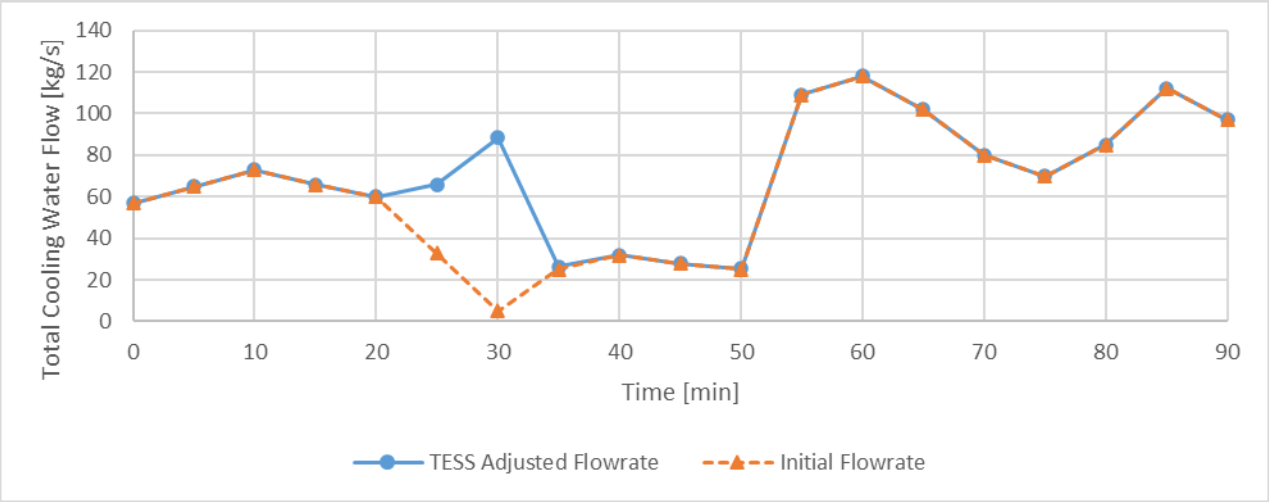


Figure 8-6: Additional Flow Required to Meet Heat Requirement with TESS Compared to DAFP Flow Rate

In DAFP, the flow through the gas cooler is reduced to the minimum allowed at 25-50 min since the energy content in the flue gas is more than the required PGEN heat transfer for the restart procedure. This not only resulted in elevated temperatures for the cooling water exiting the gas cooler but also that the minimum allowable heat is transferred. This can potentially change with the integration of the TESS control algorithm with DAFP, which is investigated in the rest of the chapter.

8.2.3 Changes Required to CWFR (CWFR-T)

The CWFR formulated in Chapter 7.3 determines the allowable flow range for the cooling water. Currently, TESS control algorithm is added to the DAFP without any other changes, there is the potential that minimum flow is determined by DAFP. This will result in a high temperature cooling water exiting the gas cooler and thus being unable to transfer the required heat from the TESS. The TESS control algorithm will then, as it did in the previous section, increase the flow through an additional cooling water stream that will be able to absorb heat from the TESS.

This is not desirable since the heat transferred from the flue gas is minimised while some of the TESS capacity is used. The ideal approach is to only transfer heat from the TESS when the available heat in the flue gas is not sufficient to meet the specified heat requirement. It follows that an adjustment to the CWFC is required.

The gas cooler model used in this study indicates that the allowable flow range determined by CWFC can also indicate a potential heat transfer range with the most heat transfer expected at the maximum cooling water flow rate. This range of potential heat transfer can then be used to determine whether the specified minimum heat requirement for the cooling water can be met.

The adjusted CWFC algorithm are illustrated in Figure 8-7. The first notable difference is the provision of the specified required heat availability as an input and then the introduction of an

iterator i. This allows the formation of an array of results for $\dot{m}_{hs}$, T_{hs} and δ_{TESS}. The binary parameter of δ_{TESS} indicates whether the current flow rate of cooling water will result in available heat that is more ($\delta_{TESS} = 1$) or less ($\delta_{TESS} = 0$) than the specified heat requirement.

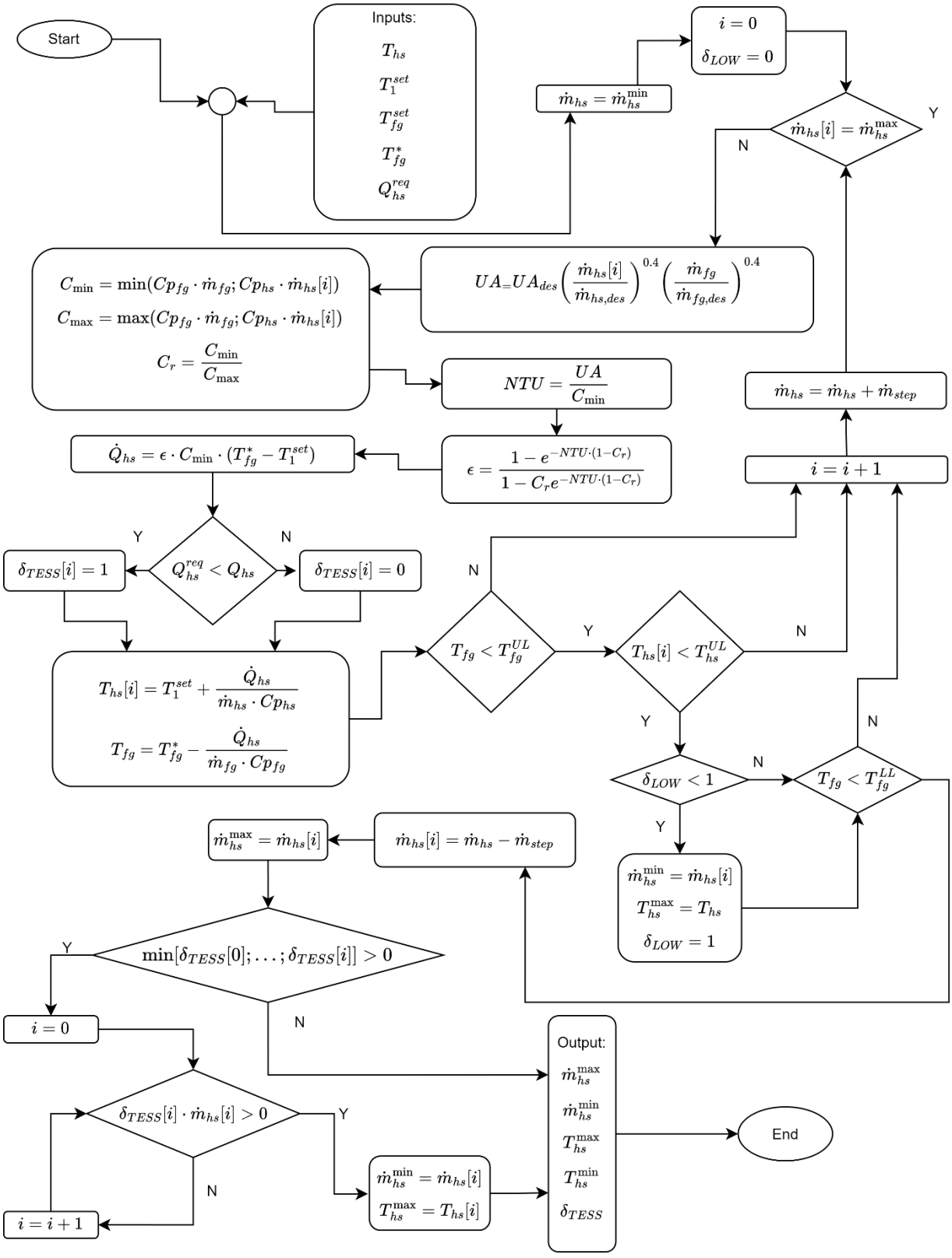


Figure 8-7: CWFR-T for Use in DAFP with an Integrated TESS

The rest of the procedure is the same as the one used in DAFP, with only a final adjustment at the end of the algorithm before the flow and temperature ranges are assigned as outputs. The adjusted CWFC determines if there is at least one result set that predicts a higher heat availability than required. If there is not, then flow and temperature ranges remain unchanged. If there is, then the algorithm iterates through the result set, starting from the minimum flow until a value of $\delta_{\mathrm{TESS}}\mathrm{i} = 1$ is found. The value of i is then used to change the minimum flow and equivalent cooling water temperature.

This approach potentially reduces the allowable flow range for DAFP but will prevent a scenario where the flow is minimised due to the unavailability of PGEN only to transfer heat from TESS to meet the specified heat availability requirement. No other sub-algorithm requires adjustment and thus in the next section, the DAFP formulation is altered to integrate the TESS control.

8.3 Formulation of DAFP with integrated TESS control (DAFP-T)

The previous section described the TESS control algorithm and illustrated the workings thereof on the demonstrative dataset. This section will provide the formulation of the DAFP integrated with a TESS control capability.

The sub-algorithms provided in earlier chapters are still used to ensure that the trip and restart of flow through the PGEN and ACHX is accurately accounted for during the execution of DAFP. The bisection method, BM-PGEN, is also still used to determine the flow distribution that will result in maximum power generation whenever there is sufficient heat to do so.

An illustration of the logic of DAFP-T is illustrated in Figure 8-8.

The notation in the formulation below is consistent with the formulation of DAFP where T℃, Q J, $\dot{\mathrm{Q}}$ W and $\dot{\mathrm{m}}$ $[\mathrm{kg/s}]$ represent temperature, heat, heat transfer rate and mass flow respectively with sub-and superscripts used to identify specific parameters and values.

The time index for the formulation is given by $\mathrm{T} = \{1,2,\dots,|\mathrm{T}|\}$. The difference in time between t and $\mathrm{t}+1$ is constant and indicated by $\Delta\mathrm{t}$. The cooling water exits the gas cooler at a temperature $\mathrm{T}_{\mathrm{hs,t}}$ ℃ and a mass flow rate of $\dot{\mathrm{m}}_{\mathrm{hs,t}}$ kg/s.

The first step of DAFP-T is to receive the maximum and minimum flow of the cooling water at time t, $\dot{\mathrm{m}}_{\mathrm{hs,t}}^{\mathrm{max}}$ and $\dot{\mathrm{m}}_{\mathrm{hs,t}}^{\mathrm{min}}$ respectively. This range is provided by the updated algorithm, CWFR-T in Chapter 8.2.3. In this algorithm, illustrated in Figure 8-7, the heat transfer for the circulating pump flow range is tested and filtered for flow rates that protect the operational envelope. The addition from CWFR to CWFR-T is to identify if any of the flow ranges result in the available heat such that $\mathrm{Q}_{\mathrm{hs,t}} > \mathrm{Q}_{\mathrm{hs}}^{\mathrm{req}}$. If identified, CWFR-T adjusts the allowable flow range accordingly to ensure that sufficient heat is available whenever possible.

After the execution of CWFR-T, the DAFP proceeds as formulated in the previous chapter where a midpoint of the allowable flow range is determined, $\dot{m}_{hs,t}^{mid}$. The UA, C_{min}, C_{max}, C_r, NTU and ϵ values are then calculated with a similar approach to that of Chapter 7.3. The heat transferred per second for the midpoint flow is then calculated after which the flue gas and cooling water exit temperatures are predicted should the cooling water through the gas cooler be adjusted to the midpoint. There is now a minimum, maximum and midpoint cooling water flow and temperature, all sustaining the operational envelope.

The TESS control, refer to Figure 8-4, is now initiated to determine the reaction of the TESS to the parameters of the cooling water exiting the gas cooler. Note that this is repeated for the minimum, maximum and midpoint flows. The TCA then provides an adjusted value for both the flow rate temperature of the cooling water that is to enter the PGEN and ACHX section of the system.

The same approach used in DAFP to determine the desired cooling water flow rate is then applied where the power generation at the three distinct points are calculated. Note that the DADP includes the maximisation of the power generation through firstly determining the ratio of flow distribution between the ACHX and PGEN and then also the PGEN settings required to reach the maximum power generation. The bisection method is then repeated until the convergence for maximum power generation is achieved.

The desired cooling water flow rate through the gas cooler is now determined along with the expected heat transferred every second, the flue gas exit temperature and the temperature of the cooling water that will enter the ACHX and PGEN section. Thus, from here an unchanged DADP can be used to determine the required flow distribution and temperature setpoints between the ACHX and PGEN.

The heat transferred from the flue gas has now been adjusted for maximum power generation or minimum power consumption, where applicable. The desired heat transfer between the PGEN and ACHX as well as the distribution of flow between the PGEN, ACHX and BP (where relevant) has now been determined for all the possible operational regimes of the system. The final requirement is to determine the desired setpoints of each component that is used by the control philosophy to continuously adjust controllable equipment such as valves and fans to ensure that the flow and temperature setpoints are reached. From $\dot{Q} = \dot{m} \cdot Cp \cdot \Delta T$ it can be stated that if these temperature setpoints are reached, the assigned thermal loads and desired total heat transfer is also reached.

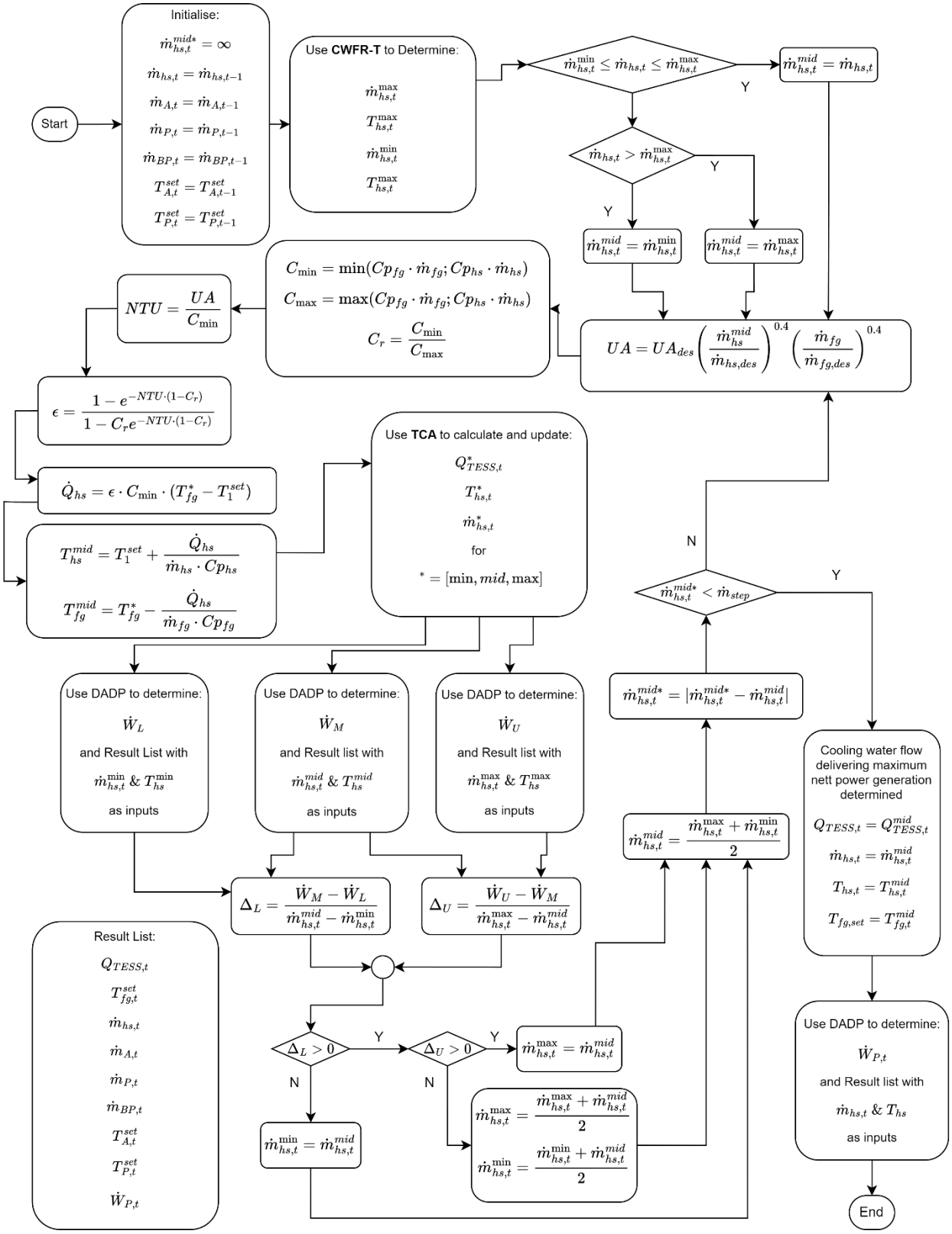


Figure 8-8: Flow Diagram of DAFP-T

A sample script of DAFP-T is provided in Appendix J.

8.4 Performance Evaluation of DAFP-T

To evaluate the operation of DAFP-T, the two datasets are used. The performance of the DAFP-T relative to WP, DADP and DAFP-T will also be illustrated and noted where relevant.

8.4.1 Demonstrative Dataset

To demonstrate the operational performance of DAFP-T, the plant parameters set out in Table 3-1, Table 3-2 and Table 3-3 are used with additional parameters being supplied where required.

The average minimum cooling water temperature entering the gas cooler is set as $\overline{T}^{LL}$ =150 ℃ as in Table 3-1. PGEN has a lower heat limit of $\dot{Q}_P^{min}$ =2 MW and a maximum thermal load of $\dot{Q}_P^{max}$ =20 MW. The cold and warm start procedure parameters for PGEN are as set out in Chapter 5.1.3. The lower and upper limit of the flue gas operational envelope is set at $\overline{T}_{fg}^{min} = \max[\overline{T}^{LL} + 10; \overline{T}_1 + 10]$ and $\overline{T}_{fg}^{max}$ =350 ℃.

In addition, the TESS capacity is set as Q_{TESS}^{max} =54 GJ as noted in Table 8-1 along with a material phase change temperature of T_{TESS} =180 ℃. The maximum temperature difference achievable in the heat exchanger of the TESS is also set as 15 ℃.

8.4.1.1 Changes in Heat Availability, Flow and Temperatures

The approach for the TCA used in the DAFP-T is to transfer heat to the cooling water should there be insufficient heat available or to transfer heat to the TESS should there be excess. This is observed in Figure 8-9. No heat is transferred before 25 min since there is sufficient heat in the cooling water. However, at time 25–30 min, heat is transferred from the TESS, resulting in lower TESS capacity levels. Note the constant heat availability at the specified value of 1.86 GJ for this period. This value is sufficient to sustain both PGEN operation and ACHX losses, thus indicating that the PGEN won't enter a tripped state in the dataset for DAFP-T.

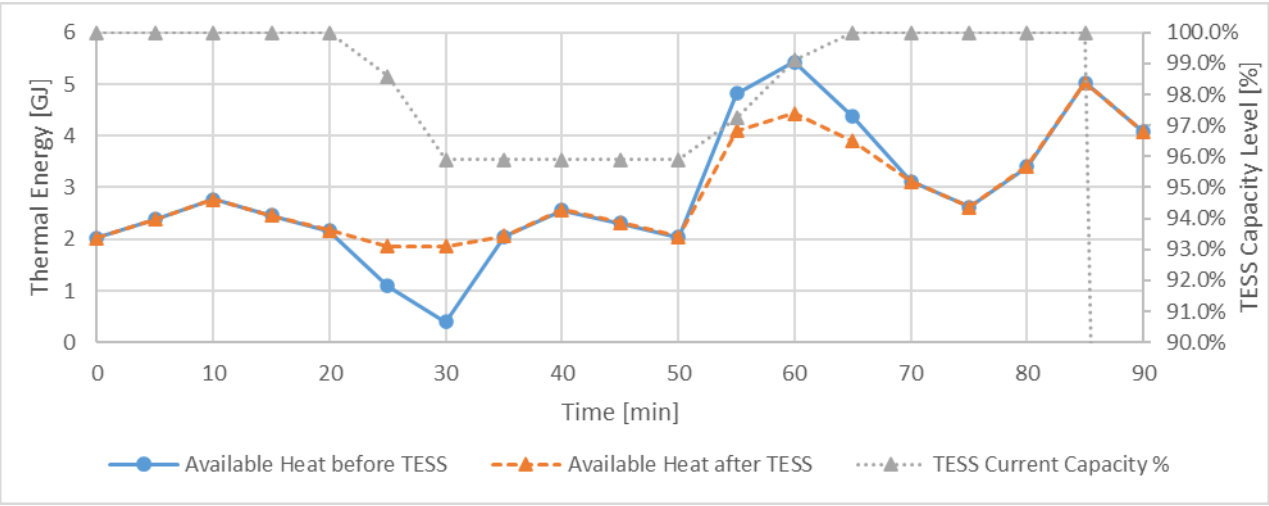


Figure 8-9: TESS Influence on Available Heat in Cooling Water for Demonstrative Dataset

Then, the TESS capacity levels remain where it is due to the temperature of the cooling water not being more than the phase change material, thus prohibiting heat transfer to the TESS. This changes at 55–65 min where some of the heat is transferred to the TESS. This results in less energy in the cooling water that can be converted to electrical power at time t.

In Figure 8-10 the resulting flow rates for the cooling water with DAFP and DAFP-T is compared. From 30–50 min, the DAFP-T resulted in a higher cooling water flow rate through the gas cooler. This is attributed to the PGEN remaining operational due to the TESS transferring sufficient heat at 25–30 min to sustain PGEN operation. All other periods indicate the same flow rate of cooling water through the gas cooler.

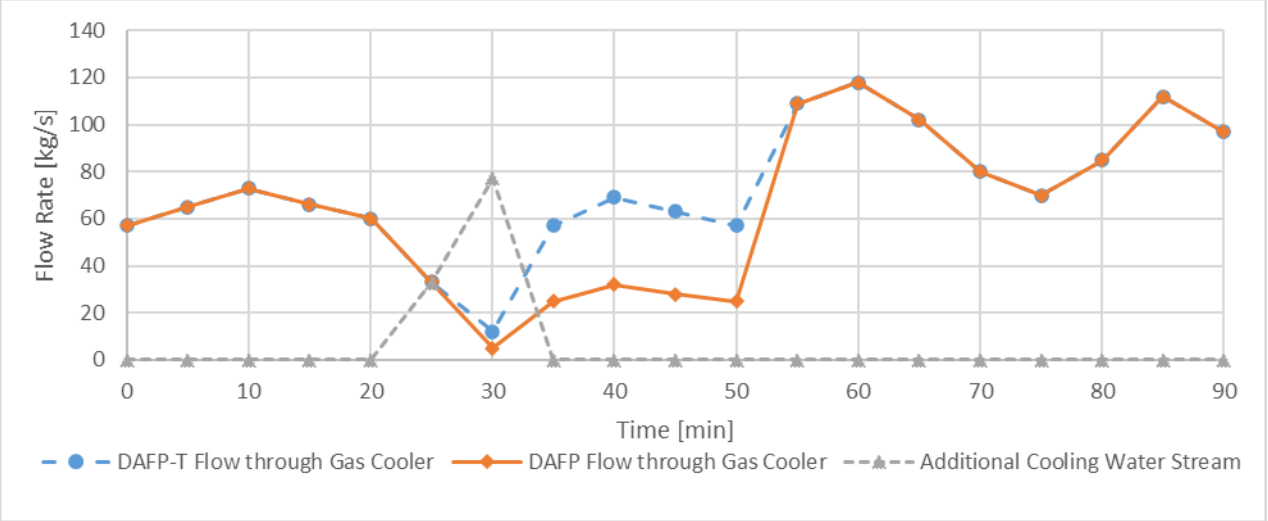


Figure 8-10: Changes in Cooling Water Flow Rate from DAFP to DAFP-T

However, the DAFP-T did initiate the additional cooling water stream to transfer heat from the TESS. This will only happen if the temperature of the cooling water is higher than the temperature of the phase change material and the heat availability is lower than the specified heat requirement.

The effect of the increased flow rates on the cooling water entering the PGEN and ACHX components are compared in Figure 8-11. During the time of increased total flow rates and heat availabilities, the cooling water temperature is reduced when comparing the temperatures for DAFP-T to DAFP.

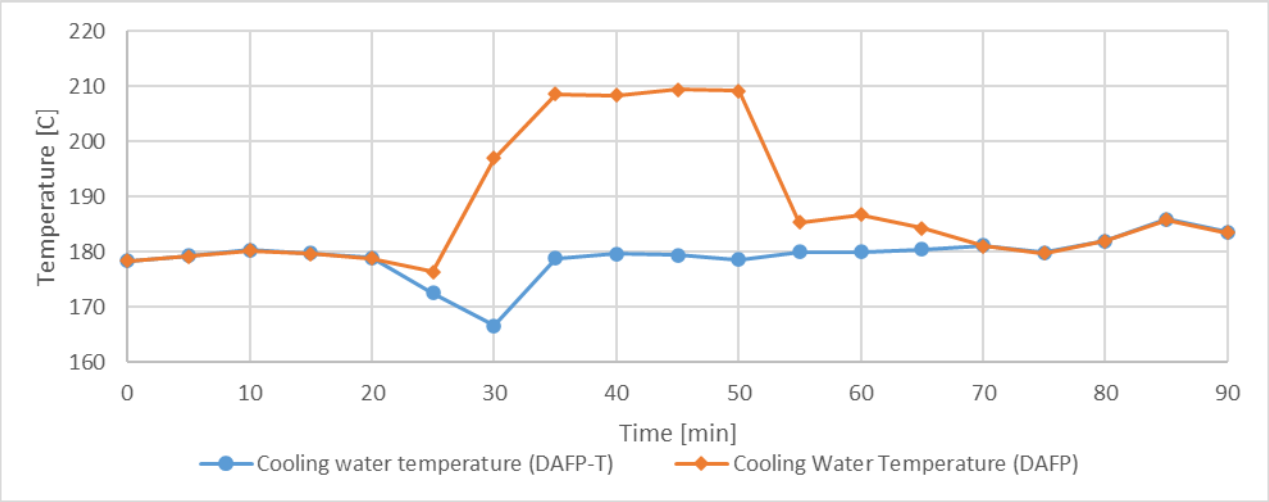


Figure 8-11: Differences in Cooling Water Temperatures T_2^* between DAFP and DAFP-T

8.4.1.2 Nett Power Generation

The main objective of investing in a TESS is to improve power generation at the PGEN, since no other financial benefit can be derived from its inclusion in the system used in this study. The influence of the TESS on the nett power generation is provided in Figure 8-12 along with the TESS capacity levels.

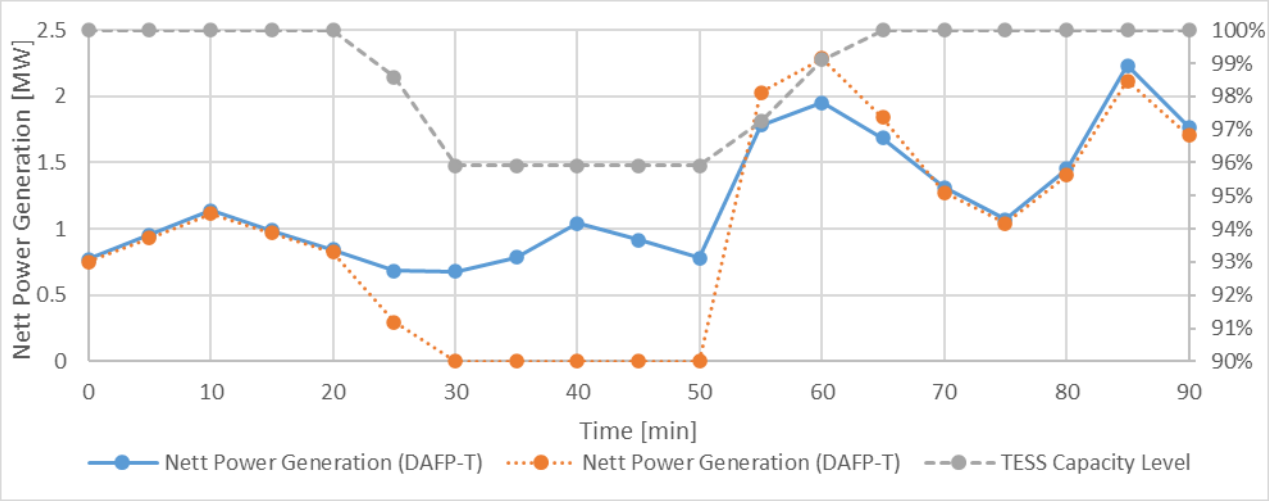


Figure 8-12: Impact of TESS on Nett Power Generation for Demonstrative Dataset

Firstly, as expected, the PGEN did not enter a tripped state due to low heat availability. The higher power generation for DAFP-T for 25–30 min can be attributed to the TESS discharging whereas the rest of the increased power generation from 35–55 min is due to the PGEN remaining operational. At 55–65 min, the power generation reduced. This is due to the charging of the TESS resulting in less energy available in the cooling water.

8.4.1.3 Summary of Demonstrative Dataset Results

The demonstrative dataset has been used from Chapter 5-8 to illustrate the differences in performance between the control philosophies and ensuring that all sub-algorithms operate as required. The table below is a summary of the results between the different philosophies.

Table 8-2: Comparison of DAFP-T, DAFP, DADP and WP on Demonstrative Dataset

Parameter	DAFP-T	DAFP	DADP	WP	Unit
Available Heat in Cooling Water	54 771	53 681	52 567	52 567	MJ
Heat transferred by PGEN	45 972	43 567	40 185	36 566	MJ
% of Total Heat	83.93	81.16	76.43	69.55	%
Average heat transfer rate at PGEN	8.07	7.64	7.05	6.42	MW
Average power generation	1.203	1.028	0.962	0.868	MW
Weighted average η_{th}	14.93	15.12	15.52	15.58	%

The available heat in the cooling water remains constant from WP to DADP, since no cooling water flow rate adjustments were made. The DAFP then adjusted the flow rate such that more heat is available in the cooling water. The DAFP-T then further increased this by transferring heat from the TESS when required to supplement the energy transferred from the flue gas.

This is expected to result in less periods where PGEN is offline and thus result in more heat being transferred to the PGEN with DAFP-T transferring 83.93% of the available heat to the PGEN. The PGEN under DAFP-T also further improved on the average power generation with a value of 1.203 MW. Note that the weighted average thermal efficiency of the system reduced from DAFP to DAFP-T.

8.4.2 Historical Dataset

The previous section illustrated the differences between DAFP-T and DAFP on a demonstrative dataset. The sub-algorithm of TCA prevented a trip of the PGEN in this dataset but since no changes were made to the sub-algorithms of SAAR, SAPR it can be assumed that the reaction of the system to a trip remains consistent with WP. The difference in heat availability, cooling water temperatures and flow rate are observed between the two philosophies.

To evaluate the realistic changes in performance for the heat rejection system, the control philosophy needs to be applied to the signature historical dataset of the plant. The performance of the heat rejection system on the historical dataset is compared in this section.

8.4.2.1 Performance and Operational Parameters on Historical Dataset

The introduction of a TESS to the system is made with the intent of increasing the available heat in the cooling water to prevent PGEN trips due to low heat availability in the short term. Since the

TESS need to be recharged with heat from the cooling water, reductions in available heat to the PGEN and ACHX should also be expected.

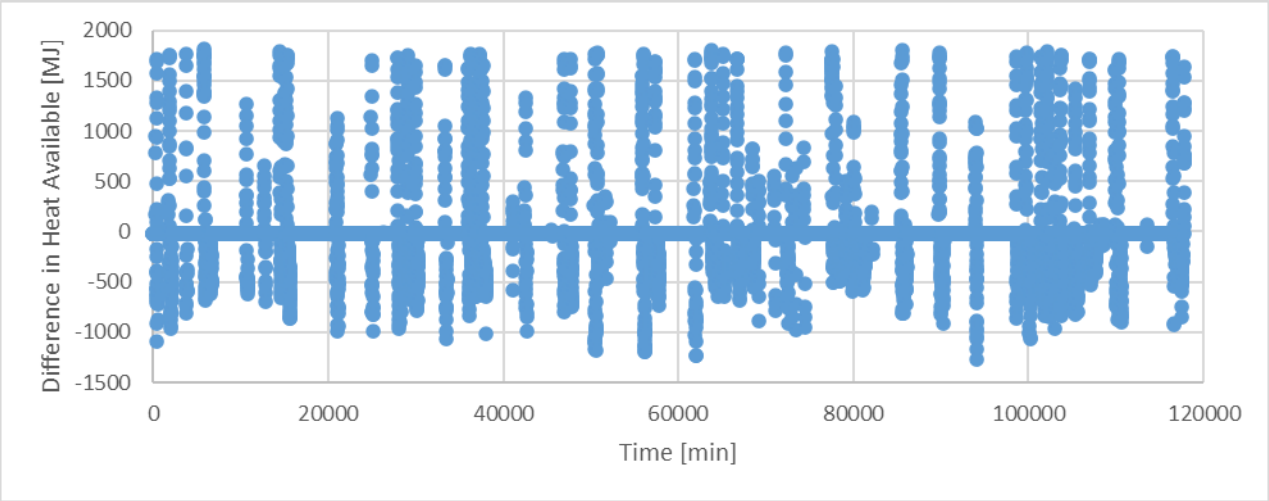


Figure 8-13: Difference in Heat Available in Cooling Water from DAFP to DAFP-T

A representation of the relative changes of the heat availability in the cooling water is provide in Figure 8-13. It can be observed that there are several periods of charging and discharging of the TESS from the difference in heat available. During periods of TESS charging, the difference in heat available in the cooling water is negative.

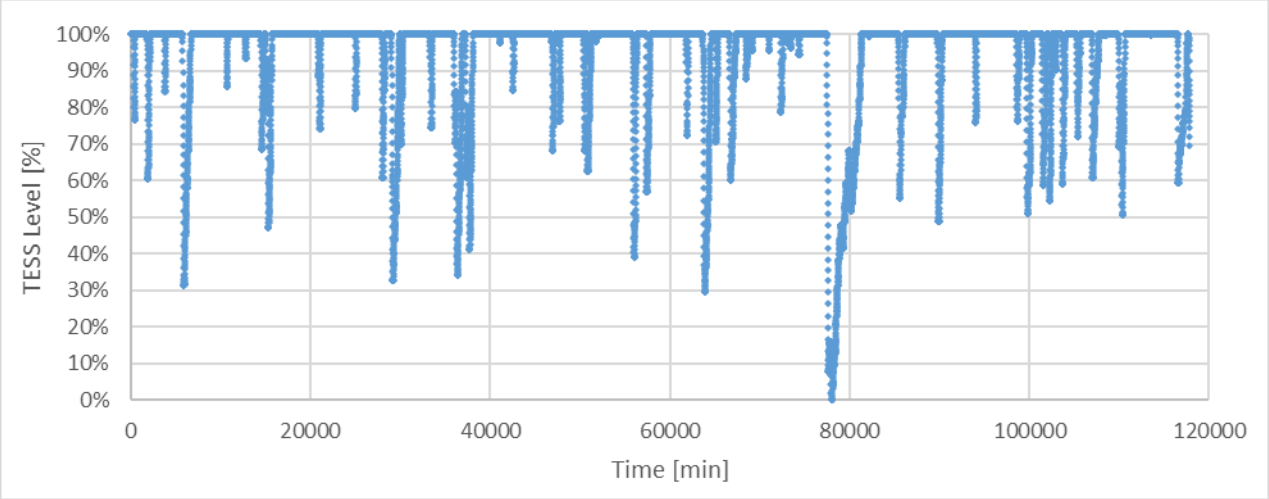


Figure 8-14: TESS Level over Time Horizon of Historical Dataset for DAFP-T

These periods of charging and discharging can also be observed by monitoring the thermal energy level in the TESS. The value of this monitor is illustrated in Figure 8-14. There are several periods where the level reduced to below 60%, however, the TESS is only fully depleted once. The expectation from this observation is that since the minimum required heat in the cooling water is set such that the PGEN operation is sustained, only a single trip due to low heat availability will occur. This will also occur at the same period that the TESS is fully depleted.

Table 8-3: TESS Depletion and Recharging in Historical Dataset

t min	$Q^{2}_{hs,t}$ GJ	ΔQ_{TESS} GJ	$Q^{2*}_{hs,t}$ GJ	$Q_{TESS,t}$ GJ	$Q_{TESS,t}$ %	$W_{PGEN,t}$ MW
77 955	0.38	-1.47	1.85	0.51	0.944	0.685
77 960	0.29	-0.51	0.80	0.00	0.000	0.000
77 965	0.34	0.00	0.34	0.00	0.000	0.000
⋮	⋮	⋮	⋮	⋮	⋮	⋮
78 070	4.10	0.17	3.93	0.17	0.319	1.638
78 075	4.50	0.22	4.28	0.39	0.723	1.768

An extract from the results is provided in Table 8-3. At 77 960 min the TESS is depleted with the last heat transferred to the cooling water being insufficient to maintain the PGEN operation. The PGEN is goes through the restart procedures and at 78 070 min the conditions for a TESS recharging phase are met. There are two PGEN trips observed over the time horizon of the historical dataset. The only other trip observed is the forced trip discussed in Chapter 3.6 which occurs at 38 520 min and has a downtime of 60 min.

As mentioned in the previous section, the purpose of the TESS is to sustain PGEN operation and as such the most important performance parameter to evaluated is the difference in power generation between DAFP and DAFP-T. The difference between the power generation with DAFP and DAFP-T for each period t in the time horizon is provided in Figure 8-15.

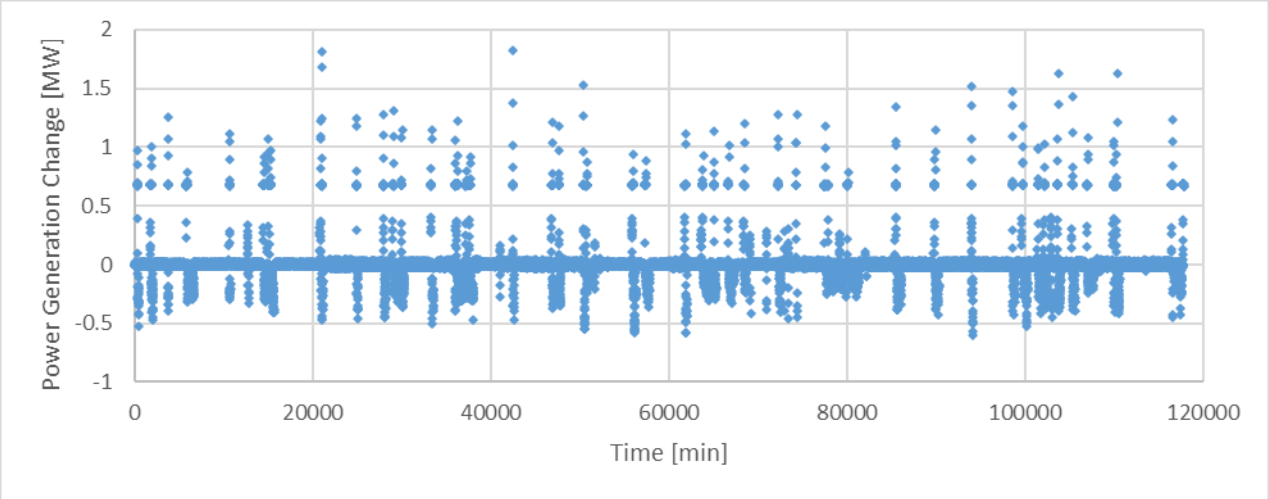


Figure 8-15: Increase in Power Generation from DADP to DAFP

It is noted that for most periods the power generation difference is relatively small. This is expected during times where heat transfer between the cooling water and TESS is also

insignificant. The heat transfer in these periods is to compensate for environmental losses only or a small difference between the available and required heat in the cooling water.

Conversely, there are also periods where significant differences between the power generation performances are noted. The reduction in power generation is observed during periods where the TESS is recharged with energy from the cooling water and there is thus less energy for PGEN considering the operational envelope needs to be maintained. Significant increases in PGEN can be attributed to either discharging of the TESS to meet the minimum heat availability requirement or a result of the PGEN not entering a tripped state and thus not have a constrained restart procedure where no power is generated.

The DAFP-T is shown to only enter a tripped state twice during the time horizon. This is a significant improvement compared to the 51 times for DAFP. The reduction of trip periods and constrained restart procedures can potentially result in improved power generation over the time horizon of the dataset. However, since there are also periods of power generation decreases, it can also be stated that the power generation performance is significantly influenced by the TESS parameters, like those mentioned in Table 8-1.

Changes to the material phase change temperature, capacity and environmental heat loss will influence the potential and rate of energy transfer between the cooling water and TESS. In addition, the required minimum heat availability setpoint used by the TCA also has a significant influence on the eventual performance parameters of the DAFP-T. Thus, evaluation of the combined effects of these parameters needs to be considered before an investment is made to procure a TESS for the current system.

8.4.2.2 Comparison to DAFP

The performance of the DAFP-T will now be compared to the results of the system under DAFP, DADP and WP in the previous chapters. A summary of these results is provided in Table 8-4.

The gas cooler operational envelope is still maintained throughout the time horizon of the historical dataset while the PGEN is in operation for 99.9% of the time. This is longer than for DAFP, DADP and WP. This can be attributed to more heat being transferred to the cooling water when required to sustain PGEN operation. The number of trips reduced from 51 in DAFP to 2 in DAFP-T while the average amount of time between a trip and completion of a restart procedure reduced from 114 min for DAFP to 78 min for DAFP-T. Note that one of these trips are the forced trip at 38 520 min with a forced downtime of 60 min.

Table 8-4: Comparison of Performance between DAFP-T, DAFP, DADP and WP

Parameter	DAFP-T	DAFP	DADP	WP	Unit
Time $\overline{T_5} < 150\,℃$	0	0	0	0	min
Minimum $\overline{T_5}$	150	150	150	150	℃
Maximum $\overline{T_5}$	185.74	185.74	185.74	185.74	℃
% of time PGEN is in operation	99.9	96.2	95.9	95.9	%
Heat transferred by Gas Cooler	88 422.8	88 238.2	81 914.9	81 914.9	GJ
% of Total Heat in Flue Gas	99.57	99.36	92.24	92.24	%
Heat transferred by PGEN	77 163.99	76 687.30	70 107.61	60 889.85	GJ
% of Total Heat	87.267	86.909	85.586	74.333	%
Average heat transfer rate at PGEN	10.913	10.846	9.916	8.612	MW
Average power generation	1.629	1.615	1.485	1.231	MW
Weighted average η_{th}	14.95	14.96	15.06	14.39	%
Energy Recovery Efficiency	12.96	12.38	11.34	9.40	%

The decrease in PGEN trips resulted in the CWFR-T being able to maximise energy transfer in the gas cooler for a larger portion of the time horizon, transferring 99.57% of the available heat in the flue gas to the cooling water.

The average heat transfer rate at the evaporator of the PGEN increased from 10.846 MW under DAFP to 10.913 MW. This resulted in an increase of 0.87% on the average power generation, increasing from 1.615 MW to 1.629 MW over the time horizon. The weighted thermal efficiency of the PGEN increased from 14.96% to 14.95%. It follows that the cooling water flow rate in the system is adjusted to generate more power, thus successfully meeting the objective of the DAFP.

The energy recovery efficiency resulted in a value of 12.96%, increasing from a value of 12.38%. This indicates that the eventual power generation from the system is 12.96% of the available energy in the flue gas.

8.5 Conclusion

This chapter illustrated the formulation and performance of the DAFP-T on a historical dataset. The first section of the chapter provided a summary of the change in approach required to improve on the performance of DAFP by adding an additional component in the form of a TESS. For the case study in this chapter, suitable TESS parameters are assumed from literature and provided.

A sub-algorithm that controls the TESS, TCA, is formulated in the second section of this chapter. The TCA controls the heat available in the cooling water entering the PGEN and ACHX based on

a specified minimum. The TCA can also initiate an additional cooling water stream from the circulation pumps of the system in a scenario where there is insufficient heat, but the current cooling water temperature is too high to expect heat transfer from the TESS. The TCA is also in control of the charging and discharging of the TESS based on cooling water parameters at time t. The TCA is formulated and illustrated on the demonstrative dataset.

It is noted in the demonstration that changes are also required to the CWFR to consider the addition of a TESS. The CWFR is adjusted to also determine whether there is more than the specified heat requirement in the flue gas. If so, then the allowable flow range provided to DAFP-T is adjusted to ensure that only ranges where the heat requirement is sufficient is considered. The updated algorithm is referred to as CWFR-T.

The Discrete Adjustment to Flow Philosophy with an integrated TESS is then formulated. The DAFP-T uses the above sub-algorithms to firstly determine the allowable cooling water flow rate and the required heat transfer between the TESS and cooling water. The DAFP-T then still uses the modified bisection method of DAFP to determine the flow rate that will deliver the maximum power generation. No changes other than the addition of TCA and the changes from CWFR to CWFR-T are made to DAFP in the process of formulating DAFP-T.

A summary of the evolution from DADP to DAFP is provided in the figure below.

In summary, the WP aimed to maximise power generation with the assigned cooling water flow by adjusting the evaporating pressure and degree of superheat in the PGEN. The assigned cooling water flow is based on a fixed distribution ratio. The DADP then improved on this power generation by adjusting the flow of cooling water distributed to the PGEN. The DAFP provided further improvement by using the operational status of the PGEN and a gas cooler model to maximise power generation or minimise power consumption. The DAFP-T further improved on this performance by dampening the effect of a fluctuating heat source by storing excess thermal energy in a TESS for use during low heat availability.

The DAFP-T approach on the historical dataset resulted in a PGEN that is operational 99.9% of the time, transferring 87.27% of the available heat from the cooling water, an increase from 86.91% under DAFP. The average power generation for the PGEN is determined to be 1.629 MW, an increase of 0.014 MW compared to 1.615 MW under DAFP. The DAFP-T also resulted in a weighted thermal efficiency of 14.95%. The energy recovery ratio for DAFP-T is determined to be 12.96%, which also increased from 12.38% under DAFP.

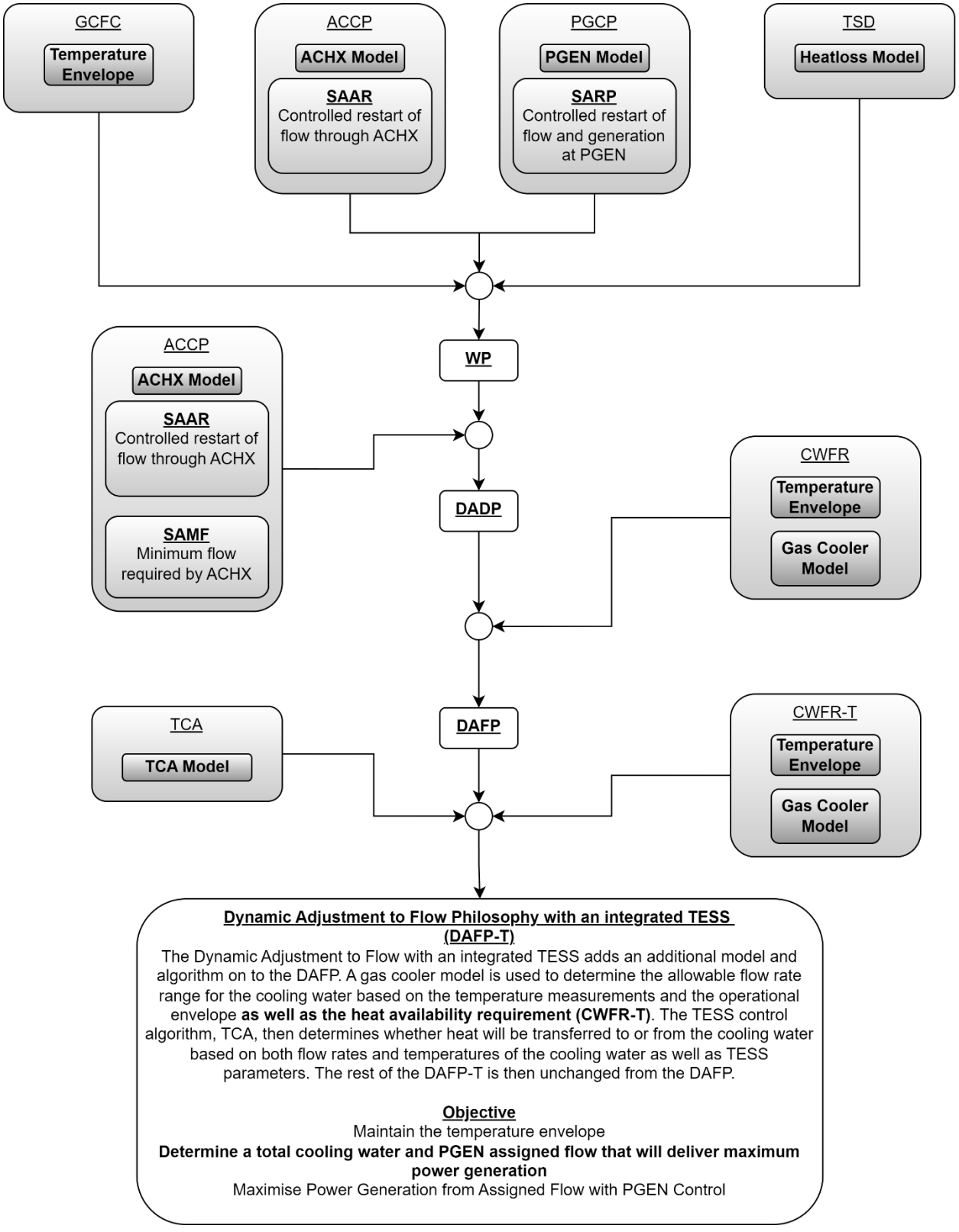


Figure 8-16: Summary of DAFP-T after Conclusion of Chapter 8.

The number of trips the PGEN experiences reduced from 51 to 2 with the time between a trip and restart also reducing from 114 min to 78 min with DAFP-T. This is due to the TCA increasing the available heat in the cooling water by transferring heat when required. Note that one of the trips

is forced, as mentioned in earlier chapters while the other trip occurred when the TESS is empty and could not transfer any heat to meet the desired heat availability.

The DAFP-T can thus be applied to a historical dataset to accurately evaluate the impact of a TESS will have on system performance, with a parametric study possible with different TESS parameters. The performance influences can also be weighed against investment requirements.

CHAPTER 9 SUMMARY AND CONCLUSION

The need for a control formulation that manages the operation of a combined power generation and air-cooled heat exchanger system is identified and addressed in this study. The frameworks are simulated in a fluctuating heat source environment with the additional need to maintain an operational envelope. Several control philosophies exist in literature, however, either design conditions or averaging of the heat source is used. Nowhere in literature could it be found that a control philosophy is formulated to control both a power generation and a cooling system in parallel, with a fluctuating heat source, with the aim of maximising power generation while also maintaining an operational envelope. By achieving it in this study, maximum power generation can now be achieved for a specific plant under its own signature heat source profile with its own power generation and cooling system design parameters.

The trip and restart procedures of the power generation and air-cooled heat exchangers are simulated along with expected heat loss from the system and from this a desired cooling water flow distribution between the two components are determined every period. This maximises power generation from the energy the cooling water absorbed in the gas cooler. The energy transferred to cooling water can then adjusted depending on the status of the power generation system, which further improves the nett power generation every period. From this, the impact of a thermal energy storage system can also be incorporated with the aim of reducing the fluctuations of available heat to the combined power generation and cooling system.

To achieve maximum power generation a comprehensive understanding into the engineering operations is required. This includes all applicable processes and laws of physics that underpin the fundamental operational principles of equipment that form part of the power generation process. An understanding of these processes and their scientific foundations is crucial for the logical reasoning process, both during the formulation process and the calculation of the fixed setpoints and input parameters.

This thesis proposed novel control philosophy formulations that address the need for maximum nett power generation in an energy recovery system that has a fluctuating heat source environment. All the contributions can accommodate any type of heat source, power generation system or cooling equipment. Furthermore, this equipment can also be of any capacity or efficiency.

The operational responses of all the contributions were demonstrated to evaluate the impact of the distinct differences between them. This is done by solving each contribution on real-world data, obtained from a metal production plant.

9.1 Chapter Summaries

Chapter 2 provides a discussion on the basic engineering definitions and theories required in formulating control philosophies. Several known control philosophies and approaches were also discussed in depth to not only identify the addressed gap in literature, but also to identify potential additions to the formulations made in the chapters to follow.

Chapter 3 provides the information on the heat rejection system used in this study. The gas cooler, PGEN and ACHX have inherent design limitations. The models used to simulate the gas cooler, ACHX and PGEN as well as the heat loss from uninsulated components are provided in this chapter. The gas cooler section also includes the fluctuating heat source profile along with the operational temperature envelope of both the flue gas and cooling water. The profile is represented with a dataset that provides average values for mass flows and temperatures and thus the total heat available and transferred can be determined.

Chapter 4 then uses the models from the previous chapter along with control requirements to formulate the control philosophies of the cooling water flow rate (CWFC), the PGEN internal operations (PGCP), the ACHX operational control (ACCP) as well as a variable setpoint determination philosophy (TSD). The CWFC is the current philosophy used to control the cooling water flow rate through the gas cooler with adjustments based on flue gas exit temperatures. The PGCP evaluates the incoming cooling water flow rate and temperature and adjusts the evaporating pressure and degree of superheat to ensure maximum power generation is achieved. The ACCP determines the minimum number of fans and the required operational speeds to achieve the desired temperature setpoint that is distributed to the ACHX. The ACCP also determines the heat loss from the cooling water should no fan be operational. The TSD uses the natural convection and radiative losses of uninsulated components in the system to determine a setpoint for the cooling water at the junction of the outflows from the PGEN and ACHX branches.

Chapter 5 provides the formulation of the current Works Philosophy (WP). The chapter first provides sub-algorithms that are used to maintain the operations of the PGEN and ACHX during low heat availability periods. The SAPR ensures that the philosophy simulation includes a realistic restart procedure for the PGEN after a trip occurrence, including a time delay as well as period of fixed heat transfer requirements before power generation can be initiated. The SAAR ensures that the ACHX bypasses all flow when heat transfer from the cooling water need to be minimised. The SAAR then also monitors the internal temperature of the ACHX and ensures that the restart of flow through the ACHX is controlled in such a way that the operational envelope is maintained.

WP then uses all the models, sub-algorithms and philosophies provided up to this point to demonstrate the current Works philosophy. Note that the use of PGCP and ACCP ensures maximum nett power generation is achieved for a specific flow distribution. The current Works

Philosophy is to operate the PGEN and ACHX as independent processes where the cooling water flow is distributed at a fixed ratio between them. The setpoint temperature of the PGEN and ACHX is also determined independently, ensuring that the water exiting the PGEN and ACHX is always within the operational envelope.

The WP approach on the historical dataset resulted in a PGEN that is operational 95.9% of the time, transferring 92.24% of the available heat from the flue gas and then also only transferring 74.33% of the available heat to the PGEN heat exchanger. The average power generation for the PGEN is determined to be 1.231 MW with a weighted thermal efficiency of 14.39%. The energy recovery ratio, defined as the ratio of power generated to energy available in the flue gas, is also determined to be 9.40%.

The final section of this chapter re-evaluated WP with different flow distribution ratios. It is observed that a higher flow to the PGEN results in higher power generation when the setpoint temperature of both the PGEN and ACHX is set to be the same. There is thus potential for improvement of the power generation performance of the system without negatively impacting the operational envelope.

In the first section of Chapter 6, a case study is shown for the off-design operation of the PGEN. In this chapter, a novel formulation, Discrete Adjustment of Distribution Philosophy (DADP), is provided that improves on the WP. This is achieved by determining the allowable flow range to the PGEN based on ACHX performance and then implementing a modified bisection method to determine the flow distribution that will result in maximum power generation. Thus, this approach maximises nett power generation with the combined use of the PGCP, ACCP and a variable flow distribution between the two components.

The DADP approach on the historical dataset resulted in a PGEN that is operational for 95.9% of the time and increasing the energy transferred from the cooling water to 85.59%. The average power generation for the PGEN with this increased energy distribution also increased to 1.485 MW with a weighted thermal efficiency of 15.05%. The DADP philosophy does not adjust the cooling water flow rate through the gas cooler and as such the amount of heat available in the cooling water is still 81 914.9 GJ over the time horizon of the dataset. This is 92.24% of the heat available in the flue gas. However, with the increased power generation the energy recovery ratio increased from 9.40% to 11.34%. Note that due to no change in the total cooling water flow in the system, the energy transferred from the flue gas is still only 92.24% of the available energy. It is noted that the energy transferred from the flue gas can potentially be improved.

In the first section of Chapter 7, approach changes to DADP are discussed such than improvement on the DADP can be made with the Discrete Adjustment to Flow Philosophy (DAFP). The approach changes include adjusting the cooling water flow rate to increase or decrease the

energy recovered from the flue gas. The decision to increase or decrease the energy recovered is based on whether the PGEN is operational. To simulate the energy recovered, a gas cooler model is introduced along with an additional sub-algorithm that determines the allowable cooling water flow rate range that will ensure the operational envelope is maintained (CWFR). The DAFP then uses a modified bisection algorithm to determine the ideal cooling water flow rate in this range. The approach to the desired flow distribution between the two components are still followed. Thus, this approach maximises nett power generation with the combined use of the CWFR to adjust energy recovery from the flue gas and then PGCP, ACCP, and a variable flow distribution between the two components.

The DAFP approach on the historical dataset resulted in an adjusted cooling water flow rate that transferred 88 238.2 GJ of energy from the flue gas, which is 99.36% of the available energy therein. The difference of energy is that during times the PGEN is non-operational. The CWFR will also reduce the cooling water flow rate and thus energy transferred. This increase in available heat in the cooling water resulted in a PGEN that is operational 96.2% of the time, increasing the energy transferred from the cooling water to 76 687.3 GJ. This resulted in a power generation performance at an average of 1.615 MW with a weighted thermal efficiency of 14.96%. The increased power generation and heat transfer from the flue gas resulted in an increased value for the energy recovery ratio of 12.38%. It is noted that even with DAFP maximising energy transfer from the flue gas with an operational PGEN, the PGEN still experienced 51 trips due to low heat availability in the cooling water.

In Chapter 8 the DAFP is modified to include a thermal energy storage system (TESS). This philosophy is referred to as DAFP-T. The purpose of the TESS is to dampen the effect of the fluctuating heat source on the PGEN operational status. In this chapter, an additional sub-algorithm, TCA, is introduced that simulates whether heat is transferred to or from the TESS and update the cooling water temperature and flow rates accordingly. The TCA is controlled around a setpoint requirement of energy for the cooling water entering the PGEN and ACHX section in the system. The CWFR, formulated in the previous chapter, is also modified to determine whether the TESS has sufficient energy to keep the PGEN operational (CWFR-T). From here, the approach in DAFP is applied as is to maximise power generation.

After simulating the historical dataset with DAFP-T, it is noted that the TESS is only fully depleted once. A depleted TESS also resulted in a tripped PGEN. The TESS had sufficient energy and is controlled by TCA such that the PGEN is operational 99.9% of the time. This increase in operational time also resulted in CWFR-T transferring more heat from the flue gas, a total of 88 422.8 GJ which is 99.57% of the available heat for the time horizon. It is noted that during times that the TCA recharged the TESS, less heat is transferred to the PGEN and as such reduced power generation. However, over the time horizon 77 163.99% of heat is transferred to the PGEN.

This is to an average power generation of 1.629 MW, resulting in a weighted thermal efficiency of 14.95%. The increased power generation and heat transfer from the flue gas resulted in an increased value for the energy recovery ratio of 12.96%.

The formulations provided in this study are successful in transferring the waste heat from the flue gas to the cooling water and then distributing the waste heat in the cooling water between air-cooled heat exchangers and power generation components in such a way that maximises energy recovery while still adhering to all process constraints.

The novel formulations can be applied to similar systems with adjustments to the power generation, cooling, TESS, heat source and heat loss components. These formulations are thus not only useable for operational improvements but also for the analysis of future investment opportunities where new equipment with different capacities, internal control parameters and efficiencies can be used.

9.2 Future research

This thesis provides novel control formulations for maximising the power generation in a heat rejection system with a fluctuating heat source while also ensuring the operational envelope for both flue gas and cooling water is maintained. Some further research from this thesis is proposed:

- The gas cooler model in this thesis is based on published literature. A higher fidelity model of the gas cooler needs to be formulated. An improved gas cooler model also needs to consider the fouling of heat transfer surfaces. Such a model can then be used to improve on the accuracy of power generation predictions as well as the potential impact of adjustments to maintenance routines.
- An improvement on the TCA can potentially be made where the cooling water heat setpoint can become a variable. The TCA can adjust this setpoint based on either the current energy content in the TESS, predictive energy content of cooling water leaving the gas cooler in the near future, or a combination of both.
- The control formulations use PGCP to control the PGEN, which consisted of one power generation system throughout the thesis. Adjustments can be made to PGCP to accommodate several individual power generation processes, allowing for a cascaded approach of different capacities to ensure some power is generated during low heat availability conditions. With this approach the PGCP would, in addition to determining the evaporation pressure and degree of superheat, also determine the ideal distribution of cooling water flow between the different power generation components.
- The addition of a TESS is modelled in this thesis. It is noted that different sizes, temperatures and heat requirement setpoints would significantly impact the performance of the nett power generation. Changes to the phase change temperatures would result in

the need use a different phase change material. All these parameters would this impact the investment required to integrate a TESS. An investment study is needed to determine the ideal sizes, temperature and setpoint of the TESS for the Work's signature waste heat profile.

- From the two proposals mentioned above, an optimal investment model is required to iterate through an array of potential TESS and PGEN combinations. These combinations should include different capacities and efficiencies. The formulation will need to determine the exact number of PGEN and TESS design parameters to maximise both power generation and nett present value.
- The current ACCP sub-model determines the number of fans, and their operational speeds required to reach the desired setpoint temperature for the cooling water. Increasing the fidelity of the ACHX component such as being able to assign individual fouling and design parameters to each heat exchanger and fan combination in the ACHX. The control formulation can then ensure that maximum heat transfer for the minimum power input to the fan by identifying the specific fan that needs to be operational and the required speed. Based on this, the modification of individual fans can also be investigated to adjust the range of operation for the ACHX.

BIBLIOGRAPHY

[1] R. Gupta, “Chapter 4.2 - Energy Resources, Its Role and Use in Metallurgical Industries,” in *Volume 3: Treatise on Process Metallurgy, Industrial Processes, Part A*, Elsevier, 2014, pp. 1425-1458.

[2] L. Zeelie, J. Marais and W. Breytenbach, “Reduction in blast furnace operational costs through optimisation of auxiliary systems,” in *2018 International Conference on the Industrial and Commercial Use of Energy (ICUE)*, 2018.

[3] H. Jalkanen and L. Holappa, “Chapter 1.4 - Converter Steelmaking,” in *Volume 3: Treatise on Process Metallurgy, Industrial Processes, Part A*, Elsevier, 2014, pp. 223-270.

[4] B. Wang, J.-A. Zhou, J.-B. Xie, Z.-Q. Liu, H. Zhang and L.-H. Zhou, “Numerical and Experimental Investigations of Converter Gas Improvement inside a Flue Using Its Waste Heat and CO2 by Pulverized Coal Injection,” *Environmental Progress & Sustainable Energy,* vol. 37, no. 4, pp. 1503-1512, 2018.

[5] E. Hajidavalloom, M. Rezaei and A. Mombeni, “Simulation of flow and heat transfer in the duct elbow of an electric arc furnace,” *Heat and Mass Transfer,* vol. 56, pp. 2171-2184, 2020.

[6] V. B. Hemadri and P. Subbarao, “Thermal integration of reheated organic Rankince cycle (RH-ORC) with gas turbine exhaust for maximum power recovery,” *Thermal Science and Engineering Progress,* no. 23, 2021.

[7] U.S. Department of Energy, “Waste Heat Recovery: Technology and Opportunities in U.S. Industry,” BCS, Incorporated, 2008.

[8] S. Lecompte, O. Oyewunmi, C. Markides, M. Lazova, A. Kaya, M. van den Broek and M. De Paepe, “Case Study of an Organic Rankine Cycle (ORC) for Waste Heat Recovery from an Electric Arc Furnace,” *energies,* vol. 10(5), no. 649, 2017.

[9] F. P. Incropera, D. P. DeWitt, T. L. Bergman and A. S. Lavine, Fundamentals of Heat and Mass Transfer, John Wiley & Sons, 2007.

[10] A. Inayat, “Current progress of process integration for waste heat recovery in steel and iron industries,” *Fuel,* vol. 338, 2023.

[11] T. Sung, E. Yun, H. Kim, S. Yoon, B. Choi, K. Kim, J. Kim, Y. Jung and K. Kim, “Performance characteristics of a 200-kW organic Rankine cycle system in a steel processing plant,” *Applied Energy,* no. 183, pp. 623-635, 2016.

[12] Y. A. Cengel and A. J. Ghajar, Heat and Mass Transfer: Fundamentals & Applications, New York: McGraw-Hill, 2015.

[13] Z. Miao, P. Yan, M. Xiao, M. Zhang and J. Xu, “Comparative study on operating strategies of the organic Rankine cycle under transient heat source,” *Energy,* no. 285, 2023.

[14] S. Ata, A. Kahraman and R. Sahin, “Thermal efficiency evaluation of an organic Rankine cycle with n-pentane as working fluid,” *International Journal of Energy Applications and Technologies,* vol. 2, no. 6, pp. 31-38, 2019.

[15] H. Tian and G. Shu, “Organic Rankine Cycle systems for large-scale waste heat recovery to produce electricity,” *Organic Rankine Cycle (ORC) Power Systems,* pp. 613-636, 2017.

[16] D. Hu, Y. Zheng, Y. Wu, S. Li and Y. Dai, “Off-design performance comparison of an organic Rankine cycle under different control strategies,” *Applied Energy,* no. 156, pp. 268-279, 2015.

[17] B. van Rooyen, Performance and fouling prediction model for finned-tube heat exchangers, Potchefstroom: North-West University, 2019.

[18] T. Gao, B. Sammakia and J. Geer, “Dynamic response and control analysis of cross flow heat exchangers under variable temperature and flow rate conditions,” *International Journal of Heat and Mass Transfer,* no. 81, pp. 542-553, 2015.

[19] Y.-q. Feng, F.-y. Zhang, J.-w. Xu, Z.-x. He, Q. Zhang and K.-j. Xu, “Parametric analysis and multi-objective optimization of biomass-fired organic Rankine cycle system combined heat and power under three operation strategies,” *Renewable Energy,* no. 208, pp. 431-449, 2023.

[20] W. Abbas and J. Vrabec, “Cascaded dual-loop organic Rankine cycle with alkanes and low global warming potential refrigerants as working fluids,” *Energy Conversion and Management,* vol. 249, no. 114843, 2021.

[21] A. Guercio and R. Bini, “Biomass-fired Organic Rankine Cycle combined heat and power systems,” in *Organic Rankine Cycle (ORC) Power Systems*, 2017, pp. 527-567.

[22] J. P. Bester, M. van Eldik and P. v. Z. Venter, “Energy Recovery Maximisation Modelling Subject to Constrained Cooling,” *energies,* vol. 17, no. 1, 2024.

[23] C. Borgnakke and R. E. Sonntag, Fundamentals of Thermodynamics, John Wiley and Sons, Inc., 2009.

[24] P. Rousseau, *Thermal-Fluid Systems Modelling [Course Notes],* Potchefstroom: Faculty of Engineering, North-West University, 2013.

[25] P. Venter, *Investment and operational optimisation of an energy recovery engineering plant,* Potchefstroom: North-West University, 2018.

[26] Y. A. Cengel, Heat Transfer: A Practical Approach, McGraw-Hill, 2002.

[27] H. Oertel, Kinematics of Fluid Flow, New York: Springer, 2009.

[28] A. R. Simpson, M. Asce and A. Marchi, “Evaluating the Approximation of the Affinity Laws and IMproving the Efficiency Estimate for Variable Speed Pumps,” *Journal of Hydraulic Engineering,* pp. 1314-1318, 2013.

[29] R. Saidur, S. Mekhilef, M. Ali, A. Safari and H. Mohammed, “Applications of variable speed drive (VSD) in electrical motors energy savings,” *Renewable and Sustainable Energy Reviews,* no. 16, pp. 543-550, 2012.

[30] K. S. Mohamed and H. A. Ashour, “Study of cooling tower system energy saving opportunities within steel production factory,” in *22nd Internation Middle East Power Systems Conference*, Assiut University, Eqypt, 2021.

[31] N. Kumar, P. Besuner, S. Lefton, D. Agan and D. Hilleman, “Power Plant Cycling Costs,” National Renewable Energy Laboratory, California, 2012.

[32] D. Peterson, “Learn about the different types of electrical and mechanical soft-start methods as well as devices to use for each method,” Control Automation, 02 April 2021. [Online]. Available: https://control.com/technical-articles/comparing-electrical-and-mechanical-motor-soft-start-methods/. [Accessed 24 June 2022].

[33] T. Erhart, Improvement of heat-led CHPs based upon ORC-technology, Glasgow: University of Strathclyde , 2015.

[34] R. Zhao, H. Zhang, S. Song, Y. Tian, Y. Yang and Y. Liu, “Integrated simulation and control strategy of the diesel engine–organic Rankine cycle (ORC) combined system,” *Energy Conversion and Management,* vol. 156, pp. 639-654, 2018.

[35] M. Trafczynski, M. Markowski and K. Urbaniec, “Energy saving potential of a simple control strategy for heat exchanger network operation under fouling conditions,” *Renewable and Sustainable Energy Reviews,* no. 111, pp. 355-364, 2019.

[36] A. Vasičkaninová, M. Bakošová and A. Mészáros, “Fuzzy Control Design for Energy Efficient Heat Exchanger Network,” *Chemical Engineering Transactions,* vol. 88, pp. 529-534, 2021.

[37] S. Faghih and A. Pourshaghaghy, “Selecting working fluids in organic Rankine cycle (ORC) for waste heat applications and optimal cycle parameters for different hot source temperatures,” *Journal of Thermal Analysis and Calorimetry,* 2022.

[38] X. Wang, R. Wang, M. Jin, G. Shu, H. Tian and J. Pan, “Control of superheat of organic Rankine cycle under transient heat source based on deep reinforcement learning,” *Applied Energy,* vol. 278, 2020.

[39] B. Xu and X. Li, “A Q-learning based transient power optimization method for organic Rankine cycle waste heat recovery system in heavy duty diesel engine applications,” *Applied Energy,* vol. 286, 2021.

[40] J. Zhang, Y. Zhou, R. Wang, J. Xu and F. Fang, “Modeling and constrained multivariable predictive control for ORC based waste heat energy conversion systems,” *Energy,* vol. 66, pp. 128-138, 2014.

[41] X. Li, B. Xu, H. Tian and G. Shu, “Towards a novel holistic design of organic Rankine cycle (ORC) systems operating under heat source fluctuations and intermittency,” *Renewable and Sustainable Energy Reviews,* vol. 147, 2021.

[42] J. Chowdhury, D. Thornhill, P. Soulatiantork, Y. Hu, N. Balta-Ozkan, L. Varga and B. K. Nguyen, “Control of Supercritical Organic Rankine Cycle based Waste Heat Recovery System using Conventional and Fuzzy Self-tuned PID Controllers,” *International Journal of Control, Automation and Systems,* vol. 17, no. 11, pp. 2969-2981, 2019.

[43] J. Zhang, Y. Li, Z. Wang and G. Hou, “Dynamic Characteristics and Predictive Control for Organic Rankine Cycle,” *7th IEEE Conference on Industrial Electronics and Applications (ICIEA),* pp. 281-284, 2012.

[44] J. Zhang, S. Gao, Y. Chen and G. Hou, “Multivariable robust control for organic rankine cycle based waste heat recovery systems,” IEEE, Beijing, 2013.

[45] G. Fan, Y. Du, H. Li and Y. Dai, “Off-design behavior investigation of the combined supercritical CO2 and organic Rankine cycle,” *Energy,* vol. 237, pp. 1215-1229, 2021.

[46] F. Dal Magro, Energy recovery systems based on high temperature phase change materials, Udine: University of Udine, 2017.

[47] M. Gelfi, A. Pola, R. Roberti, L. Vecchia and E. Galili, “Failure analysis of an electric arc furnace off-gas system,” *Engineering Failure Analysis,* no. 25, pp. 42-48, 2012.

[48] R. Khadem Hosseini and S. Yareiee, “Failure analysis of boiler tube at a petrochemical plant,” *Engineering Failure Analysis,* 2019.

[49] E. Hahne and D. Zhu, “Natural convection heat transfer on finned tubes in air,” *International Journal of Heat and Mass Transfer,* vol. 37, pp. 59-63, 1994.

[50] J. Song, C. Gu and X. Ren, “Parametric design and off-design analysis of organic Rankine cycle (ORC) system,” *Energy Conversion and Management,* no. 112, pp. 157-165, 2016.

[51] F. Calise, C. Capuozzo, A. Carotenuto and L. Vanoli, “Thermoeconomic analysis and off-design performance of an organic Rankine cycle powered by medium-temperature heat sources,” *Solar Energy,* vol. 103, pp. 595-609, 2014.

[52] M. Rezaei, M. Sameti and F. Nasiri, “An enviro-economic RAM-based optimization of biomass-driven combined heat and power generation,” *Biomass Conversion and Biorefinery,* 2023.

[53] D. Cocco, L. Migliari and F. Serra, “Influence of thermal energy losses on the yearly performance of medium size CSP plants,” in *The 28th Internation Conference on Efficiency, Cost, Optimization, Simulation and Environmental Impact of Energy Systems*, Pau, France, 2015.

[54] M. R. M. Ali, M. I. Fakhri, N. Hayati and N. A. Ramli, “The n-th section method: A modification of Bisection,” *Malaysian Journal of Fundamental and Applied Sciences,* vol. 13, no. 4, pp. 728-731, 2017.

[55] H. Ayaz, V. Chinnasamy, J. Yong and H. Cho, “Review of Technologies and Recent Advances in Low-Temperature Sorption Thermal Storage Systems,” *energies,* vol. 14, no. 6052, 2024.

[56] C. Prieto, P. D. Tagle-Salazar, D. Patino, J. Schallenburg-Rodriguez, P. Lyons and L. F. Cabeza, “Use of molten salts tanks for seasonal thermal energy storage for high penetration of renewable energies in the grid,” *Journal of Energy Storage,* vol. 86, no. 111203, 2024.

APPENDIX A – ACHX PERFORMANCE PREDICTION MODEL

The modelling approach outlined in [17] is used to formulate a mathematical model that will predict the performance of the ACHX given the cooling water temperature and flow rate with a controlled air mass flow rate.

The approach consists of 7 steps and is based on the explicit UA method as referenced from [9]. The overall heat transfer coefficient, $\mathrm{UA}\ \left[\frac{\mathrm{W}}{\mathrm{K}}\right]$, is given below in equation (A.1) with an indication of the first 6 steps.

$$\mathrm{UA} = \frac{1}{\left(\mathrm{h_w} \cdot \frac{\mathrm{A_{w_{total}}}}{\mathrm{A_{a_{total}}}}\right)^{-1} + \left(\mathrm{R_t} \cdot \mathrm{A_{a_{total}}}\right) + \left(\eta_\mathrm{o} \cdot \mathrm{h_a}\right)^{-1}} \tag{A.1}$$

Step 1: Water-side heat transfer area, denoted as $\mathrm{A_{w_{total}}}[\mathrm{m}]$

Step 2: Air-side heat transfer area, denoted as $\mathrm{A_{a_{total}}}[\mathrm{m}]$

Step 3: The unfouled total conductive resistance, denoted as $\mathrm{R_t}\left[\frac{\mathrm{K}}{\mathrm{W}}\right]$

Step 4: Cooling water convective heat transfer coefficient, denoted as $\mathrm{h_w}\left[\frac{\mathrm{Wm^2}}{\mathrm{K}}\right]$

Step 5: Air side convective heat transfer coefficient, denoted as $\mathrm{h_a}\left[\frac{\mathrm{Wm^2}}{\mathrm{K}}\right]$

Step 6: System overall heat transfer efficiency, denoted as $\eta_\mathrm{o}\ -$

Step 1: Water-side heat transfer area

In this step, the total heat transfer area exposed to the cooling water is determined through equation (A.2). This area is a function of the inner tube diameter,$\mathrm{ID_{tube}}\ \mathrm{m}$, the total length of the tube, $\mathrm{L_{tube}}$, and the number of tubes, denoted by $\mathrm{N_{tubes}}$.

$$\mathrm{A_{c_{total}}} = \pi \cdot \mathrm{ID_{tubes}} \cdot \mathrm{L_{tube}} \cdot \mathrm{N_{tubes}} \tag{A.2}$$

Step 2: Air-side heat transfer area

The air-side heat transfer coefficient is typically 10-100 times less than the water-side convection coefficient [17]. Extended surfaces in the form of fins are introduced to overcome this problem by significantly increasing the air-side heat transfer area.

The air-side heat transfer area has already been used provided earlier in the thesis through equation (3.9) to (3.12). These equations are restated through equation (A.3) below.

$$\mathrm{A} = \mathrm{A_{tube,exposed}} + \mathrm{A_{fin}} \tag{A.3}$$

$$A_{tube,exposed} = L_{tube,exposed} \cdot \pi \cdot (OD_{tube}) \cdot N_{tubes} \quad \text{(A.3.1)}$$

$$L_{tube,exposed} = L_{tube} - (\rho_{fin} \cdot L_{tube} \cdot t_{fin}) \quad \text{(A.3.2)}$$

$$A_{fin} = L_{tube} \cdot \rho_{fin} \cdot N_{tubes} \cdot t_{fin} + 2\pi \cdot (r_{fin}^2 - r_{tube}^2) \quad \text{(A.3.3)}$$

Step 3: Unfouled total conductive resistance

The unfouled conductive resistance of the tube bundle is determined from equation (A.4).

$$R_t = \frac{\ln\left(\frac{OD_{tube}}{ID_{tube}}\right)}{2 \cdot \pi \cdot L_{tube} \cdot N_{tubes} \cdot k_{tube}} \quad \text{(A.4)}$$

In equation (A.4), all parameters have been declared in earlier steps except for the outer diameter, $OD_{tube}[m]$, and the thermal conductivity of the tube, $k_{tube}\left[\frac{W}{m \cdot K}\right]$.

Step 4: Cooling water convective heat transfer coefficient

The water side convection heat transfer coefficient is a function of the Nusselt number, $Nu_w\ -$, along with the inner diameter of the tube and the thermal conductivity of the cooling water, $k_w\left[\frac{W}{m \cdot K}\right]$, as shown in equation (A.5).

$$h_w = \frac{Nu_w \cdot k_w}{ID_{tube}} \quad \text{(A.5)}$$

The Nusselt number is a function of the flow within the tube. To accurately determine the Nusselt number, the Reynolds number, $Re_w\ -$, needs to be calculated. The Reynolds number gives an indication on whether the flow inside the tube is laminar or turbulent.

Should the Reynolds number be laminar then the Nusselt number is constant value whereas empirical correlations are used to determine the Nusselt number should the flow be regarded as turbulent.

The Nusselt number can be determined through equation (A.5.1) [9];

$$Nu_w = \begin{cases} 3.66 \text{ if } Re_w \leq 2300 \text{ and } T_a \text{ is constant} \\ 4.34 \text{ if } Re_w > 2300 \text{ and } T_a \text{ is fluctuating} \\ 0.023 \cdot Re_w^{0.8} \cdot Pr_w^{0.3} \end{cases} \quad \text{(A.5.1)}$$

Where T_a °C is the ambient air temperature and Pr_w is the Prandtl number of the water flow. The Reynolds number and Prandtl number can be determined through (A.5.2) and (A.5.3) below. The Reynolds number is a function of the mass flow per tube, $\dot{m}_w\left[\frac{kg}{s}\right]$, along with the dynamic viscosity, $\mu_w\left[\frac{kg}{m \cdot s}\right]$, and internal diameter of the tube.

$$\mathrm{Re_w} = \frac{4\dot{m}_w}{\mu_w \cdot \pi \cdot \mathrm{ID_{tube}}} \tag{A.5.2}$$

$$\mathrm{Pr_w} = \frac{\mathrm{Cp_w} \cdot \mu_w}{k_w} \tag{A.5.3}$$

The Prandtl number is a function of the specific heat, $\mathrm{Cp_w}\ \left[\frac{\mathrm{J}}{\mathrm{kgK}}\right]$, the dynamic viscosity and the thermal conductivity of the water. These parameters are all dependent on the water temperature and is calculated as such [9].

Step 5: Air-side convective heat transfer coefficient

The convective heat transfer coefficient on the air-side is a function of the Colburn J-factor, which is typically obtained from the supplier, the mass flux, $\mathrm{G}\ \left[\frac{\mathrm{kg}}{\mathrm{m^2 s}}\right]$, the specific heat of the air, $\mathrm{Cp_a}\ \left[\frac{\mathrm{J}}{\mathrm{kgK}}\right]$, and the Prandtl number for the air flow, $\mathrm{Pr_a}$.

The air-side convective heat transfer coefficient can be determined through (A.6).

$$h_a = \frac{j \cdot G \cdot \mathrm{Cp_a}}{\mathrm{Pr_a^{\frac{2}{3}}}} \tag{A.6}$$

The mass flux can be determined through the air mass flow rate, $\dot{m}_a\ \left[\frac{\mathrm{kg}}{\mathrm{s}}\right]$ and the free-flow area, $\mathrm{A_{ff}}\ [\mathrm{m^2}]$, that is obtained from the supplier, as shown in in equation (A.6.1). The Prandtl number is determined through equation (A.6.2) which is similar to the water-side equation of (A.5.3). The parameters used to determine the Prandtl number for the air-side are temperature dependent.

$$G = \frac{\dot{m}_a}{\mathrm{A_{ff}}} \tag{A.6.1}$$

$$\mathrm{Pr_a} = \frac{\mathrm{Cp_a} \cdot \mu_a}{k_a} \tag{A.6.2}$$

Step 6: System overall heat transfer efficiency

The overall heat transfer efficiency is a comprehensive efficiency parameter that includes the efficiency of heat transfer for the fin, η_f, the finned area, $\mathrm{A_{f_t}}$, and the total air-side heat transfer area. The overall heat transfer efficiency can be determined through (A.7).

$$\eta_o = 1 - \left(\frac{\mathrm{A_{f_t}}}{\mathrm{A_{a_{total}}}}\right) \cdot (1 - \eta_f) \tag{A.7}$$

The efficiencies of various fin geometries are available in literature [9].

Step 7: The design heat transfer rate

The heat exchanger duty is defined by equation (A.8), where eff denotes the heat transfer effectiveness and $q_{max}[W]$ denotes the maximum heat transfer.

$$q_{des} = \mathrm{eff} \cdot q_{max} \tag{A.8}$$

The effectiveness is influenced by the heat transfer ability ratio, C_r $-$, and NTU, as shown in equation (A.8.1).

$$\mathrm{eff} = \frac{1}{C_r} \cdot \left[1 - \frac{1}{e^{\left\{C_r \cdot \left[1 - \left(\frac{1}{e^{NTU}}\right)\right]\right\}}}\right] \tag{A.8.1}$$

The heat transfer ability can be determined through (A.8.2).

$$C_r = \frac{C_{min}}{C_{max}} \tag{A.8.2}$$

Where $C_{min} = \min\left(Cp_w \cdot \dot{m}_w , Cp_a \cdot \dot{m}_a\right)$

$$C_{max} = \max\left(Cp_w \cdot \dot{m}_w , Cp_a \cdot \dot{m}_a\right)$$

The NTU can be determined through equation (A.8.3) where UA is determined through the first 6 steps whilst the total air-side heat transfer area, $A_{a_{total}}$, and minimum heat transfer ability, C_{min} $\left[\frac{W}{K}\right]$, are known from previous calculations.

$$NTU = \frac{UA \cdot A_{a_{total}}}{C_{min}} \tag{A.8.3}$$

The effectiveness for use in equation (A.8) can now be determined.

The maximum heat transfer is a function of the minimum heat transfer ability and the difference in air and water inlet temperatures, as shown in equation (A.9).

$$q_{max} = C_{min} \cdot (T_w - T_a) \tag{A.9}$$

The actual heat transfer can then be determined with equation (A.10).

$$q_{des} = \mathrm{eff} \cdot q_{max} \tag{A.10}$$

equations (A.9) and (A.10) can now be used to determine the design heat transfer duty of the heat exchanger.

Note that no fouling is considered since the current fouling condition of the air-cooled heat exchangers have not been quantified.

APPENDIX B – HEAT LOSS PREDICTION MODEL

The theory supplied in Chapter 2.1.7 from [26] and [12] is used to characterise the heat loss from the uninsulated pipes and tank in the system.

The steps of the calculation are provided, followed by a summarised block diagram illustrating the how the steps are used for both the tank and piping components.

Energy Balance Equations:

The equations provided in (3.24) and (3.25) is used in this section to measure and ensure convergence as well as determining the reduction in temperature for the cooling water.

From (3.24), the following equations are made for use in the model:

$$\dot{Q}_{LH} = \frac{2k\pi L(T_i - T_e)}{\ln\left(\frac{D_e}{D_i}\right)} \tag{B.1}$$

$$\dot{Q}_{RH} = h_e A_e(T_{\infty,e} - T_e) + \frac{T_e - T_{\infty,e}}{\epsilon\sigma\pi D_e L(T_e + T_{\infty,e})(T_e^2 + T_{\infty,e}^2)} \tag{B.2}$$

From (3.25), the following equations are made for use in the model:

$$\dot{Q}_i = h_i A_i\left(T_{\infty,i} - T_i\right) = \frac{2k\pi L(T_i - T_e)}{\ln\left(\frac{D_e}{D_i}\right)} = \dot{Q}_{LH} \tag{B.3}$$

Assumptions:

The pipe, tank and any potential insulative material conductive and radiative properties can be assigned a constant value.

It is assumed that there is no resistance to heat transfer between the cooling water and inner tank surface. This assumption is made to ensure that the heat loss predicted is conservative due to the absence of heat transfer characteristics in the tank. The inner surface of the pipe will, therefore, be modelled at a temperature equal to the bulk fluid temperature and thus:

$$T_i = T_{\infty,i} \tag{B.4}$$

Step 1:

Determine the conductive properties of the material.

$$R_{cond} = \frac{\ln\left(\frac{D_e}{D_i}\right)}{2\pi kL} \tag{B.5}$$

Step 2:

Assign guess values for T_i. Provide a range in which T_e is, such that $T_e^L < T_e < T_e^H$. As an initial value, assign:

$$T_e = \frac{T_e^L + T_e^H}{2} \tag{B.6}$$

Step 3:

Determine the value of $\dot{Q}_{LH}$ at the currently assigned T_i and T_e values.

$$\dot{Q}_{LH} = \frac{(T_i - T_e)}{R_{cond}} \tag{B.7}$$

Step 4:

Determine the film temperature of the air on the external surface and determine the relevant thermal properties at this film temperature.

$$T_f = \frac{T_e + T_{\infty,e}}{2} \tag{B.8}$$

The following properties are required at the film temperature:

- β – Thermal expansion coefficient of the air $\left[\frac{1}{K}\right]$
- k – Thermal conductivity of air $\left[\frac{W}{m \cdot K}\right]$
- μ – Dynamic viscosity of air $\left[\frac{kg}{m \cdot s}\right]$
- ν – Kinematic viscosity of air $\left[\frac{m^2}{s}\right]$
- C_p – Specific heat of air $\left[\frac{J}{kg \cdot K}\right]$

Step 5:

Determine the current resistance to heat transfer due to natural convection and radiation at the currently assigned values of T_e.

Heat Transfer Resistance of Natural Convection:

The Prandtl and Rayleigh numbers of the external air are then determined as:

$$\mathrm{Pr} = \frac{\mu \cdot C_p}{k} \tag{B.9}$$

$$\mathrm{Ra} = \frac{g \cdot \beta \cdot \left(T_e - T_{\infty,e}\right) \cdot D_e^3}{\nu^2} \mathrm{Pr} \tag{B.10}$$

The Nusselt number for the external air then determined with (2.28) [26]:

$$\mathrm{Nu} = \left[\left(0.6 + \frac{0.387 \cdot \mathrm{Ra}^{\frac{1}{6}}}{\left(1 + \left(\frac{0.559}{\mathrm{Pr}}\right)^{\frac{9}{16}}\right)^{\frac{8}{27}}} \right) \right]^2 \tag{B.11}$$

The Nusselt number can then be used to determine the natural convection heat transfer coefficient through:

$$h_e = \frac{\mathrm{Nu} \cdot k}{D_e} \tag{B.12}$$

The heat transfer resistance due to natural convection is then:

$$R_{conv} = \frac{1}{h_e \pi D_e L} \tag{B.13}$$

Heat Transfer Resistance of Radiation:

The resistance to heat transfer through radiation is dependent on the ambient and external surface temperatures. Note that these temperatures need to be supplied in units of kelvin K. The first formula converts the temperatures from ℃ to K.

$$\left[T_{e,K}, T_{\infty,e,K}\right] = \left[T_e + 273.15, T_{\infty,e} + 273.15\right]$$

$$R_{rad} = \frac{1}{\epsilon \cdot \pi D_e L \cdot \sigma \cdot \left(\left(T_{e,K} + T_{\infty,e,K}\right)\left(T_{e,K}^2 + T_{\infty,e,K}^2\right)\right)} \tag{B.14}$$

Step 6:

Determine the value of $\dot{Q}_{RH}$ at the currently assigned T_i and T_e values.

$$\dot{Q}_{RH} = \frac{T_i - T_e}{R_{conv}} + \frac{T_i - T_e}{R_{rad}} \tag{B.15}$$

Step 7:

Determine the difference between $\dot{Q}_{LH}$ and $\dot{Q}_{RH}$. If the difference is outside the convergence criteria, the guess value for T_e needs to be adjusted.

The range for a suitable guess value for T_e is updated as follows:

$$\dot{Q}_{LH} > \dot{Q}_{RH} \rightarrow T_e^L = T_e$$
$$\dot{Q}_{LH} < \dot{Q}_{RH} \rightarrow T_e^H = T_e \quad \text{(B.16)}$$

The method above indicates that if the conductive heat transfer is more than the combination of convective and radiative heat transfer, the difference between the T_i and T_e is too high and thus that the guess value of T_e is too low. The lower bound of the guess value for T_e is thus increased to T_e.

If the conductive heat transfer is less than the combination of convective and radiative heat transfer, the difference between the T_i and T_e is too low and thus that the guess value of T_e is too high. The upper bound of the guess value for T_e is thus decreased to T_e.

The range of $[T_e^L, T_e^H]$ is then used in a repeat of Step 2-7 until convergence is reached.

Step 8:

If internal convection coefficients need to be considered, as in the piping component, then the internal surface temperature of the component needs to be updated from the initial value assigned.

Heat Transfer Resistance of Internal Convection:

The film temperature of the cooling water is determined as in (B.8), only for T_i and $T_{\infty,i}$.

The following properties of water is required to determine the internal convection coefficient:

- k_w – Thermal conductivity of water $\left[\frac{W}{m \cdot K}\right]$
- μ_w – Dynamic viscosity of water $\left[\frac{kg}{m \cdot s}\right]$
- C_{p_w} – Specific heat of water $\left[\frac{J}{kg \cdot K}\right]$
- ρ_w – Density of water $\left[\frac{m^3}{kg}\right]$

The Reynolds and Prandtl number are then determined with:

$$Re_w = \frac{\rho V D_i}{\mu} \quad \text{(B.17)}$$

$$Pr_w = \frac{\mu_w \cdot C_{p_w}}{k_w} \quad \text{(B.18)}$$

The Nusselt number is then determined from the Dittus-Boelter correlation provided in Chapter 2 and from [9].

$$\mathrm{Nu_w} = 0.023 \cdot \mathrm{Re_w^{0.8}} \cdot \mathrm{Pr^{0.3}} \tag{B.19}$$

The internal convection coefficient is then used to determine the internal convection coefficient of the cooling water:

$$\mathrm{h_i} = \frac{\mathrm{Nu_w} \cdot \mathrm{k_w}}{\mathrm{D_i}} \tag{B.20}$$

The known value of $\mathrm{T_{\infty,i}}$ is then used with the current value of $\dot{\mathrm{Q}}_{\mathrm{LH}}$ to determine an updated internal surface temperature through:

$$\dot{\mathrm{Q}}_{\mathrm{LH}} = \dot{\mathrm{Q}}_{\mathrm{i}} = \mathrm{h_i A_i (T_{\infty,i} - T_i)} \tag{B.21}$$

$$\mathrm{T_i} = \mathrm{T_{\infty,i}} - \left(\frac{\dot{\mathrm{Q}}_{\mathrm{i}}}{\mathrm{h_i} \cdot \pi \mathrm{D_i L}} \right) \tag{B.22}$$

The updated value is then used during a repeat of Step 2-8 until convergence is reached. After convergence is reached, the following is true:

$$\dot{\mathrm{Q}}_{\mathrm{i}} = \dot{\mathrm{Q}}_{\mathrm{LH}} = \dot{\mathrm{Q}}_{\mathrm{RH}}$$

Step 9:

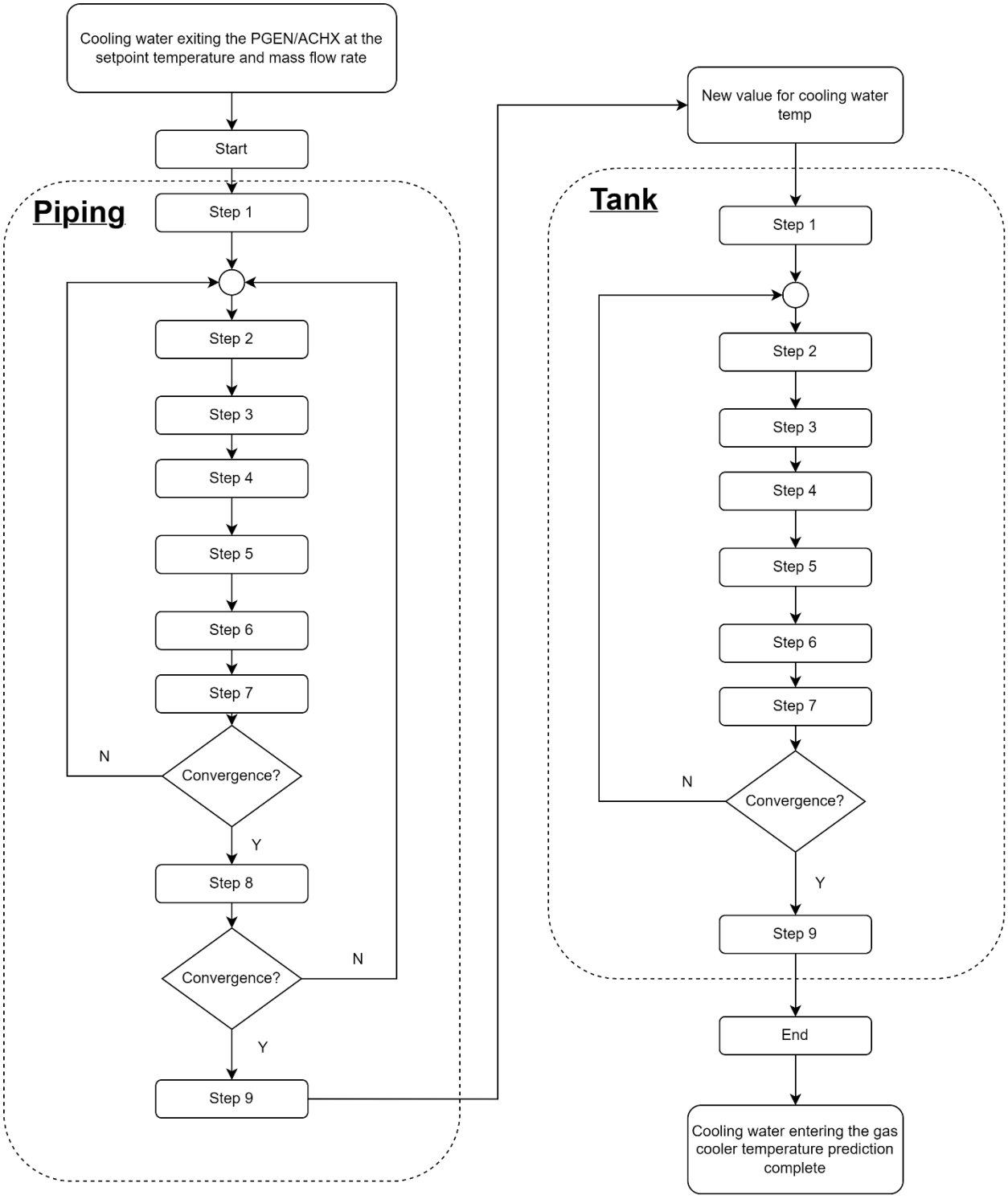
Successful convergence in Step 8 then allows the use of the heat transfer rate to determine the equivalent temperature drop and thus the temperature of the cooling water exiting the component:

$$\mathrm{T_{cw,e}} = \mathrm{T_{cw,i}} - \frac{\dot{\mathrm{Q}}_{\mathrm{i}}}{\dot{\mathrm{m}} \mathrm{C_p}} \tag{B.23}$$

The value of the $\mathrm{T_{cw,e}}$ is then either used as the bulk fluid temperature $\mathrm{T_{\infty,i}}$ in the next uninsulated component or it is designated as the predicted temperature of water entering the gas cooler.

Block Diagram:

The complete step layout used for the components in this thesis is illustrated in the following block diagram. Note that Step 8 is not used in the tank section due to the assumptions stated earlier. Also, note that the temperature entering the tank is updated from the piping heat loss calculations.



B 1: Heat loss calculation steps for the uninsulated components in the system

APPENDIX C – POWER GENERATION CONTROL (PGCP)

```
# -*- coding: utf-8 -*-
"""
PGEN Operation with varying evaporating pressure and degree of superheat
    Create dataframe of combinations and decide on combination with maximum power generation
    Provide feedback to calling function
"""

#Import Required Modules
import CoolProp.CoolProp as ct
import numpy as np

fluid_wf = 'nPentane'
rho_1 = ct.PropsSI('D','P',1.1e5,'T',35.5+273.15,fluid_wf)
T_pc1 = ct.PropsSI('T','P',1.1e5,'Q',0,fluid_wf)
phase_1 = ct.PhaseSI('P',25e5,'T',40+273.15,fluid_wf)

def PGEN_Opt(T_hs_i,m_hs_i,T_set):

    import CoolProp.CoolProp as ct
    import pandas as pd
    import math

    fluid_wf = 'nPentane'
    fluid_hs = 'water'
    fluid_cs = 'air'

    Q_evap_min = 2e6
    Q_evap_max = 20e6

    P_hs = 30e5

    #Cold Source
    T_pp_cond = 20

    # Design parameters
    p_eva = 22.8e5
    eta_pump = 0.85
    T_tur_des = 180+273.3

    rho_des = ct.PropsSI('D','P',p_eva,'T',T_tur_des,fluid_wf)

    parametric_study = pd.DataFrame(columns= ['p_eva','T1','T_sh',"T3_PP",'eta','W_net',
                                              'm_wf','Q_evap','eta_th','LMTD','UA',
                                              'T3_pc','phase_i','phase_o','H3','H4',
                                              'H4_isen','W_pump','m_wf2'])

    #Cycle parameters
    eta_pump = 0.85
    eta_turb_des = 0.8

    #Evap
    C_hs1 = ct.PropsSI('C','P',P_hs,'T',T_hs_i+273.15,fluid_hs)
    C_hs2 = ct.PropsSI('C','P',P_hs*0.98,'T',T_set+273.15,fluid_hs)
    C_hs = (C_hs1+C_hs2)/2

    Q_evap = m_hs_i*4170*(T_hs_i-T_set)
    T_set = T_hs_i-Q_evap/(m_hs_i*C_hs)
```

1

```
Q_evap = m_hs_i*C_hs*(T_set-T_hs_i)
p_eva_low = 12

results = []

def calculate_lmtd(Tc_in, Th_in, Tc_out, Th_out):
    delta_T1 = Th_in - Tc_out
    delta_T2 = Th_out - Tc_in

    if delta_T1 == delta_T2:
        return delta_T1  # If delta_T1 and delta_T2 are equal, LMTD is just delta_T1/T2

    lmtd = (delta_T1 - delta_T2) / math.log(delta_T1 / delta_T2)
    return lmtd

def find_cold_inlet_temp(LMTD_given, Th_out, Th_in, Tc_out, tolerance=0.01, max_iter=10):
    Tc_in_guess = 40  # Initial guess for Tc_in
    iteration = 0

    while iteration < max_iter:
        iteration += 1

        # Calculate the LMTD with the current guess
        lmtd_current = calculate_lmtd(Tc_in_guess, Th_in, Tc_out, Th_out)

        # Check if the calculated LMTD is within the tolerance of the given LMTD
        if abs(lmtd_current - LMTD_given) < tolerance:
            return Tc_in_guess

        # Adjust the guess for Th_in based on the difference
        Tc_in_guess -= (LMTD_given - lmtd_current) * 0.1  # Adjust factor can be tuned
        #print(Tc_out_guess)

    return Tc_in_guess

def seek(p_eva_low):
    i=0
    step = 1
    p_eva_values = np.arange(p_eva_low, 25 + step, step)
    T_sh_values = np.arange(5, 25 + step, step)
    for p_eva in p_eva_values:
        for T_sh in T_sh_values:
            try:
                i=i+1
                if -Q_evap < Q_evap_min:
                    return(0,0,0,0,0,0)
                else:
                    T1 = 35.5+273.15
                    j = 0
                    while j<4:
                        #Pump
                        P1 = 1.1e5
                        P2 = p_eva*1e5/0.9

                        H1 = ct.PropsSI('H','P',P1,'T',T1,fluid_wf)
                        s1 = ct.PropsSI('S','P',P1,'T',T1,fluid_wf)
```

```
H2_isen = ct.PropsSI('H','P',P2,'S',s1,fluid_wf)

W_isen_p = H2_isen-H1
W_p = W_isen_p/eta_pump

H2 = H1+W_p

#Evaporator Refrigerant side
P3 = P2*0.9
T3_pc = ct.PropsSI('T','P',P3,'Q',0,fluid_wf)
T3 = T3_pc+T_sh

H3 = ct.PropsSI('H','P',P3,'T',T3,fluid_wf)

m_wf2 = Q_evap/(H2-H3)
m_wf = m_wf2

delta_T1 = T_hs_i - (T3-273.15)
delta_T2 = T_set - (T1-273.15)

if delta_T1 == delta_T2:
    LMTD = delta_T1
else:
    LMTD = (delta_T1 - delta_T2) / math.log(delta_T1 / delta_T2)

m_hs_frac = (m_hs_i/m_hs_ref)**0.4
m_wf_frac = (m_wf/m_wf_des)**0.4

UA = UA_ref*m_hs_frac*m_wf_frac
LMTD = -Q_evap/UA

T1_update = find_cold_inlet_temp(LMTD, T_set, T_hs_i,
                                 T3-273.15)+273.15

#Turbine
s3 = ct.PropsSI('S','P',P3,'T',T3,fluid_wf)
P4 = P1/0.9
rho3 = ct.PropsSI('D','P',P3,'T',T3,fluid_wf)

#Determine new eta
eta_turb = eta_turb_des*math.sin(0.5*math.pi*
                                 (math.pow((m_wf*rho_des/(m_wf_des*rho3
                                           ,0.1)))

H4_isen = ct.PropsSI('H','P',P4,'S',s3,fluid_wf)
W_isen = m_wf*(H3-H4_isen)

H4 = H3 - (eta_turb*(H3-H4_isen))

phase_i = ct.PhaseSI('P', P3, 'T', T3, fluid_wf)
phase_o = ct.PhaseSI('P', P4, 'H', H4, fluid_wf)

W = eta_turb*W_isen

#Condenser
P1 = P4*0.9
T1_pc = ct.PropsSI('T','P',P1,'Q',0,fluid_wf)
```

3

```
                        T1 = T1_pc - T_pp_cond

                        H1 = ct.PropsSI('H','P',P1,'T',T1,fluid_wf)
                        rho1 = ct.PropsSI('D','P',P1,'T',T1,fluid_wf)

                        W_pump = (m_wf/rho1)*(P2-P1)
                        W_net = W - W_pump

                        eta_th = W_net/-Q_evap

                        T1 = T1_update
                        j+=1

                    lst = [p_eva,T1-273.15,T_sh,T_hs_i - T3+273.15,eta_turb,W_net,m_wf,
                           m_hs_i,-Q_evap,eta_th,LMTD,UA,T3_pc-273.15,phase_i,phase_o,
                           H3,H4,H4_isen,W_pump,m_wf2]

                results.append(lst)
                parametric_study.loc[len(parametric_study)] = lst
            except (ValueError, ZeroDivisionError) as e:
                print(f"""Skipping invalid combination: Pressure={p_eva}, Temp={T_sh} due to
                      error: {e}""")
                continue

seek(p_eva_low)
parametric_study = pd.DataFrame(results,columns= ['p_eva','T1','T_sh',"T3_PP",'eta','W_net',
                                                  'm_wf','m_pgen','Q_evap','eta_th','LMTD',
                                                  'UA','T3_pc','phase_i','phase_o','H3','H4',
                                                  'H4_isen','W_pump','m_wf2'])
parametric_study = parametric_study[parametric_study["T3_PP"]>=10]
parametric_study = parametric_study[parametric_study["T1"]>=35.5]

if parametric_study.empty:
    max_T_sh_W = 0
    max_p_eva_W = 0
    max_eta_th_W = 0
    max_W_th = 0
    max_Q_evap = 0
    max_m_wf = 0

else:
    # Find the index of the maximum value in the "eta" column
    max_W_index = parametric_study['W_net'].idxmax()

    # Extract the corresponding values from the "T_sh" and "p_eva" columns
    max_T_sh_W = parametric_study.loc[max_W_index, 'T_sh']
    max_p_eva_W = parametric_study.loc[max_W_index, 'p_eva']
    max_eta_th_W = parametric_study.loc[max_W_index, 'eta_th']
    max_W_th = parametric_study.loc[max_W_index, 'W_net']
    max_Q_evap = parametric_study.loc[max_W_index, 'Q_evap']
    max_m_wf = parametric_study.loc[max_W_index, 'm_wf']

fb_list = [max_eta_th_W,max_p_eva_W,max_T_sh_W,max_W_th,max_Q_evap,max_m_wf]

return(fb_list)
```

4

APPENDIX D – AIR-COOLED HEAT EXCHANGER CONTROL (ACCP)

```
# -*- coding: utf-8 -*-
"""
ACHX Performance Simulation Based on Masters of Van Rooyen
    Determine the desired number of fans and their operational speed
    to achieve the required heat transfer per second.
"""

import math
from pyfluids import Fluid, FluidsList, Input
import pint
import pandas as pd

u = pint.UnitRegistry(system='SI')

#ACHE Design Information
from fluids.geometry import AirCooledExchanger

import warnings
warnings.filterwarnings("ignore", message=".*UnitStrippedWarning.*")


def ACHX(T_w_in,m_w_in,Q_req,P_w_in,T_a_in, N_min, N_max,n_fan,m_a_max,p_fan_kw):
    #Assign Units to required heat transfer per second and water flow rate
    Q_req = Q_req*u.MW
    m_w_total = (m_w_in)*u.kg/u.s

    #Create empty dataframes for processing of future results
    seeking = pd.DataFrame(columns=['Q_rej','n_fan', 'rpm', 'p_fan'])

    #Function for running the ACHX with a select number of fans
    def RunACHX(Q_req,n_fan):
        q_des_M = 0
        rpm_inc = 0

        design = AirCooledExchanger(
                                    tube_rows = 6,
                                    tube_passes = 1,
                                    tubes_per_row = 43*n_fan,
                                    tube_length = 4.900*n_fan*u.m,
                                    tube_diameter = 0.03175*u.m,
                                    fin_thickness = 0.0004*u.m,
                                    pitch_normal= 0.076*u.m,
                                    pitch_parallel= 0.076*u.m,
                                    fin_diameter = 0.0635*u.m,
                                    fin_density = 433/u.m,
                                    tube_thickness = 0.00241*u.m)


        while abs(q_des_M)<Q_req and N_min+rpm_inc<=N_max:

            q_reported = q_des_M
            Q_a_total = (m_a_max*u.m**3/u.s)*((N_min+rpm_inc)/N_max)*n_fan

            #   Sub-Step 1
            #   Water-side overall heat transfer area

            D_i = design.tube_diameter-(2*design.tube_thickness)
```

1

```
L_t_total = design.tubes_per_row*design.tube_rows*design.tube_length

A_w_total = math.pi*D_i*L_t_total

#   Sub-step 2
#   Air-side overall heat transfer area

A_a_total = design.A

#   Sub-step 3
#   Total conductive resistance of clean heat exchanger

k_fin = 45*u.W/(u.m*u.K)
k_tube = 25*u.W/(u.m*u.K)
k_combo = ((2203*k_fin) + (4400*k_tube))/6603

R_total_x = math.log10(design.tube_diameter/D_i)
R_total_y = 2*math.pi*L_t_total*k_combo

R_total = R_total_x/R_total_y

#print(f"Total external heat transfer area is : {R_total}")

# Sub-Step 4
# Water-side Convection Coefficient

N_t = design.tubes
m_w_tube = (m_w_total/N_t)

fluid = Fluid(FluidsList.Water).with_state(Input.pressure(P_w_in*100e3),
                                           Input.temperature(T_w_in))

mu_w = fluid.dynamic_viscosity*(u.kg/(u.m*u.s))
Cp_w = fluid.specific_heat*(u.J/(u.kg*u.K))
k_w1 = fluid.conductivity*(u.W/(u.m*u.K))
k_w2 = fluid.conductivity*(u.J/(u.s*u.m*u.K))

Pr_w = Cp_w*mu_w/k_w2
Re_w = 4*m_w_tube/(mu_w*math.pi*D_i)

Nu_w = 0.023*(Re_w**0.8)*(Pr_w**0.3)

h_w = Nu_w*k_w1/D_i

#print(f"Internal convection coefficient is : {h_w:.3f}")

#   Sub-step 5
#   Air Side Convection coefficient

j = 0.008

air = Fluid(FluidsList.Air).with_state(Input.pressure(100e3),
                                       Input.temperature(T_a_in))
rho_a = air.density*u.kg/u.m**3
m_a_total = Q_a_total*rho_a
G = m_a_total/design.A_min
```

2

```
        mu_a = air.dynamic_viscosity*(u.kg/(u.m*u.s))
        k_a = air.conductivity*(u.J/(u.s*u.m*u.K))
        Cp_a = air.specific_heat*(u.J/(u.kg*u.K))

        Pr_a = (Cp_a*mu_a)/k_a
        h_a = (j*G*Cp_a)/(Pr_a**(2/3))*(u.W*u.s/u.J)

        ## Sub-step 6
        A_f_total = design.A_fin
        eta_f = 0.6
        eta_o = 1-(A_f_total/A_a_total)*(1-eta_f)

        ##  Final step of Part 1
        ##  Determine UA
        UA_w = (h_w*A_w_total/A_a_total)**(-1)
        UA_a = (eta_o*h_a)**(-1)

        UA = 1/(UA_w+(R_total*A_a_total)+UA_a)

        ## Part 2
        ## Optimal heat transfer rate
        C_w = Cp_w*m_w_total
        C_a = Cp_a*m_a_total

        C_max = max(C_w,C_a)
        C_min = min(C_w,C_a)

        C_r = C_min/C_max

        NTU = UA*A_a_total/C_min

        x = C_r*(1-(1/math.exp(NTU)))
        eff = (1/C_r)*(1-(1/math.exp(x)))

        delt_T = (T_a_in - T_w_in)*u.K
        q_max = C_min*delt_T

        q_des = eff * q_max
        q_des_M = q_des*(u.s/u.J)*u.MW/1e6

        q_des = -q_des*(u.W*u.s/u.J)
        C_w = C_w*(u.W*u.s/u.J)

        rpm_inc = rpm_inc+1

    rpm = N_min+rpm_inc-1

    p_fan = p_fan_kw*(rpm/N_max)*n_fan
    lst = [-q_reported.magnitude,n_fan,rpm,p_fan]

    return(lst)

for n_fan in range(1,n_fan+1,1):

    Q_a_total_min = (m_a_max*u.m**3/u.s)*(N_min/N_max)*n_fan
    Q_a_total_max = (m_a_max*u.m**3/u.s)*(N_max/N_max)*n_fan
    Q_min = CheckACHX(Q_a_total_min, design)*-1
```

```
        Q_max = CheckACHX(Q_a_total_max, design)*-1

        if Q_req >= Q_min and Q_req <= Q_max:

            lst = RunACHX(Q_req, n_fan)

            seeking.loc[len(seeking)] = lst
        elif n_fan == 4:

            lst = [Q_req,n_fan,p_fan_kw*n_fan,Q_req]
            seeking.loc[len(seeking)] = lst


    if len(seeking) > 0 :
        # Find the index of the minimum value in the power column
        min_W_index = seeking['p_fan'].idxmin()

        # Extract the corresponding values from the number of fans and speed columns
        n_fan_res = seeking.loc[min_W_index, 'n_fan']
        p_fan_res = seeking.loc[min_W_index, 'p_fan']
        rpm_res = seeking.loc[min_W_index, 'rpm']

    else:
        n_fan_res = 0
        p_fan_res = 0
        rpm_res = 0

    return(n_fan_res,p_fan_res, rpm_res)
```

APPENDIX E – TEMPERATURE SETPOINT DETERMINATION (TSD)

```
# -*- coding: utf-8 -*-
"""
Calculate the heat loss from the pipe and tank in the system given the properties of each.
Include for:
    Conductive heat transfer
    Convective heat transfer
    Radiative heat transfer
Adjust setpoint temperature to ensure cooling water entering the gas cooler >= 150C.
"""

#Import required modules
import math
from pyfluids import Fluid, FluidsList, Input

def condResist(propList):
    l,in_d,t,k = propList[0],propList[1],propList[2],propList[3]
    out_d = in_d+(2*t)

    if t == 0:
        R= 0
    if t > 0:
        R = math.log(out_d/in_d)/(2*math.pi*l*k)
    return(R)

def convResist(propList,od,l,T_se,T_amb):
    beta = propList[0]
    pr = propList[5]
    k = propList[4]
    nu = propList[2]

    Ra = (9.81*beta*(T_se-T_amb)*(od**3)/(nu**2))*pr
    numerator = 0.387*math.pow(Ra, 1/6)
    denominator = math.pow(1+math.pow(0.559/pr,9/16),8/27)

    Nu = (0.6+(numerator/denominator))**2
    h_conv = Nu*k/od

    R = 1/(h_conv*math.pi*od*l)
    return(R)

def radResist(e,od,l,T_se,T_amb):

    T_se = T_se+273.15
    T_amb = T_amb+273.15

    R = 1/(e*math.pi*od*l*5.67e-8*(T_se+T_amb)*((T_se**2)+(T_amb**2)))

    return(R)

def filmTemp(T_f):
    air = Fluid(FluidsList.Air).with_state(Input.pressure(101.325e3),
                                           Input.temperature(T_f))

    beta = 1/(T_f+273.15)
    mu = air.dynamic_viscosity
    nu = air.kinematic_viscosity
    Cp = air.specific_heat
```

1

```
    pr = air.prandtl

    air_p = [beta,mu,nu,Cp,k,pr]

    return(air_p)

def insuProp(pipe_p,i_t,i_k,i_e):
    p_l,p_id,p_t = pipe_p[0],pipe_p[1],pipe_p[2]

    i_l = p_l

    p_od = p_id+(2*p_t)
    i_id = p_od

    insu_p = [i_l,i_id,i_t/1000,i_k,i_e]

    return(insu_p)

def TankLoss(tank_p,t_insu_p,T_amb,T_si,T_loss):
    Q_diff = 10
    convergence = 1

    lim_l = T_amb
    lim_h = T_si-T_loss
    lim_h=200

    T_g = (lim_h+lim_l)/2
    i=0

    while abs(Q_diff) > convergence:
        #Guess value for external temperature
        T_se = T_g

        T_f = (T_amb+T_se)/2
        air_p = filmTemp(T_f)

        "---LH side---"
        "Calculate the conductions resistances"
        resist_tank = condResist(tank_p)
        resist_t_insu = condResist(t_insu_p)

        R_cond = resist_t_insu+resist_tank

        Q_LH = (T_si-T_loss-T_se)/R_cond

        "---RH side---"
        if resist_t_insu==0:
            od = tank_p[1]+(2*tank_p[2])
        if resist_t_insu >0:
            od = t_insu_p[1]+(2*t_insu_p[2])

        l = tank_p[0]
        e = tank_p[4]

        "Calculate the convection resistance"
        resist_conv = convResist(air_p,od,l,T_se,T_amb)
        #print(resist_conv)
```

```
        "Calculate the radiative resistance"
        resist_rad = radResist(e, od, l, T_se, T_amb)
        #print(resist_rad)

        "Calculate the total RH heat transfer"
        Q_rad = (T_se-T_amb)/resist_rad
        Q_conv = (T_se-T_amb)/resist_conv
        Q_RH = Q_rad+Q_conv

        Q_diff = Q_LH-Q_RH
        if Q_diff > 0:  #If LH is more, then T_se is too low
            lim_l = T_se

        if Q_diff < 0:  #If RH is more, then T_se is too high
            lim_h = T_se

        T_g = (lim_h+lim_l)/2
        i = i+1

    Q_rad = ((T_se-T_amb)/resist_rad)
    Q_conv = ((T_se-T_amb)/resist_conv)
    Q_cond = ((T_si-T_se)/R_cond)

    return(Q_LH,T_se)

def PipeLoss(pipe_p,insu_p,T_amb,T_si):
    Q_diff = 1000
    convergence = 0.1

    lim_l = T_amb
    lim_h = T_si

    T_g = (lim_h+lim_l)/2
    i=0

    while abs(Q_diff) > convergence:
        #Guess value for external temperature
        T_se = T_g

        T_f = (T_amb+T_se)/2
        air_p = filmTemp(T_f)

        "---LH side---"
        "Calculate the conductions resistances"
        resist_pipe = condResist(pipe_p)
        resist_insu = condResist(insu_p)

        R_cond = resist_insu+resist_pipe

        Q_LH = (T_si-T_se)/R_cond

        "---RH side---"
        if resist_insu==0:
            od = pipe_p[1]+(2*pipe_p[2])
        if resist_insu >0:
            od = insu_p[1]+(2*insu_p[2])
```

```
        l = pipe_p[0]
        e = pipe_p[4]

        "Calculate the convection resistance"
        resist_conv = convResist(air_p,od,l,T_se,T_amb)

        "Calculate the radiative resistance"
        resist_rad = radResist(e, od, l, T_se, T_amb)

        "Calculate the total RH heat transfer"
        Q_rad = (T_se-T_amb)/resist_rad
        Q_conv = (T_se-T_amb)/resist_conv
        Q_RH = Q_rad+Q_conv
        Q_conv_l = Q_conv/l
        Q_rad_l = Q_rad/l

        Q_diff = Q_LH-Q_RH

        if Q_diff > 0:  #If LH is more, then T_se is too low
            lim_l = T_se

        if Q_diff < 0:  #If RH is more, then T_se is too high
            lim_h = T_se

        T_g = (lim_h+lim_l)/2
        i = i+1

    Q_rad = ((T_se-T_amb)/resist_rad)
    Q_conv = ((T_se-T_amb)/resist_conv)
    Q_cond = ((T_si-T_se)/R_cond)
    return(Q_LH,T_se)

def CalculateQT(T_amb,T_L,m,pipe_p,insu_p,tank_p,t_insu_p):

    p_l = pipe_p[0]
    p_id = pipe_p[1]
    p_t = pipe_p[2]
    p_k = pipe_p[3]
    p_e = pipe_p[4]

    i_t = insu_p[2]
    i_k = insu_p[3]
    i_e = insu_p[4]

    insu_p = insuProp(pipe_p,i_t,i_k,i_e)

    t_l = tank_p[0]
    t_id = tank_p[1]
    t_t = tank_p[2]
    t_k = tank_p[3]
    t_e = tank_p[4]

    t_i_t = t_insu_p[2]
    t_i_k = t_insu_p[3]
    t_i_e = t_insu_p[4]
```

4

```
t_insu_p = insuProp(tank_p,t_i_t,t_i_k,t_i_e)

T_in = T_L
T_si = T_L
T_out = T_L-5

Q_int = 0
i=0
while T_out <= T_L:

    Q_pipe,T_pe = PipeLoss(pipe_p,insu_p,T_amb,T_in)

    water = Fluid(FluidsList.Water).with_state(Input.pressure(70e5),
                                               Input.temperature((T_in+T_si)/2))
    Cp_w = water.specific_heat
    mu_w = water.dynamic_viscosity
    pr_w = water.prandtl
    k_w = water.conductivity
    Re_w = m*p_id/mu_w
    Nu_w = 0.023*(Re_w**0.8)*(pr_w**0.3)
    h_w = Nu_w*k_w/p_id
    A_w = math.pi*p_id*p_l

    T_si = T_in - (Q_pipe/(h_w*A_w))
    Q_pipe,T_pe = PipeLoss(pipe_p,insu_p,T_amb,T_si)
    T_si = T_in - (Q_pipe/(h_w*A_w))

    T_loss = Q_pipe/(m*Cp_w)

    Q_tank,T_te = TankLoss(tank_p, t_insu_p, T_amb, T_in, T_loss)
    T_loss_t = Q_tank/(m*Cp_w)


    Q_total = Q_tank+Q_pipe
    T_drop = Q_total/(m*Cp_w)
    T_out = T_in-T_drop

    if T_out <= T_L:
        T_in = T_in+0.05

    i = i +1

T_delt = Q_pipe/(h_w*A_w)

return(Q_total,Q_pipe,Q_tank,T_drop,T_in)
```

5

APPENDIX F – SAMPLE SCRIPT FOR WP

```
print("Importing required modules...")
import pandas as pd
import time
import CoolProp.CoolProp as ct

import warnings
warnings.filterwarnings("ignore", message=".*UnitStrippedWarning.*")

from rankine_Organic_Optimal import PGEN_Opt
from Organic_run import regime
from ACHX import ACHX
import heatLoss

seconds = 300

#Ambient Conditions
T_amb = 25

#Operational Resistriction
T_H = 210
T_L = 150

#ACHX Properties
mas_achx = 3530
n_fan_max = 4
N_max = 333
N_min = 166
m_a_max = 42
p_fan_kw = 37

#PGEN Properties
restart_Q=20e6*0.2
trip = 1 #Number of trips
trip_time = 38520
trip_delay = 60

t_cw = 720
t_w = 20
t_c=  180

P_low = 2*1e6
P_high = 20*1e6
P_restart = 4e6


#WP Setting
ratio = 0.25

print("Importing Excel files...")
# Load Excel file
excel_file = "Heat and Flow.xlsx"
sheet_name = "Demonstrative"
sheet_name_achx = "Sheet1"
sheet_name_uninsulated = "HeatLoss"

heat_removed_name = "Gas Removed"
flow_name = "Flow_N"
```

1

```
temp_name = "Temp_N"
press_name = "Press_N"

# Read the Excel file and extract data from the specified column
df = pd.read_excel(excel_file, sheet_name=sheet_name)
df_hl = pd.read_excel(excel_file, sheet_name=sheet_name_uninsulated)

# Extract values from the specified column and populate a list
# Heat and Flow dataset
V_t = df[flow_name].tolist()
m_hs_t = V_t
T_t = df[temp_name].tolist()
Press_t = df[temp_name].tolist()

t = len(V_t)

Q_t=[0]*t
Q_hs_t = Q_t

runto = len(Q_t)

print("Initialising...")
for i in range(len(V_t)):
    Cp_w = ct.PropsSI('C','P',Press_t,'T',T_t+273.15,'water')
    Q_t[i] = V_t[i]*Cp_w*(T_t[i]-T_L)

# Ininsulated parameters
pipe_p = df_hl["pipe"].fillna(0).tolist()
insu_p = df_hl["pipe_ins"].fillna(0).tolist()
tank_p = df_hl["tank"].fillna(0).tolist()
t_insu_p = df_hl["tank_ins"].fillna(0).tolist()

# Initialisation
# ACHX parameters initialised
m_achx_min = [5]*t
Q_a = [0]*t
Q_a_o = [0]*t
Q_delta_A = [0]*t
n_fan = [0]*t
rpm = [0]*t
p_fan = [0]*t
m_achx = m_achx_min

#PGEN parameters initialised
delta_p = [1]*t
delay_p = 0
Q_p = [0]*t
W_net = [0]*t
T_boil = [0]*t
p_eva = [0]*t
Q_evap = [0]*t
m_wf = [0]*t

#Residual and Bypass Flow initialised
Q_res = [0]*t
Q_bp_a = [0]*t
```

```
#System Parameters initialised
eta_th = [0]*t

Q_loss = [0]*t
Q_pipe = [0]*t
Q_tank = [0]*t
T_drop = [0]*t
T_set = [150]*t

T_set_p = [150]*t
T_set_a = [150]*t

T_cw2 = [120]*t
T_A_int = [160]*t

m_pgen = [0]*t
m_bp = [0]*t

t_sp = 0
t_0 = 0

#Create dataframes for results

heatloss_df = pd.DataFrame(columns= ['Flow','Tset',"Q_total",'Q_pipe','Q_tank'])
results_df = pd.DataFrame(columns=['t','Flow','Temp','Q_orig','Q_tot','Q_loss',
                                   'T_set','T_set_a','m_achx','Q_achx','n','rpm',
                                   'T_set_p','m_pgen','Q_pgen','eta_th','p_eva',
                                   'T_boil','m_bp','W_net','Q_res','T_cw2','delta_p',
                                   'delta_q','t_sp','t_0','T_A_int','Q_bp_a'])


print("Initialisation done...")

print("Solving...")

for i in range(runto):
    delta_q = 0

    #Result List
    PGEN_list = eta_th[i],p_eva[i],T_boil[i],W_net[i],Q_evap[i],m_wf[i]

    "Use TSD to calculate setpoint temperature en remove this heat from available"
    TSD_list = [Q_loss[i],Q_pipe[i],Q_tank[i],T_drop[i],T_set[i]]
    TSD_list = heatLoss.CalculateQT(T_amb, T_L, V_t[i], pipe_p, insu_p, tank_p, t_insu_p)
    Q_t[i]=Q_t[i]-Q_loss[i]

    "--- Determine the heat loss from ACHX for n=0"
    Q_a_o[i] = (0.0002259*pow(T_t[i],1.701631))*1e6

    """1. Check if there is enough heat transfer available to allow min flow in ACHX
        if not, then bypass all the flow, if there is then flow can be distributed"""
    if Q_t[i] < Q_a_o[i]:
        #Bypass all the flow
        m_achx[i],m_pgen[i],Q_a[i],Q_p[i],delta_p[i] = 0,0,0,0,0
        m_bp[i] = V_t[i]

        #Update the internal heat transfer for stagnant water and update internal Temperature
```

```
        T_A_int[i] = T_A_int[i-1] - (Q_a_o[i]*seconds)/(mas_achx*Cp_w)

        #Set points for ACHX and PGEN is invalid - assign default
        T_set_a[i],T_set_p[i] = T_set[i],T_set[i]

    else:
        "There is enough heat, but was ACHX operational and internal temp above setpoint?"
        if m_achx[i-1] == 0 and T_A_int[i-1]<T_set[i]:
            #ACHX needs to be restarted - SAAR
            Q_delta_A[i] = mas_achx*Cp_w*(T_set[i]-T_A_int[i-1])

            #Required heat transfer rate at ACHX
            Q_des_bp = (Q_a_o[i]*seconds)+Q_delta_A[i]
            Q_des_bp = Q_des_bp/seconds

            if Q_t[i]-Q_des_bp > Q_a_o[i]:
                #Sufficient heat to transfer at ACHX for restart
                #No fans during startup of ACHX
                Q_a[i] = Q_a_o[i]
                m_bp[i] = (Q_delta_A[i]/300)/(Cp_w*(T_set[i]-T_A_int[i-1]))

                "Is the remaining heat such that PGEN can operate?"
                delta_p[i],delta_q, t_sp, t_0 = regime(Q_t[i], Q_des_bp, P_low,
                                                       delta_p[i-1], trip, i, restart_Q,
                                                       t_sp,t_0)

                if T_A_int[i-1]>T_set[i]:
                    m_achx[i] = Q_a[i]/(Cp_w*(T_A_int[i-1]-T_set[i]))
                else:
                    m_achx[i] = -Q_a[i]/(Cp_w*(T_A_int[i-1]-T_set[i]))

                if delta_q == 1:
                    m_pgen[i] = V_t[i]-m_achx[i]-m_bp[i]
                    Q_p[i] = restart_Q
                    PGEN_list = 0,0,0,0,Q_p[i],0
                else:
                    m_pgen[i] = 0
                    PGEN_list = 0,0,0,0,0,0

            else:
                #Insufficient heat for ACHX in one timestep
                if Q_t[i] < Q_a_o[i]:
                    #Insufficient heat overall
                    Q_a[i] = 0
                    m_achx[i] = 0
                else:
                    Q_a[i] = Q_a_o[i]
                    m_achx[i] = Q_a[i]/(Cp_w*(T_t[i] - T_set[i]))

                #Update bypass mass flow
                m_bp[i] = V_t[i]-m_achx[i]

                #No PGEN allowed during startup of ACHX or when ACHX not on
                m_pgen[i],Q_p[i],delta_p[i] = 0,0,0

        else:
            "ACHX was either operational or the internal temperature was above setpoint"
```

```
#ACHX was operational, wat is the flow through ACHX?
m_achx_min[i] = ratio*V_t[i]

m_A = m_achx_min[i]
m_P = V_t[i]-m_A

Q_A = m_A*Cp_w*(T_t[i]-T_set[i])
Q_P = m_P*Cp_w*(T_t[i]-T_set[i])

"Is the remaining heat such that PGEN can operate?"
if Q_P < P_low:
    #Heat is not sufficient to maintain PGEN operation
    delta_p[i] = 0
    delta_q = 0

else:
    #Heat is sufficient to maintain PGEN operation
    if delta_p[i-1]>0:
        #PGEN was in operation, thus maintain operation
        if i*5 >= trip_time and i*5 <= trip_time + trip_delay: #Time of forced trip
            delta_p[i] = 0
            delta_q = 0
        else:
            delta_p[i] = 1
            delta_q = 1

            t_0 = 0
            t_sp = 0

    else:
        #PGEN was not in operation, thus start-up procedure continued
        t_0 = t_0 + 5
        if Q_P > P_restart:
            t_sp = t_sp + 5
            if t_0 <= t_cw+t_sp:
                "Warm Start Procedure"
                if t_sp > t_w:
                    delta_p[i] = 1
                    delta_q = 1

                else:
                    delta_p[i] = 0
                    delta_q = 1
            else:
                "Cold Start Procedure"
                if t_sp > t_c:
                    delta_p[i] = 1
                    delta_q = 1
                else:
                    delta_p[i] = 0
                    delta_q = 1
        else:
            t_sp = 0

            delta_p[i] = 0
            delta_q = 0
```

```
if delta_q == 0:
    #Heat transfer not allowed in PGEN, all through ACHX
    m_pgen[i] = 0
    m_achx[i] = V_t[i]

    Q_p[i] = 0
    Q_a[i] = Q_t[i]

    eta_th[i],p_eva[i],T_boil[i],W_net[i],Q_evap[i],m_wf[i] = 0,0,0,0,0,0

else:
    #Heat transfer allowed in PGEN, but can it operate?
    if delta_p[i] == 0:
        #Only heat transfer allowed at PGEN currently
        Q_p[i] = P_restart
        Q_a[i] = Q_t[i]-Q_p[i]

        m_pgen[i] = Q_p[i]/(Cp_w*(T_t[i]-T_set[i]))
        m_achx[i] = V_t[i]-m_pgen[i]

        PGEN_list = 0,0,0,0,Q_p[i],0

    else:
        #PGEN can operate without restriction
        m_achx[i] = V_t[i]*ratio
        m_pgen[i] = V_t[i]-m_achx[i]

        Q_a[i] = Q_A
        Q_p[i] = Q_P

        T_set_p[i] = T_t[i]-Q_p[i]/(m_pgen[i]*Cp_w)
        T_set_a[i] = T_t[i]-Q_a[i]/(m_achx[i]*Cp_w)

        PGEN_list = PGEN_Opt(T_t[i], m_pgen[i],T_set_p[i])

#Determine residual heat if any.
res = Q_t[i] - Q_p[i] - Q_a_o[i]

if res - Q_bp_a[i] > 0.001:
    Q_a[i] = res + Q_a_o[i]
    n_fan[i],p_fan[i], rpm[i] = ACHX(T_t[i], m_achx[i], Q_a[i]/1e6)
else:
    Q_a[i] = Q_a_o[i]
    n_fan[i],p_fan[i], rpm[i] = 0,0,0

#Define setpoint temperatures for all components
if m_pgen[i] > 0:
    T_set_p[i] = T_t[i] - Q_p[i]/(m_pgen[i]*Cp_w)
else:
    T_set_p[i] = T_set[i]

if m_achx[i] > 0:
    T_set_a[i] = T_t[i] - Q_a[i]/(m_achx[i]*Cp_w)
    #print(T_set_a[i])
else:
    T_set_a[i] = T_set[i]
```

```
    #Update internal temperature of ACHX
    if m_achx[i]>0:
        T_A_int[i] = (T_t[i]+T_set_a[i])/2
    else:
        T_A_int[i] = T_A_int[i-1]-(seconds*Q_a_o[i]/(Cp_w*mas_achx))

    Q_res[i] = Q_hs_t[i]-Q_a[i]-Q_p[i]
    m_bp[i] = m_hs_t[i]-m_achx[i]-m_pgen[i]

    T_cw2[i] = T_L+(Q_res[i]/(m_hs_t[i]*Cp_w))

    lst_hl = [V_t[i],T_set[i],Q_loss[i],Q_pipe[i],Q_tank[i]]
    heatloss_df.loc[len(heatloss_df)] = lst_hl

    lst_res = [i*5,V_t[i],T_t[i],Q_t[i]+Q_loss[i],Q_t[i],Q_loss[i],T_set[i],T_set_a[i],m_achx[i],
               Q_a[i],n_fan[i],rpm[i],T_set_p[i],m_pgen[i],Q_p[i],eta_th[i],p_eva[i],T_boil[i],
               m_bp[i],W_net[i],Q_res[i],T_cw2[i],delta_p[i],delta_q,t_sp,t_0,T_A_int[i],Q_bp_a[i]]

    results_df.loc[len(heatloss_df)] = lst_res

heatloss_df.to_excel('1_WP_025.xlsx')
results_df.to_excel('1_WP_025.xlsx')
```

7

APPENDIX G – SAMPLE SCRIPT FOR DADP

```
"""
Initialisation and loading of modules the same as for WP
    Removed for conciseness of appendix
"""

print("Initialisation done...")

print("Solving...")

def maxPGEN(V_t,T_t,T_set,m_achx_min,Q_a_o):

    m_pgen_min = (Q_t-Q_a_o)/(Cp_w*(T_t-T_amb))

    m_achx_1 = m_achx_min
    m_achx_2 = V_t - m_pgen_min

    tolerance = 0.25
    T_p1 = T_set

    i=0

    m_pgen_left = m_pgen_min
    m_pgen_right = V_t - m_achx_min

    while abs(m_pgen_left-m_pgen_right) > tolerance and T_p1>T_amb:
        Q_a = Q_a_o
        Q_p = Q_t-Q_a

        m_pgen_mid = (m_pgen_left+m_pgen_right)/2

        T_pr = T_t-Q_p/(m_pgen_right*Cp_w)
        T_pm = T_t-Q_p/(m_pgen_mid*Cp_w)
        T_pl = T_t-Q_p/(m_pgen_left*Cp_w)

        eta_th,p_eva,T_boil,W_net_left,Q_evap,m_wf = PGEN_Opt(T_t, m_pgen_left,T_pl)
        eta_th,p_eva,T_boil,W_net_mid,Q_evap,m_wf = PGEN_Opt(T_t, m_pgen_mid,T_pm)
        eta_th,p_eva,T_boil,W_net_right,Q_evap,m_wf = PGEN_Opt(T_t, m_pgen_right,T_pr)

        slope_left = (W_net_mid-W_net_left)/(m_pgen_mid-m_pgen_left)
        slope_right = (W_net_right-W_net_mid)/(m_pgen_right-m_pgen_mid)

        #case1: Near midpoint, squeeze
        if slope_left > 0 and slope_right < 0:
            #Peak is near midpoint, narrow both sides
            m_pgen_left = m_pgen_left + (m_pgen_mid-m_pgen_left)/2
            m_pgen_right = m_pgen_right - (m_pgen_right-m_pgen_mid)/2
        #case2: Both slopes are positive, shift to right
        elif slope_left > 0 and slope_right > 0:
            m_pgen_left = m_pgen_mid
        #case3: Slope is decreasing left, move to left
        else:
            m_pgen_right = m_pgen_mid

        i+=1
    m_pgen = m_pgen_mid
    m_achx = V_t-m_pgen
```

1

```
    eta_th,p_eva,T_boil,W_net,Q_evap,m_wf = PGEN_Opt(T_t, m_pgen,T_pm)
    fb_list = [eta_th,p_eva,T_boil,W_net,Q_evap,m_wf,m_pgen,m_achx,Q_t,T_pm]
    return(fb_list)

def DADP(i,V_t,T_t):

    delta_q = 0

    #Result List
    PGEN_list = [eta_th[i],p_eva[i],T_boil[i],W_net[i],Q_evap[i],m_wf[i],m_pgen[i],
                 m_achx[i],Q_t[i],T_pm[i]]

    "Use TSD to calculate setpoint temperature en remove this heat from available"
    TSD_list = [Q_loss[i],Q_pipe[i],Q_tank[i],T_drop[i],T_set[i]]
    TSD_list = heatLoss.CalculateQT(T_amb, T_L, V_t, pipe_p, insu_p, tank_p, t_insu_p)
    Q_t[i]=Q_t[i]-Q_loss[i]

    "--- Determine the heat loss from ACHX for n=0"
    Q_a_o[i] = (0.0002259*pow(T_t,1.701631))*1e6

    """1. Check if there is enough heat transfer available to allow min flow in ACHX
        if not, then bypass all the flow, if there is then flow can be distributed"""
    if Q_t[i] < Q_a_o[i]:
        #Bypass all the flow
        m_achx[i],m_pgen[i],Q_a[i],Q_p[i],delta_p[i] = 0,0,0,0,0
        m_bp[i] = V_t

        #Update the internal heat transfer for stagnant water and update internal Temperature
        T_A_int[i] = T_A_int[i-1] - (Q_a_o[i]*seconds)/(mas_achx*Cp_w)

        #Set points for ACHX and PGEN is invalid - assign default
        T_set_a[i],T_set_p[i] = T_set[i],T_set[i]

    else:
        "There is enough heat, but was ACHX operational and internal temp above setpoint?"
        if m_achx[i-1] == 0 and T_A_int[i-1]<T_set[i]:
            #ACHX needs to be restarted - SAAR
            Q_delta_A[i] = mas_achx*Cp_w*(T_set[i]-T_A_int[i-1])

            #Required heat transfer rate at ACHX
            Q_des_bp = (Q_a_o[i]*seconds)+Q_delta_A[i]
            Q_des_bp = Q_des_bp/seconds

            if Q_t[i]-Q_des_bp > Q_a_o[i]:
                #Sufficient heat to transfer at ACHX for restart
                #No fans during startup of ACHX
                Q_a[i] = Q_a_o[i]
                m_bp[i] = (Q_delta_A[i]/300)/(Cp_w*(T_set[i]-T_A_int[i-1]))

                "Is the remaining heat such that PGEN can operate?"
                delta_p[i],delta_q, t_sp, t_0 = regime(Q_t[i], Q_des_bp, P_low,
                                                       delta_p[i-1], trip, i, restart_Q,
                                                       t_sp,t_0)

                if T_A_int[i-1]>T_set[i]:
                    m_achx[i] = Q_a[i]/(Cp_w*(T_A_int[i-1]-T_set[i]))
                else:
```

```
            m_pgen[i] = V_t[i]-m_achx[i]-m_bp[i]
            Q_p[i] = restart_Q
            PGEN_list = 0,0,0,0,Q_p[i],0,0,0,0,0
        else:
            m_pgen[i] = 0
            PGEN_list = 0,0,0,0,0,0,0,0,0,0

    else:
        #Insufficient heat for ACHX in one timestep
        if Q_t[i] < Q_a_o[i]:
            #Insufficient heat overall
            Q_a[i] = 0
            m_achx[i] = 0
        else:
            Q_a[i] = Q_a_o[i]
            m_achx[i] = Q_a[i]/(Cp_w*(T_t[i] - T_set[i]))

        #Update bypass mass flow
        m_bp[i] = V_t[i]-m_achx[i]

        #No PGEN allowed during startup of ACHX or when ACHX not on
        m_pgen[i],Q_p[i],delta_p[i] = 0,0,0

else:
    "ACHX was either operational or the internal temperature was above setpoint"
    #ACHX was operational, wat is the minimum flow through ACHX?
    m_achx_min[i] = Q_a_o[i]/(Cp_w*(T_t[i]-T_set[i]))

    m_A = m_achx_min[i]
    m_P = V_t[i]-m_A

    Q_A = m_A*Cp_w*(T_t[i]-T_set[i])
    Q_P = m_P*Cp_w*(T_t[i]-T_set[i])

    "Is the remaining heat such that PGEN can operate?"
    if Q_P < P_low:
        #Heat is not sufficient to maintain PGEN operation
        delta_p[i] = 0
        delta_q = 0

    else:
        #Heat is sufficient to maintain PGEN operation
        if delta_p[i-1]>0:
            #PGEN was in operation, thus maintain operation
            if i*5 >= trip_time and i*5 <= trip_time + trip_delay: #Time of forced trip
                delta_p[i] = 0
                delta_q = 0
            else:
                delta_p[i] = 1
                delta_q = 1

                t_0 = 0
                t_sp = 0

        else:
            #PGEN was not in operation, thus start-up procedure continued
            t_0 = t_0 + 5
```

```
            if Q_P > P_restart:
                t_sp = t_sp + 5
                if t_0 <= t_cw+t_sp:
                    "Warm Start Procedure"
                    if t_sp > t_w:
                        delta_p[i] = 1
                        delta_q = 1

                    else:
                        delta_p[i] = 0
                        delta_q = 1
                else:
                    "Cold Start Procedure"
                    if t_sp > t_c:
                        delta_p[i] = 1
                        delta_q = 1
                    else:
                        delta_p[i] = 0
                        delta_q = 1
            else:
                t_sp = 0

                delta_p[i] = 0
                delta_q = 0

    if delta_q == 0:
        #Heat transfer not allowed in PGEN, all through ACHX
        m_pgen[i] = 0
        m_achx[i] = V_t[i]

        Q_p[i] = 0
        Q_a[i] = Q_t[i]

        eta_th[i],p_eva[i],T_boil[i],W_net[i],Q_evap[i],m_wf[i] = 0,0,0,0,0,0

    else:
        #Heat transfer allowed in PGEN, but can it operate?
        m_achx[i] = Q_a_o[i]/(Cp_w*(T_t[i]-T_set[i]))

        if delta_p[i] == 0:
            #Only heat transfer allowed at PGEN currently
            Q_p[i] = P_restart
            Q_a[i] = Q_t[i]-Q_p[i]

            m_pgen[i] = Q_p[i]/(Cp_w*(T_t[i]-T_set[i]))

            PGEN_list = 0,0,0,0,Q_p[i],0,0,0,0,0

        else:
            #PGEN can operate without restriction
            #Find the ideal flow to be distributed to PGEN
            PGEN_list = maxPGEN(V_t, T_t, T_set, m_achx_min, Q_a_o)
            m_achx[i] = V_t[i]-m_pgen[i]

            T_set_p[i] = T_t[i]-Q_p[i]/(m_pgen[i]*Cp_w)
            T_set_a[i] = T_t[i]-Q_a[i]/(m_achx[i]*Cp_w)
```

```
                T_set_p[i] = T_t-Q_p[i]/(m_pgen[i]*Cp_w)
                T_set_a[i] = T_t-Q_a[i]/(m_achx[i]*Cp_w)

            #Determine residual heat if any.
            res = Q_t[i] - Q_p[i] - Q_a_o[i]

            if res - Q_bp_a[i] > 0.001:
                Q_a[i] = res + Q_a_o[i]
                n_fan[i],p_fan[i], rpm[i] = ACHX(T_t, m_achx[i], Q_a[i]/1e6)
            else:
                Q_a[i] = Q_a_o[i]
                n_fan[i],p_fan[i], rpm[i] = 0,0,0

            #Define setpoint temperatures for all components
            if m_pgen[i] > 0:
                T_set_p[i] = T_t - Q_p[i]/(m_pgen[i]*Cp_w)
            else:
                T_set_p[i] = T_set[i]

            if m_achx[i] > 0:
                T_set_a[i] = T_t - Q_a[i]/(m_achx[i]*Cp_w)
            else:
                T_set_a[i] = T_set[i]

    #Update internal temperature of ACHX
    if m_achx[i]>0:
        T_A_int[i] = (T_t+T_set_a[i])/2
    else:
        T_A_int[i] = T_A_int[i-1]-(seconds*Q_a_o[i]/(Cp_w*mas_achx))

    Q_res[i] = Q_hs_t[i]-Q_a[i]-Q_p[i]
    m_bp[i] = m_hs_t[i]-m_achx[i]-m_pgen[i]

    T_cw2[i] = T_L+(Q_res[i]/(m_hs_t[i]*Cp_w))

    lst_hl = [V_t,T_set[i],Q_loss[i],Q_pipe[i],Q_tank[i]]
    heatloss_df.loc[len(heatloss_df)] = lst_hl

    lst_res = [i*5,V_t,T_t,Q_t[i]+Q_loss[i],Q_t[i],Q_loss[i],T_set[i],T_set_a[i],m_achx[i],
               Q_a[i],n_fan[i],rpm[i],T_set_p[i],m_pgen[i],Q_p[i],eta_th[i],p_eva[i],T_boil[i],
               m_bp[i],W_net[i],Q_res[i],T_cw2[i],delta_p[i],delta_q,t_sp,t_0,T_A_int[i],Q_bp_a[i]]

    results_df.loc[len(heatloss_df)] = lst_res

for i in range(runto):
    DADP(i,V_t[i],T_t[i])

heatloss_df.to_excel('2_DADP.xlsx')
results_df.to_excel('2_DADP.xlsx')
```

APPENDIX H – SCRIPT FOR DAFP

```
"""
Initialisation and loading of modules the same as for DADP
DADP also not provided in full, refer to previous Appendix
    Removed for conciseness of appendix

Additional imports and initialisations shown
"""
import math
import fluids

#Gas Cooler Parameters
m_hs_des = 80
m_fg_des = 25

m_hs_min = 5
m_hs_max = 120

#Loading of Additional Gas Cooler Parameters
T_fg_name = "Temperature Flue Gas"
cp_name = "CP_fg"
mfg_name = "Mass Flow Flue Gas"

T_fg_t = df[temp_fg_name].tolist()
Cp_t = df[cp_name].tolist()
m_fg_t = df[mfg_name].tolist()

#Initialisation
T_fg_UL = 350

print("Initialisation done...")
print("Solving...")

def maxPGEN(V_t,T_t,T_set,m_achx_min,Q_a_o):
    """
    As in previous appendix, focusing on DADP
    """

def CWFR(T_t,T_set, T_set_fg,T_fg,m_hs,m_fg,Cp_fg):
    #Assign minimum flow possible from circulation pumps
    m_hs = m_hs_min

    #step for flow rate adjustment
    m_step = 0.1

    #Initialise results list
    CFWR_list = [m_hs_max, m_hs_min,T_hs_max,T_hs_min]

    while m_hs != m_hs_max:
        def CalcFlow():
            m_hs_frac = (m_hs/m_hs_des)**0.4
            m_fg_frac = (m_fg/m_fg_des)**0.4

            UA = UA_des*m_hs_frac*m_wf_frac

            hs = Fluid(FluidsList.Water).with_state(Input.pressure(P_w_in*100e3),
                                                    Input.temperature(T_w_in))
            Cp_hs = hs.specific_heat*(u.J/(u.kg*u.K))

            Cmin = min(Cp_hs*m_hs,Cp_fg*m_fg)
            Cmax = max(Cp_hs*m_hs,Cp_fg*m_fg)
            Cr = Cmin/Cmax

            NTU = UA/Cmin
```

```
            eff_n = 1-math.exp(-NTU*(1-Cr))
            eff_d = 1-(Cr*math.exp(-NTU*(1-Cr)))
            eff = (eff_n)/(eff_d)

            Q_hs = eff*Cmin*(T_fg-T_set)

            T_hs = T_set + Q_hs/(m_hs*Cp_hs)
            T_fg = T_fg + Q_hs/(m_fg*Cp_fg)

        while T_fg > T_fg_UL:
            m_hs = m_hs + m_step
            Calc_flow()
        while T_hs > T_H:
            m_hs = m_hs + m_step
            Calc_flow()

        #After breaking the "whiles", the minimum flow rate and maximum hs temperature
        #is determined
        m_hs_min = m_hs
        T_hs_max = T_hs

        while T_fg < T_fg_LL:
            m_hs = m_hs + m_step
            Calc_flow()

        m_hs = m_hs - m_step
        m_hs_max = m_hs

    if m_hs == V_t_max:
        m_hs = (m_hs_max+m_hs_min)/2
        CalcFlow()
        T_mid = T_hs

        CFWR_list = m_hs_max, m_hs_min,T_max,T_min,T_mid
    return(CFWR_list)

def DADP(i,m_hs,T_hs):
    """
    As in previous appendix, focusing on DADP
    """

def DAFP(i,m_hs,T_hs):

    #First, run CWFR to determine the range of allowable flow for cooling water
    CWFR(T_hs,T_set,T_set_fg,T_fg,m_hs,m_fg,Cp_fg)

    #Initialise iterative process
    tolerance = 0.5
    j=0

    #Determine performance at boundaries
    m_hs_left = m_hs_min[i]
    m_hs_right = m_hs_max[i]

    while abs(m_hs_left-m_hs_right) > tolerance:

        m_hs_mid = (m_hs_left+m_hs_right)/2

        lst_res_l = DADP(i,m_hs_left,T_hs_max[i])
        lst_res_m = DADP(i,m_hs_mid,T_hs_mid[i])
        lst_res_r = DADP(i,m_hs_right,T_hs_min[i])

        W_net_m = lst_res_m[20]
        W_net_l = lst_res_l[20]
        W_net_r = lst_res_r[20]

        slope_left = (W_net_m-W_net_l)/(m_hs_mid-m_hs_left)
        slope_right = (W_net_r-W_net_m)/(m_hs_right-m_hs_mid)
```

```
        #case1: Near midpoint, squeeze
        if slope_left > 0 and slope_right < 0:
            #Peak is near midpoint, narrow both sides
            m_hs_left = m_hs_left + (m_hs_mid-m_hs_left)/2
            m_hs_right = m_hs_right - (m_hs_right-m_hs_mid)/2


         #case2: Both slopes are positive, shift to right
         elif slope_left > 0 and slope_right > 0:
             m_hs_left = m_hs_mid
         #case3: Slope is decreasing left, move to left
         else:
             m_hs_right = m_hs_mid

         j+=1

    #Maximum net power generation at midpoint flow confirmed
    m_hs = m_hs_mid
    T_hs = T_hs_mid

    #Run DADP with the final adjusted cooling water flow rate and temperature
    DADP(i,m_hs,T_hs)

DAFP(i,V_t[i],T_t[i],T_set_fg[i],T_fg[i],m_hs[i],m_fg[i],Cp_fg[i])

heatloss_df.to_excel('3_DAFP.xlsx')
results_df.to_excel('3_DAFP.xlsx')
```

APPENDIX I – SCRIPT FOR DAFP-T

```
"""
Initialisation and loading of modules the same as for DAFP
Repeated formulas also removed, refer to previous appendix.
    Removed for conciseness of appendix

Additional imports and initialisations shown
"""

#Desired cooling water energy
Q_hs_req = 1.8e9
Q_hs_req_dot = Q_hs_req/seconds

#TESS Parameters
Q_tess_cap = 54e9
T_diff_max = 15
T_pc_mat = 180

Q_tess_loss = 4.1/100

print("Initialisation done...")
print("Solving...")

def maxPGEN(V_t,T_t,T_set,m_achx_min,Q_a_o):
    """
    As in previous appendix, focusing on DADP
    """


def CWFR(T_t,T_set, T_set_fg,T_fg,m_hs,m_fg,Cp_fg):
    """
    As in previous appendix, focusing on DAFP
    """


def DADP(i,m_hs,T_hs):
    """
    As in previous appendix, focusing on DADP
    """


def DAFPT(i,m_hs,T_hs):
    #First, run CWFR to determine the range of allowable flow for cooling water
    CWFR(T_hs,T_set,T_set_fg,T_fg,m_hs,m_fg,Cp_fg)

    #Initialise iterative process
    tolerance = 0.5
    j=0

    #Determine performance at boundaries
    m_hs_left = m_hs_min[i]
    m_hs_right = m_hs_max[i]

    while abs(m_hs_left-m_hs_right) > tolerance:

        m_hs_mid = (m_hs_left+m_hs_right)/2

        lst_res_l = DADP(i,m_hs_left,T_hs_max[i])
        lst_res_m = DADP(i,m_hs_mid,T_hs_mid[i])
        lst_res_r = DADP(i,m_hs_right,T_hs_min[i])

        W_net_m = lst_res_m[20]
        W_net_l = lst_res_l[20]
        W_net_r = lst_res_r[20]
```

```
        slope_left = (W_net_m-W_net_l)/(m_hs_mid-m_hs_left)
        slope_right = (W_net_r-W_net_m)/(m_hs_right-m_hs_mid)

        #case1: Near midpoint, squeeze
        if slope_left > 0 and slope_right < 0:
            #Peak is near midpoint, narrow both sides
            m_hs_left = m_hs_left + (m_hs_mid-m_hs_left)/2
            m_hs_right = m_hs_right - (m_hs_right-m_hs_mid)/2
        #case2: Both slopes are positive, shift to right
        elif slope_left > 0 and slope_right > 0:
            m_hs_left = m_hs_mid
        #case3: Slope is decreasing left, move to left
        else:
            m_hs_right = m_hs_mid

        j+=1


    #Maximum net power generation at midpoint flow confirmed
    m_hs = m_hs_mid
    T_hs = T_hs_mid

    """TESS CAPABILITY"""
    #Adjust cooling water flow rates and temperatures to be distributed between
    #PGEN and ACHX

    Q_tess_loss_t = Q_tess*Q_tess_loss

    Cp_hs = hs.specific_heat*(u.J/(u.kg*u.K))
    Q_hs_t = Cp_hs*m_hs*(T_hs-T_set)

    #Is there enough heat in cooling water:
    if Q_hs_t<Q_req:
        #Heat transfer to cooling water required
        if T_hs > T_pc_mat:
            #Heat can be transferred to the cooling water as is, but is it enough?
            Q_dis = min(m_hs*Cp_hs*seconds*(T_pc_mat-T_hs),Q_hs - Q_req, Q_tess)

            if Q_hs + Q_dis < Q_req:
                #Additional stream of cooling water required to transfer heat
                Q_add = min(Q_tess,Q_req-Q_dis-Q_hs_t)
                m_add = Q_add/(Cp_hs*T_diff_max)
        else:
            #Additional stream of cooling water required to transfer heat
            Q_add = min(Q_tess,Q_req-Q_dis-Q_hs_t)
            m_add = Q_add/(Cp_hs*T_diff_max)

    else:
        #Heat transfer to cooling not required, use excess to recharge TESS
        if T_hs < T_pc_mat:
            #Excess energy can be used to charge the TESS
            Q_charge = min(m_hs*Cp_hs*seconds*(T_hs-T_pc_mat),Q_tess_cap-Q_hs_t) + Q_tess_loss_t

    Q_tess = Q_tess + Q_charge - Q_dis - Q_add - Q_tess_loss_t
    Q_hs_t = Q_hs_t - Q_charge + Q_dis + Q_add

    T_hs = T1 + Q_hs_t/(Cp_hs*(m_hs+m_add))
    m_hs = m_hs + m_add/seconds

    #Run DADP with the final adjusted cooling water flow rate and temperature
    DADP(i,m_hs,T_hs)


DAFPT(i,V_t[i],T_t[i],T_set_fg[i],T_fg[i],m_hs[i],m_fg[i],Cp_fg[i])

heatloss_df.to_excel('4_DAFPT.xlsx')
results_df.to_excel('4_DAFPT.xlsx')
```

APPENDIX J – PUBLISHED ARTICLE

energies

MDPI

Article

Energy Recovery Maximisation Modelling Subject to Constrained Cooling

Johannes Petrus Bester [1,*], Martin Van Eldik [1] and Philip van Zyl Venter [2]

[1] School of Mechanical Engineering, North-West University, Potchefstroom 2520, South Africa; martin.vaneldik@nwu.ac.za
[2] School of Industrial Engineering, University of Stellenbosch, Stellenbosch 7602, South Africa; philipzventer@sun.ac.za
* Correspondence: 23461357@mynwu.ac.za

Abstract: The primary heat rejection cycle, which is critical for the stability and integrity of the metal production process and equipment, involves the transfer of heat from flue gas to a fluid circulated through a gas-cooler. The rate of heat transfer from the flue gas is influenced by several parameters, including the temperature of the cooling fluid. Heat transfer rates that are too high or too low can negatively impact equipment's life, emphasising the need for a temperature operational envelope in the cooling fluid prior to entering the gas-cooler. Rejected heat is used for power generation, transferred to the environment, or both. This study examines the impact of control philosophies on both temperature and power generation, while maintaining the exit temperature within the desired range as the highest priority. A more advanced philosophy that combines bypass control with feedforward parameters can maintain temperatures within safe operating limits at all times, while improving the power generation, compared to a typical works approach which is used as a baseline. This study presents a formulation that increased power generation from an average of 6.11 MW for a typical works philosophy to 10.68 MW, while maintaining the temperature within the operating temperature envelope.

Keywords: thermal management; heat rejection; air-cooled heat exchanger; waste heat; transient modelling; temperature control

check for updates

Citation: Bester, J.P.; Van Eldik, M.; Venter, P.v.Z. Energy Recovery Maximisation Modelling Subject to Constrained Cooling. *Energies* **2024**, *17*, 131. https://doi.org/10.3390/en17010131

Academic Editor: Marco Marengo

Received: 30 October 2023
Revised: 7 December 2023
Accepted: 19 December 2023
Published: 25 December 2023

Copyright: © 2023 by the authors. Licensee MDPI, Basel, Switzerland. This article is an open access article distributed under the terms and conditions of the Creative Commons Attribution (CC BY) license (https://creativecommons.org/licenses/by/4.0/).

1. Introduction

Steel production accounts for approximately 4.8% of global energy use, with an estimated 48.0% of wasted energy input [1]. Production processes, such as a blast furnace (BF), a basic oxygen furnace (BOF), and an electric arc furnace (EAF), use energy to convert input materials into desired products. These processes also produce an energy stream as a secondary product in the form of high-temperature flue gas [2]. The carbon–oxygen reaction within a BOF converter produces flue gas at temperatures between 1200 and 1500 °C [3].

Heat is transferred from the flue gas in the gas-cooler. A gas-cooler is a heat exchanger that typically has internal channels for a fluid to pass through and absorb heat from a high-temperature flue gas. The flue gas leaving the gas-cooler needs to be at least below 727 °C at all times to prevent the short-term overheating of downstream pipes and equipment [4]. This temperature requirement drops to below 454 °C to reduce the risk of long-term overheating [4]. A lower temperature limit is also in place to prevent acid-dew point corrosion, with the specific value dependent on the composition of the flue gas [5].

Among other factors, the rate of heat transfer from one fluid to another is influenced by the temperature and mass flow of both fluids [6]. The mass flow rate and the temperature of the flue gas typically depend on a specific process. It follows that the mass flow and the temperature of the heat-absorbing fluid are controlled to ensure that sufficient cooling of the flue gas is achieved.

Studies such as [7] can be used to design a heat exchanger for maximum heat transfer performance by considering the expected hot and cold stream parameters. The study by the authors of [7] determines the required number and height of fins to maximise heat transfer from exhaust gases.

The heat transferred from flue gas is referred to as waste heat. A fluctuating waste heat profile is commonly encountered in practical industrial scenarios such as steel production [8]. This variability arises from changes in production demand, fluctuations in ambient conditions, and other dynamic factors inherent to the process. Therefore, the effective management of the fluctuating waste heat profile is essential for maintaining the efficiency and the performance of the heat exchange system, while ensuring the cooling fluid is operated within the allowable temperature envelope. A temperature setpoint is a predetermined target temperature value used for reference in temperature control systems.

Advanced control strategies and predictive algorithms have been developed to manage the waste heat fluctuations effectively. These methods dynamically adjust the temperature setpoint in response to variations in the waste-heat source. This adaptive approach ensures that the temperature of the heat-absorbing fluid remains within the desired envelope, even when faced with fluctuations in the waste-heat source.

Furthermore, the temperature of the heat-absorbing fluid entering the gas-cooler is typically constrained within a specific range, defined by the lower and upper threshold temperature values. This heat-absorbing fluid circulates in a closed-loop cycle, in which the absorbed heat must be efficiently transferred to the surrounding environment or another industrial process. In this study, heat was transferred to the environment or to a power generation system.

This process of transferring heat to the environment or to a power generation system is hereafter referred to as the "heat rejection process". The conventional approach to heat rejection from the flue gas involves the use of air-cooled heat exchangers to release heat into the environment [9]. However, with the increasing need for metal producers to stay competitive, waste-heat utilisation is becoming more prevalent in production plants.

In response to this shift, production plants are continuously exploring integrated heat rejection processes that combine both conventional heat removal and waste-heat utilisation methods. The development of specific control strategies is essential for the effective temperature management of these integrated systems.

Controlled heat transfer processes can be applied to ensure that the setpoint temperature is maintained. A study [10] attempted to automate and control a thermal mixing process. To achieve this, an accurate dynamic model of the process was formulated based on the conservation of mass and energy. The dynamic model was then used to predict the temperature response in the tank when process changes were implemented. This prediction was then used to adjust the heat-transfer rate to limit the difference to the target temperature.

A study by the authors of [11] focused on an organic Rankine cycle (ORC) that operates under fluctuating and intermittent heat sources. Solutions to the challenges posed by a fluctuating heat source can be grouped into two main categories: the damping of fluctuations and the accommodation through stream control. Conventional stream control methods include bypassing the energy source and transferring thermal energy to the ambient environment [12]. Within the ORC, adjustments are made to the flow rate of the working fluid to match the heat-source fluctuations [13].

The study by the authors of [11] also investigated multiple proportional-integral-derivative (PID)-based controllers and concluded that, even though PID controllers are easy to implement, control performance is often unsatisfactory with a fluctuating heat source. The study then evaluated advanced control methods, including both linear and nonlinear predictive control [14], supervisory predictive control [15], dynamic programming [16], optimal control [17], and extremum-seeking control [18]. These control methods delivered higher control performance, but this performance is highly dependent on the accuracy of the fluctuation prediction.

Heuristic control methods are, therefore, advised in the studies of [19,20]. Fluctuating heat sources also present challenges owing to the mechanical restrictions of rotating equipment, poor control performance, and an inability to achieve real-time optimal control, owing to the nonlinearity of an ORC system [11].

All the methods investigated above focus on controlling the rate of heat transfer in a single heat transfer process to match a fluctuating supply. A relevant addition to the current study is the use of multiple heat transfer components and the designation of the flow distribution for each component.

The work in [21] focused on a neural-network-based, model-predictive controller (MPC) for temperature control within a heat exchanger network (HEN). Parallel heat exchangers were observed within the HEN. The control method proved to be a significant improvement on a conventional MPC; however, the temperature controller did not adjust the flow rates to individual heat exchangers. This resulted in the flow being equally split between the heat exchangers.

A study conducted in [22] used fuzzy logic controllers to improve the energy efficiency of a small HEN. Within this HEN, the high-temperature fluid was distributed between two branches that had a total of three identical heat exchangers. This resulted in a difference in the heat-transfer rate capability between the branches. None of the heat exchangers within the HEN could be used to generate electrical power. The efficiency improvement was realised by minimising the coolant fluid flow induced by the pump. No additional objectives have been reported.

In [23], the conventional approach to flow distribution control in an HEN was changed in an attempt to increase heat recovery. The conventional approach involves an even split in the volume flow between the branches. The heat exchangers within each branch have different heat transfer capabilities. In the study, a PID controller was used to adjust the flow split between the two branches to maintain identical temperatures between the outlets of each branch. This resulted in an improvement in the total heat recovery.

The heat rejection process used in this study can distribute the waste heat to two separate processes: a power generation cycle and an air-cooled heat exchanger. In addition, the power-generation component has varying efficiencies based on the supplied flow and temperature.

The goal of this paper is to formulate a control philosophy that uses both the air-cooled heat exchanger and the power generation methods in parallel to maximise energy recovery, while still adhering to all critical process constraints.

The novel contribution of this paper includes the formulation of three control philosophies that consider the stochastic effect of a fluctuating heat source and maximise the energy recovered, even in the event of sudden changes in heat transfer capabilities, such as the power generation system becoming unavailable.

2. System and Model Description

2.1. Process Description

The original cooling cycle consisted of a circulation pump, gas-cooler, multiple air-cooled heat exchangers, and a holding tank. The design of this cooling cycle was completed with water as the selected cooling fluid. With the aim of waste-heat recovery, a power generation cycle was designed and retrofitted in parallel to the existing air-cooled heat exchangers.

During the design and construction phase of the power generation cycle, no other changes were made to the existing cooling cycle. Water remained the designated cooling fluid absorbing heat from the flue gas.

The resulting cooling cycle is displayed in Figure 1. Valves were used to designate the flow to each stream by adjusting the opening from 0 to 100%. From Figure 1, three distinct heat streams can be identified.

The first heat stream flows to air-cooled heat exchangers (ACHX). In the ACHX, ambient air is used to absorb heat from the high-temperature water through forced convection.

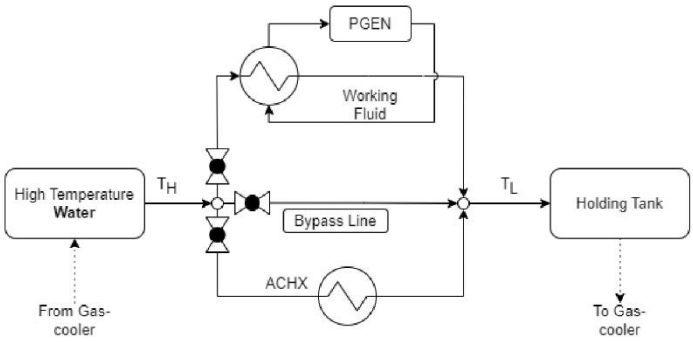


Figure 1. Rejecting the heat from the cooling fluid.

The second heat stream flows to a power generation cycle (PGEN). In the PGEN, a working fluid is used to absorb heat from the high-temperature water. This heat is then used as the heat source in a Rankine cycle to generate electrical power.

The last heat stream is the bypass line (BP) where no heat is transferred. Therefore, this will typically be used in low-heat conditions. The water exiting the gas-cooler at a temperature near the target temperature for water entering the gas-cooler is regarded as a low-heat condition.

After the high temperature water passes through a combination of the three branches, it then enters the holding tank at a lower temperature, T_L.

2.2. The Applicable Component and Process Limitations

To demonstrate the control philosophy, a typical production process and historical data are required. In this section, the relevant representative processes and design parameters are discussed.

The supplied design and operational parameters in this section are from an actual plant with additional information taken from the relevant literature to assign realistic parameters, where required.

The gas-cooler temperature limitations are listed in Table 1, along with the setpoint temperature of the control philosophy.

Table 1. Process and temperature envelope values for the cooling water.

Node	Parameter	Unit	Value
-	Maximum Pressure	bar	90
Exit of Gas-cooler	Upper Temperature	°C	280
	Lower Temperature	°C	230
Entry of Gas-cooler	Temperature Setpoint	°C	180
	Lower Threshold Temperature	°C	180
	Upper Threshold Temperature	°C	220

The temperature range expected for the cooling water exiting the gas-cooler is 230–280 °C, according to historical data for this specific plant. Note that the flue gas is at a significantly higher temperature. The Carnot thermal efficiency indicates that higher efficiencies can be achieved in the power generation cycle if the heat source temperature is increased. A higher temperature for the water exiting the gas-cooler can theoretically be achieved by reducing the flow rate.

However, the maximum pressure is achievable within the cooling cycle in combination with water, as the cooling fluid does not allow for higher temperature. Higher temperatures would lead to phase changes within the gas-cooler, significantly impacting the heat transfer

achieved. The loss of cooling in localised areas of the gas-cooler can have potentially severe consequences.

The potential increase in thermal efficiencies, as a result of higher temperatures entering the power generation cycle, can therefore not be pursued. It also follows that the mass flow of the cooling water should not be reduced in order to increase the temperature.

The gas-cooler design and the process parameters are used to determine the operational temperature envelope for the cooling water entering the gas-cooler. The upper threshold value of 220 °C would, according to design calculations and flow rates, result in water exiting the gas-cooler below the upper temperature limit. For this system and this specific process, a lower threshold limit of 180 °C will prevent acid-dew point corrosion on the gas-cooler walls. With the objective of maximum waste heat utilisation, the target temperature is set as low as possible within the operational temperature envelope.

The individual components also have their own sets of limitations and operational ranges.

The PGEN process converts the heat to electrical power with varying thermal efficiency. The thermal efficiency is the ratio of net power generation to the total heat supplied. The efficiency can be influenced by various parameters, one of which is the heat source temperature, as shown in Figure 2.

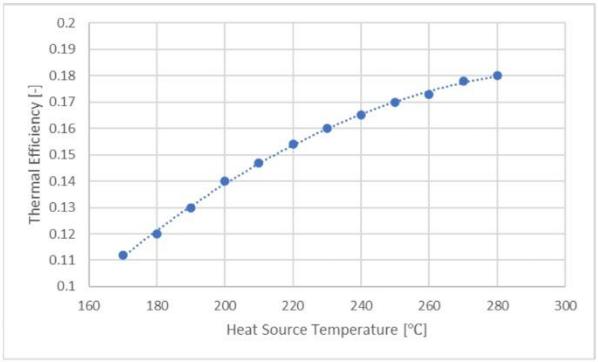


Figure 2. Thermal efficiency of converting waste heat to electrical power as a function of heat source temperature [24] for a fixed mass flow of cooling water.

The PGEN cycle in this system is similar to that used in [24], with pentane as the selected working fluid. A thermal efficiency curve similar to that in [24] is, therefore, used to determine the power generated within the cooling process, as shown in Figure 2.

The thermal efficiency curve in Figure 2 is for a fixed mass flow of the heat source. However, since the heat source has a fluctuating temperature and flow rate profile, a varying mass flow rate is also considered in this study.

The operational limits of the PGEN system are supplied in Table 2. The maximum heat that can be assigned to the PGEN system is 100 MW. In combination with the thermal efficiency curve, the PGEN has a maximum power generation of 18 MW. According to [25], a PGEN cycle similar to the one used in this study can operate at partial load of 10%. This results in a minimum assigned heat transfer of 10 MW, which results in 1.8 MW of power generation at maximum thermal efficiency.

The pinch point (PP) is the minimum temperature difference between the hot and the cold stream of a heat exchanger. The minimum pinch point achievable in both the evaporator and the condenser of the PGEN is 5 °C, as used in [24].

Note that the power generation can only adjust to the heat supplied at 2%/min, in line with the study in [26]. This is only a restriction on the power generated and not on the heat transferred by PGEN, since this restriction is based on controlled turbine adjustments rather than heat exchanger limitations.

Table 2. Design limitations of PGEN.

Parameter	Unit	PGEN
Assigned Heat Transfer	MW	$10 \leq Q_{PGEN} \leq 100$
Thermal Efficiency	-	$\eta_{th} \leq 0.18$
Power Generation [1]	MW	$1.8 \leq P_{PGEN} < 18$
Evaporator PP	°C	$T_{PP,e} \geq 5$
Condenser PP	°C	$T_{PP,c} \geq 5$
Power Generation Adjust	%/min	$P_{PGEN}^{Adj} \leq 2$

[1] Power generation limits assigned at maximum efficiency for heat source temperature.

When the flow to the PGEN is such that the PGEN cannot operate within this set of limitations, a trip will occur to limit potential damage to critical process equipment, such as turbines and pumps. A trip refers to any event where the PGEN does not transfer any heat from the cooling water and, therefore, also does not generate any power.

A trip occurrence is harmful to PGEN components such as the turbine [27]. To avoid frequent trips, a time delay is typically introduced. This delay is to ensure that sufficient heat is available for a certain period of time before restarting the PGEN.

The design limits for the ACHX system are displayed in Table 3. The term ACHX refers to a network of air-cooled heat exchangers. The collective capability of the ACHX can transfer all the available heat at 100 MW.

Table 3. Design and operational limitations of ACHX.

Parameter	Unit	ACHX
Assigned Heat Transfer	MW	$0 \leq Q_{ACHX} \leq 100$
Adjustment Rate	MW/min	$Q_{ACHX}^{adj} \leq 4$

The thermal inertia in the heat exchanger tubes and the use of ambient air in the ACHX results in a delay for the ACHX to transfer the required heat from the distributed flow. In addition, the production plant also has a fixed rate at which the fan speed on the ACHX can be increased. This is due to an extreme scenario where the plant and the national power utility entered into an agreement regarding power demand. The failure to comply with the agreement can lead to financial penalties. As a result, the fixed rate of increasing the fan speed at the ACHX enables the plant to reduce the power demand in other processes.

Should the power demand of the production plant not be at critical levels, the only limitation on the performance adjustment is the transient response of the ACHX.

To ensure that the control formulation works as required at all times, a scenario where the production plant power consumption is at critical levels is used in this study.

In this scenario, the adjustment rate of the ACHX is constrained at 4 MW/min.

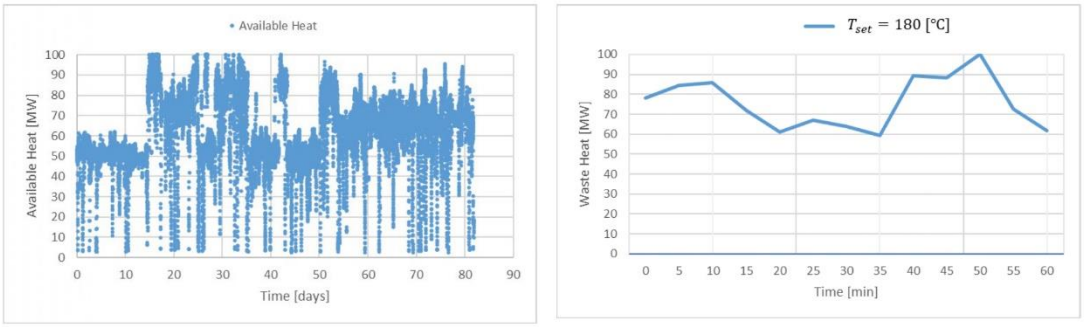
2.3. The Dataset for the Case Study

In this section, the historical dataset used to demonstrate the control philosophy is discussed.

A South African smelting plant provided a historical dataset for this study, under the condition that the values would be reworked and scaled to ensure anonymity. The gas-cooling systems in this study are applicable to various smelting operations, albeit under a different name.

In Figure 3a, a representative waste heat profile is illustrated, consisting of 83 days of entries at 5 min intervals. From this plot, significant fluctuations over time can be observed. A demonstrative dataset ranging 60 min is used for illustrative purposes, as shown in Figure 3b. This dataset enables the demonstration of the adjustments to the flow and heat

distributions between the three streams, including the influences on T_L and the changes observed with each formulation.



(**a**) (**b**)

Figure 3. (**a**) Representative dataset of available heat that can be transferred from the cooling fluid over 83 days. (**b**) Demonstrative dataset used in the demonstration.

The evaluation of power production and other performance parameters were still performed on the representative waste-heat profile in Figure 3a.

The modelling was completed within Microsoft Excel 2016 and Python 3.8, where several modules, such as NumPy 1.26.2 and Pandas 2.1.3, were used. The provided algorithms can be reproduced either within Pandas or other suitable codes.

3. The Formulation of the Control Philosophy

This section demonstrates the formulation of a control philosophy that aims to maximise power generation while ensuring that the temperature entering the gas-cooler is maintained within a suitable range when the production process is in operation.

The purpose of the control philosophy is to maximise power generation while adhering to all constraints. Unplanned stoppages of the PGEN can be used to evaluate the behaviour and the performance of the control philosophy adapting to the change in heat transfer capability. An unplanned stoppage is an unforeseen and sudden halt in the normal operation of a process that causes disruptions and potential production delays. For PGEN, this results in a loss in heat transfer capacity and power generation.

An unplanned stoppage is introduced in the use of both datasets in Figure 3. The average mean time between failures (MBTF) for the PGEN used in this study indicates that no more than one unplanned event can be introduced for both profiles. This is in agreement with the literature of [28]. Trips due to low heat availability are also included, as is discussed in the formulations below.

The importance of the heat rejection process in the main production process has been described in detail in previous sections. The flue gas leaving the gas-cooler needs to be within the safe operational temperature envelope. This is achieved by controlling the temperature of the cooling water entering the gas-cooler, referred to as T_L. A loss in the heat rejection capacity of the cooling system can potentially cause the cooling water temperature to move outside the operational envelope. This increases the risk of disruptions to the production process.

The gas-cooler operation adjusts the mass flow rate of the water depending on the temperature entering the gas cooler to ensure that a sufficient heat transfer is maintained. The mass flow of the cooling water, therefore, inherently considers the current gas-cooler heat transfer efficiency. The mass flow and temperature of the cooling water can thus be used alongside a target temperature to determine the available waste heat.

3.1. A Typical Works Philosophy

A typical works philosophy is proposed as a baseline. In this philosophy, the heat and flow distributions are fixed between all heat exchangers.

The control philosophy is described using binary operators and condition statements. Therefore, this section first describes all relevant parameters and the writing conventions and symbols used for each.

The conservation equation for energy, reproduced from [6], is:

$$Q_{res} = Q_{in} - Q_{out} \tag{1}$$

where Q_{res} is the change in energy for the control volume, while Q_{in} and Q_{out} are the energy flowing into and out the control volume. Since heat is either transferred out of the control volume through the PGEN or the ACHX, Equation (2) can be rewritten as:

$$Q^T = Q^P + Q^A - Q^{BP} + Q_{res} \tag{2}$$

where Q^T is the total available heat and Q^P, Q^A, and Q^{BP} are the heat in MW distributed to the PGEN, ACHX, and bypass, respectively. Failing to remove Q^T between the PGEN and ACHX components will result in residual heat, where $Q_{res} > 0$. This heat term is an indication of the difference between the temperature exiting the heat rejection cycle, T_L [°C], and the target temperature set out in Table 1. The exit temperature can be calculated as:

$$Q_{res} = \dot{m}_{Tot} \cdot C_p \cdot (T_L - T_{set}) \tag{3}$$

where $\dot{m}_{Tot}$ and C_p are the mass flow rate and specific heat of the cooling water. It follows that, in a scenario where sufficient heat transfer is performed, $Q_{res} = 0$, and, therefore, $T_L = T_{set}$.

The time index for the formulation is given by $\mathrm{T} = \{1, 2, \ldots, |\mathrm{T}|\}$. The cooling water enters the heat rejection cycle at a temperature of T_{in} [°C] and a mass flow rate of $\dot{m}_{Tot}$ [kg/s]. At time t, a process model uses the desired temperature of the cooling water entering the gas-cooler, T_{set} [°C], to determine the heat to be transferred, Q^T [MW].

A binary parameter, δ^P, is introduced, where a non-zero value indicates that the power generation process is operational and available to transfer heat. A value of zero indicates that the power generation cycle is not available.

To prevent frequent trips to the PGEN in low heat conditions, a time delay is introduced for a PGEN currently offline. This ensures that the PGEN does not start until n periods have passed, where sufficient heat is available. Other reasons for a stoppage will externally force the value of δ^P to be zero until rectified.

The heat assigned to the PGEN, Q^P, must be more than the lower limit, L_P [MW], of the power-generating process. The process control within PGEN will adjust working pressures and the mass flow rates of the refrigerant to transfer the required heat, within the constraints of the PGEN design. The PGEN component converts Q^P to electrical power at a heat source temperature-dependent thermal efficiency, as shown in Figure 2.

It follows that a higher value for Q^P results in a higher power generation. It can also be argued from (3) that a higher Q_{res} value results in a higher T_L for the cooling water entering the gas-cooler. The formulations to follow, therefore, attempt to minimise Q_{res} while also attempting to maximise Q^P.

Any heat not transferred by the PGEN needs to be assigned to the ACHX. The heat distributed to ACHX is Q^A [MW]. Due to the use of a fan and ambient air to transfer heat, the heat transfer rate increase is limited at Q^A_r. Note that ACHX can consist of multiple air-cooled heat exchanger units. The distribution of heat and mass flows between the individual units does not fall within the scope of this study. Therefore, the ACHX is treated as a single system with a relatively wide operational range.

For the typical works philosophy, a parameter, ϕ_P [-], is introduced that represents the share of heat distributed to the PGEN. This parameter is predetermined and fixed, independent of heat source parameters.

The heat distributions to the ACHX, PGEN, and BP at time t are determined through the algorithm illustrated in Figure 4.

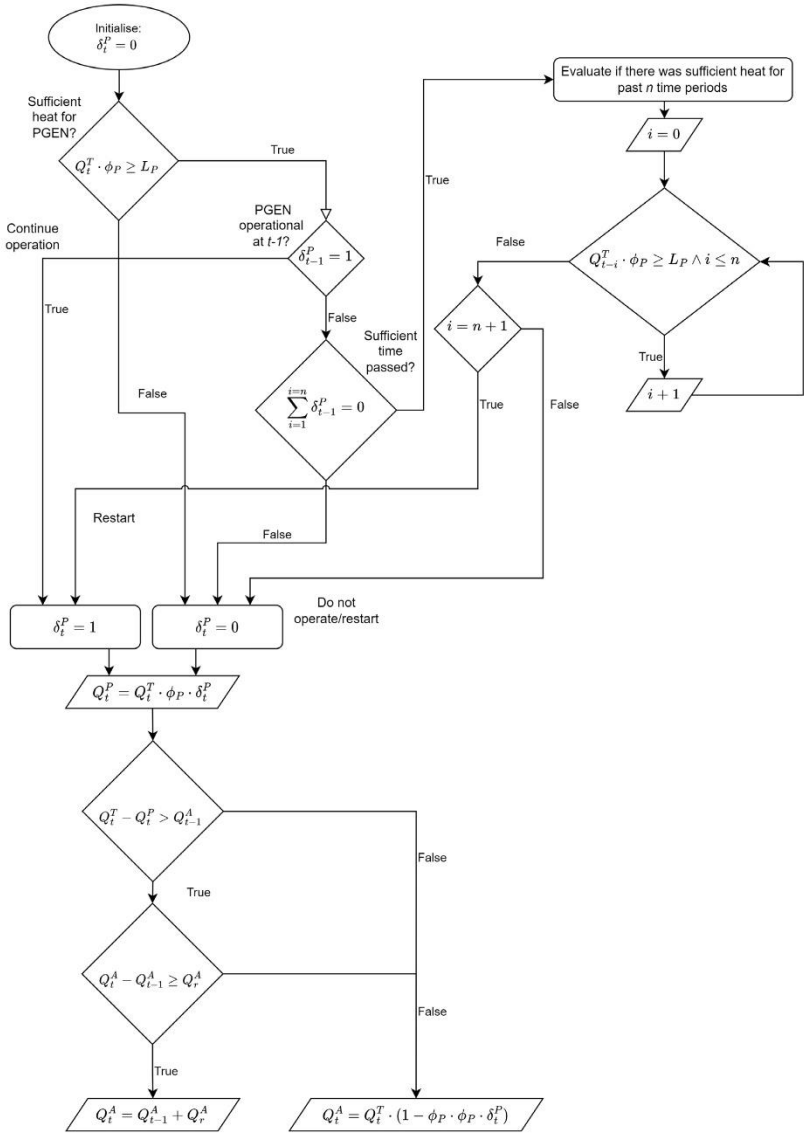
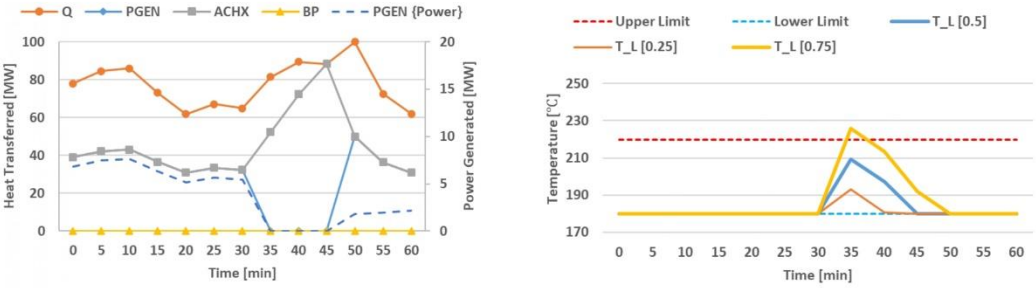


Figure 4. Block diagram for Algorithm 1 (WPLC).

To demonstrate the behaviour of the control formulations, the plant parameters set out in Tables 2 and 3 will be used, with additional parameters being supplied where required. The setpoint temperature $T_{set} = 180$ °C, as in Table 1. The PGEN has a lower heat limit of $L_P = 10$ MW. The heat of Q^P is converted to power according to the curve in Figure 2. The ACHX can only increase its heat transfer capability by 4 MW/min. The time period of the sufficient heat required before a restart is 15 min; $n = 3$. The formulation will be applied to the demonstrative dataset in Figure 3b.

3.1.1. The Results of WPLC on the Demonstrative Dataset

In Figure 5a, the heat distribution between the components based on the demonstrative dataset (Figure 3b) is illustrated.



(**a**) (**b**)

Figure 5. (**a**) Heat distribution between the PGEN, ACHX, and BP over time for WPLC. An overlay of the available heat (Q) is included. (**b**) Illustration of temperature entering the gas-cooler over time for WPLC, with $\phi_{PGEN} = 0.5$ as well as $\phi_{PGEN} = 0.25$ and 0.75.

The fixed ratio of heat distribution between components are notable, with both components following the curve of the waste heat, with the exception of 35–45 min, where the PGEN was unavailable due to an unplanned event. It is also noted that during time periods where PGEN was unavailable, the ACHX attempted to transfer as much of the waste heat as possible within its adjustment constraint. Note that the power generation after the PGEN restarted was at the lower limit and only increased by the 2 %/min, while the heat transferred by the PGEN did not follow this restriction.

The value of T_L over the same time span is shown in Figure 5b. The unplanned unavailability of the PGEN results in the ACHX needing to transfer all the required heat. However, since the ACHX can only realistically increase the heat transfer by 4 MW/min, the required heat transfer cannot be instantaneously satisfied by the ACHX. It follows that this scenario will result in $Q_{res} > 0$, and from (3), it follows that $T_L > T_{set}$.

The results in the demonstrative dataset indicate clearly that the conservation principles given in Equation (2) are adhered to, with temperature increases noted where $Q_{res} > 0$.

The value of ϕ_P can be adjusted in an attempt to maximise power generation. The value of T_L remains within the temperature envelope even with the unplanned availability of the PGEN, as shown in Figure 5b. The ACHX is able to adjust quickly enough to transfer the heat that would have been distributed to the PGEN.

This can indicate that the fixed ratio is too conservative and that more heat can be distributed to the PGEN to increase the power generated by the system. Using the same formulation, the value of ϕ_P is adjusted to a more aggressive approach, where $\phi_P = 0.75$.

The temperature curve for T_L with this approach indicates that the temperature moved outside the operational envelope. This was due to the ACHX receiving only 25% of the heat before needing to adjust to transfer 100% of the heat. This approach can, therefore, be seen as too aggressive, given the supplied demonstrative dataset.

The opposite can also be shown for the more conservative approach, where $\phi_P = 0.25$ results in only a small increase in T_L when the PGEN becomes unavailable. This is due to the ACHX initially receiving 75% of the heat before having to adjust to transfer 100% of the heat.

It is concluded that a conservative value for ϕ_P will not result in maximum power generation but will have reduced risk, whereas an aggressive value will deliver more power generation but with increased risk of breaching the temperature envelope.

The above results are only for a demonstrative dataset to illustrate the effect of changes made to parameters. In the next section, the formulation will be applied to the historical dataset shown in Figure 3a.

3.1.2. The Results of WPLC on the Historical Dataset

The WPLC is applied to the larger dataset for four different ϕ_P values. The value of ϕ_{PGEN} is changed from 0.1 to 0.9 to determine the ideal ratio for the specific heat profile shown in Figure 3a. An unplanned stoppage is also forced on three different time periods to evaluate the influence of heat source properties on the preferred value of ϕ_P.

It has been indicated in the previous section that a higher value for ϕ_P will result in a higher heat distribution to the PGEN. This indicates that more power will be generated. The value of ϕ_P is, therefore, varied between 0.5 and 0.8 to determine the highest value that is still conservative enough to ensure adequate cooling in the event of an unplanned trip. Unplanned events 1, 2, and 3 take place at 8.5, 24.75 and 32.6 days into the timeline of the historical dataset.

Since the objective of this study is to maximise power generation whilst keeping within the operational temperature envelope, the maximum value for ϕ_P needs to be identified where the T_L is still within the operational envelope.

This value is indicated with a shaded column in Table 4. A value of 0.7 for ϕ_P causes the cooling water to move out of the operational temperature envelope for only one of the unplanned events. This indicates that the impact that the distribution ratio has is dependent on the heat source parameters at the time of the unplanned event.

Table 4. Results for heat rejection cycle for a range of ϕ_P and unplanned events.

		ϕ_P			
		0.5	**0.6**	**0.7**	**0.8**
T_L [°C] at unplanned events	Event 1	187.1	193.8	200.5	207.2
	Event 2	207.1	213.8	220.8	227.2
	Event 3	191.3	197.9	204.5	211.1

A value of 0.6 for ϕ_P is thus identified as the desired setting, which delivers adequate cooling at all times, while also being conservative enough that the highest value for T_L after an unplanned trip is inside the envelope at 213.8 °C.

The impact of $\phi_P = 0.6$ on the power generation is supplied in Table 5 along with more aggressive and conservative values. Evaluating the average power generation along with the maximum temperatures indicates that the more conservative value for ϕ_P delivers a lower temperature and lower power generation. This is due to a significant share of heat being distributed to the ACHX to ensure that it can readily adjust to transfer Q_{Tot} if the PGEN were to become unavailable.

Table 5. Results for heat rejection cycle for a $\phi_{PGEN} = 0.6 \pm 0.1$.

		Typical Works Philosophy		
		ϕ_P = 0.5	ϕ_P = 0.6	ϕ_P = 0.7
P_{PGEN} [MW]	Maximum	8.7	10.4	12.1
	Average	5.1	6.1	7.1
T_L [°C]	Maximum	207.1	213.8	220.8
	Minimum	180	180	180

The opposite is also true; the more aggressive value delivers a higher average power generation as well as a value for T_L that breaches the temperature envelope. This is due to the PGEN receiving a larger share of the heat, resulting in ACHX having to increase over a longer time to meet the heat transfer requirement in case of an unplanned event.

This results section shows that a fixed value for the distribution ratio is not the desired approach for a fluctuation in the heat source.

The results and discussions above conclude that the ratio of distribution should be dependent on the parameters of the heat source at any given time. It follows that the ratio of distribution needs to be continuously adjusted.

3.2. The Ongoing Readiness of the ACHX

The WPLC is a typical works philosophy where the heat is distributed at a fixed ratio between the PGEN and the ACHX. The WPLC shows that a fixed ratio of heat distribution between the PGEN and the ACHX is not ideal due to the potential of unplanned stoppages.

This section formulates a control algorithm that ensures an adequate heat transfer is maintained at all times by continuously being ready for an unplanned stoppage. This will be achieved by calculating and distributing a share of the heat to the ACHX that mitigates any risk of temperatures outside the operational envelope for the gas-cooler.

For this purpose, a binary parameter, δ^{OR}, is introduced. A value of one indicates that the control philosophy must anticipate an unplanned stoppage every time period. To determine the value of δ^{OR}, a minimum heat transfer, Q_L^A [MW], is firstly calculated. Determining Q_L^A is carried out through Equation (4) below:

$$Q_L^A = \max\left(\dot{m}_{Tot} \cdot C_p \cdot \left(T_{in} - T_L^U\right); 0\right) \tag{4}$$

where T_L^U is the upper temperature limit of the operational temperature envelope. Note that if $T_{in} < T_L^U$, the term will be negative, and that Q_{ACHX}^L is set to zero. In this scenario, all the heat can be assigned to the PGEN for power generation without risk, since failing to transfer any heat will only result in $T_L = T_{in}$ and thus $T_L < T_L^U$.

The heat distribution between the PGEN and the ACHX is determined through the algorithm illustrated in Figure 6.

To demonstrate the behaviour of the ORLC, the same plant parameters set out in Section 3.1 are used. In addition, the upper temperature limit for the operational envelope, $T_L^U = 220$ °C, is used, as noted in Table 1.

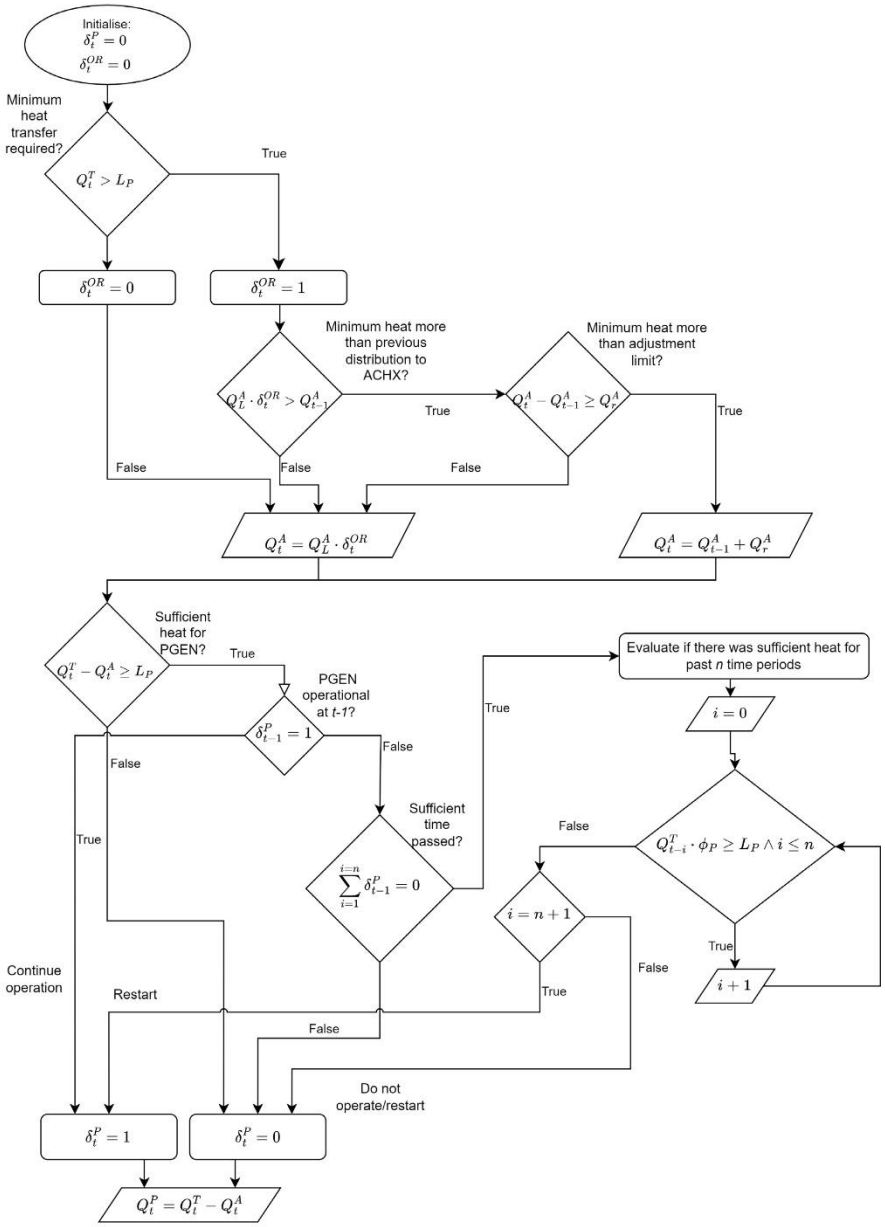


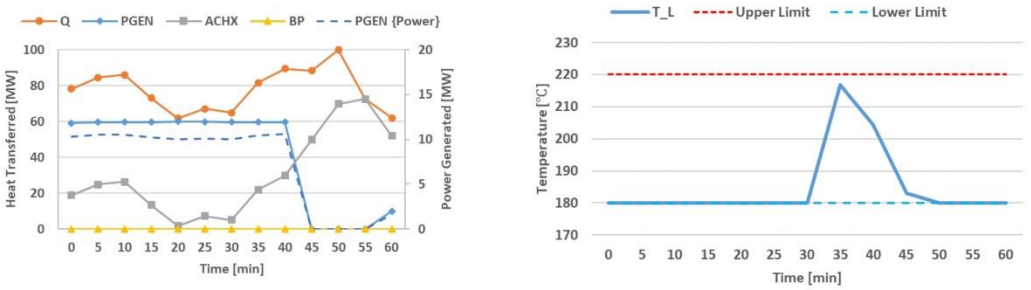
Figure 6. Block diagram for Algorithm 2 (ORLC).

3.2.1. The Results of the Continuous Readiness of the ACHX on the Historical Dataset

The results of applying this formulation to the demonstrative dataset in Figure 3b is shown in Figure 7a,b.

The first significant difference noted in Figure 7 is in the heat transferred by the PGEN and the ACHX. Previously, these curves followed the same values, whereas, in this

formulation, they differ. The fluctuation of T_{in} results in a varying value of Q^{L}_{ACHX}. This is due to the difference between T_{in} and T_{set} being used in its calculation. Note that this results in a constant value for Q_{PGEN}. It can be argued that the heat transfer assigned to the ACHX reduces the cooling water to the upper temperature limit, T^{U}_{L}, whereas the PGEN then transfers the residual heat contained between T^{U}_{L} and T_{set}.



(**a**) (**b**)

Figure 7. (**a**) Heat distribution between the PGEN, ACHX, and BP over time for the formulation in Section 3.2. An overlay of the available heat (Q) is included. (**b**) Illustration of temperature entering the gas-cooler over time for the formulation in Section 3.2.

Through the comparison of Figures 5 and 7, the heat distributed to the PGEN clearly has lower fluctuations for the ORLC compared to the WPLC. By comparing the resulting power generation, as is done in Figure 8, it can be noted that the PGEN with the WPLC observed higher power generation figures for only 10 min of the 60 min range. It is expected that the ORLC will result in an increase in power generation on the demonstrative dataset. This is dependent on the signature waste-heat profile and will need to be evaluated in the historical dataset for an accurate conclusion.

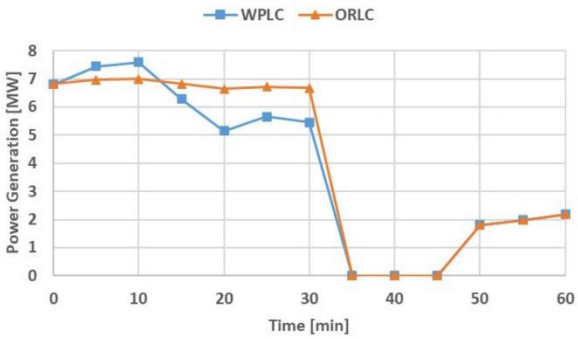


Figure 8. Power generation comparison between ORLC and WPLC.

3.2.2. The Results of the Continuous Readiness of the ACHX on the Historical Dataset

The control philosophy given above can be demonstrated on the historical set of data illustrated in Figure 3a. The results are summarised in Table 6.

It is noted that the power generation increased from an average of 6.11 MW to 6.41 MW with this philosophy. The maximum power generation, however, reduced from 10.4 MW to 9.61 MW. The maximum temperature for T_L reduced from 217.1 to 204.5 °C, which indicates that the current formulation is a definite improvement of the typical works philosophy.

This formulation is definitely successful in its objective to adjust the distribution between the ACHX and the PGEN to the extent that a sufficient heat transfer can be guaranteed at all times.

Table 6. Results for heat rejection cycle for ORLC.

		Control Philosophy	
		WP (ϕ_{PGEN} = 0.6)	**ORLC**
P_{PGEN} [MW]	Maximum	10.4	9.61
	Average	6.11	6.41
T_L [°C]	Maximum	213.8	204.5
	Minimum	180	180

3.3. *Advanced Bypass Utilisation*

In ORLC, it is noted that T_L did not exceed any of the temperature limits for any given period. By ensuring that the heat transfer demand is always met, additions to the control formulation can now be made in an attempt to maximise power generation.

To increase the observed power generation, a binary parameter, δ^{BP}, is introduced. A non-zero value indicates that the control philosophy will make use of the bypass line to maintain a desirable value for T_L while assigning as much heat transfer to the PGEN process as possible. The conservation of energy and mass in (2) and (3) will still hold, with the heat and mass flows assigned to the bypass compensating for the higher heat transfer rate achieved in the PGEN.

When $\delta^{BP} = 1$, the value of the minimum heat assigned to the ACHX, Q_L^A, is also bypassed. If successful, it follows from Equation (1) that a larger Q^P is observed in comparison to the previous section.

The heat distribution to the ACHX, PGEN and BP streams are determined through the algorithm illustrated in Figure 9.

3.3.1. The Results of the Advanced Use of Bypass on the Demonstrative Dataset

Figure 10 can be compared to Figures 5 and 7. A significant difference is the consistent use and adjustment of flow in the BP. This allows the ACHX to maintain the minimum required heat transfer while allowing the PGEN to operate at maximum capacity whenever possible. This can be confirmed through the evaluation of the power generated being significantly higher than for previous formulations.

The power generation performance between WPLC, ORLC, and ABLC are illustrated in Figure 11. The control formulation in ABLC shows an increase in the heat distributed to the PGEN and it is, therefore, expected that the ABLC will result in an increase in observed power generation. Figures 10 and 11 shows that ABLC includes all operational constraints and limitations as required.

The formulation of ABLC is, therefore, suitable to be tested on the historical dataset.

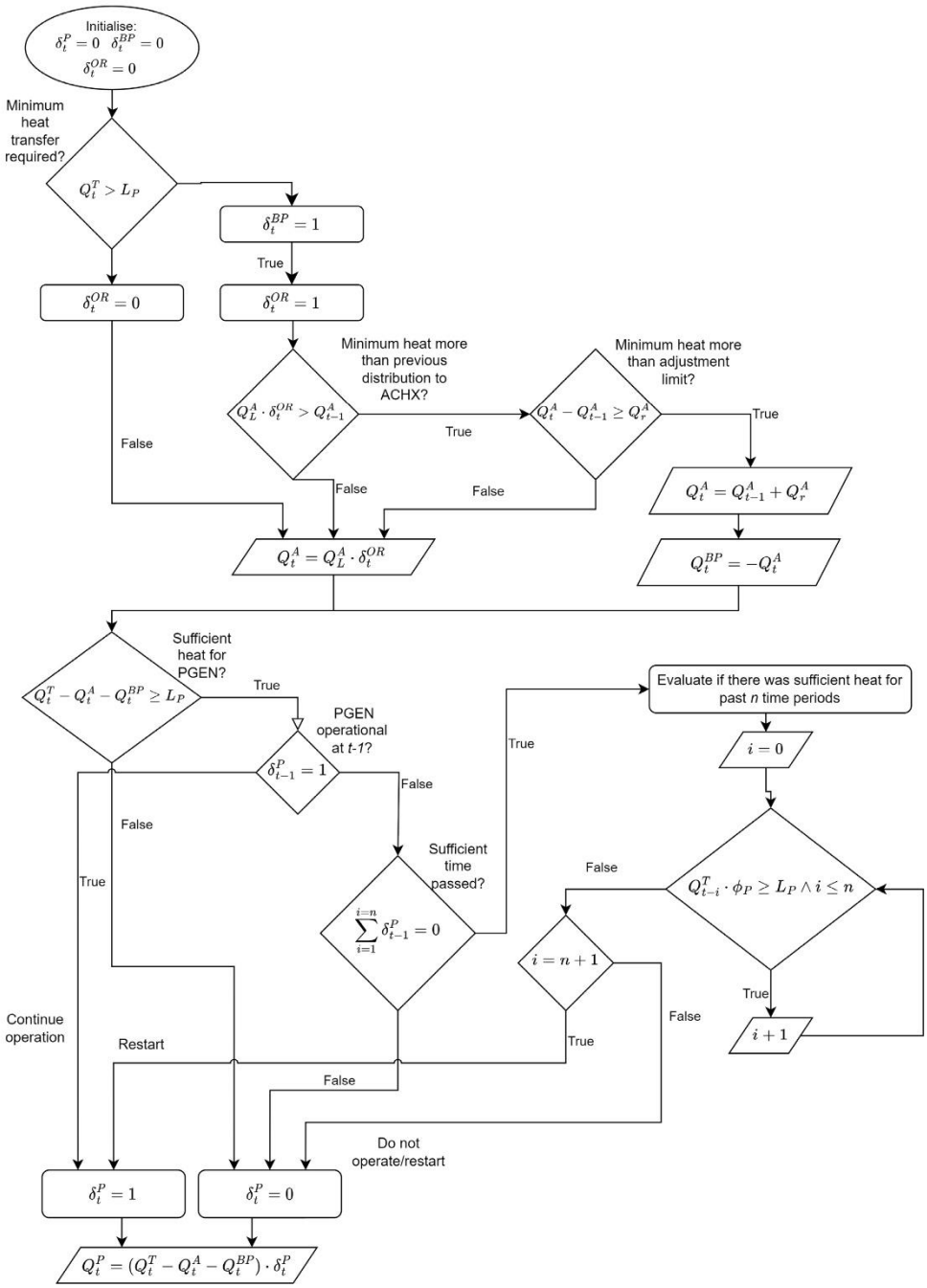
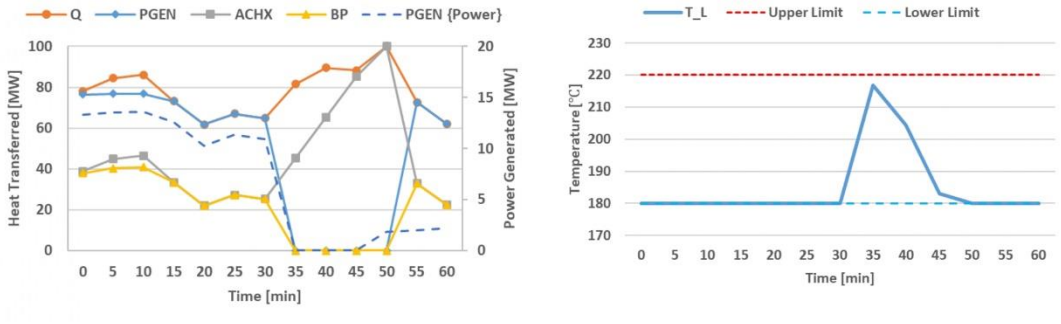


Figure 9. Block diagram for Algorithm 3 (ABLC).



(**a**) (**b**)

Figure 10. (**a**) Heat distribution among PGEN, ACHX, and BP over time for the formulation described in Section 3.3. Overlay of the available heat is included. (**b**) Illustration of temperature entering the gas-cooler over time for the formulation in Section 3.3.

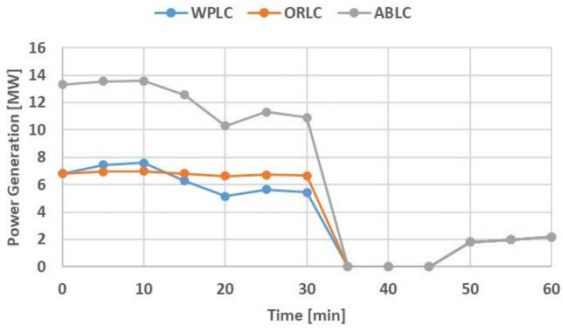


Figure 11. Power generation comparison between ORLC, WPLC and ABLC (demonstrative data).

3.3.2. The Results of Advanced Use of Bypass on Historical Dataset

The formulation in Section 3.3 is now applied to the historical dataset in Figure 3a. The results are summarised in Table 7.

Table 7. Results for heat rejection cycle for ABLC.

		Control Philosophy		
		WPLC	**ORLC**	**ABLC**
P_{PGEN} [MW]	Maximum	10.40	9.61	17.31
	Average	6.11	6.41	10.12
T_L [°C]	Maximum	213.8	204.5	204.5
	Minimum	180	180	180

A significant increase in average and maximum power generation are noted. The average power generation increased by 57.8% from 6.41 MW to 10.12 MW. This is achieved without any increase in the value for T_L, indicating that there is no added risk to this formulation in terms of moving outside the operational temperature envelope.

From the above results, it is clear that the formulation of ABLC is successful in significantly increasing the power generation by PGEN. This is achieved while still ensuring that ACHX is always ready to transfer all the required heat at a rate fast enough that there is no risk of moving outside the temperature envelope, even in case of an unplanned trip.

3.4. The Use of Predictive Parameters

The ABLC was successful in significantly increasing the power produced whilst still ensuring that T_L stayed within the desired temperature envelope at all times.

From historical plant data and process models, future heat transfer requirements can be predicted with a level of certainty. This may allow adjustments to the heat distribution to further improve on power generation without adding risk.

Plant operational models and historical datasets can be used to determine the feedforward parameters that indicate whether an increase in available heat can be expected in the following n periods.

It is noted in Table 1 and discussed in Section 2 that the PGEN has a limit on how fast the power generation can be adjusted. It is also noted that this constraint originates from turbine control and not from the heat exchanger's capability. From this, it can be argued that increasing the heat transferred to the PGEN before a significant increase is observed in Q^T can result in the PGEN increasing the power generation without adding significant risk. By increasing the power generation earlier, the PGEN will have smaller adjustments to make once a significant increase in Q^T is observed.

From historical datasets, certain process procedures can be identified that lead to a required relative heat transfer increase in α in the next m time periods. A binary parameter, δ^{PP}, is introduced, where a non-zero value indicates that $\alpha > 0$. If an increase in heat is expected, then the heat transfer required from the PGEN will either be the maximum operational limit or a product of α with its previous value, Q^P_{t-1}.

Since the philosophy of ORLC is still present in this formulation, the value of α needs to be limited to ensure that the ACHX can still meet the heat transfer requirements in case the PGEN becomes unavailable.

This ensures that the operational limits of all components are adhered to, while maintaining a safe value for T_L.

Note that the ACHX minimum heat distribution, Q^A_L, is still assigned. Therefore, this philosophy can potentially lead to assigning more heat transfer requirements to the ACHX and PGEN than is required at time t. It follows that the bypass must be used to maintain the temperature T_L above the lower limit, according to Equation (1). Therefore, this control philosophy only allows the use of predictive parameters to maximise power generation if the value of δ_{BP} is also a non-zero value.

The heat distribution between the PGEN, ACHX, and BP are determined through the algorithm illustrated in Figure 12.

3.4.1. The Results of Using Predictive Parameters on the Demonstrative Dataset

Figure 13 can be compared to Figures 5, 6 and 10. A minor increase in the heat distributed to the PGEN is noted. To ensure $Q_{res} \geq 0$, the BP is also increased slightly to prevent breaching the temperature envelope on the lower limit. No changes are noted in the heat distribution to the ACHX.

The power generation performances of WPLC, ORLC, ABLC, and PPLC are illustrated in Figure 14. Note that the slight increase in heat distribution to PGEN has resulted in a small increase in power generation compared to the previous formulation of ABLC.

Figures 12 and 13 show that PPLC includes all operational constraints and limitations as required, and is working as required and expected.

The formulation of PPLC is therefore suitable to be tested on the historical dataset.

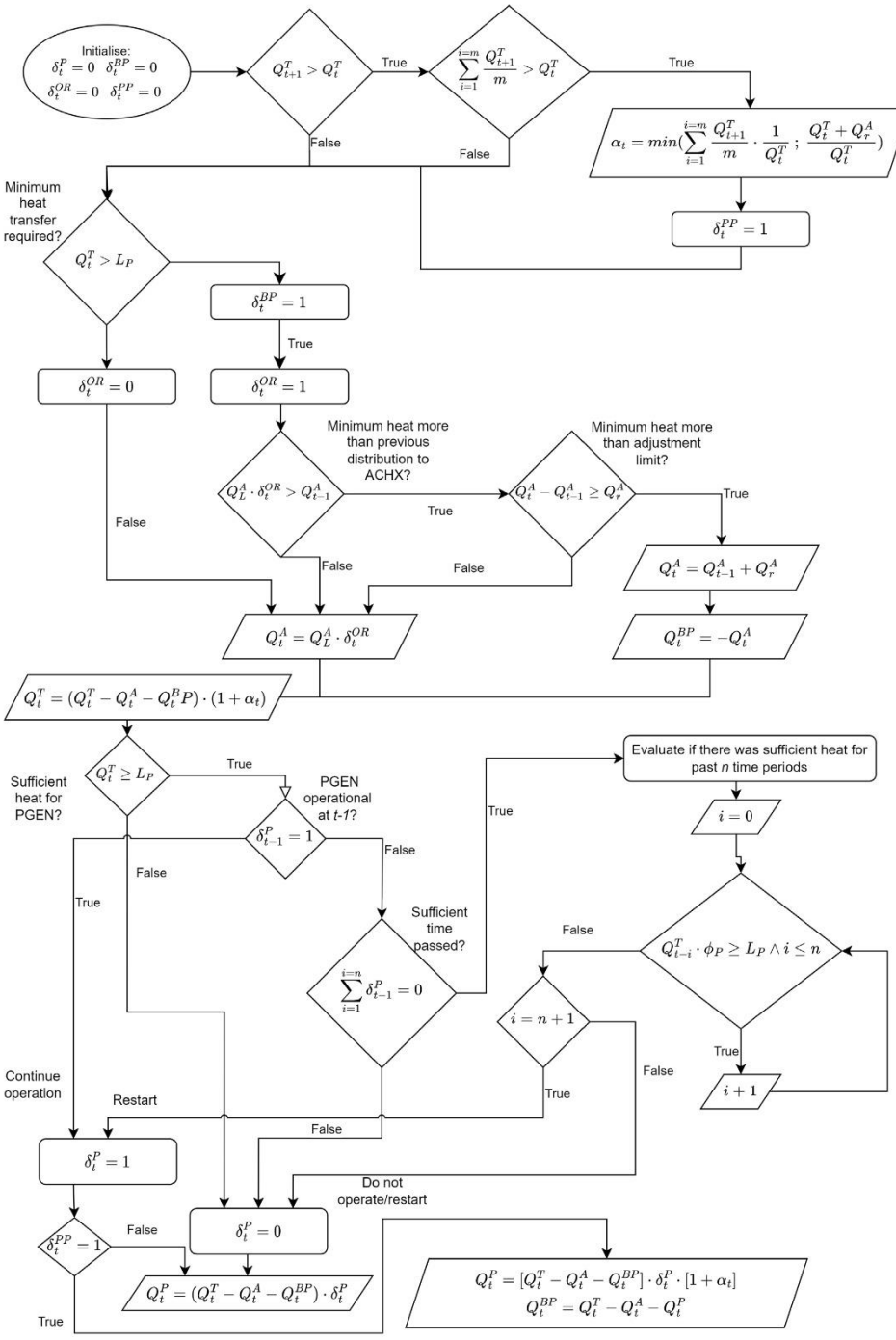
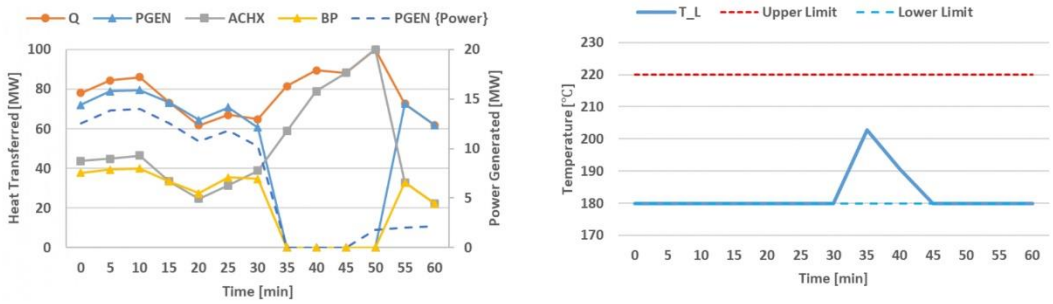


Figure 12. Block diagram for Algorithm 4 (PPLC).



(**a**) (**b**)

Figure 13. (**a**) Heat distribution among PGEN, ACHX, and BP over time for the formulation described in Section 3.4. Overlay of the available heat is included. (**b**) Illustration of temperature entering the gas-cooler over time for the formulation in Section 3.4.

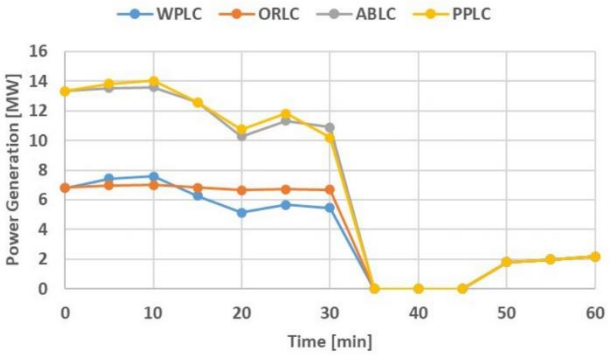


Figure 14. Power generation comparison between WPLC, ORLC, ABLC and PPLC for the demonstrative dataset.

3.4.2. The Results of Using Predictive Parameters on the Historical Dataset

The formulation is applied to the historical dataset of Figure 3a with the results summarised in Table 8.

Table 8. Results for heat rejection cycle for PPLC.

		Control Philosophy			
		WP	**ORLC**	**ABLC**	**PPLC**
P_{PGEN} [MW]	Maximum	10.40	9.61	17.31	17
	Average	6.11	6.41	10.12	10.68
T_L [°C]	Maximum	213.8	204.5	204.5	204.5
	Minimum	180	180	180	180

The average power generation increased by 5.5% from 10.12 MW to 10.68 MW. The maximum values observed for T_L indicate minimal added risk. The unplanned event is triggered in a time period where $\delta^{PP} = 1$. As noted in Section 3.4.1, the flow through the bypass increased. However, no change in maximum temperature is noted. This is due to the value of α^{PP} being influenced by the adjustment capability of the ACHX every time.

4. Conclusions

The formulation of a control philosophy for the heat rejection process was demonstrated. The main priority of the control philosophy is to ensure that the heat rejection process transfers sufficient heat from the cooling fluid to other components or processes. This ensures that the temperature of the cooling fluid entering the gas-cooler remains within the required range. A failure to do so can result in production interruptions that can be associated with significant losses for the plant owner. In addition, the availability of a power generation cycle also makes waste-heat recovery and power generation a priority.

Therefore, the control philosophy needs to calculate both the heat and mass flow distributions between the ACHX, PGEN, and BP. The control algorithm also needs to adjust to changes in the received flow from time $t-1$ to t.

Note that all control formulations in this study consider a scenario where the power consumption of the plant is at critical levels. As discussed, this results in the need to constrain the ramp-up rate of the ACHX. The results of the control formulations shown in this study are for the most extreme scenario to ensure that the control formulations perform as required at all times. Should power consumption not be near critical levels, only a transient response will constrain the heat transfer adjustment of the ACHX.

The formulation starts with a typical works control philosophy. In this formulation, the distribution of heat between the ACHX and PGEN is fixed, independent of the fluctuating heat source. Based on the historical data, a suitable ratio is selected that satisfies the heat transfer requirement, even in the event of an unplanned trip of the PGEN. It is shown that the ratio of distributions needs to adjust according to the heat source parameters to ensure maximum power generation without any added risk of moving out of the temperature envelope.

This is rectified with the next formulation, where the minimum heat is always assigned to the ACHX with the residual heat then distributed to the PGEN. This resulted in the temperature remaining within the operational limits, but with an improvement in power generation. An average power generation of 6.41 MW was observed.

The advanced use of BP ensures that T_L is maintained within the desired temperature envelope while also allowing the PGEN to transfer significantly more heat than previously allowed. This significantly improved the average power generation to 10.12 MW.

The addition of feedforward parameters to predict the increase in available heat increased the average power generation by another 5.5%, resulting in an average of 10.68 MW.

Through the formulation process, the control algorithms are simulated on a demonstrative dataset for evaluation to ensure the scientific soundness of the results once applied to the larger historical dataset. All evaluations have shown that the WPLC, ORLC, ABLC, and PPLC work as intended. The limitations of components are never breached, and adjustments are always made within the capability of each component. The changes in formulations also deliver the expected changes in heat distribution between the components.

The formulated control philosophy successfully maximised energy recovery while ensuring that the temperature was maintained in the desired temperature envelope.

The novel contributions of this paper are the three control philosophies that consider the stochastic effect of a fluctuating heat source. These formulations then successfully distribute the waste heat between the ACHX, PGEN, and BP in such a way that maximises energy recovery without any risk to the production process, even with a sudden loss in heat transfer capabilities such as an unplanned trip event for the PGEN.

A potential future study could include the formulation of a control philosophy for an ACHX that consists of multiple heat exchangers, where each individual heat exchanger has different design parameters. The formulation can then attempt to ensure a maximum heat transfer for a minimum power input to forced convection equipment. An additional study could be carried out to increase the fidelity of the PGEN component. The internal control of the PGEN can lead to an improved conversion ratio of the power generated to the heat transfer.

Author Contributions: Conceptualisation, J.P.B., M.V.E. and P.v.Z.V.; Formal analysis, J.P.B. and P.v.Z.V.; Investigation, J.P.B., M.V.E. and P.v.Z.V.; Methodology, J.P.B., M.V.E. and P.v.Z.V.; Validation, J.P.B. and P.v.Z.V.; Visualisation, J.P.B. and P.v.Z.V.; Writing—original draft, J.P.B.; Writing—review and editing, M.V.E. and P.v.Z.V. All authors have read and agreed to the published version of the manuscript.

Funding: This research received no external funding.

Data Availability Statement: Data are contained within the article. Historical dataset not publicly available due to NDA with data provider.

Conflicts of Interest: The authors declare no conflict of interest.

Nomenclature

C_p	Specific heat of Fluid, $\left[\frac{\text{J}}{\text{kgK}}\right]$
T	Temperature, [°C]
m	Mass flow rate $\left[\frac{\text{kg}}{\text{s}}\right]$
Heat Streams	
Q^T	Waste heat stream, [MW]
Q^P	Heat distributed to PGEN, [MW]
Q_L^A	Minimum heat distributed to ACHX, [MW]
Q^A	Heat distributed to ACHX, [MW]
Q^{BP}	Heat distributed to Bypass, [MW]
Limits/Setpoints	
Q_r^A	Heat Adjustment Limit for ACHX, [MW]
T_L^U	Upper temperature for envelope, [°C]
T_L	Setpoint temperature, [°C]
L_p	Lower operational limit of PGEN
Greek Letters	
η_{th}	Thermal efficiency
ρ	Density, $\left[\frac{\text{kg}}{\text{m}^3}\right]$
α	Expected relative increase in Q^T
ϕ	Fixed distribution ratio to PGEN
δ^{BP}	Binary decision variable for ABLC
δ^{PP}	Binary decision variable for PPLC
δ^{OR}	Binary decision variable for ORLC
δ^P	Binary decision variable for PGEN availability
Subscripts	
h	Hot fluid
w	Wall of heat exchanger
out	Outlet
c	Cold fluid
in	Inlet
max	Maximum
min	Minimum
res	Residual

References

1. Gupta, R. Chapter 4.2—Energy Resources, Its Role and Use in Metallurgical Industries. In *Treatise on Process Metallurgy*; Industrial Processes, Part A; Elsevier: Amsterdam, The Netherlands, 2014; Volume 3, pp. 1425–1458.
2. Jalkanen, H.; Holappa, L. Chapter 1.4—Converter Steelmaking. In *Treatise on Process Metallurgy*; Industrial Processes, Part A; Elsevier: Amsterdam, The Netherlands, 2014; Volume 3, pp. 223–270.
3. Wang, B.; Zhou, J.-A.; Xie, J.-B.; Liu, Z.-Q.; Zhang, H.; Zhou, L.-H. Numerical and Experimental Investigations of Converter Gas Improvement inside a Flue Using Its Waste Heat and CO_2 by Pulverized Coal Injection. *Environ. Prog. Sustain. Energy* **2018**, *37*, 1503–1512. [CrossRef]
4. Hosseini, R.K.; Yareiee, S. Failure analysis of boiler tube at a petrochemical plant. *Eng. Fail. Anal.* **2019**, *106*, 104146. [CrossRef]
5. Hemadri, V.B.; Subbarao, P. Thermal integration of reheated organic Rankince cycle (RH-ORC) with gas turbine exhaust for maximum power recovery. *Therm. Sci. Eng. Prog.* **2021**, *23*, 100876. [CrossRef]
6. Incropera, F.P.; DeWitt, D.P.; Bergman, T.L.; Lavine, A.S. *Fundamentals of Heat and Mass Transfer*; John Wiley & Sons: Hoboken, NJ, USA, 2007.
7. Ravi, R.; Pachamuthu, S.; Shivaprasaf, K.; Kasinathan, P.; Anandan, S.; Sundarababu, J. CFD analysis of innovative protracted finned counter flow heat exchanger for diesel enginer exhaust waste heat recovery. *AIP Conf. Proc.* **2021**, *2316*, 030024.
8. Jiménez-Arreola, M.; Pili, R.; Margo, F.D.; Wieland, C.; Rajoo, S.; Romagnoli, A. Thermal power fluctuations in waste heat to power systems: An overview on the challenges and current solutions. *Appl. Therm. Eng.* **2018**, *134*, 576–584. [CrossRef]
9. Inayat, A. Current progress of process integration for waste heat recovery in steel and iron industries. *Fuel* **2023**, *338*, 127237. [CrossRef]
10. Parra-Camacho, L.; Rodriguez-Bayona, A.; Carreno-Zagarra, J. Automation and control of the thermal mixing process. *Syst. Sci. Control Eng.* **2023**, *11*, 2177769. [CrossRef]
11. Li, X.; Xu, B.; Tian, H.; Shu, G. Towards a novel holistic design of organic Rankine cycle (ORC) systems operating under heat source fluctuations and intermittency. *Renew. Sustain. Energy Rev.* **2021**, *147*, 111207. [CrossRef]

12. Zhao, R.; Zhang, H.; Song, S.; Tian, Y.; Yang, Y.; Liu, Y. Integrated simulation and control strategy of the diesel engine–organic Rankine cycle (ORC) combined system. *Energy Convers. Manag.* **2018**, *156*, 639–654. [CrossRef]
13. Shu, G.; Li, X.; Tian, H.; Shi, L.; Wang, X.; Yu, G. Design condition and operating strategy analysis of CO_2 transcritical waste heat recovery system for engine with variable operating conditions. *Energy Convers. Manag.* **2017**, *142*, 188–199. [CrossRef]
14. Yebi, A.; Xu, B.; Liu, X.; Shutty, J.; Anschel, P.; Onori, S.; Filipi, Z.; Hoffman, M. Nonlinear model predictive control strategies for a parallel evaporator diesel engine waste heat recovery system. In Proceedings of the ASME 2016 Dynamic Systems and Control Conference, Minneapolis, MN, USA, 12–14 October 2016.
15. Ponce, C.; Sáez, D.; Bordons, C.; Bordons, C.; Nú, A. Dynamic simulator and model predictive control of an integrated solar combined cycle plant. *Energy* **2016**, *109*, 974–986. [CrossRef]
16. Peralez, J.; Tona, P.; Nadri, M.; Dufour, P.; Sciarretta, A. Optimal control for an organic Rankine cycle on board a diesel-electric railcar. *J. Process Control* **2015**, *33*, 1–13. [CrossRef]
17. Rathod, D.; Xu, B.; Filipi, Z.; Hoffman, M. An experimentally validated, energy focused, optimal control strategy for an Organic Rankine Cycle waste heat recovery system. *Appl. Energy* **2019**, *256*, 113991. [CrossRef]
18. Hernandez, A.; Desideri, A.; Ionescu, C.; De Keyser, R.; Lemort, V.; Quoilin, S. Real-Time Optimization of Organic Rankine Cycle Systems by Extremum-Seeking Control. *Energies* **2016**, *9*, 334. [CrossRef]
19. Wang, X.; Wang, R.; Jin, M.; Shu, G.; Tian, H.; Pan, J. Control of superheat of organic Rankine cycle under transient heat source based on deep reinforcement learning. *Appl. Energy* **2020**, *278*, 115637. [CrossRef]
20. Xu, B.; Li, X. A Q-learning based transient power optimization method for organic Rankine cycle waste heat recovery system in heavy duty diesel engine applications. *Appl. Energy* **2021**, *286*, 116532. [CrossRef]
21. Carvalho, C.; Carvalho, E.; Ravagnani, M. Implementation of a neural network MPC for heat exchanger network temperature control. *Braz. J. Chem. Eng.* **2020**, *37*, 729–744. [CrossRef]
22. Vasičkaninová, A.; Bakošová, M.; Mészáros, A. Fuzzy Control Design for Energy Efficient Heat Exchanger Network. *Chem. Eng. Trans.* **2021**, *88*, 529–534.
23. Trafczynski, M.; Markowski, M.; Urbaniec, K. Energy saving potential of a simple control strategy for heat exchanger network operation under fouling conditions. *Renew. Sustain. Energy Rev.* **2019**, *111*, 355–364. [CrossRef]
24. Abbas, W.; Vrabec, J. Cascaded dual-loop organic Rankine cycle with alkanes and low global warming potential refrigerants as working fluids. *Energy Convers. Manag.* **2021**, *249*, 114843. [CrossRef]
25. Tian, H.; Shu, G. Organic Rankine Cycle systems for large-scale waste heat recovery to produce electricity. In *Organic Rankine Cycle (ORC) Power Systems*; Elsevier: Amsterdam, The Netherlands, 2017; pp. 613–636.
26. Guercio, A.; Bini, R. Biomass-fired Organic Rankine Cycle combined heat and power systems. In *Organic Rankine Cycle (ORC) Power Systems*; Elsevier: Amsterdam, The Netherlands, 2017; pp. 527–567.
27. Venter, P.; Terblanche, S.; van Eldik, M. Turbine investment optimisation for energy recovery plants by utilising historic steam profiles. *Energy* **2018**, *155*, 668–677. [CrossRef]
28. Rezaei, M.; Sameti, M.; Nasiri, F. An enviro-economic RAM-based optimization of biomass-driven combined heat and power generation. *Biomass Convers. Biorefinery* **2023**, 1–16. [CrossRef]

Disclaimer/Publisher's Note: The statements, opinions and data contained in all publications are solely those of the individual author(s) and contributor(s) and not of MDPI and/or the editor(s). MDPI and/or the editor(s) disclaim responsibility for any injury to people or property resulting from any ideas, methods, instructions or products referred to in the content.